



# University of HUDDERSFIELD

## University of Huddersfield Repository

Al-Yarubi, Qahtan

Phase flow rate measurements of annular flows

### Original Citation

Al-Yarubi, Qahtan (2010) Phase flow rate measurements of annular flows. Doctoral thesis, University of Huddersfield.

This version is available at <http://eprints.hud.ac.uk/id/eprint/9104/>

The University Repository is a digital collection of the research output of the University, available on Open Access. Copyright and Moral Rights for the items on this site are retained by the individual author and/or other copyright owners. Users may access full items free of charge; copies of full text items generally can be reproduced, displayed or performed and given to third parties in any format or medium for personal research or study, educational or not-for-profit purposes without prior permission or charge, provided:

- The authors, title and full bibliographic details is credited in any copy;
- A hyperlink and/or URL is included for the original metadata page; and
- The content is not changed in any way.

For more information, including our policy and submission procedure, please contact the Repository Team at: [E.mailbox@hud.ac.uk](mailto:E.mailbox@hud.ac.uk).

<http://eprints.hud.ac.uk/>

# PHASE FLOW RATE MEASUREMENTS OF ANNULAR FLOWS

QAHTAN S. K. AL-YARUBI  
B.Eng., M.Sc.

A thesis submitted to the University of Huddersfield in  
partial fulfilment of the requirements for the degree of  
Doctor of Philosophy.

University of Huddersfield

**March 2010**

---

The author of this thesis (including any appendices and/or schedules to this thesis) owns any copyright in it (the “Copyright”) and he has given The University of Huddersfield the right to use such Copyright for any administrative, promotional, educational and/or teaching purposes.

- i. Copies of this thesis, either in full or in extracts, may be made only in accordance with the regulations of the University Library. Details of these regulations may be obtained from the Librarian. This page must form part of any such copies made.
- ii. The ownership of any patents, designs, trademarks and any and all other intellectual property rights except for the Copyright (“the Intellectual Property Rights”) and any reproductions of copyright works, for example graphs and tables (“Reproductions”), which may be described in this thesis, may not be owned by the author and may be owned by third parties. Such Intellectual Property Rights and Reproductions cannot and must not be made available for use without the prior written permission of the owner(s) of the relevant Intellectual Property Rights and/or Reproductions.

---

## DECLARATION

---

## DECLARATION

No portion of the work referred to in this thesis has been submitted in support of an application for another degree or qualification of this or any other university or other institute of learning.

---

## DEDICATION

---

## DEDICATION

*In the memory of **Mahir** (12 years old), 10<sup>th</sup> January 2008. A wonderful boy with great fondness who will be missed very much.*

## ABSTRACT

In the international oil and gas industry multiphase annular flow in pipelines and wells is extremely important, but not well understood. This thesis reports the development of an efficient and cheap method for measuring the phase flow rates in two phase annular and annular mist flow, in which the liquid phase is electrically conducting, using ultrasonic and conductance techniques. The method measures changes in the conductance of the liquid film formed during annular flow and uses these to calculate the volumetric and mass flow rates of the liquid film. The gas velocity in the core of the annular flow is measured using an ultrasonic technique. Combined with an entrainment model and the liquid film measurements described above, the ultrasonic technique enables the volumetric flow rate of the gas in the core and the volumetric and mass flow rates of entrained liquid droplets to be measured.

This study was based on experimental work and the use of modelling techniques. The practical investigation comprised a series of experiments conducted on a purpose built flow loop in which the test section was a Perspex pipe of 50mm ID. The experimental work was limited to two-phase air-water flow. The flow loop was specifically designed to accommodate the different instruments and subsystems designed in this investigation including bespoke flow meters and a film extraction system. Most flow loop controls were automated using a MATLAB program. Reference measurement of the total water flow rate was made using a calibrated turbine flow meter and of the air flow rate using a calibrated rotameter.

For the combined ultrasonic/conductance method investigated in this thesis, the velocity of the gas in the core was found using a novel Ultrasonic Flow Meter (USFM). The positioning and arrangement of the transducers have never been used previously. The flow velocity of the liquid film and the thickness of the film were measured using a novel Conductance Flow Meter (CFM). The CFM measured the liquid film thickness using novel wall conductance probes. By cross correlating the signals from a pair of such probes the film velocity was obtained. Good agreement of the experimental results obtained from the CFM and USFM with results published in the literature was found.

Although not investigated experimentally in the work described in this thesis, annular flows encountered in the oil industry may contain a liquid phase comprising a mixture of oil and water. For such flows, the volume fractions of the oil and water can be measured using an automated bypass system developed during this project. The bypass system periodically extracts part of the liquid film, measures its density and then releases the sample back into the pipeline. The liquid phase volume fractions are determined from this density measurement which can be performed more than once per minute.

An entrainment model was developed, which is required by the ultrasonic/conductance flow metering technique described in this thesis, in which the mass fraction of the liquid flowing as entrained droplets in the core can be determined from the liquid film thickness and velocity measurements. A mathematical model was also developed to describe the properties of the liquid film, such as liquid velocity profile within the film, and the model's results were found to agree with the experimental results obtained during the project and also with previous work cited in the literature. The complexity of this latter model was reduced by making a number of simplifying assumptions, which are presented and discussed in the thesis, including the assumption that in annular flow there is a dynamic balance liquid entrainment and droplets being deposited back onto the film.

The combination of the designed CFM and USFM with the bypass tube and the entrainment model offer the opportunity for a 'wet gas' flow meter to be developed to measure two and three phase annular flows at relatively low cost and with enhanced accuracy. Such a device would have the advantage that it would be substantially smaller than systems using separators and it could even be retrofitted onto off-shore platforms. The integration of the subsystems developed in this project into a single system capable of giving on-line measurements of annular flow would be a major benefit to the author's sponsor, **Petroleum Development of Oman**.

**LIST OF CONTENTS**

DECLARATION .....	3
DEDICATION .....	4
ABSTRACT .....	5
LIST OF CONTENTS .....	6
LIST OF FIGURES .....	9
LIST OF TABLES .....	14
LIST OF NOMENECLATURE .....	15
ACKNOWLEDGMENTS .....	20
CHAPTER 1 INTRODUCTION .....	21
1.1 Flow measurement .....	21
1.2 Motivation.....	22
1.2.1 Multiphase flow metering in the petroleum industry.....	22
1.2.2 Annular flow .....	25
1.2.3 Wet gas metering .....	27
1.2.4 Annular flow analysis .....	29
1.3 Aims and objectives.....	32
1.4 Thesis outline .....	33
CHAPTER 2 LITERATURE SURVEY .....	36
2.1 Multiphase flows.....	36
2.1.1 Flow regimes in multiphase gas-liquid flow.....	36
2.1.2 Vertical Gas-liquid flow patterns.....	37
2.2 Multiphase flow applications.....	38
2.2.1 Flow rate measurements in multiphase flow .....	39
2.2.2 Separation metering systems for multiphase flow .....	46
2.2.3 Review of dedicated multiphase metering systems .....	50
2.3 Annular flow .....	57
2.3.1 Film thickness .....	59
2.3.2 Measurement techniques for film thickness .....	62
2.3.3 Cross-correlation technique .....	68
2.3.4 Entrainment.....	70
2.4 Gas velocity measurements in annular flow .....	81
2.4.1 Wet gas metering systems in industry .....	85
2.4.2 Ultrasonic flow meters.....	86
CHAPTER 3 PRELIMINARY WORK AND THEORETICAL ANALYSIS .....	92
3.1 Conditions for establishing annular flow .....	92
3.1.1 Flow rates and superficial velocities.....	92
3.1.2 Pressure drops .....	95
3.2 Investigation of conductance flow meter.....	97
3.2.1 Spacing between the conductance probes when using only water ....	100

---

## LIST OF CONTENTS

---

3.2.2	Effect of oil phase in the liquid on film measurements (water-oil mixture) 103		
3.3	Preliminary Investigation of ultrasonic technique .....	105	
3.3.1	Signal cross-talk between transducers .....	106	
3.3.2	Recesses or “dead zones” effect .....	116	
3.3.3	Beam reflection .....	117	
3.3.4	Calculation methods.....	119	
<b>CHAPTER 4 DESIGN AND CALIBRATION OF SENSOR TUBE, CFM AND USFM.....</b>			<b>127</b>
4.1	Film extraction by sensor tube .....	127	
4.1.1	Principle of operation of sensor tube .....	127	
4.1.2	Liquid film extraction procedure .....	130	
4.2	Conductance flow meter .....	131	
4.2.1	Principle of operation of CFM.....	131	
4.2.2	Electronic circuitry.....	132	
4.2.3	Design and calibration of CFM.....	136	
4.2.4	Signal optimization of the CFM device .....	142	
4.2.5	Cross-correlating the CFM probe signals .....	144	
4.2.6	CFM operation with both gas and liquid variations.....	147	
4.3	Ultrasonic Flow Meter .....	148	
4.3.1	Principle of operation.....	148	
4.3.2	Electronic control unit.....	149	
4.3.3	Design and testing of USFM with air only .....	152	
4.3.4	Liquid film effect on the performance of the USFM.....	157	
4.3.5	Temperature effect on USFM readings.....	161	
4.3.6	USFM operation with both gas and liquid flows .....	162	
<b>CHAPTER 5 FLOW LOOP AND EXPERIMENTAL PROCEDURES ...</b>			<b>165</b>
5.1	Flow loop Facility .....	165	
5.1.1	Air supply and monitoring .....	169	
5.1.2	Water supply and monitoring.....	173	
5.1.3	The test section .....	176	
5.2	Integrating the test section components .....	178	
5.3	Data acquisition & Control system .....	179	
5.3.1	LABJACK U12.....	179	
5.3.2	System interface.....	180	
5.3.3	Sampling frequency: .....	181	
5.3.4	.m files (MATLAB programming codes) .....	181	
5.4	Experimental runs .....	181	
5.4.1	Parameters and flow conditions .....	181	
5.4.2	Data collection process .....	183	

---

## LIST OF CONTENTS

---

CHAPTER 6 RESULTS AND DISCUSSION.....	185
6.1 Liquid film .....	185
6.1.1 Film thickness .....	185
6.1.2 Film velocity .....	192
6.1.3 Film velocity profile .....	200
6.2 Entrainment.....	209
6.2.1 Comparison of measured entrainment fraction with recent studies...	212
6.2.2 Development of an entrainment fraction correlation .....	215
6.3 Prediction of the liquid film thickness from film velocity and entrainment data .....	217
6.4 Volume fraction .....	218
6.4.1 Volume fraction of water film ( $\alpha_{w,f}$ ).....	219
6.4.2 Volume fraction of entrained water droplets ( $\alpha_{w,c}$ ) .....	222
6.4.3 Total water volume fraction ( $\alpha_{w,tot}$ ) .....	225
6.4.4 Gas volume fraction ( $\alpha_{g,c}$ ).....	227
6.5 Gas core velocity.....	229
6.5.1 USFM accuracy in measuring gas core velocity.....	229
6.5.2 Measuring core gas velocity using USFM.....	232
6.6 Comparison of reference and measured flow rates .....	236
6.6.1 Water flow rate ( $Q_w$ ).....	236
6.6.2 Gas flow rate ( $Q_g$ ).....	238
CHAPTER 7 WET GAS FLOW METER PROPOSAL .....	241
7.1 Proposed Flow meter hardware .....	241
7.2 Proposed flow meter electronics .....	243
7.3 Proposed flow meter analysis .....	244
7.3.1 Three phase annular flow [oil, water, gas].....	244
7.3.2 Two-phase annular flow [conducting liquid and gas].....	248
7.4 Proposed flow meter discussion and summary .....	250
CHAPTER 8 CONCLUSIONS .....	252
8.1 Conclusions.....	252
8.2 Present contribution .....	256
CHAPTER 9 FURTHER WORK.....	258
9.1 Alternative method for measuring volume fraction in multiphase annular flows: 258	
9.2 Integrate the flow metering devices developed in this thesis into a multiphase flow rig: .....	265
9.3 Investigate the robustness of the system:.....	266
9.4 Commercial development of an online flow meter: .....	266
REFERENCES .....	267

**LIST OF FIGURES**

*Figure 1.1 Damage caused by the breakdown of Chernobyl nuclear reactor.....26*

*Figure 2.1 Flow regimes in vertical gas-liquid flows (Martyn, 1999) .....38*

*Figure 2.2 Venturi tube (Thomas and Paul, 2008).....41*

*Figure 2.3 Turbine flow meter (Zheng et al, 2008) .....42*

*Figure 2.4 Modern industrial Coriolis meter (efunda, [online] accessed 10/01/2009)  
.....43*

*Figure 2.5 Electromagnetic flow meter (Al-Yarubi, 2006).....45*

*Figure 2.6 Simplified oil well separator (Al-Yarubi, 2006).....47*

*Figure 2.7 Typical three phase separator (for gas wells) (Al-Yarubi, 2006) .....47*

*Figure 2.8 A typical process gas plant separation system (PDO, 2008).....49*

*Figure 2.9 Chambers in positive displacement meter (Yeung, 2003).....52*

*Figure 2.10 Framo multiphase flow meter (Olsen and Hanssen, 1994) .....53*

*Figure 2.11 Fluenta multiphase flow meter (AMS, [online] accessed 05/08/2009)....54*

*Figure 2.12 Kongsberg type multiphase flow meter (Halto and Sorensen, 1999) .....57*

*Figure 2.13 Typical two-phase annular flow regime.....58*

*Figure 2.14 Weighing Method, (Aragaki, et al, 1987).....63*

*Figure 2.15 Absorption of Electromagnetic Radiation, (Jackson, 1955) .....64*

*Figure 2.16 Interfacial Reflection Techniques (Hurlburt and Newell, 1996) .....66*

*Figure 2.17 A representation of the cross-correlation function Ferrari et al, 2005)..69*

*Figure 2.18 Bag break-up mechanism (wave) (Azzopardi, 1997) .....72*

*Figure 2.19 Ligament break-up mechanism (wave) (Azzopardi, 1997) .....73*

*Figure 2.20 Bag break-up and ligament break-up mechanisms (of large drops in the  
core) (Azzopardi, 1997) .....73*

*Figure 2.21 Schematic representation of film disturbance causing entrainment  
(Azzopardi, 1997).....74*

*Figure 2.22 Sampling technique by an isokinetic probe, (Tayebi, et al, 2000) .....79*

*Figure 2.23 Liquid film removal method .....80*

*Figure 2.24 Pitot-static principle (Richard, 2001).....81*

*Figure 2.25 Laser-Doppler technique (Lioumbas, 2005).....83*

*Figure 2.26 A typical V-Cone flow meter design (Svedeman, 1997).....86*

*Figure 2.27 Massa transducer, model E-152/40 .....89*

*Figure 2.28 USFM common configuration.....89*

*Figure 3.1 Flow patterns based after Govier and Aziz (1972).....93*

*Figure 3.2 Electrode dimensions .....98*

*Figure 3.3 Meniscus effect on overestimating the film thickness .....100*

*Figure 3.4 Results for 20 mm spacing between electrodes (water only) .....101*

*Figure 3.5 Mean error between estimated water level and the measured values (water  
only) .....102*

*Figure 3.6 Results for 20 mm spacing distance between the electrodes (oil-water  
( $\alpha_o=0.07$ )) .....104*

*Figure 3.7 Mean error between estimated water level and the reference value (oil-  
water ( $\alpha_o=0.07$ )) .....104*

---

## LIST OF FIGURES

---

<i>Figure 3.8 Different acoustic paths in Ultrasonic Flow Meters, Dell’Isola et al. (1997)</i> .....	106
<i>Figure 3.9 Critical separation between receivers (50mm pipe)</i> .....	108
<i>Figure 3.10 Transducers placed in plastic wedges</i> .....	108
<i>Figure 3.11 Configuration A</i> .....	110
<i>Figure 3.12 Results for configuration A – Yellow signal is received signal at Rx1 and blue signal is cross-talk signal received at Rx2</i> .....	111
<i>Figure 3.13 Configuration B</i> .....	112
<i>Figure 3.14 Results for configuration B – Yellow signal is received signal at Rx1 and blue signal is cross-talk signal received at Rx2</i> .....	112
<i>Figure 3.15 Configuration C</i> .....	113
<i>Figure 3.16 Results for configuration C – Yellow signal is received signal at Rx1 and blue signal is cross-talk signal received at Rx2</i> .....	114
<i>Figure 3.17 Configuration D</i> .....	115
<i>Figure 3.18 Results for configuration D - Yellow signal is received signal at Rx1 and blue signal is cross-talk signal received at Rx2</i> .....	115
<i>Figure 3.19 Dead zones or recesses</i> .....	117
<i>Figure 3.20 Beam reflection analysis (50mm pipe)</i> .....	118
<i>Figure 3.21 Ultrasonic wave directions</i> .....	122
<i>Figure 3.22 Relation between change in phase and the velocity</i> .....	124
<i>Figure 3.23 Theoretical output of the USFM electronic circuit</i> .....	125
<i>Figure 4.1 Sensor tube, to the left and outside the red line</i> .....	128
<i>Figure 4.2 Liquid film extraction and DP measurement set up</i> .....	129
<i>Figure 4.3 First stage of the electronic circuit showing the principle of the initial conductivity measurement</i> .....	132
<i>Figure 4.4 Conductance monitoring circuit</i> .....	135
<i>Figure 4.5 Conductance flow meter installed in the flow loop</i> .....	136
<i>Figure 4.6 Sketch of a side view of the CFM (not to scale)</i> .....	137
<i>Figure 4.7 Top view showing the boss connection (not to scale)</i> .....	138
<i>Figure 4.8 CFM calibration process using non-conducting plugs</i> .....	139
<i>Figure 4.9 Output responses of both sensors; simultaneously</i> .....	140
<i>Figure 4.10 Calibration curve for probe separation 20mm</i> .....	141
<i>Figure 4.11 Percentage error in liquid film thickness measurement</i> .....	142
<i>Figure 4.12 CFM output voltage at 50Hz sampling frequency</i> .....	143
<i>Figure 4.13 CFM film thickness reading at 1 kHz sampling frequency (Upstream sensor blue, downstream sensor green)</i> .....	144
<i>Figure 4.14 Correlogram of the two signals, 50Hz sampling rate</i> .....	145
<i>Figure 4.15 Correlogram of the two signals after ensemble averaging, 1kHz sampling rate</i> .....	146
<i>Figure 4.16 Mean water film thickness as a function of increasing water flow rate measured using the CFM</i> .....	147
<i>Figure 4.17 Mean water film thickness as a function of increasing gas flow rate measured using the CFM.</i> .....	148
<i>Figure 4.18 Ultrasonic electronic circuit</i> .....	151
<i>Figure 4.19 Ultrasonic flow meter installed in the flow loop</i> .....	152
<i>Figure 4.20 Sketch of a side view of the USFM (not to scale)</i> .....	153
<i>Figure 4.21 Characteristic curve for the designed USFM (air only)</i> .....	154
<i>Figure 4.22 <math>V_{out}</math> expressed in term of the gas superficial velocity (air only)</i> .....	155

---

## LIST OF FIGURES

---

Figure 4.23 Calibration equation (4.20) against measured data (air only).....	157
Figure 4.24 Transducers configurations. ....	158
Figure 4.25 $V_{out}$ expressed in term of the reference core gas velocity (air and water) .....	159
Figure 4.26 The calibration curve fitting with the measured data (air and water)..	160
Figure 4.27 Modified version of Equation 4.27 against the measured data (air and water).....	161
Figure 4.28 Temperature effect on the USFM at different gas flow rates (air and water).....	162
Figure 4.29 Response of the USFM to the increase in the gas volume flow rate ....	163
Figure 4.30 Response of USFM to the increase in the water volume flow rate .....	164
Figure 5.1 Diagram of designed flow loop.....	168
Figure 5.2 ABLE (50PTnAAI75) VAFM.....	170
Figure 5.3 I/V converter circuit.....	170
Figure 5.4 Output voltage $V_{out}$ from the ABLE VAFM flow meter against gas volume flow rate.....	171
Figure 5.5 VAFM flow meter and support frame. ....	172
Figure 5.6 FAIRCHILD Flow Pressure Regulator.....	173
Figure 5.7 ABLE (AT13T) turbine flow meter.....	174
Figure 5.8 Calibration of ABLE (AT13T) turbine flow meter using the gravimetric system.....	175
Figure 5.9 Honeywell ST-3000 DP sensor.....	177
Figure 5.10 Burkert 6013 solenoid valve.....	177
Figure 5.11 Relay on/off switching circuit.....	178
Figure 5.12 LABJACK U12.....	179
Figure 5.13 System interface and wiring diagram.....	180
Figure 5.14 Flow chart of data collection process.....	184
Figure 6.1 Film thickness signal for $Q_{g,ref} = 100m^3/hr$ , $Q_{w,ref} = 0.333m^3/hr$ .....	187
Figure 6.2 Film thickness signal for $Q_{g,ref} = 175m^3/hr$ , $Q_{w,ref} = 0.333m^3/hr$ .....	187
Figure 6.3 Film thickness signal for $Q_{g,ref} = 100m^3/hr$ , $Q_{w,ref} = 1.84m^3/hr$ .....	188
Figure 6.4 Film thickness signal for $Q_{g,ref} = 175m^3/hr$ , $Q_{w,ref} = 1.84m^3/hr$ .....	188
Figure 6.5 Effect of water superficial velocity on liquid film thickness at different constant gas superficial velocities.....	190
Figure 6.6 Effect of gas superficial velocity on liquid film thickness at constant water superficial velocity.....	190
Figure 6.7 Percentage error in measured liquid film velocity at different constant gas superficial velocities.....	193
Figure 6.8 Effect of water superficial velocity on liquid film velocity at constant gas superficial velocity.....	196
Figure 6.9 Effect of gas superficial velocity on liquid film velocity at constant water superficial velocity.....	197
Figure 6.10 Comparison of film mass flow rate when varying the gas mass flow rate with results of Zabaras and Dukler (1986).....	199
Figure 6.11 Illustration of force balance on the control volume of liquid film for upward annular flow.....	203

---

## LIST OF FIGURES

---

<i>Figure 6.12 Illustration of force balance on the control volume of gas core of upward annular flow</i> .....	205
<i>Figure 6.13 Film velocity profile for <math>Q_{g,ref}</math> high, <math>Q_{w,ref}</math> high</i> .....	206
<i>Figure 6.14 Film velocity profile for <math>Q_{g,ref}</math> low, <math>Q_{w,ref}</math> low</i> .....	207
<i>Figure 6.15 Film velocity profile for <math>Q_{g,ref}</math> low, <math>Q_{w,ref}</math> high</i> .....	207
<i>Figure 6.16 Film velocity profile for <math>Q_{g,ref}</math> high, <math>Q_{w,ref}</math> low</i> .....	208
<i>Figure 6.17 A comparison of liquid film radial velocity distribution profiles at different flow conditions</i> .....	209
<i>Figure 6.18 Effect of water superficial velocity on entrainment fraction at constant gas superficial velocity</i> .....	211
<i>Figure 6.19 Effect of gas superficial velocity on entrainment fraction at constant water superficial velocity</i> .....	212
<i>Figure 6.20 Entrainment fraction vs. gas superficial velocity at different water Reynolds numbers from Sawant et al., (2008).</i> .....	213
<i>Figure 6.21 Comparison of entrainment rate when varying the gas flow rate with Zabaras and Dukler. (1986)</i> .....	214
<i>Figure 6.22 Estimated entrainment fraction as a function of the gas superficial velocity (pipe ID = 50mm)</i> .....	216
<i>Figure 6.23 Comparison of measured and predicted liquid film thickness</i> .....	218
<i>Figure 6.24 Schematic of flow phases distribution in annular flow</i> .....	219
<i>Figure 6.25 Effect of gas superficial velocity on volume fraction of water film at different water superficial velocities</i> .....	221
<i>Figure 6.26 Effect of water superficial velocity on volume fraction of water film at different gas superficial velocities</i> .....	221
<i>Figure 6.27 Effect of water superficial velocity on volume fraction of entrained water droplets at different gas superficial velocities</i> .....	224
<i>Figure 6.28 Effect of gas superficial velocity on volume fraction of entrained water droplets at different water superficial velocities</i> .....	225
<i>Figure 6.29 Effect of gas superficial velocity on overall water volume fraction at different water superficial velocities</i> .....	226
<i>Figure 6.30 Effect of water superficial velocity on overall water volume fraction at different gas superficial velocities</i> .....	226
<i>Figure 6.31 Effect of water superficial velocity on gas volume fraction at constant gas superficial velocity</i> .....	228
<i>Figure 6.32 Effect of gas superficial velocity on gas volume fraction at constant water superficial velocity</i> .....	228
<i>Figure 6.33 Percentage error in measured gas core velocity at different constant water superficial velocities</i> .....	231
<i>Figure 6.34 Percentage error in measured gas core velocity at different water superficial velocities</i> .....	231
<i>Figure 6.35 Effect of gas superficial velocity on gas core velocity at different water superficial velocities</i> .....	233
<i>Figure 6.36 Effect of water superficial velocity on gas core velocity at different gas superficial velocities</i> .....	234
<i>Figure 6.37 of water flow rate on core gas velocity and film thickness at different gas flow rates</i> .....	235
<i>Figure 6.38 Effect of gas flow rate on core gas velocity and film thickness at different water flow rates</i> .....	236

---

## LIST OF FIGURES

---

<i>Figure 6.39 Percentage error in the measured water flow rate at different constant gas flow rates.</i>	238
<i>Figure 6.40 Percentage error in the measured gas flow rate at different constant water flow rates.</i>	239
<i>Figure 7.1 Hardware components of the proposed flow meter</i>	242
<i>Figure 7.2 Measurement sources for the proposed flow meter</i>	251
<i>Figure 9.1 Principle of operation of Flush Mounted Sensor</i>	259
<i>Figure 9.2 Flush Mounted Sensor configurations (not to scale)</i>	260
<i>Figure 9.3 Flush Mounted Sensor calibration curve (Config.1)</i>	261
<i>Figure 9.4 Voltage output of Flush Mounted Sensor for different liquid conductivities (Config.1, bench test)</i>	261
<i>Figure 9.5 Voltage output of Flush Mounted Sensor for different probe separations (Config.II, COMSOL prediction)</i>	262
<i>Figure 9.6 Voltage output of Flush Mounted Sensor for different liquid conductivities (Config.2, COMSOL)</i>	263
<i>Figure 9.7 Voltage output of Flush Mounted Sensor for different liquid conductivities (Config.2, bench test)</i>	264
<i>Figure 9.8 Voltage output of CFM device for different liquid conductivities (bench test)</i>	264

**LIST OF TABLES**

*Table 3.1 Phase shift calculation*..... 123

*Table 5.1 Water volumetric flow rates and superficial velocities* ..... 182

*Table 5.2 Air volumetric flow rates and superficial velocities* ..... 182

*Table 5.3 Constant operating conditions*..... 182

*Table 6.1 Film thickness and film velocity for four different combinations of flow conditions*..... 186

*Table 6.2 Gas flow rates used throughout the investigation* ..... 186

*Table 6.3 Gas and water flow rates used throughout the investigation* ..... 189

*Table 6.4 Corresponding liquid film Reynolds numbers and water superficial velocities* ..... 198

*Table 6.5 Summary of some experiments on entrainment fraction*..... 215

## LIST OF NOMENECLATURE

### Acronyms

CFD	Computational Fluid Dynamics
CFM	Conductance Flow Meter
CO <sub>2</sub>	Carbon dioxide
Cos	Cosine
DP	Differential Pressure
FMS	Flush Mounted Sensor
GVF	Gas Volume Fraction
I-V	Current-Voltage
LCV	Level Control Valve
PCV	Pressure Control Valve
PDO	Petroleum Development Oman
PVC	Polyvinyl Chloride
PVT	Pressure, Volume and Temperature
Sin	Sine
USFM	Ultrasonic Flow Meter
VAFM	Variable Area Flow Meter
VR	Variable Resistor

### Symbols

$A$	Cross-sectional area
$A_{c,\delta}$	Cross-sectional area of the core
$A_f$	Cross-sectional area of the film
$A_{w,c}$	Cross-sectional area of water in the core

---

## LIST OF NOMENECLATURE

---

$\hat{c}$	Constant given by $\frac{4\pi f d}{c^2} \cos \theta$
$c$	Speed of sound
$D$	Pipe inner diameter
$d$	Length of the acoustic path in USFM
$dP/dZ$	Pressure gradient
$E$	Entrainment fraction
$f$	Frequency
$f_{factor}$	Friction factor
$G$	Mass flux
$\bar{G}$	Gradient
$g$	Gravity
$h_{wall}$	Pipe wall thickness
$h$	Height
$i_o$	Incident intensity
$i$	Emergent intensity
$K$	Constant
$L/D$	Length-diameter ration
$l_{sp}$	Distance between the transducers pair in the USFM
$l_p$	Separation distance between the electrodes in the CFM sensors
$l_n$	Recess depth
$m^+$	Non-dimensional film thickness
$Q_d$	Droplet flow rate
$Q_f$	Film volumetric flow rate
$Q_{f,crit}$	Critical film flow rate
$Q_{f,feed}$	Liquid feed flow rate per unit perimeter
$Q_g$	Gas volumetric flow rate
$Q_{g,ref}$	Reference gas volumetric flow rate
$Q_{o,f}$	Oil flow rate in the liquid film
$Q_{o,d}$	Oil volumetric flow rate in the droplets
$Q_w$	Water flow rate
$Q_{w,c}$	Water volumetric flow rate in the core

---

## LIST OF NOMENECLATURE

---

$Q_{w,d}$	Water volumetric flow rate in the droplets
$Q_{w,f}$	Water flow rate in the liquid film
$Q_{w,ref}$	Reference water volumetric flow rate
$R$	Pipe radius
$R_{fb}$	Feedback resistance
$R_m$	Resistance of the electrodes
$R_o$	Contribution due to wall thickness
$R_{ref}$	Distance between the point source and the white coating
$R_{xy}(\tau)$	Cross-correlation function
$Re_w$	Reynolds number
$Rx$	Receiver transducer in USFM
$S$	Conductance
$S_m$	Mixture conductance
$T$	Total time period in cross-correlation
$Tx$	Transmitter transducer in USFM
$t$	Time
$\bar{U}$	Average velocity
$U$	Flow velocity
$U_f$	Liquid film velocity
$U_{f,ref}$	Reference film velocity from turbine flow meter
$U_{g,c}$	Gas core velocity
$U_{g,c,ref}$	Reference gas core velocity
$U_{g,s}$	Gas superficial velocity
$U_{w,c}$	Water velocity in the core
$U_{w,s}$	Water superficial velocity
$V$	Voltage
$v$	Velocity of the moving medium in USFM theory
$\mathcal{G}^*$	Liquid friction velocity
$v_d$	Velocity of ultrasonic along the downstream path
$v_u$	Velocity of ultrasonic along the upstream path
$W_d$	Droplet mass flow rate
$W_f$	Film mass flow rate
$We$	Weber number
$w, h$	Width and height of electrodes in CFM theory

---

## LIST OF NOMENECLATURE

---

$x, y$	Reference to sensors in CFM device
$Z$	Axial coordinate
$z$	Pipe wall thickness

### **Greek symbols**

$\alpha$	Volume fraction
$\beta$	Surface tension
$\delta$	Liquid film thickness
$\varepsilon$	Resistivity
$\eta$	Viscosity
$\theta$	Angle
$\lambda$	Wavelength
$\mu$	Water viscosity
$\nu$	Water kinematic viscosity
$\xi$	Percentage error
$\rho$	Density
$\varphi$	Linear absorption coefficient
$\sigma$	Conductivity
$\hat{\tau}$	Shear stress
$\tau$	Transit time in cross-correlation
$\phi$	Phase angle
$\omega$	Angular frequency

---

## LIST OF NOMENECLATURE

---

### Subscripts

<i>a</i>	Atmospheric air
<i>c</i>	Gas core
<i>crit</i>	Critical
<i>d</i>	Droplet
<i>d</i>	Downstream (USFM)
<i>e</i>	Entrainment
<i>est</i>	Estimated value
<i>f</i>	Liquid film
<i>fric</i>	Frictional
<i>g</i>	Gas
<i>i</i>	Interfacial
<i>in</i>	Input/Inlet
<i>l</i>	Liquid
<i>m</i>	Mixture
<i>o</i>	Oil
<i>out</i>	Output/Outlet
<i>p</i>	Peak value
<i>ref</i>	Reference value
<i>t</i>	Transient
<i>tot</i>	Total value
<i>u</i>	Upstream
<i>w</i>	Water
<i>xcor</i>	Cross-correlation

## **ACKNOWLEDGMENTS**

First and foremost, all thanks and praises are due to God the Almighty for his blessing that made this work possible and to be completed on time.

Secondly, I would like to express my sincere thanks (with an honorary bow) to Professor Gary Lucas, my academic supervisor, for his guidance and support. His very active part in initiating this work, and his valuable suggestions during all its phases were indispensable. Special thanks for his help in reviewing and his constructive comments and continuous support during the preparation of this thesis. He was also a source of inspiration throughout my study in the University of Huddersfield in my academic and social life. The completion of this work owes much to his valuable and endless assistance. To all his present and future students - you are very fortunate.

I would like to thank the technicians at the University of Huddersfield for their help in manufacturing, and repairing, the varied equipment that I have needed. I would particularly like to thank Mr. Peter Norman for putting up with my endless requests during the construction and modification of the flow loop.

I would like to acknowledge my fellow research students for their many and interesting conversations, in particular: Ahmad Al-Shihri, Abdulrazaq, Sulaiyam, Abbas, Hussam, Yousif, and Teerachai. A special word of gratitude is due to Dr. Zhao Xin for his helpful suggestions and encouragement which were responsible in a large measure for completing this work.

I also thank my Paddock's friends especially Abid and Sajid's families. With you guys, I always felt part of your community which alleviated my homesickness. Thank you very much for giving me that feeling and the support you provided for my family from the day I have arrived to Huddersfield.

I wish to thank Petroleum Development Oman (PDO) for financially supporting my education in the U.K which made this study possible. My deepest gratitude goes to the following personnel at PDO: Suleiman Al Tobi, Dr. Khamis Al Busaidi, Salim Al Sibani and Dr. Nasser Al-Hatmi for their support, help and advice.

Many thanks to my family in Oman especially my parents for their support and substantial encouragements from the time I was in my primary school till now. By no means least, my special thanks to my wife: Najmaa and my children: Taymaa, Yarub and Bel'arab, for their support, encouragement and patience over the last years. I promise you to make amends for the past years with much fun in the coming years.

*The time I spent in the United Kingdom; the 4 years at University of Huddersfield (MSc & PhD 2005-2009), the 3 years at Teesside University (BEng 2002-2005) and 2 years at Grimsby College (A Levels 2000-2002), will always be in my memory.*

## CHAPTER 1 INTRODUCTION

### 1.1 Flow measurement

In the oil and gas industry, a broad knowledge of the fluids (liquids, gases, steam, etc.) being handled is essential. It is necessary to know if each of these fluids has well defined pressure, volume, temperature and density (P,V,T, $\rho$ ) relationships, has a predictable flow pattern based on Reynolds number and contains no foreign material (e.g. solids carried in a gas or liquid flow) that will adversely affect flow meter performance.

In the field it is important to know if a fluid: (a) is flowing at a sufficiently constant rate such that the rate of change of flow is not more rapid than the meter system response time and, in particular, is non-pulsating; (b) has a non-swirling flow pattern entering the meter; (c) fills the circular pipe which is carrying it; (d) has had any trapped air (in liquid) or liquid (in gas) removed prior to the meter. Individual meters may have special features that can cope with some of these problems, but each meter must be carefully evaluated to ensure its suitability for the given fluid conditions. An important factor in choosing a meter is that experience has shown it is acceptable for a specific application. Reference to previous users within the industry, or industry standards, are important points to consider when choosing the best meter for a given application (Upp and LaNasa, 2002).

Accurate measurements of fluid flow rates can be achieved only if flow conditions are suitable. On the other hand, the cost of preparing the fluid and/or the flow may sometimes outweigh the value of the flow measurement, and a lower accuracy should be accepted. Consider a metering station measuring the flow of a product worth \$1 million a day, here an inaccuracy of only  $\pm 0.2\%$  represents nearly \$750,000 a year. For a station measuring a flow worth \$1,000 a day the same inaccuracy represents less than \$1,000 a year. The law of diminishing returns means that in the latter case there is little motivation to invest to improve measurement accuracy (Upp and LaNasa, 2002).

Each type of flow measurement requires specific consideration, including a balance between the accuracy requirements, the cost of the measurement, and the usefulness of the flow information obtained. This poses the general question of what type of flow meter is best? Any answer must begin by considering the flow characteristics and the fundamental nature of the fluid to be measured. Care needs to be exercised in evaluating any measurement device because, for example, the gases and liquids routinely handled in the field are not clean, and this can lead to debris in the meter or build up of heavy oil on moving parts which means the measurements made could have been seriously flawed.

## 1.2 Motivation

### 1.2.1 Multiphase flow metering in the petroleum industry

The need for increased cost, quality and safety control in many different branches of industry, including chemical processing plants, power stations (especially nuclear), and the petroleum industry, has meant the metering of multiphase flow has substantially increased in importance over the last few decades. In particular, gas-liquid flow is encountered in a wide range of applications in different branches of industry, including heat transfer equipment such as steam generators, refrigeration equipment, evaporators and condensers.

Commercial and safety considerations make the accurate measurement of multiphase fluid flow rates in the petroleum industry of great importance. Recent off-shore and on-shore discoveries, and the consequent requirement of transporting the fluids produced to central processing areas, has resulted in longer flow lines in which more than one phase is flowing. The difficulties experienced in handling gas-liquid flow in pipelines have emphasized the need for additional research efforts to provide more accurate and reliable methods for the effective prediction and operation of gas-liquid flow systems.

Accurate multiphase measurement is essential for the successful management of a reservoir, because optimisation of the primary, secondary and tertiary oil recovery

processes requires knowledge of the distribution of production over individual wells. Control of production from individual wells requires metering of the production rate of individual fluids both to optimise production performance under changing conditions, and to determine whether or not any remedial work is required. In addition, individual flow rate measurement will be required by government agencies for fiscal purposes.

The current practice for calculating the cumulative production of the different fluids produced by oil and gas wells involves well-testing to determine the flow rate of the various phases at a nominal choke opening, and continuous monitoring of an approximate production performance of each well. This is relatively complicated and requires manual intervention. The most reliable measurement technique for multiphase flow is to first separate the mixture and then use single-phase conventional devices for measuring the flow. Thus well-testing carried out by means of a test separator requires that the various phases are first separated and then metered in single phase flow lines. Unfortunately, high flows result in incomplete separation and consequent erroneous metering by single-phase flow measuring devices. To avoid such an occurrence, more complicated and expensive separators have to be installed.

However, in many cases separation is just not practical from either the technical or economic points of view and well-testing is achieved in a less desirable way by observing the loss in production from the main separator when the well is closed. This approach to the measurement of multiphase flows in crude oil production has the two major disadvantages of not being accurate while incurring high costs. The limited results obtained from test wells do not provide sufficient information on which to design a separator able to cope with the wide ranges of flow rates and mixtures expected from wells in different fields, nor the changes with time of relative proportions of the different phases at one field.

In petroleum operations, a separate test line is constructed from every production platform to the central processing platform for the purpose of flow rate measurement from the individual wells. Such a method results not only in an increase in field

development costs but it is inherently inaccurate because the flow measurements will change due to the difference in back pressure experienced by the well during the test and normal production operations.

A desirable alternative solution is on-line multiphase flow metering. Such a system would, typically, consist of a combination of devices for measuring volume fractions and velocities. There is a growing interest in the development of such systems because of their convenience and expected economic benefits. There are already in existence a number of possible measurement methods including; turbine and/or vortex flow meters, Venturi orifice plates and ultrasonic Doppler techniques. Presently there is considerable research being conducted into this field to develop a suitable flow meter which can be used for on-site measurement in the petroleum industry. Many research groups are actively engaged in developing a new and more reliable and precise multiphase flow rate measurement system. An important requirement before such a multiphase flow meter can be used in oil and gas fields is its accuracy for well testing applications. It should provide the reservoir engineer with an accuracy of  $\pm 5\%$  of reading over the required flow range of each phase. To meet the standards of fiscal metering the required accuracy would be  $\pm 0.5\%$  (Alimonti and Bilardo, 2002)

In addition to the accuracy requirements, there are a number of constraints on the design of any proposed multiphase flow meter: it should not occupy a footprint of more than 0.5m x 1.0m and should be less than 2.0m high; the straight lengths of inlet and outlet pipes upstream and downstream of the flow meter should be the minimum possible; the sampling frequency of the meter should be not less than 10Hz (to get a meaningful response of the different flow regimes); the working pressure should be up to 350bar and the pressure drop should not exceed 1bar and, finally, the multiphase flow meter should be easily removed for servicing (Atkinson et al., 2004-2005).

### 1.2.2 Annular flow

In general, flow in pipelines can be grouped into classes commonly called flow regimes or flow patterns. A wide variety of classifications exist in the literature which are mainly due to the subjective nature of the characterisation method. A flow regime that has received much attention, both analytically and experimentally, is annular flow because of its great practical importance and the relative ease with which analytical treatment can be applied. Annular flow is one of the most common flow regimes encountered in pipelines serving natural gas well-bores. It occurs at high gas flow rates accompanied by low to medium liquid flow rates. In annular flows, most of the liquid gathers and travels on the pipe wall as a wavy film while the gas travels in the centre of the pipe. However, a part of the liquid travels as drops in the centre of the pipe with the gas (Geraci, 2007). Vertical annular flow is similar to horizontal annular flow, provided allowance is made for gravity having a greater effect on more dense liquids, slowing them relative to less dense liquids or gases.

In certain older oil wells in the Middle East, the fluid flow is predominantly natural gas which flows at very high rates (e.g. 50,000m<sup>3</sup>/day). Smaller quantities of crude oil (e.g. 50m<sup>3</sup>/day) and water (e.g. 950m<sup>3</sup>/day) are also produced. Given the relatively much higher flow rate of the gas the flow regime is annular with most of the liquid flowing in a thin film on the pipe wall.

The Author's sponsor, Petroleum Development Oman (PDO), is an oil company in the Arabian Gulf which is located in the Sultanate of Oman. The company has met a problem measuring the liquid flow rate in very high gas rate annular flows. This study is aimed at developing a possible measurement technique to overcome this issue by using a combination of experimental and analytical investigations. For even a small quantity of crude oil produced per day, say 50m<sup>3</sup>/day (an oil barrel is 159 litres, to an accuracy of better than 0.01%) then at a price of \$80 dollars a barrel, the oil well will produce oil with a value of about \$9 million in a year. It is obvious that it is economically important to be able to measure the oil flow rate on-line.

Certain annular flow applications in which excessive liquid entrainment occurs, can lead to “dry out”, in which the liquid film is completely removed from contact with the channel’s walls. In certain non-oil field applications, e.g. in the nuclear power industry, from a safety point of view this can be disastrous, leading to such catastrophic events as the breakdown of the Chernobyl nuclear reactor.

Figure 1.1 shows the extensive damage to the main reactor hall caused by the breakdown of the reactor. It is thus very important to be able to predict and/or measure the onset of “dry out” to avoid its actual occurrence.



*Figure 1.1 Damage caused by the breakdown of Chernobyl nuclear reactor*

This accident happened during an experiment that was proposed to test a safety emergency core cooling feature (of a particular reactor) during the shutdown

procedure by testing the backup power supply in case of a power loss. A very large amount of cooling water is needed to maintain a safe temperature in the reactor core. The reactor consisted of about 1,600 individual fuel channels and each operational channel required a flow of 28 tons of water per hour. The experiment involved shutting down the coolant pumps, which caused the coolant to rapidly heat up and boil. The power fell too low, allowing the concentration of xenon-135 to rise and pockets of steam formed in the coolant lines.

In order to control the rising levels of xenon-135, the control rods were pulled out. When the coolant expanded in this particular reactor, the power level went up. All control rods were ordered to be inserted. As the rods were inserted, they became deformed and stuck. The reaction could not be stopped. The rods melted and the steam pressure caused an explosion, which blew a hole in the roof. A graphite fire also resulted from the explosion (Nottingham Trent University, 2009).

A second safety issue is corrosion of e.g. pipe work, especially when carbon dioxide ( $CO_2$ ) is present in the flow either as a product or being injected in enhanced oil recovery techniques. This is an issue that can result in fatalities. With annular flow, the  $CO_2$  concentration in the gas phase affects the corrosion rate because  $CO_2$  when dissolved in water forms carbonic acid. The resulting acidity of the water combined with high flow rates, can cause high levels of corrosion in the pipe. More accurate measurement of the phase flow rates and a deeper understanding of annular flow will help control and predict the corrosion rate, and hence reduce damage to equipment, avoid loss in production and increase the safety of operatives.

### 1.2.3 Wet gas metering

World natural gas consumption grew by 3.3% in 2004, compared with a 10-year average of 2.3%. Gas production rose in every region except North America (BP Review, 2005). International trade in natural gas increased by 9% in 2004 (BP Review, 2005). Pipeline shipments rose by more than 10% (BP Review, 2005). Compared with oil fields, gas fields tend to be more environment-friendly because of lower  $CO_2$  emissions and cleaner combustion.

However, the production of gas is, in most cases, associated with the production of liquid hydrocarbons, free formation water and condensed vapour (that form in the reservoir, in the wellbore and at the surface as pressure and temperature drop). This is why, from a metering point of view, the techniques normally implemented for dry gas metering cannot be always applied.

The term "wet gas" has no agreed definition, but the natural gas production industry accepts that the term denotes a relatively small amount of liquid in a production flow of natural gas, usually in the context of the production of gas from natural reservoirs. Wet gas metering (WGM) is becoming increasingly important to the oil and gas industry and part of this study deals with WGM for the measurement of the gas core velocity in annular flow.

One of the greatest problems in wet natural gas metering is the lack of knowledge of the liquid content in wet natural gas flows. So far, no WGM technique for any meter type comes close the industry's desired standards for the simultaneous metering of the liquid and gas phase flow rates. The most obvious reason for this is that the operators are not willing to allow meter tests on actual production flows because of possible financial penalties that might be incurred due to consequential production delays. Meter manufacturers are forced to test their meters on wet gas laboratory test loops which have the major drawback that nowhere does the test equipment available replicate the real flow conditions found in wet natural gas production lines.

However, such flows are becoming increasingly common because as a "dry" natural gas well ages the line pressure gradually reduces which invariably results in the flow containing a higher proportion of heavier hydrocarbon gases, which are more likely to condense in the pipe. WGM is becoming increasingly important because many gas wells worldwide are now reaching the later stages of their production life. In addition the industry is eager to maximise the return from off-shore platform investment, which means many natural gas producers are developing "marginal" fields which produce two-phase flows of natural gas with sea water and/or natural gas condensate from the outset. These fields have their wet natural gas production flows combined with that from the main wells' dry or wet natural gas production flow upstream of the

separator facilities.

If the flows from wells owned by different companies are mixed before reaching a common separator, accurate measurement of their individual flows is commercially vital. This is an additional reason why improvement in the accuracy of WGM is important to the oil and gas industry. Nederveen (1989) showed that if the need for bulk separators on offshore platforms was removed significant savings could be made. While each bulk separator costs up to \$30 million during its life they are presently an integral part of the platform, so the likely actual savings is unknown. An accurate WGM could also lead to the elimination of on-shore separators at wet gas fields, saving at least \$600,000 each. It is clear, however, that the possible saving could reduce the cost of developing a well sufficiently so that many wells that are presently unviable may become financially viable, thus increasing an important resource available to humanity.

Presently there are two approaches to the metering of wet gas. The first is to separate the two phases and meter each separately. The second consists of metering the overall two phase flow with a dry gas flow meter for which correction factors have been established to take into account the presence of the liquid phase. From an economic point of view, this second method seems to be of growing interest.

Ultrasonic flow meters are already widely used by the oil companies and much work has been carried out on wet gas metering using ultrasonic flow meters (Mus, et al., 2001). Lynnworth and Liu (2006) carried out a review that showed that ultrasonic flow meters offer the most satisfactory results in wet gas metering. This conclusion has led the author to choose the ultrasonic technique for use in this project.

#### 1.2.4 Annular flow analysis

Much research has been undertaken over the past forty years to gain a better understanding of the fundamental physics of annular flows for the purpose of developing a model for the design of new two-phase flow systems. Despite extensive study, accurate and detailed data on the liquid-gas interface and interface dynamics

are still lacking. These interface dynamics are essential to developing reliable laws for flow modelling.

Experimental work is key for multiphase flow research, and provides the most direct and reliable way of understanding the physical mechanisms, because of the complexity of the problems involved. The data obtained from experiments allows models to be developed and tested directly. However, a deeper and fuller understanding of multiphase flow in pipes requires a combined approach: experimental and theoretical (Bilgesu, 1994).

The same fundamental conservation laws of mass, momentum and energy govern the wide variety and combinations of phase and flow regimes occurring in multiphase flows. However, the complexity of the actual conditions means there is still no general model for predicting the behaviour of flows in even the simplest geometries. Taitel et al., (1995) have classified the different approaches and levels to the solution of engineering problems; from rigorous solution of the Navier-Stokes equations, through modelling techniques, to observation and derived empirical correlations.

Historically, empirical correlation has been very useful in engineering, and a large number of such correlations appear in the literature. This approach has had success in predicting such parameters as heat transfer coefficients, usually where an extensive database of measured values exists, and a number of these empiric parameters are still very widely used in the oil and gas industry. However, empirical correlations are generally valid only for the parameter ranges for which they were generated, and they become very uncertain when extrapolated to conditions outside the original database.

Another approach is to use Computational Fluid Dynamics (CFD), an approach which calls for the solution of the continuity, momentum and energy equations for e.g. two-phase flow to determine the gas-liquid interface. However, the leading CFD codes are still not able to calculate the thickness of liquid films in such flows (Morud and Skjetne, 2005), and they struggle to evaluate the interactions between the liquid film and the droplets in the gas core. Such a situation is only to be expected when the physical mechanisms for the deposition of droplets and atomization/re-entrainment of

liquid from the film into the gas are not well understood. For example, when Morud (2005) attempted to develop a model for liquid films at walls he limited his validation to a bench test, and there has been no subsequent independent validation.

Clearly such CFD models are difficult and time-consuming and, in any case, they tend to rely to a greater or lesser extent on empirical "constitutive" relations and each model applies only to the range of specified flow conditions. Modelling techniques lie between empirical correlations and numerical solutions of the Navier-Stokes equations. They approximate the problem by considering the most important physical phenomena and neglecting those effects which complicate the problem but do not significantly improve the accuracy of the solution.

The major difficulties in experimental investigations of annular flows are the extremely thin films, relatively fast velocities, and random nature of the formation of the interface waves. Commonly available velocity measurement techniques such as hot wire anemometry disturb the films, and even non-intrusive techniques such as Laser Doppler Anemometry (LDA) cannot provide instantaneous velocity profiles within the film. These restrictions have limited experimental measurements to the time variations of film thickness and wall shear stress. This has meant that many analytical models have been developed not knowing the actual flow conditions that exist in the liquid film.

In the current study a simple liquid film modelling work has been introduced, see Section 6.1.3, in order to characterize the liquid film velocity profile. The back flow phenomenon, which usually occurs when the gas flow lacks the ability to lift up the entire segment of the liquid film in the annular flow, was then investigated.

A mathematical expression known as the "Triangular Relationship" is being used to predict the liquid film velocity distribution, see Section 6.1.3. The expression relates three variables: mean film thickness, film flow rate and wall shear stress. If any two of the variables are known, the triangular relationship can be used to find the third. For example, if a relationship between wall shear stress and mean film thickness is known

then the liquid film flow rate may be calculated for given values of mean film thickness and wall shear stress.

### 1.3 Aims and objectives

The main aim of this research program is to develop new techniques for accurate phase flow rate measurement of annular flow. The intention is to design novel but simple devices to successfully measure the liquid film thickness and velocity and the velocity of gas in the core, and to integrate these separate devices into a single multiphase measurement system (Note that if the liquid film thickness is known, the size of the core gas is easily determined). A further aim is to be able to determine the flow rate of entrained liquid in the gas core.

This aim is to be achieved by the following work plan which is set up in order of its objectives:

- To carry out a literature review regarding annular flow in general, and specifically about measurement techniques for this regime. This includes an investigation of different combinations of measurement techniques.
- To design and build a flow loop to develop an annular flow regime which can be used with different diameters of test sections and pipe orientations.
- To develop a mathematical model for the annular flow, predicting the liquid film velocity distribution.
- To develop a novel automated bypass system to implement film removal to measure the volume fractions of different liquids present in multiphase annular flows.
- To investigate the film thickness measurement by using a conductance probe.
- To develop a correlation technique to measure the liquid film velocity.

- To build and implement an ultrasonic flow meter to measure the core gas velocity.
- To investigate core gas flow measurement using the ultrasonic flow meter.
- To integrate all of the above methods and techniques into a measurement system.
- To characterise and calibrate the integrated system.

#### 1.4 Thesis outline

This thesis is organised in nine chapters describing the work that was done to achieve the aims and objectives of this project. This thesis is laid out as follows:

**Chapter 2** presents a literature survey that explains the concept of multiphase and two-phase flow. Also, it gives an outline of different multiphase flow metering techniques proposed for on-line flow rate measurement. Flow regimes in horizontal and vertical two-phase flow are briefly described. Because it is of particular interest, the annular flow regime is discussed in most detail. The different techniques that have been previously used in measuring different features of the fluid film and entrainment are summarised. The core gas velocity measurement is introduced in the context of wet gas metering. Some related techniques to wet gas metering are also discussed in this chapter.

**Chapter 3** concentrates on preliminary work including annular flow requirements in term of pressure drop and critical flow rates, as it is the first time that annular flow has been included in the University of Huddersfield's research programs. The chapter also reports the investigation of the design requirements for both a Conductance Flow Meter (CFM) and an Ultrasonic Flow Meter (USFM). The signal cross-talk phenomenon and sensor optimization are introduced prior to the design stage. Results of all the preliminary studies are presented.

**Chapter 4** describes the liquid-gas experimental facility designed and built at the University of Huddersfield. It also introduces different device designs i.e. CFM, USFM and the novel film removal technique. The chapter also reports the design of the relevant electronic circuitry of each device. The calibration methods for each device are explained and illustrated in this chapter. A description of the performances of the different designed devices is also reported in this chapter. The main aim of the work in this chapter is to optimise the performance of the whole system before actually using it to collect the raw data.

**Chapter 5** introduces the flow loop experimental apparatus and the experimental work. The reference measurement devices and their specifications are discussed. This is followed by investigating the best configurations for integrating the designed devices (CFM, USFM and film removal system) into the test section. The chapter also presents the data acquisition system and control units. The chapter also describes the automation of the multiphase system, data acquisition system and the developed program codes to automate the multiphase system and collect the data. The chapter ends with an introduction to the experimental flow conditions that were used in this study and reasons are given for their selection. This includes the procedures followed in carrying out the experiments and collecting the data.

**Chapter 6** of this report presents the results obtained using the novel measurement techniques (CFM, USFM and film removal system). Most results are presented in a graphical format and interpretations are provided. It also describes how the liquid film was mathematically modelled and the film velocity profile was characterized. Errors in the predicted results are discussed and possible improvements are suggested. The results of the current study were compared with previous work carried out by different researchers. Differences and similarities between these results were discussed to justify the results obtained in the current study.

**Chapter 7** presents the final proposal a novel wet gas flow meter developed by the author. The different aspects of the flow meter include: hardware of the flow meter, electronics of the flow meter, the mathematical approaches and testing and calibration of the flow meter. The accuracy of the novel flow meter is assessed by

finding the mean percentage error in the predicted gas and water flow rates based on the results discussed in Chapter 6.

**Chapter 8** gives a comprehensive list of the main findings and conclusions of this project and their novel aspects. The contribution to knowledge made by the project is given at the end of the chapter.

**Chapter 9** is the final chapter of this thesis. It lists some suggestions for future work and further investigations.

## CHAPTER 2 LITERATURE SURVEY

### 2.1 Multiphase flows

“Multiphase flow” is a rather imprecise term used to describe many types of flow occurring in industrial processes, (Martyn, 1999). As the name suggests, multiphase flow is a combination of one or more components (gas, liquid or solid) generally, but not necessarily, flowing in a pipeline. Such flow occurs when two or more immiscible substances flow together, and can be gas-solid (air carrying dust particles), liquid-solid (water and sedimentation from a mining process), liquid-liquid (oil in water) or gas-liquid flows (natural gas and oil) (Keshock and Lin, 1996; Fukano and Furukawa, 1998; Ariyadasa and Rezkallah, 2001). In this research project multiphase represents a gas-liquid flow.

#### 2.1.1 Flow regimes in multiphase gas-liquid flow

A flow regime is a geometrical configuration taken up by the gas and liquid. In general four main flow regimes have been proposed as adequate to describe the different flow behaviour. These are bubble flow, slug flow, churn flow and annular flow, see Figure 2.1. However, the physics of multiphase flows is complex and traditionally subjective characterisation has been used, so a wide variety of classifications exist in the literature. For the purpose of illustration the liquid velocity is assumed constant.

In fact bubble, slug and churn flow, may be considered as special cases of one type in which the continuous phase contains dispersed bubbles of gas, or where the gas phases tend to form slugs or plugs. The available literature shows that flow patterns in *horizontal pipes* have a non symmetrical distribution. As a result of gravitational forces, the liquid phase has the tendency to occupy the lower part of the tube (stratified or stratified wavy flows) while the gas phase occupies the upper part. On the other hand, flow patterns in *vertical pipes* are generally axisymmetric since the effect of gravitational forces is parallel to the direction of the flow. Annular vertical

flow will be discussed in some detail as it's the core of this study.

Usually flow patterns are recognized by visual inspection, though other means such as analysis of the spectral content of the unsteady pressures or the fluctuations in the volume fraction have been used where visual access is difficult, (Omebere-Iyari and Azzopardi, 2007). For some of the simpler flows, such as those in vertical or horizontal pipes, a substantial number of investigations have been conducted and the results are often displayed in the form of flow regime maps that identify the flow patterns occurring in various parts of a parameter space defined by the component flow rates. The flow rates used may be the volume fluxes, mass fluxes, momentum fluxes, or other similar quantities depending on the author. Perhaps the most widely used of these flow pattern maps is that for vertical gas/liquid flow constructed by Baker (in Dziubinski and Fidos, 2004).

### 2.1.2 Vertical Gas-liquid flow patterns

The major flow regimes found in vertical gas-liquid flow in a pipe of circular cross-section are shown in Figure 2.1, from left to right in order of increasing gas flow rate (Dou, 1996; Martyn, 1999). At low gas flow rates, the flow regime known as *bubble* flow predominates, where the gas flows as bubbles of approximately uniform size in a liquid matrix.

As the gas flow rate increases, collisions between bubbles are more frequent and they coalesce, eventually forming large bullet shaped bubbles called slugs. The flow has now moved into the *slug* flow regime. The pipe wall is permanently wetted and a film of liquid is present at the wall surface as the gas slug passes. Smaller gas bubbles are distributed throughout the liquid phase between slugs. The flow becomes unstable with increasing gas flow rate and the slugs distort and eventually break up as the flow moves into the *churn* flow regime. The gas now exists predominately as large irregularly shaped bubbles with smaller bubbles entrained in the liquid phase.

When the gas flow rate is sufficiently high as to support a liquid film on the surface of the pipe, the gas flows continuously through the centre of the pipe and the flow

enters the *annular* flow regime. The liquid flows along the pipe wall as an annular film, and is also carried along in the gas core as small liquid droplets.

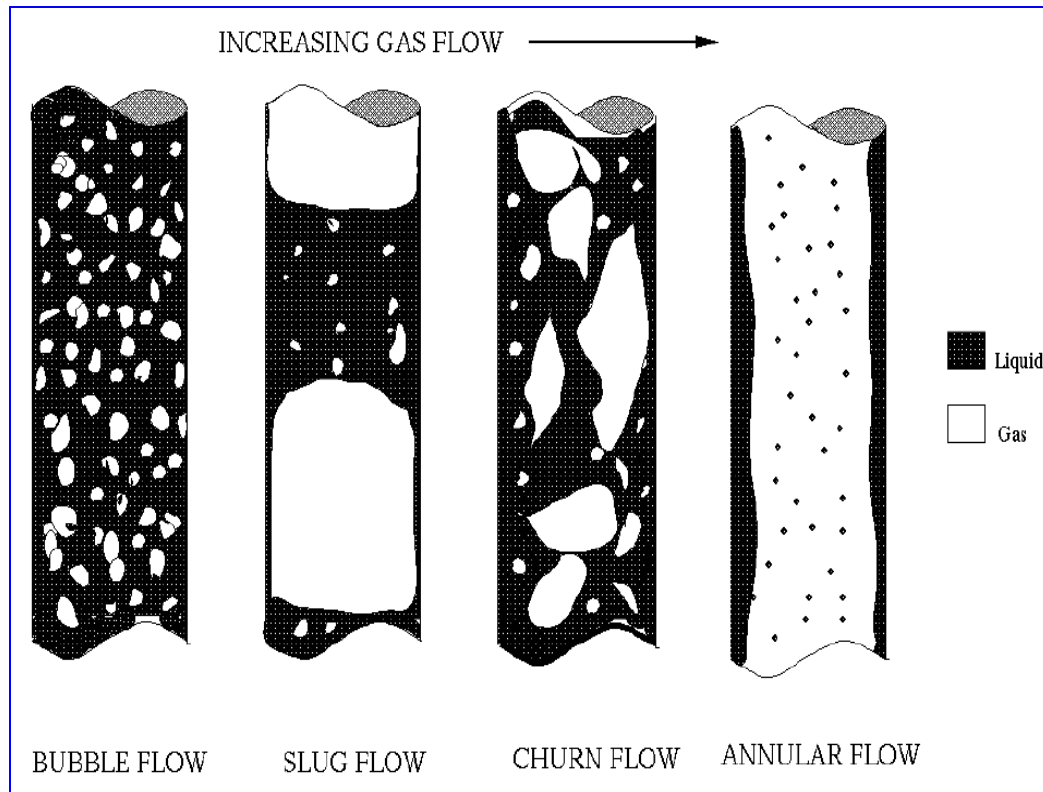


Figure 2.1 Flow regimes in vertical gas-liquid flows (Martyn, 1999)

The accuracy of multiphase design and predictive tools is poor compared to single-phase systems (Keshock and Lin, 1996). There have been many studies of various fluids in multiphase flows, but the effects due to varying the gas properties are not so well understood and often appear contradictory. By gaining a better understanding of the properties of the fluids involved, it may be possible to optimise a multiphase system by choosing the gas-liquid combination. To help gain such an understanding, the author has successfully designed and built a flow loop that will produce annular flow.

## 2.2 Multiphase flow applications

Gas-liquid multiphase flows, in particular annular flow, can occur in a variety of industrial situations as already mentioned in Chapter 1. Another application worth mentioning is phase-change heat transfer which is important where very high rates of

heat extraction are required, such as in supercomputers, in aerospace systems and in satellite cryogenic cooling systems. In phase-change heating applications, steam is invariably used to give up its heat of vaporisation when it condenses on e.g. tube walls. High-pressure steam can help extract oil from the ground, and the multiphase flow resulting will be a mixture of steam, water and oil. Generally, thermal transport systems involving multiphase flow are more expensive but are lighter, more compact and more efficient than single-phase systems. However, of interest to this project is the situation where the multiphase flow is a natural phenomenon (Lowe and Rezkallah, 1999; Zhao and Bi, 2001).

### 2.2.1 Flow rate measurements in multiphase flow

In 1995 the world market in flow meters was estimated to be worth \$2500 million and was expected to grow steadily for the foreseeable future. The value of the product being measured by these meters is very large. For example, in the U.K. alone, it was estimated that in 1994 the value of crude oil produced was worth \$15 billion (Webster, 2000).

Texaco appears to have pioneered the development of multiphase flow metering, but from the mid-1980s the oil industry generally took an interest in multiphase flow metering (Lyons and Plisga, 2004). As a result of this industry-wide effort, a number of measurement techniques are now emerging as commercially available field test hardware.

The first series of papers on the review of the development in the field of multiphase flow rate measurements in crude oil production systems were published by Ashkuri and Hill (1985). They predicted that future developments would fall into one of two categories: improvements in the design of test separators, which they considered as a short term development, or introducing new on-line techniques which did not involve phase separation. A more recent review by Whitaker (1997) showed that although test separators have improved, on-line techniques have gained more attention. This is because of the promising experimental results produced from industry supported laboratories. However, the latest review found by the author (Yeung, 2003) shows

that the on-line techniques have replaced the test separators in different parts of the world due to their great measurement results.

The available literature categorises the multiphase devices as (i) devices traditionally used as single phase devices (Sections 2.2.1.1 – 2.2.1.6), (ii) separation metering systems (Section 2.2.2) and (iii) devices designed specifically as multiphase flow meters and incorporating multiple measurement techniques (Section 2.2.3).

Oddie and Anthony (2004) have described possible choices for single phase flow rate measurement devices and techniques:

- Differential pressure devices (see Section 2.2.1.1)
- Turbine flow meters (see Section 2.2.1.2)
- Tracer techniques (see Section 2.2.1.3)
- Coriolis-type mass flow meters (see Section 2.2.1.4)
- Electromagnetic Meters (see Section 2.2.1.5)
- Ultrasonic Meters (see Section 2.2.1.6)

### *2.2.1.1 Differential pressure devices*

Differential pressure (DP) devices constitute one of the simplest methods of measuring the flow rate of gas-liquid flow in pipelines. DP devices include orifice plates, nozzles or Venturi meters. The use of such devices for multiphase flow metering has a long history and has been described by many authors including Murdock (1962), James (1965; 1966), Collins and Gacesa (1971), Lin (1982) and Pascal (1983). Provided the instruments can be properly calibrated, with reproducible upstream flow conditions and steady flow, a good degree of accuracy can be obtained. Richard (2001) stated that uncalibrated orifice meters that conform to ISO 5167-1 are assumed to have an uncertainty of  $\pm 0.5\%$ . Venturi manufacturers tend to claim uncertainties in the order of  $\pm 1\%$  after calibration (although in reality it may be higher).

One of the major advantages of DP devices is that measurement uncertainty can be predicted without the need for calibration, if the device has been manufactured and installed in accordance with one of the relevant International Standards. Sekoguchi, et al., (1978) have presented a new approach of utilising two orifices in series to meter multiphase flow systems. This technique underwent further development by Pascal (1984) who emphasized the observable influence of the diameter ratio of the two orifices and the distance between them on their performance and the accuracy of measurements.

The Venturi flow meter has recently gained the great attention from researchers. This is a metering device that has a tapered inlet and outlet with a constricted straight middle section, see Figure 2.2. The Venturi tube is suitable for clean, dirty and viscous liquid and some slurry services. It's reported that Venturi has a typical accuracy of 1% of full range (Thomas and Paul, 2008).

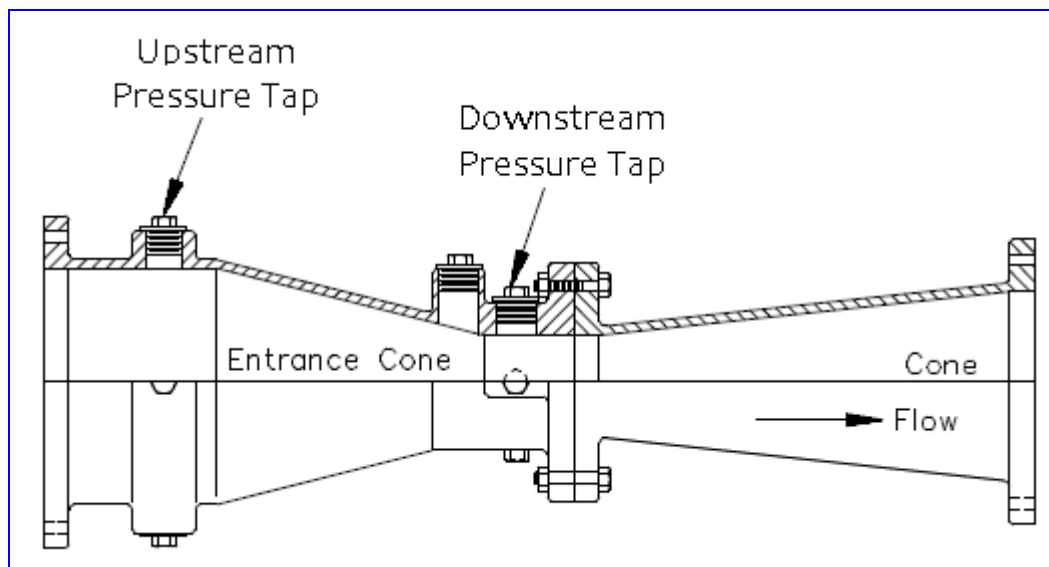


Figure 2.2 Venturi tube (Thomas and Paul, 2008)

### 2.2.1.2 Turbine flow meters

Turbine flow meters are one of the oldest methods of flow measurement, here the flow drives a turbine and the speed of revolution gives an indication of the flow rate. The use of such devices, see Figure 2.3, has been fully described by Zheng et al, (2008) who discuss the many problems associated with using turbine flow meters for

flow metering. They are prone to mechanical failure, particularly in the bearings if subject to large amounts of buffeting and are sensitive to abrasive flow components.

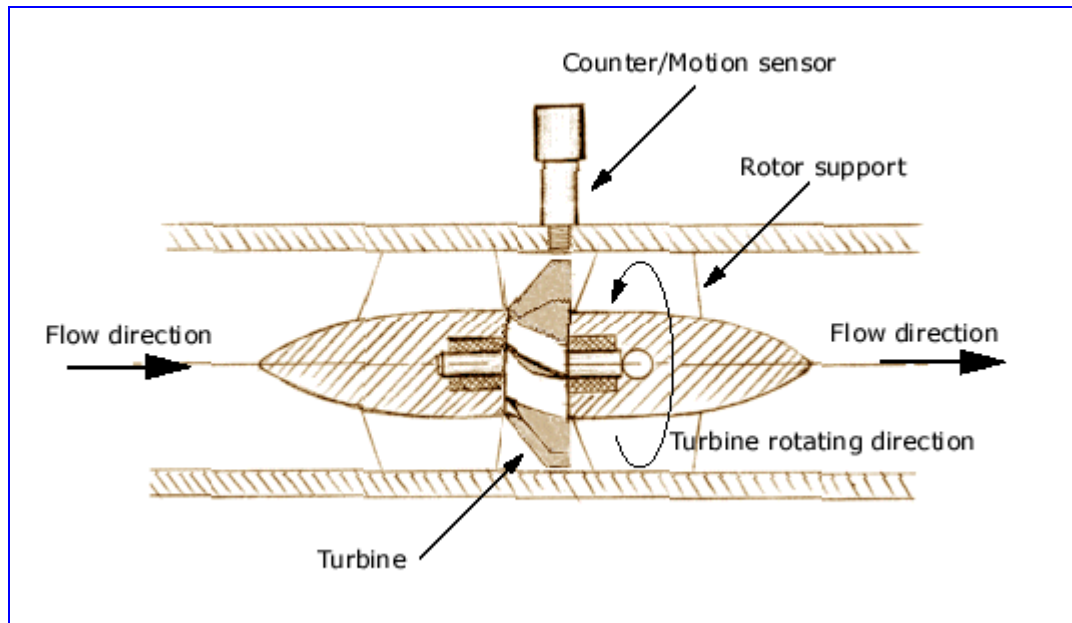


Figure 2.3 Turbine flow meter (Zheng et al, 2008)

The performance of turbine meters also depends on rotor design and the region of the normal meter operating range over which the tests were done. Finally, the results of turbine flow meters are flow pattern dependent. Turbine flow meters can show an accuracy of 0.25% of measurement (Zheng et al., 2008).

### 2.2.1.3 Tracer techniques

This must be the simplest method of determining flow velocity. A suitable tracer, usually small spherical pellets of much the same density as the fluid but discernible in the fluid flow are added to the fluid at a given point and the time they take to flow past two points downstream, a known distance apart, is measured. These techniques are widely used in metering single phase flow and were adapted for two-phase over thirty years ago (Mcleod et al., 1971). Some of the difficulties associated with the application of tracer techniques to flow metering are: **1)** obtaining a uniform distribution of the tracer throughout the flowing liquid; **2)** interphase mass transfer and mixing gives rise to a non-uniform modulation of the tracer; **3)** changes in flow pattern and velocity between the point where the tracer was added and the point of

detection, 4) the tracer must be of a suitable density and must be clearly visible within the liquid.

#### 2.2.1.4 *Coriolis-type mass flow meters*

Coriolis flow meters, see Figure 2.4, are claimed to have the greatest accuracy of any flow meter, typically 0.1% to 0.15% in liquids and 0.5% in gases. However, the range of flows over which they are applicable is small, AMI Instrumentation and Calibration in a press release of 09/08/2006 (AMS-Instrumentation-and-Calibration, 2006) publicising a new high flow rate meter gave the upper limit of its range as 2.2m<sup>3</sup>/hr. Such a device is only of use for those wells with relatively small outputs (about 50m<sup>3</sup>/day).

Coriolis meters have been used for two phase gas-liquid flows, but are of limited application because the upper limit to the void fraction is low (possibly as low as 2%), below that found in the oil and gas industry. Coriolis flow meters have traditionally suffered from another drawback, that dirty and/or abrasive liquids clogged the U-shaped design. However, the development of a single straight tube design is expected to largely overcome this difficulty (efunda, [online] accessed 10/01/2009). In general, where Coriolis-type mass flow meters have been used in the oil and gas industry it was for steady flow with a low gas void fraction.

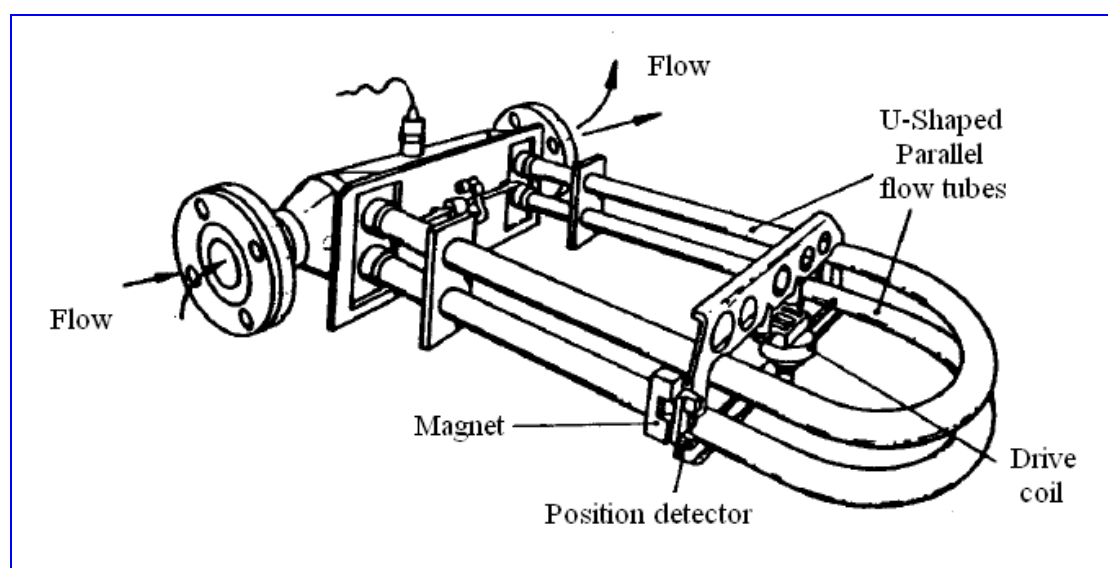


Figure 2.4 Modern industrial Coriolis meter (efunda, [online] accessed 10/01/2009)

### 2.2.1.5 *Electromagnetic Meters*

Magnetic flow meters, see Figure 2.5, have been widely used in industry for many years. Unlike many other types of flow meters, they offer true non-invasive measurements. They are easy to install and use to the extent that existing pipes in a process can be turned into meters simply by adding external electrodes and suitable magnets. They can measure reverse flows and are insensitive to viscosity, density, and flow disturbances. Electromagnetic flow meters can rapidly respond to flow changes and they are linear devices for a wide range of measurements. As in the case of many electric devices, the underlying principle of the electromagnetic flow meter is Faraday's law of electromagnetic induction. In multiphase flows the induced voltage in an electromagnetic flow meter is linearly proportional to the mean liquid velocity. However, the liquid phase must be continuous and must be electrically conducting.

Magnetic flow meters do not require continuous maintenance, except for periodic calibrations. Nevertheless electrode coating, damage to the liners, and electronic failures can occur. Any modification or repair must be treated carefully because, when installed again, some accuracy can be lost. After each modification or repair, recalibration is usually necessary. For electromagnetic flow meters to operate accurately, the process liquid must have minimum conductivity of 1mS/cm to 5mS/cm. Most common applications involve liquids with conductivities greater than 5mS/cm. Nevertheless, for accurate operation, the requirement for the minimum conductivity of liquid can be affected by length of leads from sensing electrodes to transmitter electronics (Al-Yarubi, 2006).

Electromagnetic flow meters cannot measure gas phase, so for electromagnetic flow meters to be successfully used in multiphase flow the gas must be independently measured. In multiphase flow  $\bar{U}_w$  the mean water velocity, is given by:

$$\frac{Q_w}{A(1-\bar{\alpha}_g)} = \bar{U}_w \quad 2.1$$

where:  $Q_w$  is water volumetric flow rate,  $\bar{\alpha}_g$  is gas mean volume fraction and  $A$  is pipe cross-sectional area.

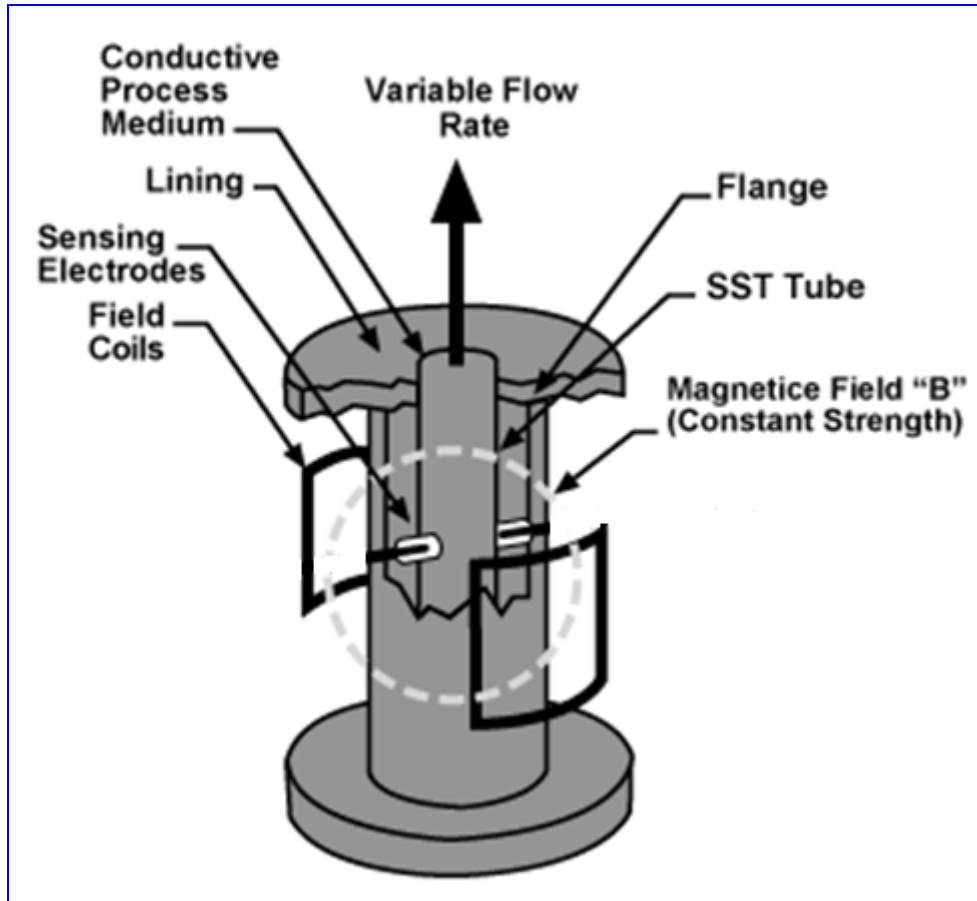


Figure 2.5 Electromagnetic flow meter (Al-Yarubi, 2006)

### 2.2.1.6 Ultrasonic Meters

The ultrasonic meter category contains a number of different designs for measuring an average velocity in a flowing system. They are all based on an ultrasonic signal being changed by stream velocity or reflected from interfaces or solids in the stream. Meter measurement accuracy can be in the range of 1% of flow rate, and reflects the ability of the system to represent the average velocity over the whole stream passing through the meter body's hydraulic area - which affects installation requirements and accuracy of the results obtained. Meters are made in several types; one type requires installation of transducers into the flowing stream, the other is a strap-on model that can be installed without shutting down the flow stream. Whereas electromagnetic flow meters require a minimum electric conductivity of the liquid for operation,

ultrasonic flow meters can be applied in nearly any kind of flowing liquid. Ultrasonic flow meter is discussed in details in Section 2.4.2.

### 2.2.2 Separation metering systems for multiphase flow

This is the traditional and extensively tested method for multiphase flow measurement. Oil, gas and water in the incoming stream are first separated and then metered by volumetric flow meters in individual flow lines. Test separator design depends upon the type of production, oil or gas. In oil gathering stations the test separator is a horizontal vessel with a top crude inlet and three outlets for gas from top, and water and oil from bottom, each outlet line containing a single phase flow meter, see Figure 2.6.

To get accurate results from a well-test it is necessary to control pressure levels and measure accurately the amount of oil, water and gas produced. Pressure is controlled by a Pressure Control Valve (PCV) on the gas outlet line. Pressure control is very important because a fluctuating pressure invalidates the test result. The gas produced from the well is measured by an orifice flow meter which allows the replacement of the orifice plate while the separator and gas line are under pressure. Using the correct size orifice plate is essential to obtain accurate readings.

Water and oil levels are controlled by separate Level Control Valves (LCVs), connected to Emergency Shut Down (ESD) valves. The amounts of water and oil produced are measured by separate suitable single phase flow meters. The LCV for the oil usually works on gap control which gives sufficient residence time for the oil to release any trapped gas. The gas, oil and water produced over a given test period are measured and totalled.

PDO has recently introduced a vertical three-phase gas well separator Type SM (V6203) in its newly discovered Kauther gas field, see Figure 2.7, as part of the Kauther Gas Plant (KGP) project at a cost of \$160,000,000. The V6203 gas test separator has a cross-flow plate-pack coalescer which acts as a filter.

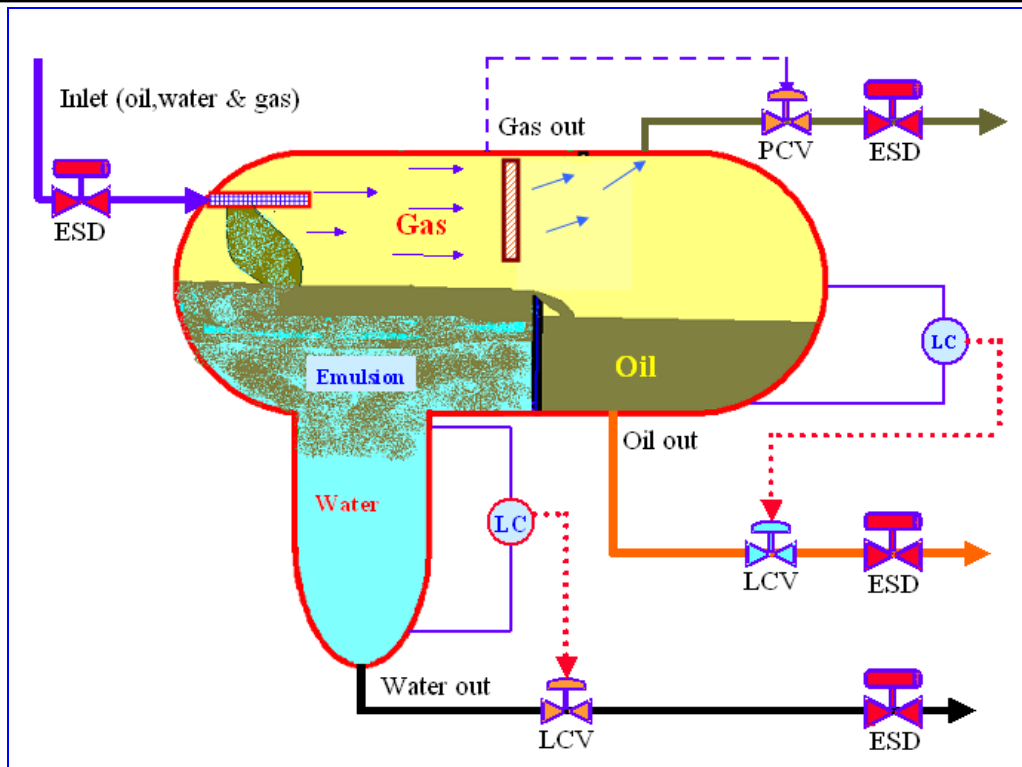


Figure 2.6 Simplified oil well separator (Al-Yarubi, 2006)

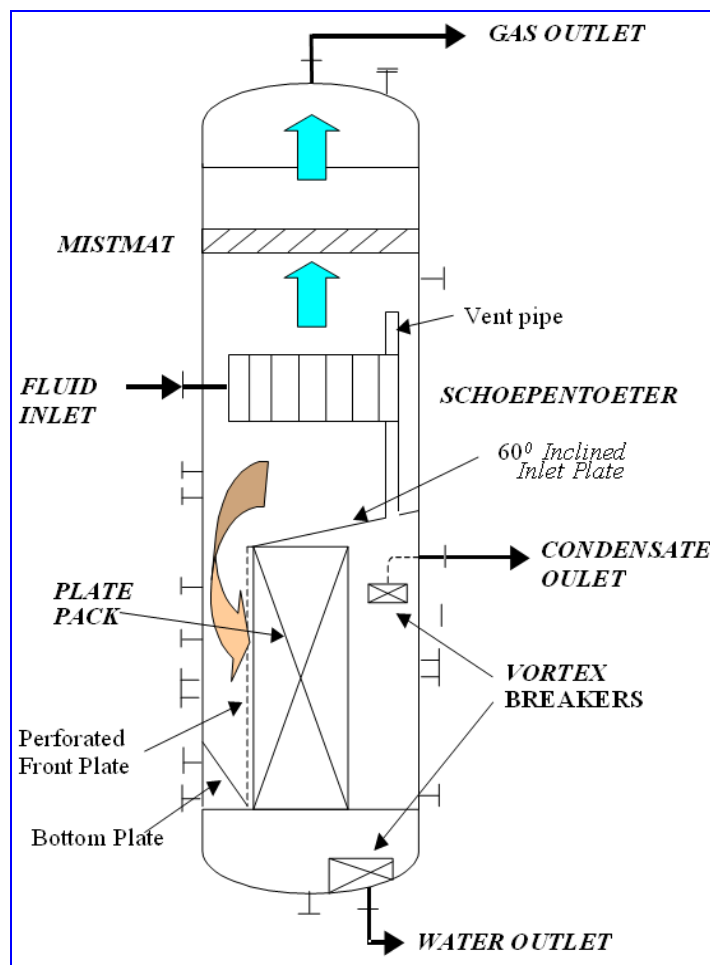


Figure 2.7 Typical three phase separator (for gas wells) (Al-Yarubi, 2006)

Generally, a three-phase separator for both oil and gas wells would be expected to accomplish the following:

- Liquid must be separated from gas in a primary separating section.
- Gas velocity must be lowered to allow liquids to drop out.
- Gas must be scrubbed through an efficient mist extractor.
- Water and oil must be diverted to a turbulence-free section of the vessel.
- Liquids must be retained in the vessel long enough to allow separation.
- The water-oil interface must be maintained.
- Water and oil (referred to as condensate in Figure 2.7) must be removed from the vessel at their respective outlets.

With the KGP project the well fluid to be tested is routed by a dedicated test header to the test separator. Primarily gas and liquid are separated. Then the gas flows from the top of the separator via a flow meter to a wet gas cooler under a pressure control unit. The liquid collected in the test separator is further separated into water and condensate (oil and hydrocarbons in general). Water is drawn from the bottom of the test separator by an inter-phase level/flow cascade control unit. The condensate is drawn from a condensate outlet nozzle, which is located in the middle of the hydrocarbon section of the plate pack, by a level/flow cascade control unit.

Figure 2.8 shows a typical gas process plant involving a V6203 multiphase separator shown in Figure 2.7. Gas plant is much more complicated than oil plant. Crude enters the gathering plant at high pressure, so the separator must be vertical to separate liquid particles from the gas by means of gravity. Normally in gas plant there will be first, second and third stage separation. Water will be collected from the first stage separation while condensate (heavier hydrocarbons) is gathered from the second and third stage separation. Condensate will be treated and transferred to Liquefied Petroleum (LPG) process plant within the gathering station. Methane gas is then cleaned of acid and sour gases and then purified and compressed. The gas must be dried and free of water vapour and heavier hydrocarbons components before transporting it to customers.



Such a process requires a great attention to many different aspects as it deals with different phases of flow. The main disadvantage of using conventional test separators is that they are heavy, bulky and expensive (\$750,000 approximately). Furthermore, they are unrepresentative because they only sample a fraction of the total production and do not operate continuously. The complexity of the process could be minimised if an online measurement device were installed. The following section will review some of these devices used to overcome the need for bulky separators. PDO has started to use multiphase flow meters to test each well production. The required accuracy by PDO for the well test is  $\pm 10\%$ , which can be achieved easily by a multiphase flow meter with lower operational cost compared to test separators.

### 2.2.3 Review of dedicated multiphase metering systems

The first commercial dedicated multiphase flow meter appeared about ten years ago, as a result of several multiphase metering research projects that took place in the early 1980's. The driving force to develop multiphase flow meter technology was the forecast decline of production, accompanied by the necessity to tie future smaller discoveries to existing infrastructure. Increasing gas and water fractions, inherent in a mature producing province, would create more unstable flow conditions in existing production facilities and require more flexible multiphase solutions.

A critical review of the multiphase flow meter solutions currently available in the market is far from being an easy task. Most multiphase flow meter research projects are now driven by the oil and gas industry and usually end up with a patented solution. Thus, scientific and commercial interests often tend to overlap in a sector of the oil and gas market where competition is intense. Multiphase flow meter manufacturers have to act quickly in order to secure the implementation of a particular technology before their rivals. This results in a very limited amount of published information on the performance of the various multiphase flow meters. Unless operators are ready to pay non-negligible sums to gain access to the results of independent multiphase flow meter assessments carried out at well-established labs, they are usually offered "black-box" packages where very little is unveiled about the technical principles behind the multiphase flow meters.

This section presents a review of multiphase metering systems which PDO has used or tested in its production fields. This encompasses what are believed to be all the most advanced and soundly based technologies. This provides a review of the state of the art of emerging technologies. It includes information on current capabilities and costs as well as describing the different measurement concepts. *This type of information is commercially sensitive due to the high competition in the market for commercial multiphase flow meter.* In the following review, it's worth defining the terms used to avoid confusion and ambiguity:

Standard terms are used in quoting accuracy or error percentages:

*Absolute error*: an error or deviation expressed as a percentage of full scale.

*Accuracy*: ability to provide a reading close to the true value of the parameter being measured.

*Relative error*: error or deviation expressed as a percentage of actual flow rate.

*Uncertainty*: the dispersion of the readings (usually the standard deviation).

### 2.2.3.1 Positive displacement screw meter

This flow meter was licensed by ISA Controls Ltd. in 1994, and is believed to be the most advanced in terms of flow loop and field test experience. A full range of flow conditions of up to 0.95 gas volume fraction (GVF) has been tested and several thousand run-hours experience gained. The meter measures total volumetric and total mass throughput of the multiphase fluid stream and uses water cut ( $C_w = Q_w / Q_{total}$ ) to measure the flow rates of oil, water and gas.

The principle behind the screw meter is that the positive displacement elements constrain the phases to move at a single velocity. The meter housing has chambers, see Figure 2.9, which are continuously filled and emptied, and this process is transmitted through suitable gearing to a counter that reads total volume.



Figure 2.9 Chambers in positive displacement meter (Yeung, 2003)

A densitometer beam passes through a cavity between the screws mid-way along the meter axis. In principle, if slip between the phases were fully eliminated between the screws, the densitometer reading would equate to the true mixture density relating to the overall proportions of oil, water and gas flowing in the pipeline. Coupled with the water cut reading from a second instrument, the mixture density and total swept volume readings can then be used to solve for the flow rates of oil, water and gas at line conditions (Yeung, 2003). (This assumes that the individual phase densities are known as a function of pressure and temperature which are also measured at the multiphase metering section).

The test data obtained this far indicates that relative error uncertainty increases with GVF. The relative error of the flow rate increases from  $\pm 5\%$  (GVF of 0.8) to  $\pm 10\%$  (maximum GVF of 0.95). Cost to supply such a flow meter can only be estimated at present but is expected to be of order \$150,000. Cost of a complete ISA multiphase measurement system is, of course, application dependent.

### 2.2.3.2 Framo multiphase metering system

The system, see Figure 2.10, was developed by Framo Engineering AS in Norway and is based on a technique which should, in principle, be insensitive to the

randomness in multiphase flow. The device has a novel mixer, or flow conditioner which, unlike conventional mixers, can mix slugs and gas pockets to produce a steady exit stream from intermittent regimes. Dual energy gamma ray attenuation measurements are used to determine the ratios of oil, water and gas.

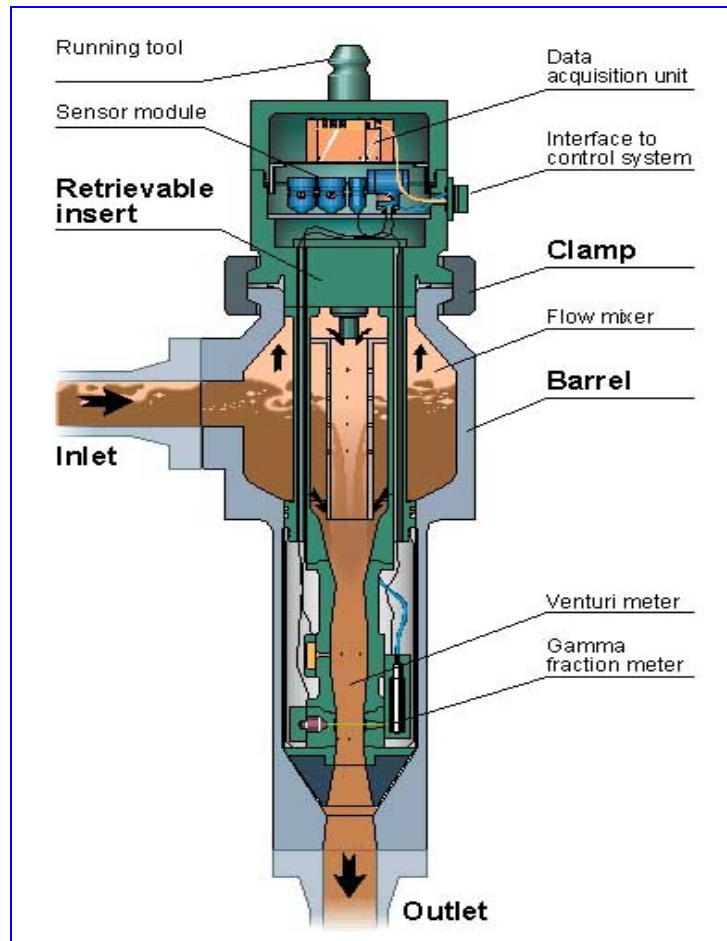


Figure 2.10 Framo multiphase flow meter (Olsen and Hanssen, 1994)

Calibration of the Framo system would rest with the type of measurement used. For the Venturi meter, it is primarily a matter of subjecting the pressure sensors to accurately known fluid pressure. This assumes that a universal or repeatable and predictable Venturi discharge coefficient can be established for well-mixed multiphase flow. The dual energy gamma system requires calibration on fluids of known density and attenuation coefficient.

Test results show relative measurement errors in phase flow rates and total flow of 20% to 30% (Olsen and Hanssen, 1994). The field prototype is barrel shaped, approximately 1.4m long and 0.5m diameter and total cost approximately \$900,000.

### 2.2.3.3 *Fluenta system*

The Fluenta multiphase flow meter has an inline spool piece that measures flow without separation of phases. The meter was 0.076m in diameter and 1.5m long. The Fluenta multiphase flow meter combines conductance (**A**), capacitance (**B**) and  $\gamma$ -ray (**C**) sensing techniques to monitor vertical up-flows see Figure 2.11. If the flow is oil continuous then capacitive sensors are used, if the flow is water continuous conductance sensors are fitted, and used to measure the water content of the flowing liquid. The meter also includes a Venturi to be used in gas velocity measurements.

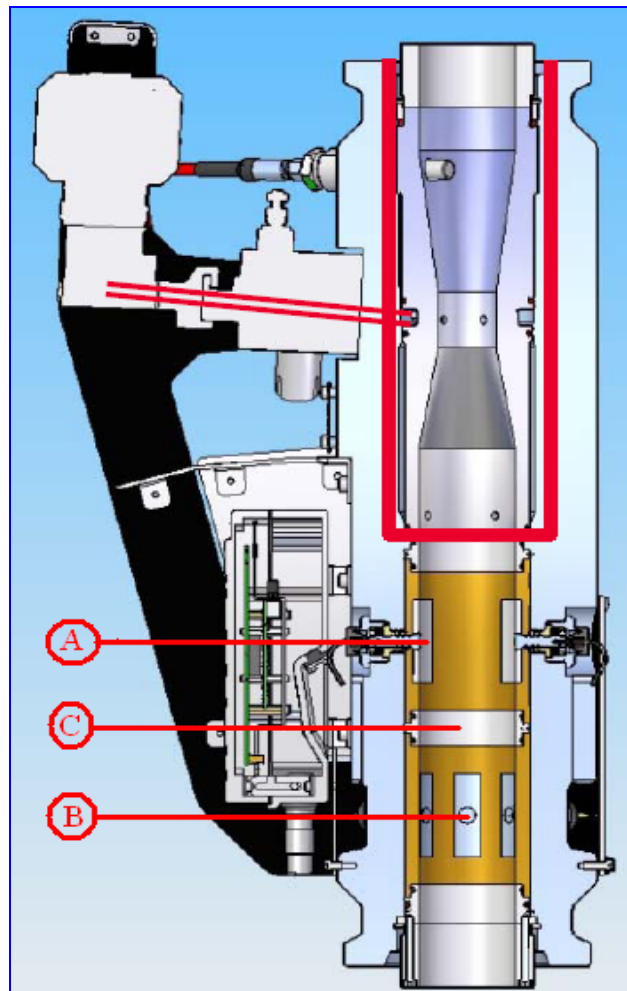


Figure 2.11 Fluenta multiphase flow meter (AMS, [online] accessed 05/08/2009)

A second set of sensors placed a known distance along the pipe provide cross-correlation measurement of the flow velocity. By using cross-correlation techniques on the signals, the meter measures the velocity of both the gas and the liquid, enabling the meter to operate in all kinds of flow regimes - bubbly, churn and slug flow - for water cuts of 0-1 and gas volume fractions up to about 0.95.

Calibration of the system for the field trial was completed at the CMR laboratory. Absolute errors of  $\pm 2\%$  phase fraction have been demonstrated by the test programme for gas volume fractions of up to 0.5. In the past Fluenta have quoted \$300,000 for one of their multiphase metering systems, but this latest development is likely to be significantly more expensive.

#### *2.2.3.4 The Multi Fluid International system*

First marketed by Multi Fluid International, this system is now known as Roxar Flow Measurement. This microwave instrument measures the dielectric constant and gamma ray attenuation for the flow mixture to determine the in-situ volume fractions of oil, water and gas across the cross-section of the pipe. In one configuration, the instrument functions in both water continuous and oil continuous emulsions, this version of the instrument is known as the “full range meter”.

Velocity measurements are performed by a momentum meter which can be combined with a microwave device. In conjunction, the two meters allow liquid and gas velocities to be measured more accurately over a wide range of flow regimes. The meter operates in water cuts of 0-1. The ‘low price’ version, which uses a similar microwave technology, operates only in oil continuous flow, up to a water cut of 0.4-0.6. Phase fraction results obtained from laboratory loop tests had absolute errors within  $\pm 2\%$ . Cross-correlation of data measurements to obtain mixture velocity and phase flow rates, were more erratic with relative errors of  $\pm 10\%$  to  $20\%$  reported.

The calibration of the MFI phase fraction system, in principle, should rely primarily on factory or laboratory set-up prior to installation. The system uses commercially available Cs137 gamma ray densitometers which can be calibrated on fluids such as

air and tap water. The microwave unit requires data including density of the dead crude, produced water density and conductivity. The MFI system then relies on application specific prediction equations of the variation of these quantities and gas density as a function of line pressure and temperature.

The 'low price' oil-continuous instrument is currently quoted at an estimated price of \$200,000. This includes the twin sensor arrangement which permits a single velocity measurement by cross-correlation (Purvey, 1998).

#### *2.2.3.5 Texaco Starcut meter*

This water content monitor has been developed by Texaco EPTD. The instrument measures the water content of emulsions containing little or no free gas. It uses measurements of the phase shift and attenuation of 10GHz microwaves caused by the flow stream to determine water cut. The instrument is already developing a field track record ahead of other phase fraction/water cut devices, although these devices have, of course, already demonstrated a measurement capability on gas fractions significantly higher than 0.25. The sensing flow path is of rectangular cross-section of approximately 10mm by 5mm normal to the flow path. This limits the device to rely on a slip stream sample arrangement in the majority of applications since it clearly imposes a throughput limitation

Calibration of the Starcut monitor is essentially a factory/laboratory exercise. It subsequently performs its own auto-calibration once installed in service. Tests indicated that the combination of the screw meter, see Section 2.2.3.1, with the Starcut system would be expected to provide the latter with a well mixed and representative sample from which to derive water cut. The present pricing for an off-shelf unit is approximately \$70,000.

#### *2.2.3.6 Kongsberg multiphase flow meter*

In 1992, Kongsberg Offshore launched a multiphase meter developed by Shell Exploration and Production Laboratory (KSEPL) in the Netherlands. The meter

measures the flow rates of oil, gas and water for slug flow. The measurement spool comprises two closely spaced parallel conductance plates mounted across the centre of the pipe. Two more capacitance electrodes are positioned one near the top and one close to the bottom of the pipe, see Figure 2.12. The gas-liquid interface is sensed by the conductance electrodes, and flow perturbations sensed at upstream and downstream capacitance electrodes are cross-correlated to obtain the flow velocity.

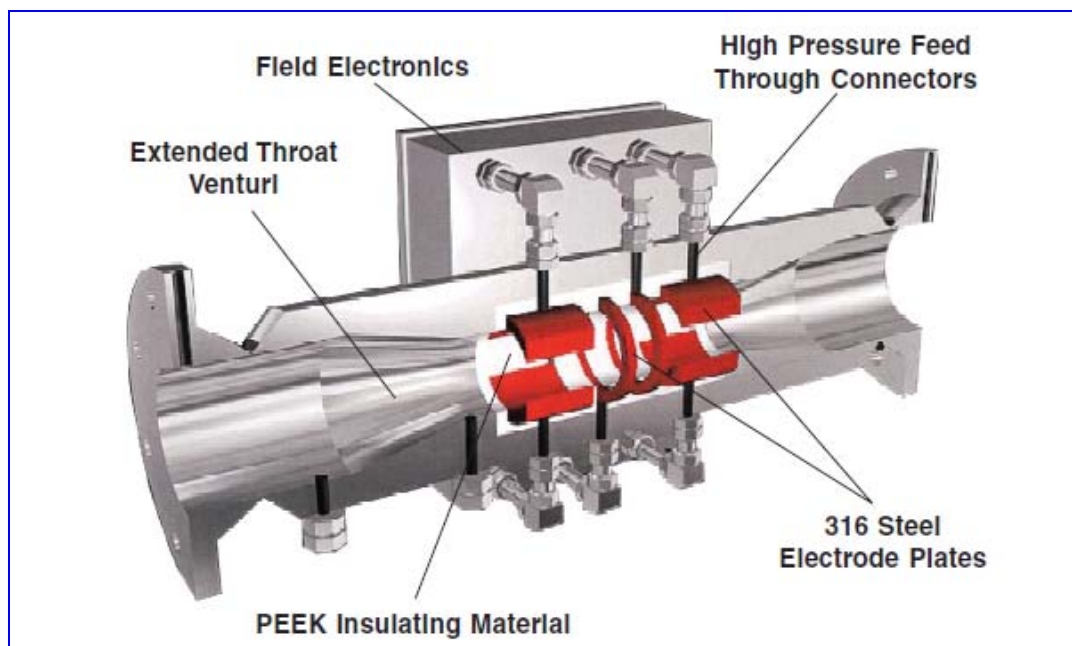


Figure 2.12 Kongsberg type multiphase flow meter (Halto and Sorensen, 1999)

Prototype units have been undergoing field trials in Oman which Shell report (Halto and Sorensen, 1999) as giving “consistent” results compared to test separator equipment, although with some bias error. Shell claim to have a number of such applications and state that the level of accuracy achievable with the unit (quoted at between 10% to 20% of flow rate) is acceptable. Shell compensate for the lower accuracy of these meters by having a relatively low cost unit, less than \$100,000 including an industrial PC.

### 2.3 Annular flow

Annular two-phase flow is the focus of this research. It is characterized by gas core flow in the centre of the tube, a liquid film flowing on the inner tube wall, and a wavy gas-liquid interface. The gas core also carries entrained liquid droplets. The interface

between the liquid film and the gas core is highly dynamic and constantly changing and the droplets are believed to be transported into the gas core as crests of the waves are sheared off by the gas stream (Sawanta et al., 2008). A feature of the interface is the presence of large disturbance waves along with smaller ripple waves. Figure 2.13 shows a schematic plot of a typical annular flow regime.

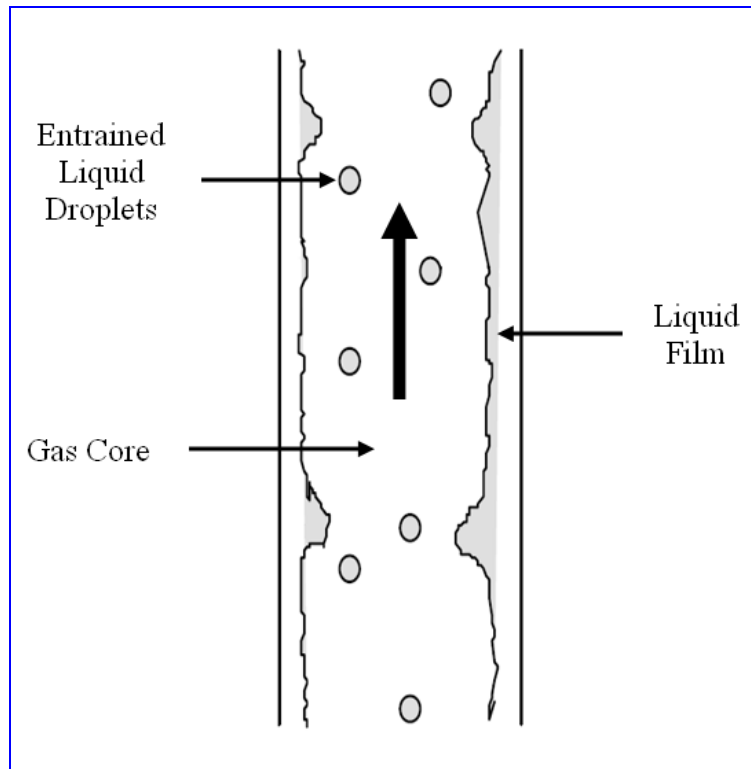


Figure 2.13 Typical two-phase annular flow regime

Annular flow can occur at all pipe orientations. In vertical flow the time averaged film properties are uniform around the pipe circumference, but for inclined and horizontal pipes, gravity causes a significant asymmetry of the film, much higher mass flow rates and film thicknesses are found at the lower side than at the upper side of the pipe. The importance of liquid films has led to extensive experimental investigations.

In this study, the four major features of the annular flow regime that were studied are: (i) the liquid film thickness  $\delta$ , (ii) the liquid film velocity  $U_f$ , (iii) the entrainment fraction  $E$  and (iv) the gas core velocity  $U_{g,c}$ . This study is concerned with measurement of the flow rate of the phases rather than the behaviour of the liquid

film, but the study of latter is necessary when considering the flow behaviour in more detail.

### 2.3.1 Film thickness

In many situations concerning annular flow, determining the flow characteristics is important for improving system performance or ensuring safety. As explained earlier (see Section 1.2.2) a good understanding of liquid film behaviour is critical to prevent dry-out situations and subsequent catastrophic events. The general trend is for the mean film thickness to decrease to some minimum value as the gas flow rate increases or with a decrease in the liquid flow rate (Ariyadasa, 2002; Fukano and Furukawa, 1998). For upward vertical, co-current flow, this behaviour of the mean film thickness is due to the film becoming smoother as the gas flow rate increases (Ariyadasa, 2002).

MacGillivray (2004), has reported an empirical relationship for calculating the film thickness, based on the interfacial shear or the entrainment, as follows:

$$m^+ = \left[ \left( 0.707 \text{Re}_w^{0.5} \right)^{2.5} + \left( 0.03379 \text{Re}_w^{0.9} \right)^{2.5} \right]^{0.4} \quad 2.2$$

where:  $m^+$  is non-dimensional film thickness and  $\text{Re}_w$  is the Reynolds number defined by:

$$\text{Re}_w = \frac{4 G_l \bar{P}}{\mu} \quad 2.3$$

where:  $\bar{P}$  is the perimeter wetted by the film (m),  $\mu$  is the liquid viscosity (kg/ms) and  $G_l$  is the liquid film mass flux ( $\text{kg/m}^2\text{s}$ ), calculated from the mass flow rate ( $\text{kg/s}$ ) of the liquid film:

$$G_l = \frac{W_l}{\pi D^2} \quad 2.4$$

where:  $W_l$  is the liquid mass flow rate ( $\text{kg/s}$ ) and  $D$  is the pipe diameter (m).

The dimensionless film thickness,  $m^+$ , is given as:

$$m^+ = \frac{\delta \mathcal{G}^*}{\nu} \quad 2.5$$

where:  $\delta$  is the film thickness (m),  $\nu$  is the liquid kinematic viscosity ( $\text{m}^2/\text{s}$ ), and  $\mathcal{G}^*$  is the liquid friction velocity (m/s), calculated from:

$$\mathcal{G}^* = \left( \frac{\tau_i}{\rho_l} \right)^{0.5} \quad 2.6$$

where:  $\tau_i$  is the interfacial shear stress and  $\rho_l$  is the liquid density ( $\text{kg}/\text{m}^3$ ).

Ambrosini et al., (1991) recommend using a slightly different relationship;

$$m^+ = A \text{Re}_w^B \quad 2.7$$

where:  $A = 0.34$ , and  $B = 0.6$  for  $\text{Re}_w < 1000$

and  $A = 0.0512$ , and  $B = 0.875$  for  $\text{Re}_w > 1000$ .

Fukano and Furukawa (1998) were amongst the first to develop a relation that included the effect of the gas flow rate on the mean film thickness, and an estimate for the film thickness within 15% of the data was claimed. They conducted their experiments on annular flow using air-water and air-glycerine solutions. This relationship is given as:

$$\frac{\delta}{D} = 0.0594 \exp\left(-0.34 Fr_g^{0.25} \text{Re}_w^{0.19} x^{0.6}\right) \quad 2.8$$

where:  $\delta$  is the film thickness (m),  $D$  is the pipe diameter (m),  $x$  is the gas quality (ratio of the mass flow rate of the gas divided by the total mass flow rates of gas and liquid) and  $Fr_g$  is the gas Froude number is calculated from:

$$Fr_g = \frac{U_{g,s}}{(gD)^{0.5}} \quad 2.9$$

where:  $g = 9.81\text{m/s}^2$ ,  $U_{g,s}$  is the gas superficial velocity (m/s) and here the Reynolds number is defined by:

$$Re_w = \frac{U_{w,s} D}{\nu} \quad 2.10$$

where:  $U_{w,s}$  is the water superficial velocity (m/s),  $D$  is the pipe diameter (m) and  $\nu$  is the liquid kinematic viscosity ( $\text{m}^2/\text{s}$ ).

These relations are not very useful for practical design purposes since they require either knowledge or calculation of such quantities as the interfacial shear stress, which is not readily available. In addition, these relations do not identify the influence of the gas mass flow rate on the average film thickness. Also, of course, other flow parameters affect the mean film thickness. Hori et al., (1979) reported that an increase in the viscosity of the liquid resulted in an increase in the film thickness. Bousman (1995) has shown that an increase in either the viscosity or the surface tension resulted in a thicker liquid film and larger amplitude waves. The observation was also noted by Han and Gabriel, (2006) in their study of the effect of the gas on the wave characteristics in two-phase gas-liquid annular flow.

Kwon et al., (2001) suggest that for constant mass flow rate (both gas and liquid), as the gas density increased so the film thickness increased. This might have been expected since for a constant mass flow rate the gas volumetric flow rate will decrease as the gas density increases. In a sense these findings confirmed those of Ariyadasa (2002) and Fukano and Furukawa (1998). For the same gas velocity, the film thickness increased with decreasing gas density. These results were based on comparison of data obtained by researchers for tests made at different absolute pressures, test section lengths and tube diameters.

Typical film thicknesses in two-phase flows are often less than a few millimetres, so accurate measurement is difficult, and this has led to a wide range of measurement

techniques (Clark, 2002). An initial review of the literature found some twenty film thickness measurement techniques, and these have been divided into three groups:

- Film average methods (see Section 2.3.2.1)
- Localised methods (see Section 2.3.2.2)
- Point methods (see Section 2.3.2.3)

## 2.3.2 Measurement techniques for film thickness

### 2.3.2.1 Film average methods

These techniques belong to a larger group of “liquid hold-up” techniques that have been widely reported in the literature. To obtain an average film thickness value measured over a considerable length of film using these methods is possible only through the assumption that all the liquid present is in the form of a uniform symmetrical film. There has been little study using film average methods due predominantly to their inability to provide information on local interface phenomena i.e. waves.

The ***Weighing Method*** (Aragaki et al., 1987), involves an arrangement that allows the weighing of the experimental test section during operation, see Figure 2.14. The ***Hold-up measurement***, (Burns et al., 2003), simply consists of isolating a section of film and measuring the liquid volume within this isolated section. The ***Conductance method*** (Kang and Kim, 1992), involves the measurement of the conductance of a length of film and then relating the measured conductance value to the thickness of the film. In many instances, it is necessary to make the film conducting by adding appropriate electrolytes.

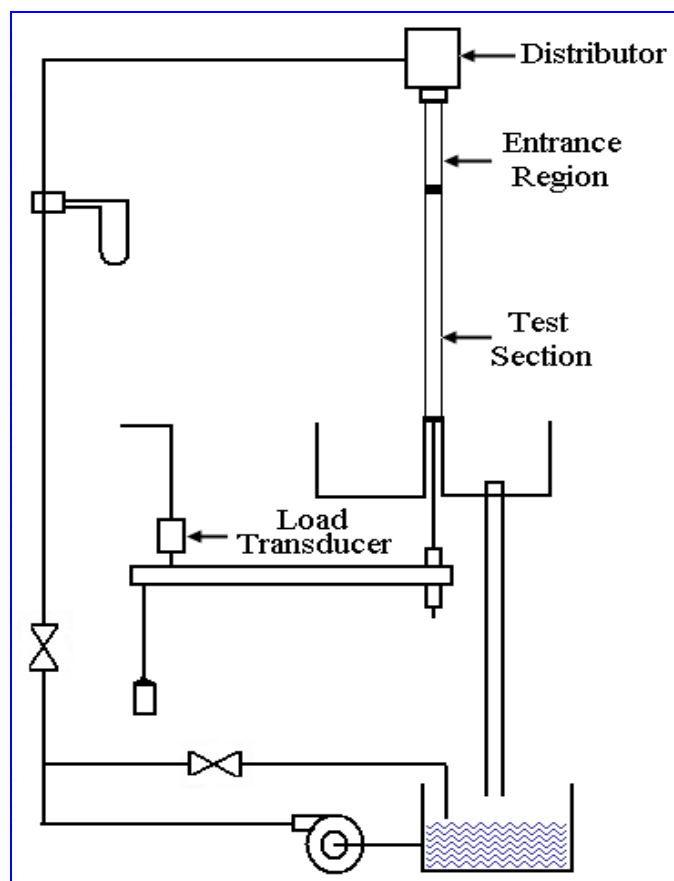


Figure 2.14 Weighing Method, (Aragaki, et al, 1987)

### 2.3.2.2 Localised methods

This group of methods includes techniques that give localised measurements of the thickness of the film (of the order of a few millimetres to a few centimetres averaged over a given area), from which it is not possible to obtain an instantaneous point value. This group includes the most common techniques used for film thickness measurement, probably because of their relative ease of use and general applicability to most flow systems. The *Capacitance probe* (Huang et al., 2005), comes into this category and it works on the principle that a pair of electrodes will give a measurement of the local capacitance which be function of the thickness of the film between them. The *Conductance probe* (Geraci et al., 2007), is probably the single most widely used device for measuring the time varying film thickness. Essentially, the conductance is measured using a circuit containing a pre-determined electrode configuration and the readings are amplified and displayed by some output device. Film thickness can be determined from such conductance measurements if a

calibrated linear relationship can be established between the two parameters within the range of measurements.

A large number of measurement techniques are based on the *Absorption of Electromagnetic Radiation*, (Tibirića et al., 2009), for which Beer's law applies:

$$\delta = -\frac{1}{\varphi} \ln\left(\frac{i}{i_o}\right) \quad 2.11$$

where:  $\delta$  is the thickness of the material,  $\varphi$  the linear absorption coefficient of the material,  $i$  the emergent intensity, and  $i_o$  the incident intensity of the monochromatic collimated beam.

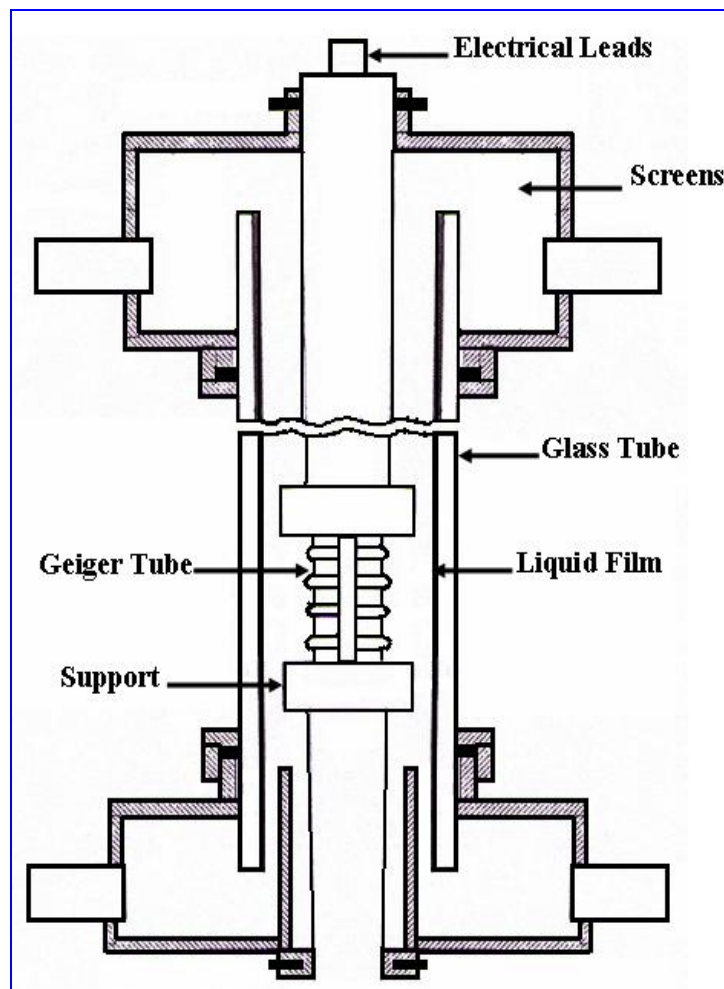


Figure 2.15 Absorption of Electromagnetic Radiation, (Jackson, 1955)

First the system is calibrated. Then a collimated beam of radiation is passed through the liquid film, and the intensity of emergent radiation is measured by a suitable detector. This can be used to determine the thickness  $\delta$ . An old, rarely used and somewhat dangerous technique is *Radioactive Emission*, (Jackson, 1955), where a radioactive substance is dissolved in the flowing liquid and radiation emission measured by a Geiger-counter or other suitable detector, see Figure 2.15. The local volume of liquid (i.e. the film thickness) will be proportional to the radiation detected. This is an averaging technique which gave reasonable results but was largely abandoned for health and safety reasons.

A measurement method with considerable advantages in industrial applications is the *Ultrasonic Pulse-Echo Method* (Wada, et al., 2006). This involves the measurement of the transit time of a sound wave transmitted and received by a single ultrasonic transducer. The transit time can be combined with knowledge of the speed of sound in the liquid to determine the film thickness.

### 2.3.2.3 Point methods

This group includes all methods in which continuous or statistical information is obtained at a point in a liquid film where film thickness can be measured over small areas i.e. up to  $1\text{mm}^2$  or  $1\mu\text{m}^2$ , (Franco, 2007). These methods have not been as extensively used as localised methods because, generally, they are harder to implement and the results more difficult to analyse. Because of its relative simplicity of operation and its wide applicability to most types and thicknesses of conducting liquid films, the *Needle Contact Probe* (Fossa, 1998) is the most popular film thickness measurement device. The probe consists of a needle, the body of which is electrically insulated, mounted on a moveable rod. An electrode is inserted flush into the wall over which the film flows.

The needle and moveable rod are placed directly opposite the electrode. The rod is gradually moved forward until the conducting tip of the needle just makes contact with the surface of the film. A conduction path now exists between the needle and the electrode and a current flows. The distance moved by the rod will, by subtraction,

give the thickness of the film. A similar technique to the needle contact probe is the *Hot-wire Method* (Franco, 2007), where the simple needle probe is replaced with a hot-wire probe. However, this technique suffers from inaccuracy when waves are present in the film surface.

The *Fibre-Optic Techniques* (Addlesee and Cornwell, 1997; Ohba et al., 1984) uses a sensor pick-up head mounted flush in the wall surface over which the liquid film flows. This sensor consists of a central optic fibre carrying a beam from a laser, and six receiving fibres surround the transmitting fibre and are joined tightly to it. Light from the laser travels along the transmitting fibre into the liquid where some of it is reflected at the surface of the liquid film at the gas core interface. Some of this reflected light enters the six receiving fibres, each of which has a photo-detector at its end. The intensity of the reflected laser light will have a different value depending on film thickness, the angle made by the film surface with respect to the wall, and the position of the individual fibre. By suitably processing the output from all six photo-detectors film thickness can be found, (Yu and Tso, 1995).

The *Interfacial Reflection Techniques* (Hurlburt and Newell, 1996), has the laser outside the pipe carrying the multiphase flow, aimed at a translucent white coating on the outer surface of the pipe, see Figure 2.16.

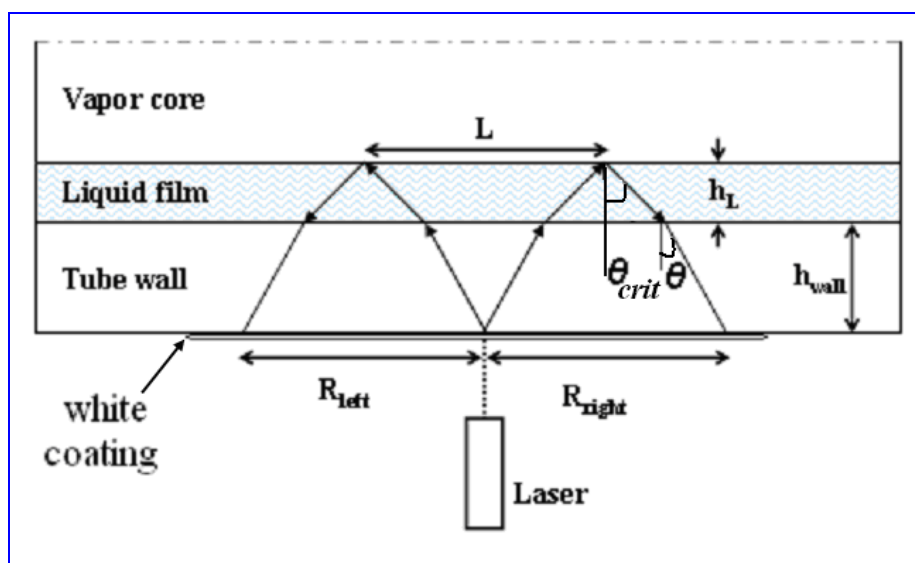


Figure 2.16 Interfacial Reflection Techniques (Hurlburt and Newell, 1996)

This generates a single wavelength hemispherical light wave travelling outwards from the point where the laser met the coating. The wave front will follow the laws of reflection and refraction and will be symmetrically reflected from the liquid surface at the critical angle. By detecting the reflected beam and knowing the optical properties of the liquid the film thickness can be found. Of course, the liquid and the pipe must be transparent to the wavelength of light used.

The reflected light images were recorded using a video camera with approximately 16 sample frames processed at each operating condition. The distance between the point source and the point where the light reflected from the film surface reaches the white coating ( $R_{ref}$  - shown as  $R_{right}$  and  $R_{left}$ ) can be geometrically related to the film thickness ( $\delta$ ) by the following expression:

$$R_{ref} = R_o + 2\delta \tan \theta_{crit} \quad 2.12$$

where:  $\theta_{crit}$  is the critical angle, and  $R_o$  is the contribution due to wall thickness given by:

$$R_o = 2h_{wall} \tan \theta \quad 2.13$$

where:  $h_{wall}$  is pipe wall thickness.

The wide range of film thickness measurement methods available makes a single recommendation difficult. It is more appropriate to consider a technique's suitability depending on the type of film and the thickness measurements required (Clark, 2002). However, for information on local film thickness, conductance/capacitance probes are probably the best unless such factors as measurement location or fluid properties prevent their use. These devices are relatively easy to use, not too expensive and reasonably accurate.

In this present work the flows used are vertical, i.e. axisymmetric film properties can be assumed, hence either point of localised methods are suitable to give the averaged film thickness and velocity. The conductance method (localised technique) was

chosen to measure the film thickness and the film velocity (with the aid of the cross-correlation technique), see Sections 3.3.3, 4.2 and 6.1.

### 2.3.3 Cross-correlation technique

Consider two pairs of identical sensors separated by a known distance  $L$  along a pipe axis. As a disturbance passes the upstream sensor there is a momentary change in its output signal. The disturbance is carried with the flow with minor changes (due for example to turbulence) to the downstream sensor where it causes a similar but not identical change in the output signal. The time delay between these changes in output signal at the two sensors is equal to the time taken for the particle to travel the distance between the sensors. This is inversely proportional to the mean flow velocity. To determine the mean flow velocity, the time lag between the changes in output signal is found by using statistical methods known as cross-correlation, (Ferrari et. al, 2005).

This method can be summarised by:

$$R_{xy}(\tau) = \lim_{T \rightarrow \infty} \frac{1}{T} \int_0^T x(t - \tau) \cdot y(t) dt \quad 2.14$$

where:  $R_{xy}(\tau)$  is defined as the cross-correlation function between the output from the two sensors which are referred to as  $x(t)$  (from the upstream sensor) and  $y(t)$  (from the downstream sensor).  $T$  is the total time period for which data was acquired.

$R_{xy}(\tau)$  reaches a maximum value when  $\tau$  is equal to the mean time for the perturbations in the relevant property of the flow to travel from upstream sensor X to downstream sensor Y. This maximum value occurs when  $\tau = \tau_p$ . Hence,  $\tau_p$  can be found by determining the value of  $\tau$  at which  $R_{xy}(\tau)$  is a maximum, see Figure 2.17.

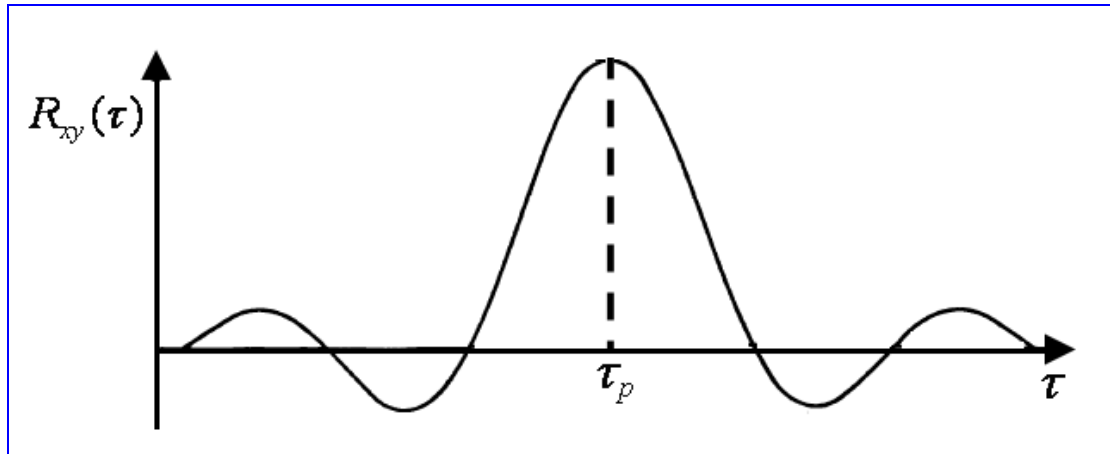


Figure 2.17 A representation of the cross-correlation function Ferrari et al, 2005)

The average flow velocity  $\bar{U}$  can be calculated, as:

$$\bar{U} = \frac{L}{\tau_p} \quad 2.15$$

where:  $L$  is the separation distance between the two pairs of identical sensors.

Since Beck, Beck and Plaskowski (1987), successfully used cross-correlation for flow measurement this technique has been increasingly used. The outstanding advantages of cross-correlation flow measurement systems make them particularly suitable for industrial applications where they provide flexibility for measuring multiphase fluid flow in hostile environments. Importantly, a large number of different types of transducer can be used with this technique which enables the probes to be designed so that they do not present an obstruction to the flow. Many practitioners believe that cross-correlation is superior to other existing methods for gas-liquid two phase measurement.

The cross-correlation technique has been developed extensively by different researchers, including Lucas, et al., 1987. Other researchers have built sensor systems including capacitance sensors, conductivity sensors, and electrodynamic sensors, (Beck and Plaskowski, 1987). All of these systems have been successfully operated in the laboratory and a wealth of accumulated experience is available. Cross-correlation has been adopted in this research to measure the liquid film velocity.

In this study a conductance cross-correlation technique has been used. Sensors which are sensitive to the disturbances in the properties of the liquid film in annular flow were constructed. It was possible to build a film velocity measurement system using two of these conductance sensors to measure the actual speed with which disturbances in the film propagate downstream.

#### 2.3.4 Entrainment

The liquid forming the film is continuously entrained drawn into the gas core as droplets and, simultaneously, the droplets in the gas core are continuously deposited onto the film in a process called droplet deposition. A fully developed annular flow means that the two processes are in dynamic balance and the mass flow rate of liquid droplets in the gas core remains constant. The liquid entrainment fraction (or liquid entrained fraction or liquid atomisation) is the ratio of the: mass flow rate of the liquid droplets in the gas core to the total mass flow rate of the liquid phase, both core and film (Pan and Hanratty, 2002).

$$E = \frac{W_d}{W_d + W_f} \quad 2.16$$

where:  $W_d$  is the mass flow rate of the liquid droplets (kg/s) and  $W_f$  is the mass flow rate of the liquid in the film (kg/s).

In this study, liquid entrainment is limited to the process where part of the liquid phase is entrained into the gas core as a result of gas flow “shearing off” the wave crests and carrying them in the form of droplets. Knowledge of the entrainment fraction and the amount of the liquid flowing as a liquid film is needed to develop better design procedures for vertical annular gas-liquid flows but the entrainment rate of the droplets from the liquid film is the greatest uncertainty in the mass balance of the liquid film (de Bertodano, et al., 1997).

A number of regimes of film behaviour have been identified in upwards annular two-phase flow (Pu et al., 2006). At low film flow rates it has been found that there is little or no entrainment of drops because the film experiences only small ripples. The critical value below which no entrainment occurs has been given by Owen and Hewitt, (1987) in terms of a film Reynolds number:

$$\text{Re}_{w,crit} = \exp\left(5.8504 + 0.4249 \frac{\mu_g}{\mu_l} \sqrt{\frac{\rho_l}{\rho_g}}\right) \quad 2.17$$

where:  $\mu_g$  and  $\mu_l$  are the gas and liquid dynamic viscosities (kg/ms) respectively and  $\rho_g$  and  $\rho_l$  are the gas and liquid densities (kg/m<sup>3</sup>) respectively.

In a number of reported investigations (Drosos, et al., 2006; Rodríguez and Shedd, 2004; Nigmatulin, et al., 1996), the critical liquid flow rate increased with increasing gas flow rate.

### 2.3.4.1 *Entrainment mechanisms*

There are three well-known mechanisms by which the liquid film is entrained into the gas core in vertical upward annular flow: **(a)** wave entrainment, **(b)** entrainment by bubble bursts, and **(c)** entrainment by droplet impingement. It is widely accepted that after waves have been generated in the flow, wave entrainment is the dominant entrainment mechanism, and the other two mechanisms may be neglected. This is supported by the findings of William, et al., (1996, 2007), Azzopardi and Sanaullah (2002) and de Bertodano, et al., (2001). Two different mechanisms were identified for the wave entrainment. The first, termed bag break-up, occurs at lower gas and liquid flow rates, see Figure 2.18.

At higher flow rates Azzopardi (1983) has reported that a second mechanism occurs in which the crests of roll waves were elongated and thin ligaments were torn from the film, see Figure 2.19. These ligaments immediately broke down into drops. These mechanisms are similar to those which occur when large drops are distorted and broken up by a gas stream (Azzopardi, 1997), see Figure 2.20.

The bag break-up mechanism, Figure 2.18, occurs at lower gas velocities (those that are easier to observe) and is considered to be the more important. However, the ligament mechanism, Figure 2.19, is relevant over greater ranges of flow rates.

It was observed that when two waves within the liquid film collided, a number of drops were ejected from the film and entrained into the gas core. This effect is described as the wave coalescence entrainment mechanism. Hewitt and Govan, (1990) studied the mechanism of bubble impact. With annular flow some liquid drops in the gas core will be re-deposited onto the liquid film and their impact will cause some smaller droplets to be ejected from the film and entrained into the gas core, see Figure 2.21.

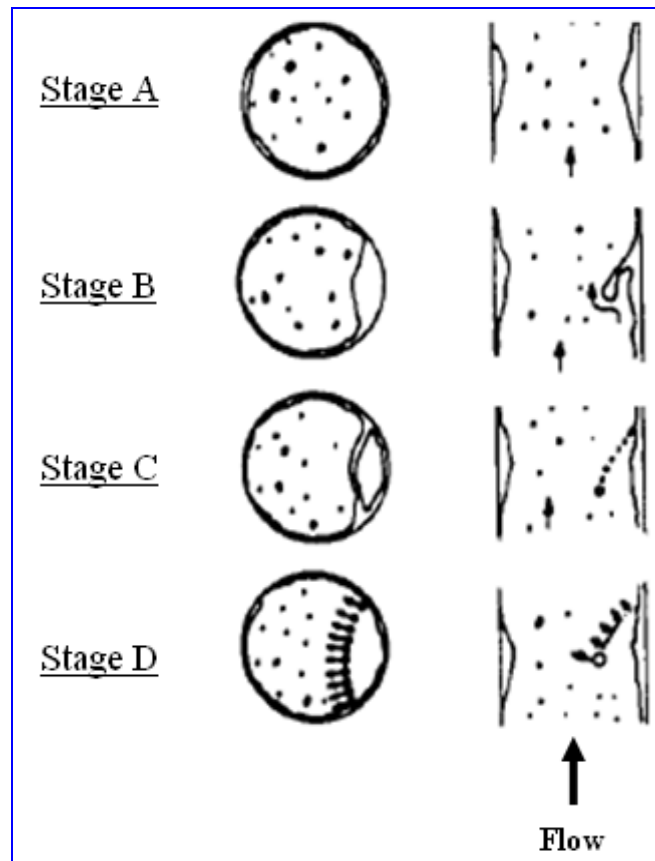


Figure 2.18 Bag break-up mechanism (wave) (Azzopardi, 1997)

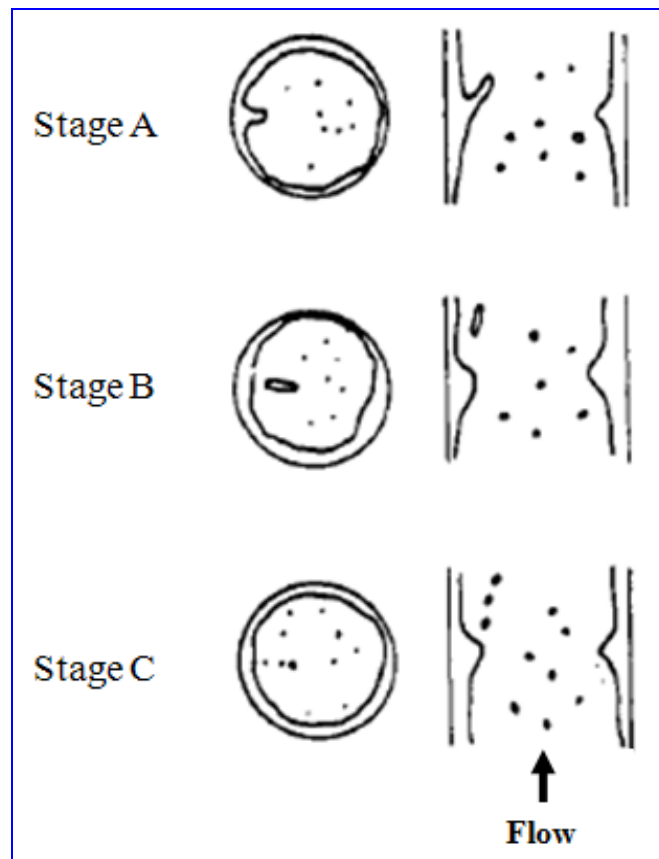


Figure 2.19 Ligament break-up mechanism (wave) (Azzopardi, 1997)

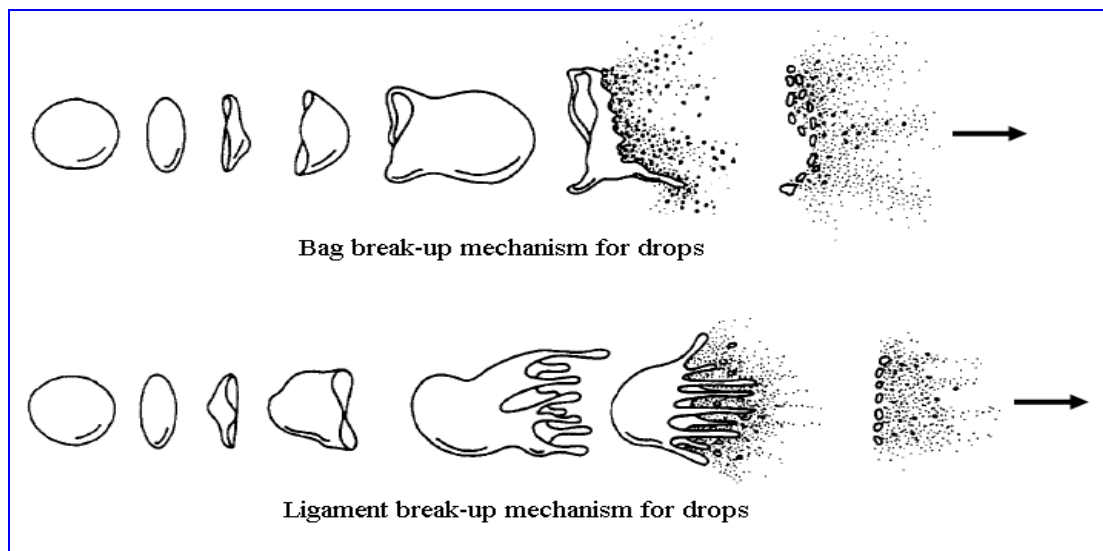


Figure 2.20 Bag break-up and ligament break-up mechanisms (of large drops in the core) (Azzopardi, 1997)

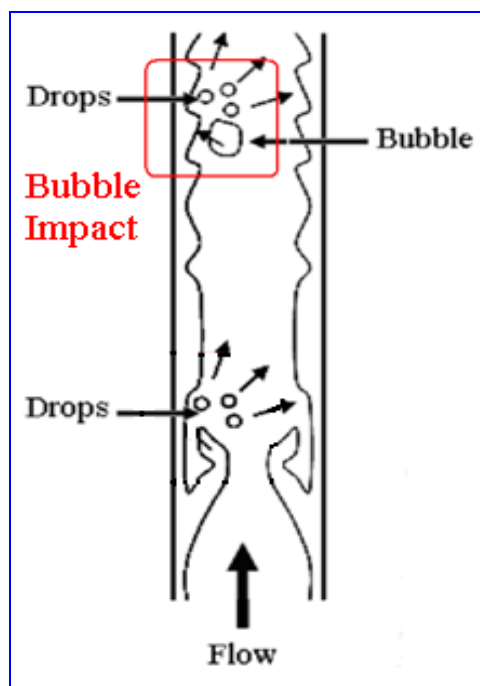


Figure 2.21 Schematic representation of film disturbance causing entrainment (Azzopardi, 1997)

While the detailed exact mechanism as to how the liquid droplets are generated out of a disturbance wave is still controversial, there is fundamental recognition that liquid entrainment is due to the wave crest being sheared-off into the gas core. Several wave entrainment mechanisms have been proposed to fully or partially explain this shearing-off process but so far there is no solid and direct evidence to favour any particular one.

#### 2.3.4.2 Correlations for Entrainment

So far no simple scheme has been developed for measuring entrainment rates and it is not yet possible to remove drops from the gas core without causing substantial disturbance to the flow. Unfortunately, while initial rates of entrainment immediately after the creation of the liquid film may be found, it is not possible to use these values as the steady state entrainment rate because the flow is developing and some time and development length is required before equilibrium is established. Equally, it is not possible to get close to the disturbance waves from which the drops are created because they are moving along the tube.

In annular two-phase flow, the droplet entrainment usually coexists with the droplet deposition. Thus, the measurement of entrainment rate is difficult and few results of direct measurement were reported in literature. Consequently, many correlations for the entrainment rate were developed from experimental data. The literature review indicated that a number of experimental and theoretical works have been conducted for the droplet transfer in annular two-phase flow but further improvements of the correlations for the deposition and entrainment rates are still required because of their significant importance in many practical applications.

Basing their ideas on the experimental observation that the disturbance waves traversing the liquid film surface are the main source of droplet entrainment, Nigmatulin, et al., (1996) developed the following equation for the prediction of the entrainment fraction  $E$  in quasi-equilibrium annular flow:

$$E = \tanh(7.25 \times 10^{-7} We_w^{1.25} Re_w^{0.25}) \quad 2.18$$

where:  $We_w$  and  $Re_w$  are liquid Weber number and Reynolds number, respectively.

They are defined as:

$$We_w = We_g \left( \frac{\Delta\rho}{\rho_g} \right)^{1/3}, \quad We_g = \frac{\rho_g U_{g,s}^2 D}{\beta} \quad 2.19$$

where:  $We_g$  is the gas Weber number,  $\rho_g$  is the gas density ( $\text{kg/m}^3$ ),  $U_{g,s}$  is the gas superficial velocity (m/s),  $D$  is the pipe diameter (m),  $\Delta\rho$  is the difference between the water and gas densities ( $\text{kg/m}^3$ ) and  $\beta$  is the surface tension (N/m).

and

$$Re_w = \frac{\rho_w U_{w,s} D}{\mu_w} \quad 2.20$$

where:  $\rho_w$  is the water density ( $\text{kg/m}^3$ ),  $U_{w,s}$  is the water superficial velocity (m/s),  $D$  is the pipe diameter (m) and  $\mu_w$  is the water dynamic viscosity (kg/ms).

Pan and Hanratty (2002) extended an idea first developed by Kataoka et al. (1983), that the entrainment mechanism was only present when the film mass flow rate was above a critical film flow rate  $W_{f,crit}$  (kg/s) and gave an entrainment relation based on the atomization of the film due to the Kelvin–Helmholtz mechanism:

$$E = \frac{K_A U_{g,s}^2 \sqrt{\rho_g \rho_f}}{\beta} \left( U_f - \frac{W_{f,crit}}{f_f(z)} \right) \quad 2.21$$

where:  $K_A$  is approximately  $3 \times 10^{-6} \text{ s}^2/\text{kg}$ ,  $U_{g,s}$  is the gas superficial velocity (m/s),  $U_f$  is the liquid film velocity (m/s),  $\beta$  is surface tension (N/m), and  $\rho_g$  and  $\rho_f$  the gas and film densities respectively (kg/m<sup>3</sup>).

Recently, Sawanta, et al., (2008) published a new and simpler entrainment correlation derived from non-dimensional analysis which successfully collapsed trends in experimental entrainment data. They correlated their entrainment fraction  $E$  to the standard Weber number  $We$  as:

$$E = E_m \tanh(a We_g^{1.25}) \quad 2.22$$

where:  $We_g$  is the gas Webber number:

$$We_g = \frac{\rho_g U_{g,s}^2 D}{\beta (\Delta\rho/\rho_g)^{1/4}} \quad 2.23$$

$$E_m = 1 - \frac{Re_{w,crit}}{Re_w} \quad 2.24$$

where:  $Re_{w,crit}$  is the limiting Reynolds number under which no entrainment occurs and is defined in Equation 2.17.

$$a = 2.31 \times 10^{-4} Re_w^{-0.35}, \beta = 0.00719 \text{ N/m} \quad 2.25$$

The relationships representing the entrainment rate available in literature have been reviewed by Patruno (2009), Azzopardi and Wren (2004), Matsuura (1995) and Schadel, et al., (1990) amongst others. They carried out experimental investigations to find a relationship for the deposition rate and have reported that the relationship they deduced predicted the experimental data well. However, this is somewhat circular since the relationships were based primarily on the respective experimental data. It means, however, that the validity of the expressions over wider ranges of flow and thermal conditions is clear.

Okawa, et al., (2000), Govan and Hewitt, (1990) and Sugawara (1990) have all attempted to use available experimental databases to develop expressions for the entrainment rate which would be useful to the better understanding of the relative influence of different parameters such as gas velocity, fluid properties and droplet concentration. Unfortunately, good agreement with the accumulated experimental data was not obtained. Recently Peng (2008) gathered experimental data on deposition rates measured in dilute particle concentrations. It was found that the particle relaxation time (droplet responsiveness to a change in fluid velocity, Barbosa, et al., 2002) correlated well with the deposition mass transfer coefficient (the ratio between the rate of droplet deposition and droplet concentration in gas core, Okawa, et al., 2000).

#### *2.3.4.3 Measurement techniques for entrainment*

Most experimental studies have concentrated on measurements of the liquid film attached to the wall or the entrained liquid droplets dispersed in the gas core in order to obtain an entrainment fraction. The most common methods reported in the literature for entrainment fraction measurements can be categorized into two main groups: **(a)** the sampling probe method, and **(b)** the liquid film removal method. The former method is used to sample the entrained liquid droplets in the gas core while the latter is used to collect the liquid film flowing on the inner tube wall. In addition, a tracer measurement method was also reported.

*The sampling probe method*, also called the *isokinetic probe method*, involves droplet flux measurements at different positions across the diameter of the tube. The average is obtained from the integral of the droplet flux over the tube cross-section. Figure 2.22 shows the main parts of the isokinetic probe for flow sampling used by Tayebi et al., (2000). It consists of a spool piece; a sampling tube with an L shape sampling probe inserted in the pipe core to collect the liquid droplets; a traverse mechanism; a manual valve to control rate of withdrawal to assure isokinetic conditions i.e. the superficial velocity of air flowing through the sampling probe is equal to that in the test section; a small separator and a glass measuring cylinder.

The isokinetic probe method requires removing some of the flowing mixture from the pipe. The simplest way is to insert a small sampling probe into the flow at a relevant position in the gas core. Those small droplets in the gas stream which impact the mouth of the probe will flow more or less unobstructed into the probe and are collected downstream. In this way, the droplet flux and the gas velocity at the location of the probe mouth can be found, and the total liquid entrainment can be determined from the integration of the droplet flux over the cross-sectional area of the tube.

A differential pressure-cell,  $D_p$ , is used to achieve the pressure measurement required to establish the isokinetic conditions. One side of the  $D_p$  can be connected to the tip of the probe and the other side is connected to the probe body. Usually, there is a connection to high pressure gas which is used to clean the pressure tapings when a new sampling is prepared. The channels used to measure the pressure difference are usually filled with some liquid after sampling for some time. There is, therefore, a limited time available to adjust the flow to isokinetic conditions.

Barbosa et al, (2002) amongst others have developed this method (i.e. isokinetic probe method) but one remaining limitation is its inability to take measurements near the core/film interface due to the sampling of part of the liquid in the waves.

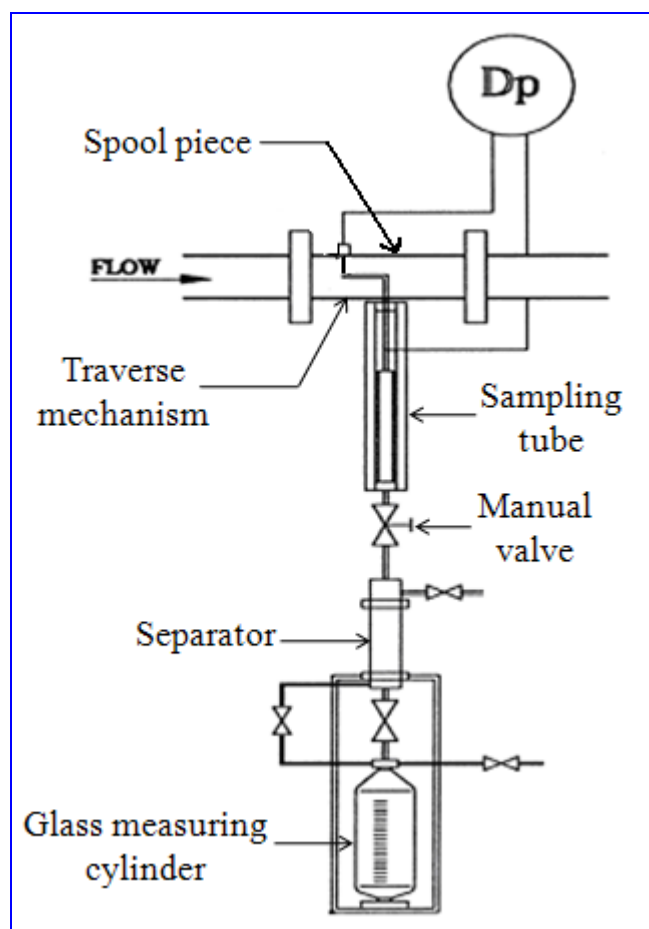


Figure 2.22 Sampling technique by an isokinetic probe, (Tayebi, et al, 2000)

The *liquid film removal* (also known “*liquid film withdrawal*” or “*liquid film extraction*”) is a technique for liquid film extraction through a porous wall or a small opening on the tube wall, see Figure 2.23. Gamisans et al., (2004), Wadekar (2002) and Richardson and Rubin (2001) have all used this method. The advantage of this method is that the liquid entrainment fraction can be directly measured by collecting the liquid droplets after a separation process has been performed. Also, the entrainment fraction can be calculated from the difference between the total liquid flow rate and the liquid film flow rate which is measured by collecting the liquid film through the porous wall.

For low entrainment there are two serious disadvantages with this technique. First, it is difficult to completely separate the droplets from the gas stream. Second, the liquid entrainment fraction is calculated from the difference between total liquid and film flow rates, but if the entrainment is low enough, the difference between film flow rate and total liquid flow rate will be within the practical measurement error. Finally, this

method relies heavily on a subjective judgement on the basis of unaided eye observations, to judge the point of complete removal of the liquid film which can result in large measurement error.

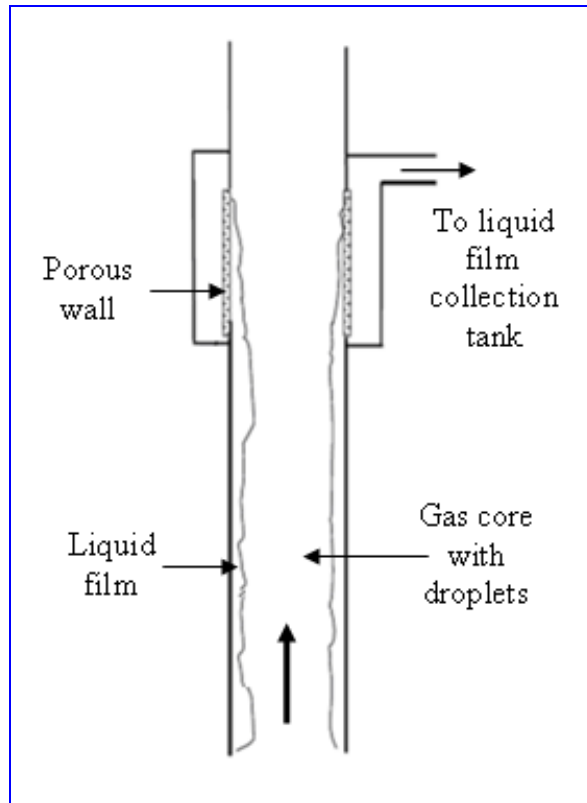


Figure 2.23 Liquid film removal method

However, this technique is widely used and it is generally believed that it is a technique that produces some of the more accurate results.

**The tracer measurement technique** involves the injection of a tracer, a dye or some other solution, into the liquid film and the measurement of its concentration at different locations downstream. Quandt (1965) was the first to report this method followed by Schadel, et al, (1990) who used it to determine the entrainment and deposition rates for vertical annular flows in various diameter tubes. Jonathan (2002) developed this technique into a novel method for measuring shear-stress. More recently Oriol, et al, (2008) used this technique to characterize two-phase flow regimes and liquid dispersion in horizontal and vertical tubes by using coloured tracer and a non-intrusive optical detector. Because it is a cumbersome technique with little accuracy it is not often used today.

## 2.4 Gas velocity measurements in annular flow

In gas extraction from high pressure natural reservoirs, a liquid phase appears as hydrocarbon condensates and water. In many applications the gas volume fraction is so high that the flow can be regarded as a wet gas. Presently there are two methods for the metering of this wet gas which have been described above - separating the two phases and metering each separately, and metering the overall two phase flow with a dry gas flow meter for which correction factors have been established. The latter is of growing interest these days.

In the laboratory there are a number of techniques used to measure the velocity or flow rate of a gas; including orifice plates, nozzles, Venturi tubes, Pitot tubes, vane anemometers and rate-of-cooling anemometer, etc. The difficulty in measuring the velocity of the gas in the core of annular flow arises from the presence of the liquid film. Below is list of some of the methods presently being used to measure the gas velocity in the gas core in annular flow.

A ***Pitot tube***, see Figure 2.24, is a simple and convenient device for measuring local velocity in fluid flow.

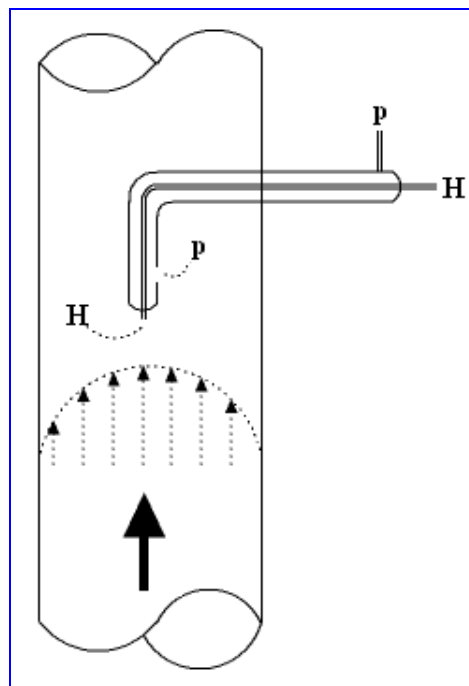


Figure 2.24 Pitot-static principle (Richard, 2001)

The Pitot tube, along with a differential pressure measuring device, generates a signal which represents the difference between the total or Pitot pressure  $H$  and the static pressure  $p$ . Static pressure,  $p$ , is the pressure measured at right angles to local flow velocity. The legs of the static pressure and total pressure tubes are connected to the legs of a manometer or to another appropriate device to measure the pressure difference ( $H-p$ ). If the Pitot tube is properly designed and the density of the gas  $\rho_g$  passing over the Pitot tube is known, the velocity  $v$  of the gas over the Pitot tube can be calculated using a standard formula:

$$\frac{1}{2} \rho_g v^2 = (H - p) \quad 2.26$$

**Hot-film anemometry** is based on the cooling of a high temperature metal film by a fluid flowing over it. The film is usually very thin (~0.05mm) and its electrical resistance will be proportional to its temperature. If the relationship between resistance and temperature of the film is known for static conditions, the difference in heat loss to the surrounding fluid can be measured and the local fluid velocity determined. Hot-film anemometry uses King's Law:

$$V_{wire}^2 = A + B u^n \quad 2.27$$

where:  $V_{wire}$  is the voltage across the wire (V),  $u$  is the velocity of the flow normal to the wire (m/s) and A, B and n are constants.  $n = 0.45$  is a common value for hot-wire probes (although in a research setting, it should be determined experimentally along with A and B). A and B can be found by measuring the voltage,  $V_{wire}$ , obtained for a number of known flow velocities and performing a least squares fit for the values of A and B which best fit the data.

These types of sensors have proven very efficient in turbulent flows. Velocity measurement using hot-film anemometer has some advantages in the direct continuous measurement of the gas-phase velocity field. It is also possible to measure the turbulence energy spectrum relatively easily. The uncertainty of this method is about 0.07% at 10 m/s velocity or less (Yoshida, 2005).

*Laser Doppler anemometry* uses the Doppler effect whereby the frequency of a wave is changed if it is reflected from a moving object. The Doppler shift in frequency occurs as light is dispersed from the surface of moving particles. The shift in the frequency of the light source (laser beam) is proportional to the velocity of the particles. The frequency shift is very different (from 1kHz up 100kHz) from the frequency of the light in the laser beam and thus it can be directly measured. Therefore, the arrangement using a prism to split the laser beam into two is usually used, see Figure 2.25.

The two beams from the laser source intersect each other in the measurement zone, because the path difference between the two beams is small where they meet a set of interference fringes are formed, provided that the liquid is transparent to the laser light. Particles in the fluid flow will not only disrupt the interference pattern then they pass through they will also reflect some light whose frequency is changed because of the Doppler effect. The system thus defines the position and speed of the particle, and these are obtained by analysis of the signals from the photo multiplier (Lioumbas, 2005).

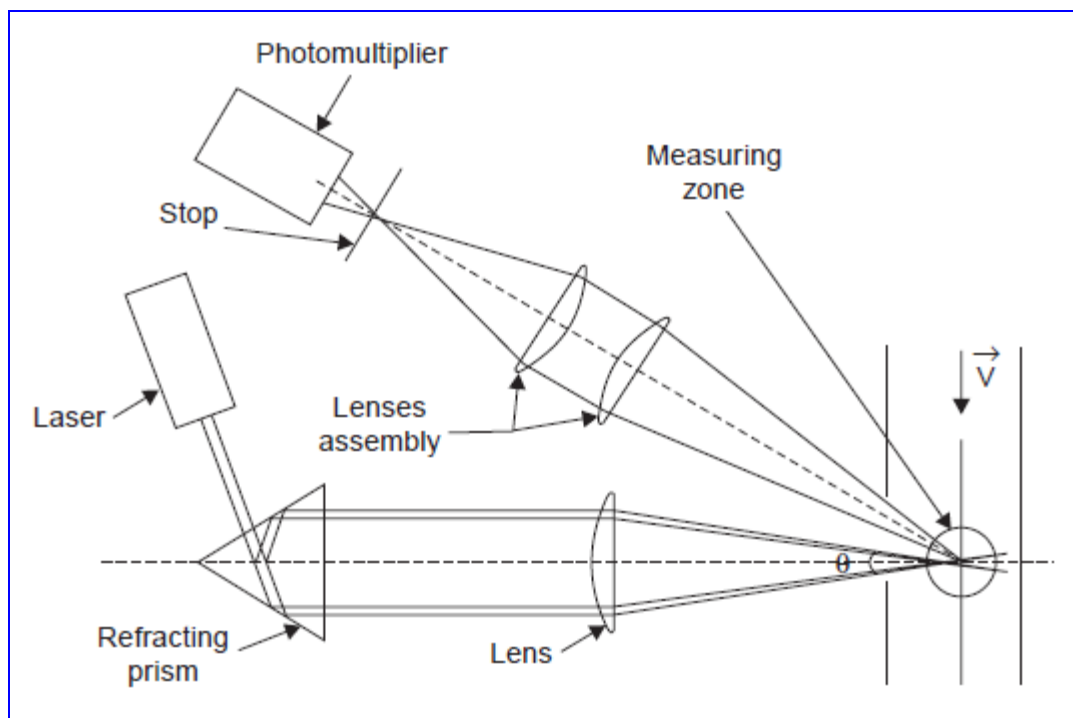


Figure 2.25 Laser-Doppler technique (Lioumbas, 2005)

These techniques, i.e. *Laser Doppler anemometry*, *Pitot tube* and *Hot-film anemometry*, are local gas velocity measurement (not global) which are used mainly in laboratories (not field applications). If the gas flow rate  $Q_g$  is required then the following expression is used:

$$Q_g = \int_A U_g dA \quad 2.28$$

where:  $Q_g$  is the gas volume flow rate ( $\text{m}^3/\text{s}$ ),  $U_g$  is the gas velocity ( $\text{m}/\text{s}$ ) and  $A$  is the pipe cross-sectional area ( $\text{m}^2$ ).

*Tracer techniques* used by e.g. Van't Westende, et al., (2007) measured the gas-velocity using '*tracer*'-droplets. Because the relaxation-time of the tracer-droplets (the time taken by the tracer droplets to attain equilibrium with the other droplets in the gas core of the annular flow) is less than, or of the same order as, the time-scale of the large-scale turbulence structures, the tracer-droplets are expected to follow the mean gas-velocity. An advantage of using droplets as tracers is that they are often already present in the flow.

The tracer technique is a measurement technique that offers little or no obstruction to the fluid flow and is capable of operating over a wide range of conditions including unsteady flow and both single and two phase flow (Hans and Windorfer, 2003). The ultrasonic flow meter will be introduced and discussed later in this chapter (see Section 2.4.2), and will also be used in this study.

These two techniques i.e. *Tracer techniques* and *Ultrasonic Flow Meters* are global techniques and can be used in laboratories or in the fields.

Baker (2000) has reported numerous other methods also exist. For example: positive displacement flow meters, vortex flow meters, thermal flow meters, etc., but these are not sufficiently relevant to this thesis for a review of them to be included here.

### 2.4.1 Wet gas metering systems in industry

The meters currently being used in the oil and gas industry to measure unprocessed natural gas flows are orifice plates, Venturi meters and (more recently) ultrasonic meters. Until quite recently, the vast majority of two-phase metering used orifice plate meters and only in the last few years have Venturi meters become the meter of choice. Industry now favours the Venturi meter despite it being more expensive, probably because orifice plates are more susceptible to damage by intermittent "slugs" in the pipeline or pressure pulses. However, the Venturi does offer a smaller total head loss than the orifice plate (Richard, 2001).

Of the four types of differential pressure (DP) meters available only the orifice plate and Venturi meters are in widespread use for unprocessed natural gas metering. The V-Cone (a patented device designed and manufactured by McCrometer Ltd.) is not in general use because it is relatively new and largely untested, and so not yet trusted by many industries (Svedeman, 1997).

The V-Cone, see Figure 2.26, is a differential pressure type flow meter with a design that conditions the flow prior to measurement. The V-Cone creates an annular opening, forcing the fluid to flow around a cone positioned in the centre of the pipe which creates a differential pressure.

The cone is shaped so that it "flattens" the fluid velocity profile in the pipe, creating a more stable signal across wide flow downturns ratios (downturn ratio is the ratio of the maximum water flow to minimum water flow). Flow rate is calculated by measuring the difference between the pressure upstream of the cone at the meter wall and the pressure downstream of the cone through its centre.

The original DP meter is the orifice plate. It has a tradition of use in all industries and an enormous amount of research has been carried out on it. Hence the simple orifice plate is cheap and is still in use. However, dry or wet natural gas wells invariably contain periodic slugs and pressure pulses both of which can cause substantial damage to the orifice plate. These slugs and pressure pulses are also why turbine meters are

not used in unprocessed natural gas production lines. As Ting and Jones (1996) said "the damage to turbine meters in this service would be unacceptable".

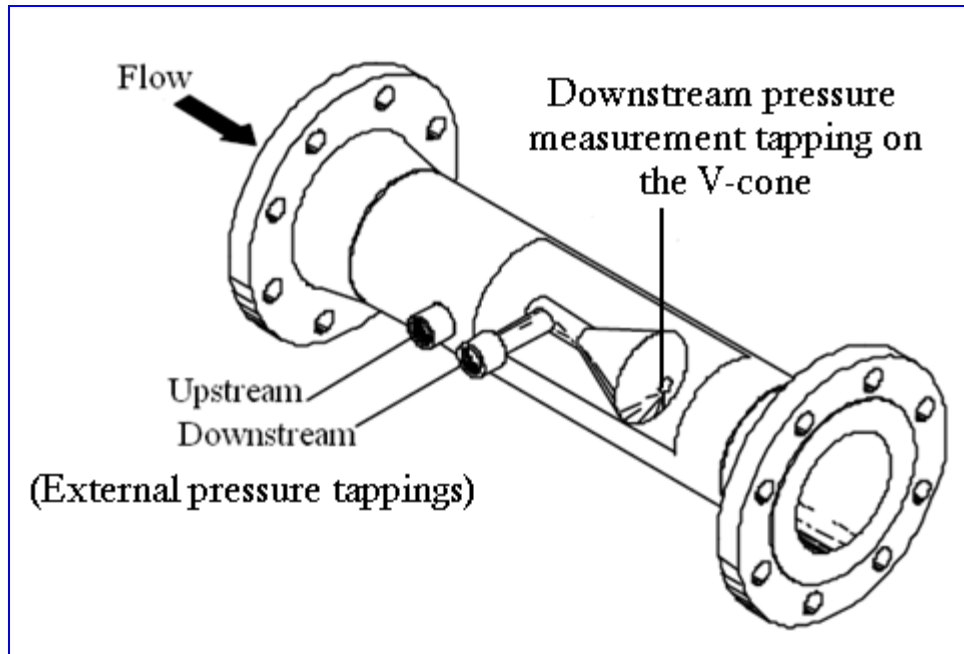


Figure 2.26 A typical V-Cone flow meter design (Svedeman, 1997)

#### 2.4.2 Ultrasonic flow meters

Ultrasonic waves are sound waves which have frequencies higher than those to which the human ear can respond. The engineering applications of ultrasonic waves can be divided into two categories: low-amplitude vibrations and high energies. In the former the effect of the medium on the incident waves is important, but in the latter the changes brought about on the medium by the waves is important. For measurement systems only low-amplitude ultrasonic waves alone are used.

The basic principle is that the required information about the measured medium can be obtained by using the reflection, absorption, and scattering effects of the medium on the incident ultrasonic waves. The first ultrasonic meters were available over half a century ago and manufacturers are now producing fourth or fifth generation products which have shown promise in both single-phase and two-phase flow metering tests (Lynnworth and Liu, 2006).

The ultrasonic signals required for flow measurement are transmitted and received by ultrasonic transducers so these are most important parts of any ultrasonic sensor. The transducers convert an electrical signal (e.g. a voltage pulse) into an acoustic signal (e.g. a sound pressure pulse), and vice versa. The temporal and spatial radiation characteristics of these components are the prime determinants of sensor performance. It is necessary to match the characteristics of any pair of sensors for use in an USFM, to avoid zero drift problems.

Real transducers must have a finite size in order to generate ultrasonic beams at adequate sound levels. The ultrasonic beam generated will have a definite directionality, the shape of the beam, its width, the number of side lobes, etc., are determined by the ratio of the acoustic wavelength to the effective size of the transducer. The smaller this ratio the more directional the transducer, that is the narrower the ultrasound beam. All acoustic beams spread so the sound pressure level gradually decreases along the beam.

For gas flow meters, the ultrasonic transducers are usually directly exposed to the inside of the pipe and have to endure corrosive gases, traces of liquids and particles, and large variations in pressure, temperature and humidity without compromising their acoustic performance to any significant degree. Thus in the real world many aspects of the functioning of ultrasonic transducers need to be taken into account to ensure an accurate, operationally safe and reliable metering system.

Piezoelectric transducers are generally used in such meters. Usually the surface of the transducer is a plane circle. However, the acoustic impedance of the piezoelectric element is much higher than that of the fluid and a matching layer or layers of suitable materials can be used between the fluid and the transducer to maximize the acoustic efficiency. The acoustic impedance of the matching layer will be between that of the fluid and that of the piezoelectric crystal.

Ultrasonic flow meters with piezo-electric transducers are commonplace for single phase liquids. However, difficulties arise when attempts are made to measure gas flow because of the big difference in acoustic impedance between the transducer and the

gas. Ultrasonic techniques as a new measuring method in multiphase systems have now been introduced by several teams of researchers (Lynnworth and Liu, 2006). The results show the possibility of simultaneously measuring both solids and gas volume fractions in a three-phase system.

There are strict limits on the applicability of ultrasonic flow meters to multiphase mixtures. Users who select an ultrasonic flow meter often do so for one (or more) of the following reasons: ultrasonic equipment provides a useful measurement whether or not the fluid is single-phase; the equipment is relatively easy to use; the flow regime can be laminar, transitional or turbulent; transducers are minimally invasive; there is no extra pressure drop; the instrument has a fast response; the instrument is generally reliable except at extreme temperatures; the capital and running costs are reasonable.

The most accurate ultrasonic flow meters recently available are quadrature or other special-path or multi-path configurations, with laboratory calibration accuracies typically 0.5% of reading, or better, over most of the meter's flow range (Lynnworth and Liu, 2006). Flow conditioners and straight piping contribute to achieving such accuracy despite flow disturbances in the upstream pipeline. With the meters ideally installed, the ultrasonic meter manufacturers claim an uncertainty of  $\pm 0.5\%$  for their products in dry natural gas flows, and as the meter uses a velocity based measurement it does not have the restrictions at high Reynolds number that DP meters do.

In this study, the Massa Model E-152/40, see Figure 2.27, was used in the designed USFM. This type is a miniature air ultrasonic transducer having many applications in short range sensing and remote control where non-contact is desired.

The transducer operates at 40kHz, its fundamental resonant frequency, thereby producing a relatively broad directional response, free of minor lobes. The corresponding wavelength at 25°C is 8.6mm. The housing and diaphragm are one piece and made from stainless steel to provide high resistance to corrosive atmospheres. Each transducer is provided with about 500mm of twisted pair cable potted in at the back of the housing. The same model was used all through the project

either as transmitter or receiver. One of the benefits of this model is that it operates at a fundamental resonant frequency which means other signals less or greater than 40kHz will not be detected.

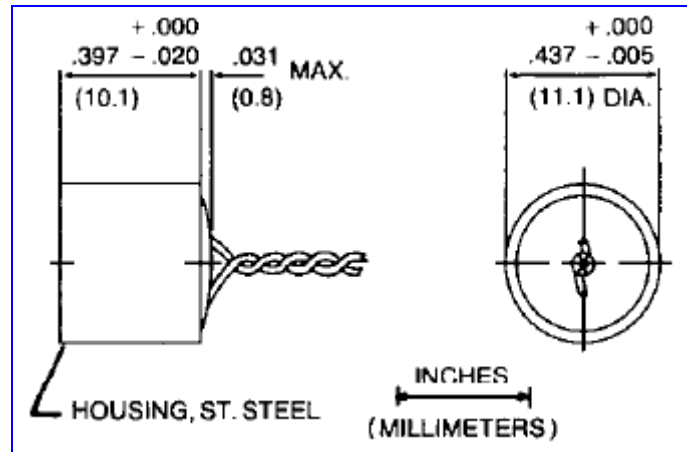


Figure 2.27 Massa transducer, model E-152/40

There is a wide range of ultrasonic flow meters available because the basic principles of these meters allow flexibility in design. Today, ultrasonic flow meters use contra-propagating transmission, single and multiple transducers, single and multiple paths, passive and active principles for liquid level sensing, for determination of flow rates in open channels or partially-full conduits, or pipes, and other interactions (Murakawa, et al., 2005). Ultrasonic meters measure the velocity of the gas flowing through the meter body. By knowing the velocity and the cross-sectional area, uncorrected volume flow rates can be found. The diagram below, Figure 2.28, shows a schematic of a commonly used configuration for an USFM.

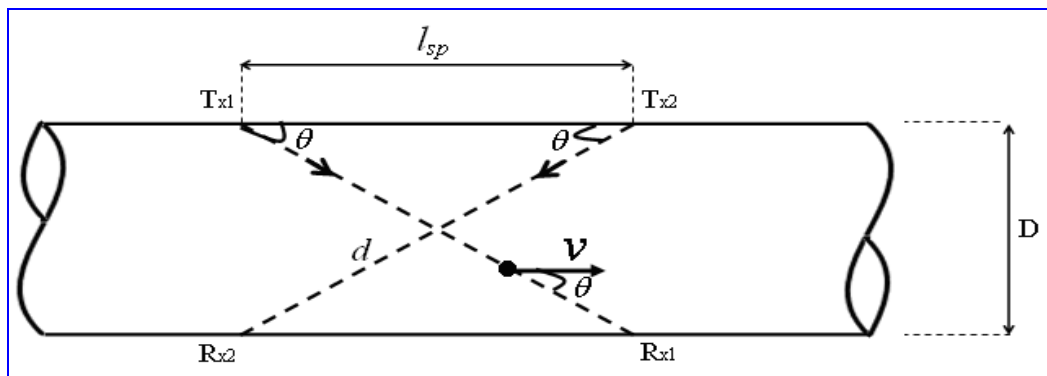


Figure 2.28 USFM common configuration

In Figure 2.28  $D$  is the inner pipe diameter (m),  $l_{sp}$  is the axial separation (m) between the transmitters (Tx1 and Tx2) and receivers (Rx1 and Rx2),  $d$  is the length (m) of the acoustic path,  $\theta$  is the angle (in degrees) between the acoustic path and a vector representing the direction in which the medium moves and  $v$  is the velocity of the moving medium (m/s).

To determine average velocity in a flow using the ultrasonic method, several assumptions are made, including constant path length  $d$ , constant speed of sound  $c$  and a mean velocity profile for a coordinate system. The distance which is travelled by the ultrasonic beam is given by:

$$d = \frac{D}{\sin \theta} \quad 2.29$$

The velocity of ultrasonic beam along the downstream path from Tx1 to Rx1  $v_d$  is given by:

$$v_d = c + v * \cos \theta \quad 2.30$$

The velocity of ultrasonic along the upstream path from Tx2 to Rx2  $v_u$  is given by:

$$v_u = c - v * \cos \theta \quad 2.31$$

where:  $v$  is the fluid velocity as shown in Figure 2.28.

We can see that the local propagation velocity of an acoustic signal in a moving medium is a function of both the velocity of sound in the fluid at rest and the velocity of the fluid. Since the value of  $c$  depends on the nature of the medium and on its thermodynamic state, it is opportune to use two different wave trains that have the same directions but opposite propagation modes. This gives rise to a difference between the downstream propagation velocity  $v_d$  and the upstream one  $v_u$  (see Equations 2.30 and 2.31).

Spendel (1985) stated three basic modes of operation used for the measurement of the time difference between upstream and downstream times of flight. The modes of operation are:

- the leading edge system
- the phase comparison system
- the frequency (sing-around) system

These systems and the one chosen for research project will be discussed later in detail in Chapter 3.

Ultrasonic meters appear to be giving good results for dry natural gas production flows (they appear to give similar accuracy to the Venturi meter, Hans and Windorfer, (2003) provided they are installed in the pipe work far enough from any disturbance to the flow. The system has no moving parts, does not create an additional pressure drop and is insensitive to fluctuations in gas composition. Its fast response allows measurement in transient or pulsating flows and it provides bi-directional flow measurement. Finally, this system can greatly reduce installation and maintenance costs.

However, these significant advantages of ultrasonic meters in dry natural gas are offset by some significant problems when they are used to meter natural gas in the production environment. Poor meter location seriously affects the ultrasonic meter. If the meter is too close to bends, valves or other obstructions, the resulting swirl and/or turbulence can seriously affect the velocity profile and hence the accuracy of the flow rate measurement. In addition, the bonding material used in the manufacture of the ultrasonic transducers tends to fail at temperatures in excess of 150°C and when there is a sudden pressure fluctuation (Richard, 2001).

## CHAPTER 3 PRELIMINARY WORK AND THEORETICAL ANALYSIS

This Chapter presents a number of important preliminary tasks that were carried out concerning the experimental procedures and design work. These tasks were a necessary prerequisite for making decisions about certain aspects of the design and modelling of the wet gas metering technique. Additional information on each system will be given in Chapter 4 when describing their design and calibration.

### 3.1 Conditions for establishing annular flow

#### 3.1.1 Flow rates and superficial velocities

The conditions for air-water annular flow were obtained from the Govier and Aziz (1972), flow pattern map, see Figure 3.1. For a 1 inch (25mm) pipe we get annular flow when the gas superficial velocity is about 100 times the water superficial velocity:

$$U_{g,s} \cong 100 U_{w,s} \quad 3.1$$

where:  $U_{g,s}$  is the gas superficial velocity (m/s) and  $U_{w,s}$  is the water superficial velocity (m/s).

The superficial velocity is defined as the equivalent velocity that each phase would have, when passing through the pipe on its own. In terms of the volumetric flow rates:

$$\frac{Q_g}{A} \cong 100 \frac{Q_w}{A} \quad 3.2$$

where:  $Q_g$  and  $Q_w$  are the volumetric gas and water flow rates (m<sup>3</sup>/s) respectively and  $A$  is the pipe cross-sectional area of the pipe (m<sup>2</sup>).



To find the mean flow velocities for each phase for the onset of annular flow we must know the gas volume fraction. For a 50mm ID pipe ( $A=1.963 \times 10^{-3} \text{ m}^2$ ), the values for gas and water superficial velocities (25.8m/s and 0.25m/s, respectively) of Han are assumed to give achieve annular flow. Since we are dealing with high gas flow rate and volume fraction, the gas volume fraction was taken as  $\alpha_g \cong 0.95$ :

$$\therefore U_g = \frac{U_{g,s}}{\alpha_g} = 27.2 \text{ m/s} \quad 3.3$$

The water volume fraction is assumed (to be consistent with the gas volume fraction assumption of 0.95)  $\alpha_w \cong 0.05$  then:

$$U_w = \frac{U_{w,s}}{\alpha_w} = 5 \text{ m/s} \quad 3.4$$

To predict the approximate volume flow rates of gas and water to establish an annular flow rate in a pipe of 50mm internal diameter (cross-sectional area  $A=1.963 \times 10^{-3} \text{ m}^2$ ), will be (from Equations 3.3 and 3.4):

$$Q_w = U_w \alpha_w A = 5 \times 10^{-4} \text{ m}^3/\text{s}$$

$$\therefore Q_w \cong 29 \text{ litre/min} \quad 3.5$$

$$Q_g = U_g \alpha_g A = 0.049 \text{ m}^3/\text{s}$$

$$\therefore Q_g \cong 3034 \text{ litre/min} \quad 3.6$$

This step is essential in the selection of the right monitoring instruments for the flow loop, see Chapter 5 and indicates that to establish an annular flow in the 50mm pipe, it will require values of water and gas volumetric flow rates of at least 29 litre/min and 3034 litre/min, respectively. Thus an air supply of at least 3034 litre/min ( $178 \text{ m}^3/\text{hr}$ ) is required and so it was ensured that the available laboratory air supply, from a compressor, could maintain that flow rate.

### 3.1.2 Pressure drops

Pressure drop or head loss, occurs in all piping systems because of elevation changes, turbulence losses caused by abrupt changes in direction, and friction within the pipes and fittings. The following calculation was carried out in order to obtain the pressure drop over the 2m length test section in the annular flow rig i.e. the minimum required pressure into the test section. The total pressure drop  $\Delta P_{Total}$  is a combination of the hydrostatic pressure drop  $\Delta P_{hydrostatic}$  and the frictional pressure drop  $\Delta P_{fric}$ :

$$\Delta P_{Total} = \Delta P_{hydrostatic} + \Delta P_{fric} \quad 3.7$$

$$\Delta P_{fric} = \frac{\rho_a h_{ts} f_{fric} U_a^2}{R} \text{ (Darcy's Law)} \quad 3.8$$

where:  $\Delta P_{fric}$  is the pressure drop due to frictional losses,  $h_{ts}$  is the length of pipe forming the test section of the flow loop (m),  $\rho_a$  is the air density ( $1.25\text{kg/m}^3$ ),  $f_{fric}$  is the friction factor of the pipe = 0.007 (MacGillivray, 2004),  $U_a$  is the mean flow velocity of the air (m/s).  $R$  is the pipe radius (m).

In a 50mm diameter pipe and 2m long, considering  $U_g = 27.2\text{m/s}$  is a good approximation of the gas velocity because water friction is low then using Equation 3.8  $\Delta P_{fric}$  yields:

$$\Delta P_{fric} = \frac{1.25 \times 2 \times 0.007 \times (27.2)^2}{25 \times 10^{-3}} = 465.9 \text{ Pa} \quad 3.9$$

If the water volume fraction is, say, 5% water then to a first approximation the density of the air/water mixture is  $\rho_m = 1.25 \times 0.95 + 0.05 \times 1000 = 51.2\text{kg/m}^3$ . For a vertical pipe of length 2m, the hydrostatic pressure drop will be:

$$\therefore (\Delta P)_{hydrostatic} = \rho g h = 51.2 \times 9.81 \times 2 = 1004.5 \text{ Pa} \quad 3.10$$

For a 2m vertical pipe carrying 5% water in an air-water mixture at  $U_g = 27.2$  m/s, the total pressure drop will be about:

$$\Delta P_{Total} = 1470.4 \text{ Pa} = 0.015 \text{ bar}$$

The pressure drop across the test section for the wet gas flow rate of 3034 litre/min air and 29 litre/min is about 0.015bar. Hence, pressure required at test section is about 1.015 bar (atmospheric pressure + 0.015).

Dry air at a pressure of 1bar has a density of  $\rho_a = 1.29 \text{ kg/m}^3$ , so at 6 bar gauge, compressor delivery pressure, it will have a density  $\rho_c$  of:

$$\rho_c = \rho_a \times \left( \frac{6+1}{1} \right) = 9.03 \text{ kg/m}^3 \quad 3.11$$

If the requirement is  $178 \text{ m}^3/\text{hr}$  at 0.985bar (1-0.015) then at a pressure of 6 bar gauge a volume flow rate of  $25 \text{ m}^3/\text{hr}$  will be required =  $6.94 \times 10^{-3} \text{ m}^3/\text{s} = 0.064 \text{ kg/s}$  3.12

The airline from the main compressor house is connected to the high pressure flow regulator, see Section 5.1.1, in the lab via a  $\frac{3}{4}$  inch (19mm) diameter pipe which was installed many years ago. From the high flow regulator to the test section a 2 inch (50mm) diameter pipe is used. Using the Darcy equation, see Equation 3.8, the pressure drop in the initial length of pipe of  $\frac{3}{4}$  inch ( $\Delta P_{\frac{3}{4}'' \text{ Pipe}}$ ) and the pressure drop in the 2 inch pipe ( $\Delta P_{2'' \text{ Pipe}}$ ) can be calculated:

$$\Delta P = \Delta P_{2'' \text{ Pipe}} + \Delta P_{\frac{3}{4}'' \text{ Pipe}} \quad 3.13$$

$$\begin{aligned}
\Delta P &= \left\{ (9.03 \times 50 \times 0.007) \times \left( \frac{0.072}{9.03 \times 2.027 \times 10^{-3}} \right)^2 \times \frac{1}{0.0254} \right\} \\
&+ \left\{ (9.03 \times 20 \times 0.007) \times \left( \frac{0.072}{9.03 \times 2.85 \times 10^{-4}} \right)^2 \times \frac{1}{0.00952} \right\} \\
&= 105 \text{ kPa} \\
&\cong 1 \text{ bar}
\end{aligned} \tag{3.14}$$

So, delivering air from the university compressor house to the test section will result in a pressure loss of 1bar upstream of the regulator used to control the air flow into the annular flow rig. Therefore, we can expect the pressure at this regulator to be at least 5bar (gauge). With this inlet pressure of 5bar to the regulator, gas flow of 178m<sup>3</sup>/hr can be generated at 1.015bar in the test section.

### 3.2 Investigation of conductance flow meter

In a recent comprehensive review of measurement methods for film thickness, Clark (2002) identified that the most widely used techniques are based on the difference in impedances. Conductance probes are two electrodes a short distance apart where the gap is closed by the liquid film bridging between them. As stated earlier, Section 2.3.2, the conductance probe is proposed for use in this current investigation. Section 4.2 will further describe this technique and its mechanisms.

For an item of resistivity  $\psi$  (ohm-meter -  $\Omega m$ ), cross-sectional area  $A$  (m<sup>2</sup>) and length  $l_p$  (m), the reciprocal of the resistance  $R_p$  (ohms) is the conductance  $S_m$ :

$$S_m = \frac{1}{R_p} = \frac{A}{\psi l_p} \tag{3.15}$$

The resistivity,  $\psi$ , is the reciprocal of the conductivity  $\sigma$  and so  $S_m$  could also be written as:

$$S_m = \frac{A}{l_p} \sigma \tag{3.16}$$

The designed CFM, see Section 4.2.1, has two conductance probes and each probe has two electrodes. The two electrodes are separated by a distance  $l_p$ . The dimensions of

the electrode, Figure 3.2, within the fluid are width ( $w$ ) and height ( $h_{el}$ ) so that

$$A = w h_{el}. \quad 3.17$$

Therefore, from Equations 3.16 and 3.17, we may write the conductance  $S_m$  between the electrodes as:

$$S_m = \frac{w h_{el}}{l_p} \sigma_w \quad 3.18$$

However, the purpose of this technique is to measure the height of the liquid so  $h_{el}$  can be replaced by  $h_s$  to represent the height of the liquid. Hence:

$$S_m = \frac{w h_s}{l_p} \sigma_w \quad 3.19$$

where:  $\sigma_w = 143 \mu\text{S}/\text{cm}$ , is the conductivity of water used in laboratory and monitored using a commercial conductivity meter. Equation 3.19 suggests that for fixed  $w$ ,  $l_p$  and  $\sigma_w$  then  $S_m$  is proportional to  $h_s$ .

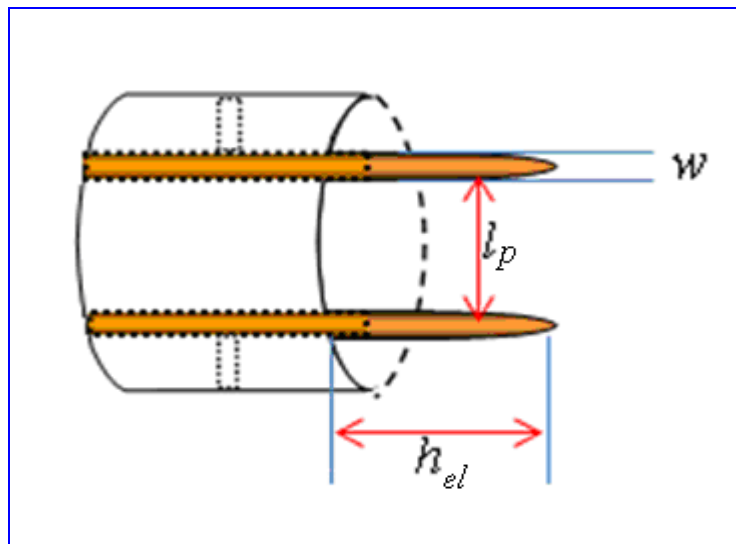


Figure 3.2 Electrode dimensions

Electronically, the mixture conductance,  $S_m$ , is measured using a circuit containing a pre-determined electrode configuration and the readings are displayed by the output

voltage,  $V_{out}$ , from an output device, see Section 4.2. Since  $S_m$  is linearly related to  $h_s$  (Equation 3.19) and  $V_{out}$  is linearly related to  $S_m$  (Equation 3.20a), film thickness can be determined from this measurement by obtaining a calibrated linear relationship between  $V_{out}$  and  $h_s$  within the range of measurements in the form of:

$$V_{out} = K \frac{w h_s}{l_p} \sigma_w \quad 3.20$$

where:

$$V_{out} = K S_m \quad 3.20a$$

Re-arranging Equation 3.20 we can obtain the height  $h_s$  of the fluid around the electrode which is a representative of the thickness  $\delta$  of the liquid film in the annular flow:

$$h_s = V_{out} K' = \delta \quad 3.21$$

where:

$$K' = \frac{l_p}{w K \sigma_w} \quad 3.21a$$

In a bench test, a reference value  $\delta_{ref}$  for the liquid film height can be measured directly using a ruler or travelling microscope, where the output voltage  $V_{out}$  is read on a digital voltmeter. A graph can be obtained for  $V_{out}$  vs.  $\delta_{ref}$ . This relationship was expected to be a straight line, and can be expressed in terms of Gradient  $\bar{G}$  where:

$$\bar{G} = \frac{V_{out}}{\delta_{ref}} \quad 3.22$$

From Equations 3.21 and 3.22:

$$\bar{G} = \frac{1}{K'} \quad 3.23$$

where:  $K'$  is given by Equation 3.21a.

Thus, by measuring the gradient  $\bar{G}$  of the calibration curve the value of  $K'$  can be obtained from Equation 3.21. Subsequently, a measured value for the liquid film thickness  $\delta_{est}$  can be deduced from a voltage measurement using Equation 3.24:

$$\delta_{est} = V_{out} K' \quad 3.24$$

### 3.2.1 Spacing between the conductance probes when using only water

The aim of carrying out this part of investigation is to minimise the meniscus effect. This section will investigate the effect of meniscus when the liquid is water. The next section will investigate the effect of meniscus when introducing oil-water mixture.

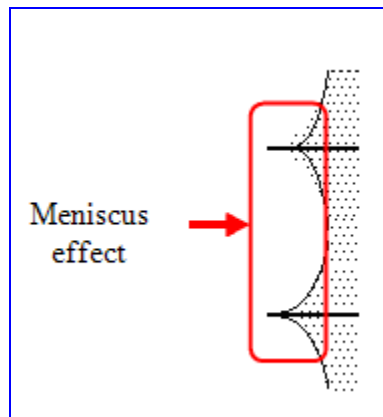


Figure 3.3 Meniscus effect on overestimating the film thickness

The meniscus usually is attributed to surface tension forces. In our case, the liquid film is expected to form a meniscus around the electrodes of the conductance flow meter (CFM). As can be seen, Figure 3.3, the presence of the meniscus will appear as extra height and so will cause inaccuracy in the flow meter readings. To attempt to reduce this effect, an experimental investigation examined the separation between the

probes maximise the accuracy of the relationship between liquid height and voltage output.

The electrode spacing distance  $l_p$  was varied in steps of 5mm from 5mm to 30mm, and the chosen spacing was that one that gave the most linear voltage output from the electronic circuit. The excitation signal of the electronic circuit was set with AC frequency of 50kHz and  $V_{p-p}$  of 2.2volts, see Section 4.2.2. Figure 3.4 shows the electronic circuit voltage output variation when the liquid film thickness was varied from 0-20mm at a spacing distance between the electrodes of 20mm.

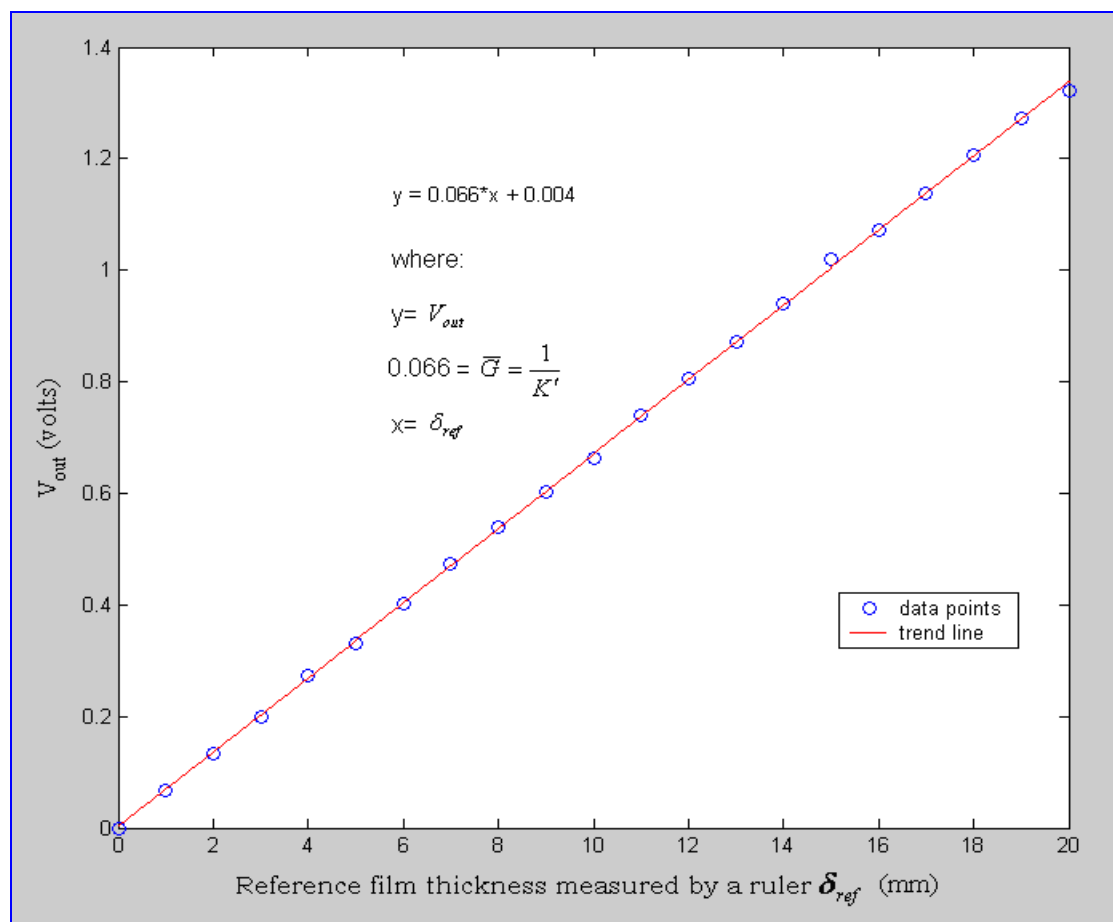


Figure 3.4 Results for 20 mm spacing between electrodes (water only)

The result of the experiment shows that an electrode spacing  $l_p$  of 20mm gives an almost perfectly linear relationship between the voltage output  $V_{out}$  and the height of the film  $\delta_{ref}$ , see Figure 3.4. This result also validates the theoretical analysis in which a linear relationship between the voltage output of the electronic circuit and the liquid film thickness  $\delta_{ref}$  was predicted.

At this stage, a percentage error can be calculated:

$$\xi_{\delta, \text{measured}} = \frac{\text{measured film height } \delta_{\text{est}} - \text{reference film height } \delta_{\text{ref}}}{\text{reference film height } \delta_{\text{ref}}} \times 100 \% \quad 3.25$$

Where the reference film height is the height measured by the ruler.

The errors were obtained by using the measured values of  $V_{\text{out}}$ , Equation 3.24 (where  $K'$  is obtained from  $\bar{G} = 0.066 \text{ V/mm}$ , Figure 3.4), to get  $\delta_{\text{est}}$  and simultaneously for each  $V_{\text{out}}$  reading the film thickness was measured using a ruler to an accuracy of about 0.5mm, neglecting the dispersion effect of the pipe. The equation of the calibration curve shows a very small offset of 0.004 which can be ignored. Figure 3.5 shows the percentage error in the measured film height  $\delta_{\text{est}}$ . This probe configuration,  $l_p = 20\text{mm}$ , shows a good accuracy with a mean percentage error in  $\delta_{\text{est}}$  of 1.68% when the measured heights were compared with the reference heights. The maximum error was 4%. Error decreased with film thickness.

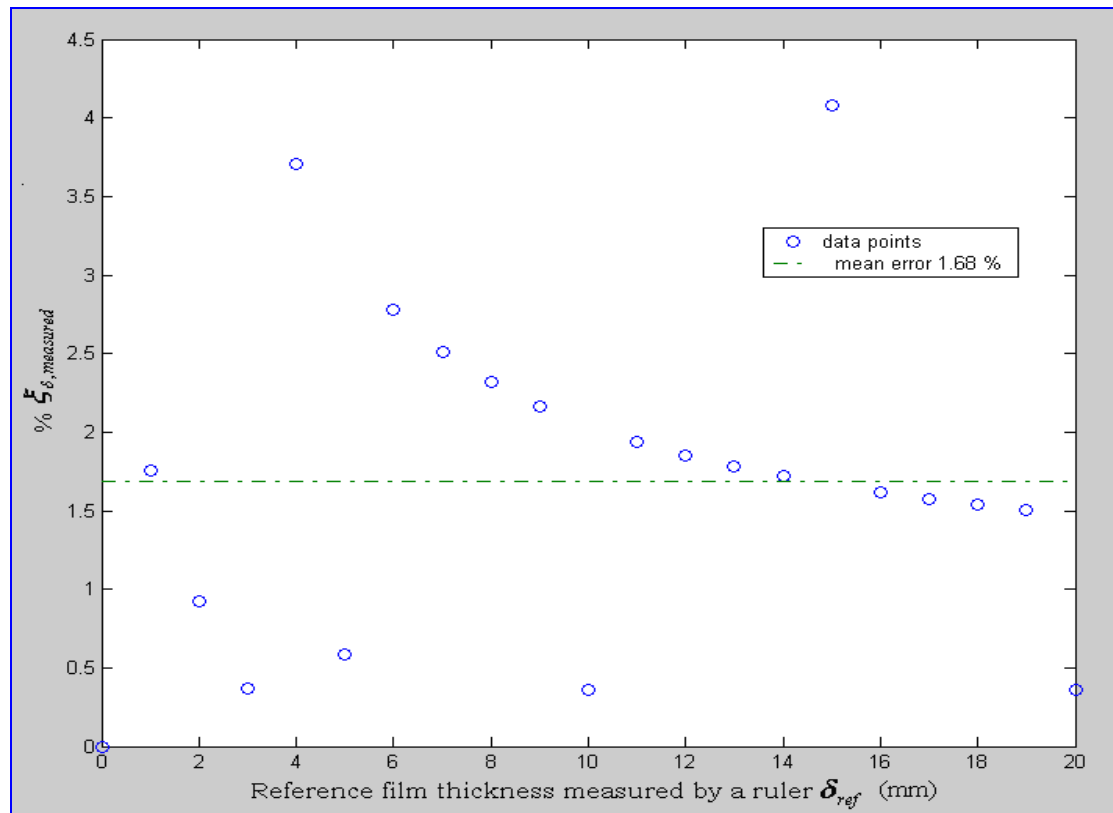


Figure 3.5 Mean error between estimated water level and the measured values (water only)

### 3.2.2 Effect of oil phase in the liquid on film measurements (water-oil mixture)

Electrical impedance techniques have proven attractive for many applications because of their generally fast response and relative simplicity of operation. Measurements obtained from these devices rely upon the variation of the capacitance (permittivity) or the conductance of a two phase mixture with the volume fraction of the disperse phase. Non-conducting liquid mixtures (such as oil continuous mixtures) are amenable to capacitance measurement, whereas conducting liquids (such as water continuous mixtures) require conductance measurements. In conducting mixtures, the conductance decreases with increasing gas or oil volume fractions, and increases with increasing water volume fraction.

The experiment, described in Section 3.2.1, was repeated but with oil introduced into the water. A constant volume fraction of the oil ( $\alpha_o = 0.07$ ) was used. The aim of this investigation was to evaluate the effect of the oil phase in the liquid film height measurement. This was aimed at providing a better understanding of the proposed technique and gives an initial step for any proposed further work when including an oil phase into the system. The oil-water mixture was assumed well-mixed after being shaken by hand. Since the oil volume fraction is constant ( $\alpha_o = 0.07$ ), all the oil does is change the effective conductivity of the mixture that is used. The electronic settings, see Section 4.2, were kept the same as in the previous experiment using the same mathematical theory used in the previous section, see Section 3.2.1. However, the signal wave frequency was increased to 80kHz as the circuit struggled to respond with a 50kHz signal. Figure 3.6 shows the variations in the voltage output when the film height of the oil-water mixture was increased from 0-20mm.

Equation 3.25 was used once again to calculate the percentage error in the measured film height of the oil-water mixture. In comparison with the results in Section 3.2.1, there is slightly more variation in the reading but the linear relationship can be clearly seen in Figure 3.6. The probe configuration showed a mean percentage error in the measured film height of -0.5%. The error range is from a maximum negative value of -17% to a maximum positive error of 15%, see Figure 3.7.

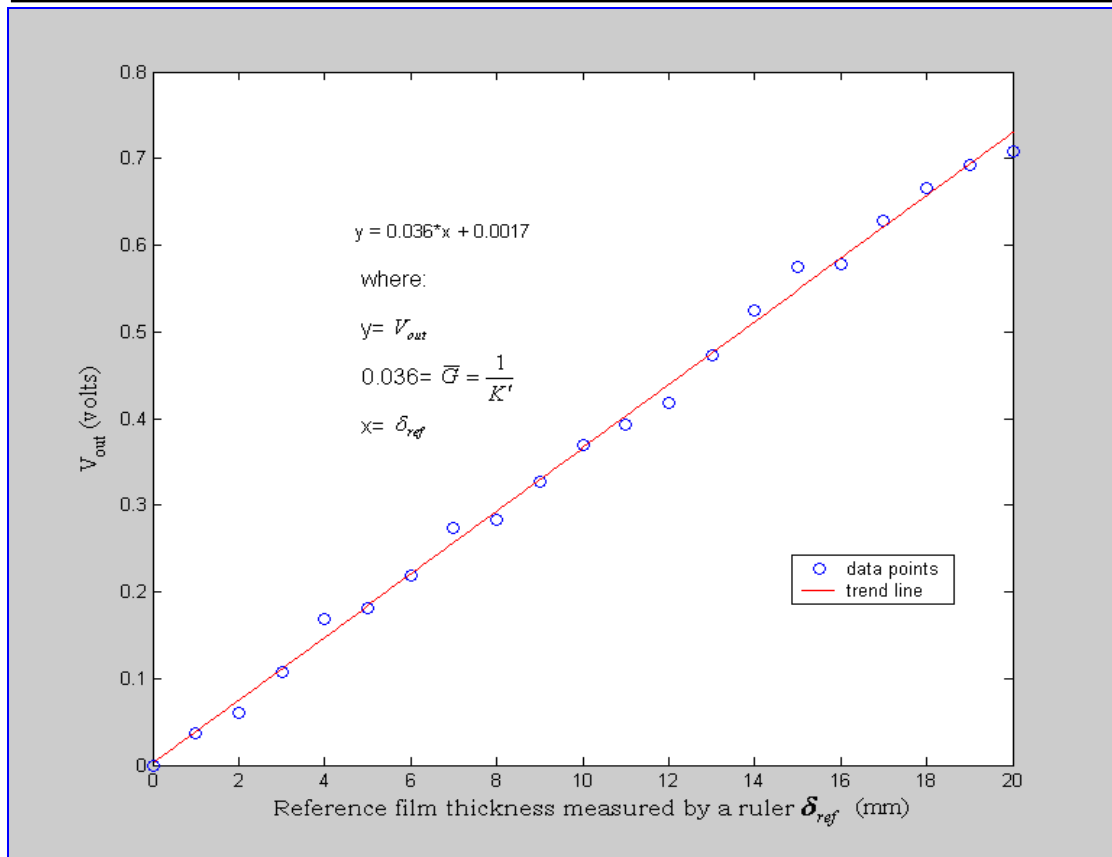


Figure 3.6 Results for 20 mm spacing distance between the electrodes (oil-water ( $\alpha_o=0.07$ ))

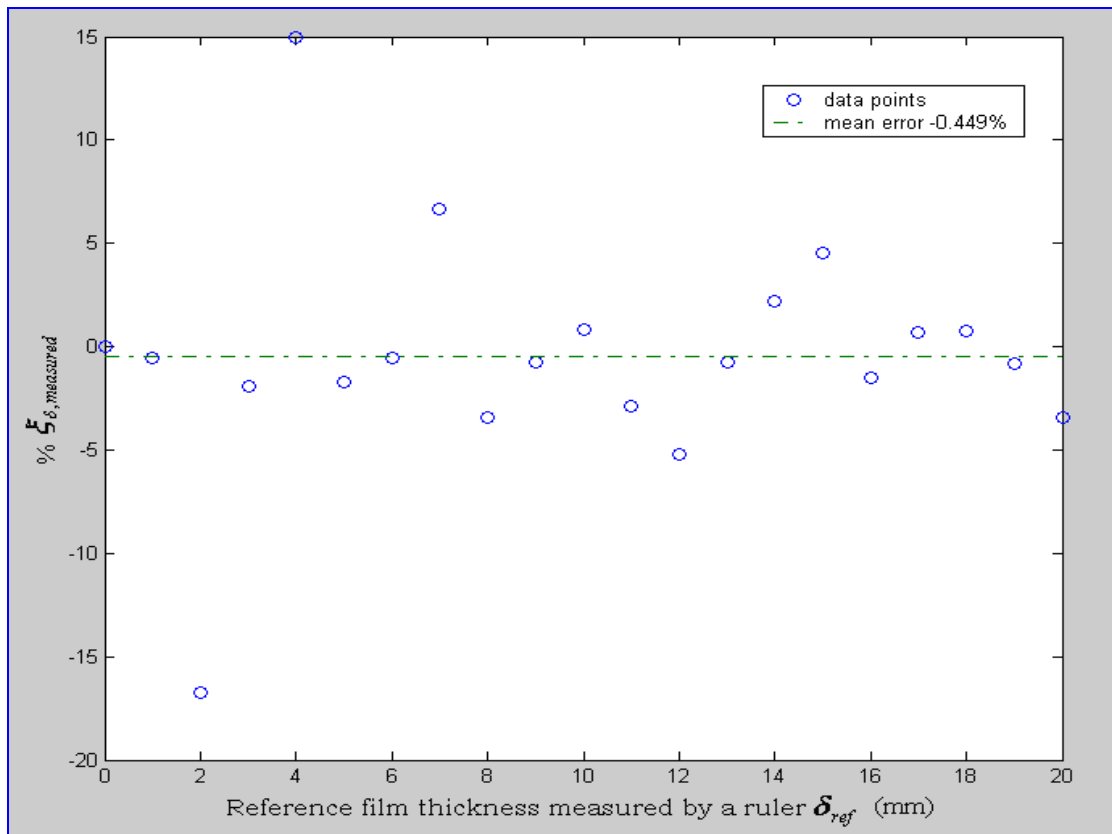


Figure 3.7 Mean error between estimated water level and the reference value (oil-water ( $\alpha_o=0.07$ ))

The gradient value  $\bar{G}$  showed a change from 0.066 (water only) to 0.036 (oil-water mixture). The author attributes this change to the effect of the presence of the 7% of oil. Also, this change in the gradient value could also be influenced by the change in the excitation frequency which was increased from 50kHz (water only) to 80kHz (oil-water mixture). In both experiments the total error is an accumulation of different physical error sources that could affect the measurement. These physical errors are (i) presence of the meniscus, (ii) accuracy of the conductance measurement, (iii) accuracy of  $\delta_{ref}$  measurement, (iv) accuracy of  $V_{out}$  measurement and (v) accuracy of separation of the electrodes  $l_p$  measurement. However, in real applications, the error for the oil-water mixture experiment can be reduced by compensating for the presence of oil by calculating the oil-water mixture conductivity.

### 3.3 Preliminary Investigation of ultrasonic technique

Sections 1.2.3 and 2.4 have introduced the reasons behind proposing an ultrasonic technique for use in this investigation. A detailed description of the proposed technique is presented in Section 4.2. Prior to considering the design of the proposed ultrasonic flow meter (USFM), some basic fundamentals of the ultrasonic wave properties are reviewed in this section.

In this section, Pulse Wave (PW) ultrasound is being used here by the author (for preliminary work only) to investigate the cross-talk and the beam deflection phenomenon. However, the final design of the system is based on a Continuous Wave (CW) ultrasound. The reason behind considering the PW in the preliminary investigation is because they have a wider range of wave spread (i.e. wider beam angle) in the travelling medium (Pavlović, 1997), resulting in a greater possibility of interacting with neighbouring PW transmitters and receivers which gives a greater possibility for beam reflection. In comparison to the PW, the CW has a defined effective beam deflection which can be avoided, see Section 3.3.3. On the other hand, the CW was favoured for the final design because the CW has the possibility of detecting all the various velocities encountered by the ultrasound beams in a flowing fluid. Also, a PW system is very poor in detecting small phase shifts in gas metering because of its pulsating nature, Pavlović (1997).

### 3.3.1 Signal cross-talk between transducers

Figure 3.8 shows a selection of the wide range of ultrasonic flow metering techniques found in the literature and in industry. Here they are classified depending on whether they use of one or more pairs of transducers. The basic types of beam path are axial, diametral and chordal (Figure 3.8(a-c)). The transmission of the acoustic signal between two transducers can be direct or reflected (Figure 3.8(d)). The transmission path of the acoustic signal between two transducers need not be direct, it can be reflected from the inner wall of the pipe. In commercially available devices up to four such reflections are possible.

In order to minimise the influence of the fluid velocity distribution in multi-path meters, the different acoustic paths can be associated in different ways by using (i) various parallel paths on the same plane (plane arrangement), (ii) paths that are symmetrically or asymmetrically crossed over compared to the axis (criss-cross arrangement), or (iii) by forming a network arrangement more complex arrangements (Figure 3.8(e-g)).

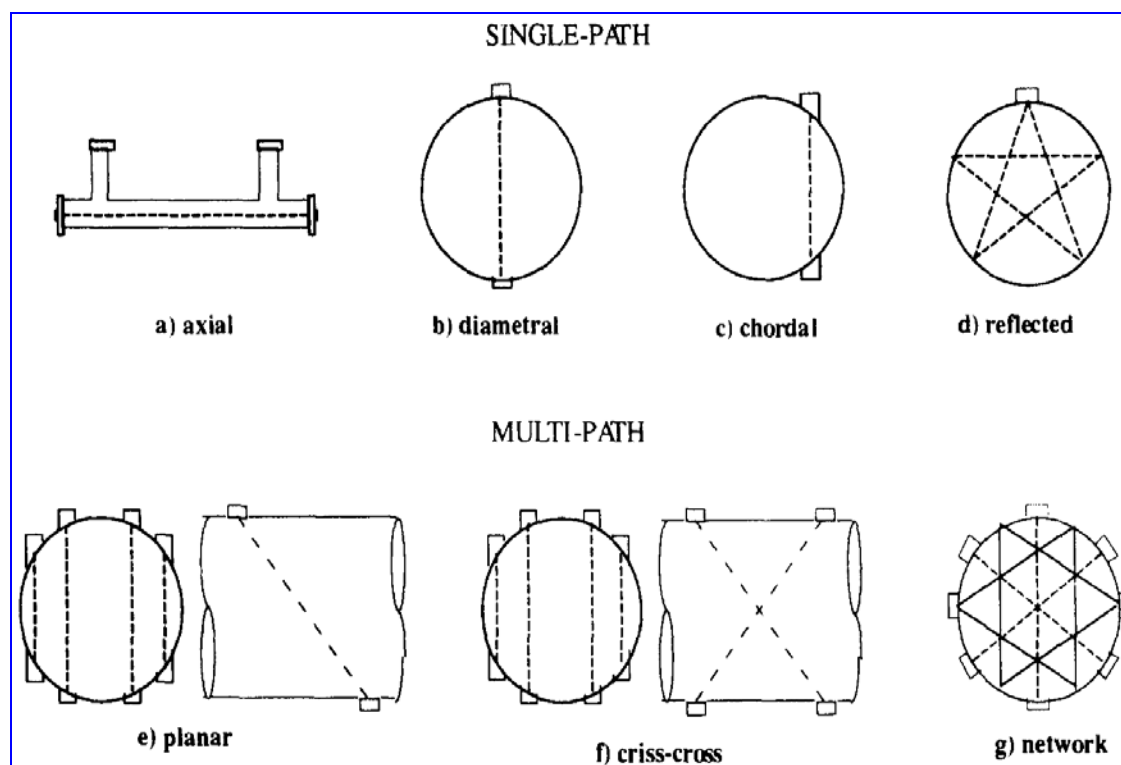


Figure 3.8 Different acoustic paths in Ultrasonic Flow Meters, Dell'Isola et al. (1997)

As the number of acoustic transducers and paths increases, measurement uncertainty decreases because the presence of swirl and lack of symmetry in the velocity distribution does not have such an important effect on the measurement. However, multiple transducers invariably experience a degree of unwanted inter-element cross-coupling or cross-talk. Cross-talk is usually overcome by either additional electronic circuitry or by design manipulation (Ferrari et al., 2005).

Introducing another stage into the electronic circuitry will introduce additional delay in the system, which may cause inaccuracy in the measurement. The author of this thesis decided to concentrate on a design configuration which ensures minimum or zero cross-talk between the transmitter of one pair of transmitter-receiver and the receiver of another pair of transmitter-receiver, taking into account a minimum size of the device. A novel transducer configuration was investigated which is described below.

Cross-talk takes the form of a system error which is a function of the strength of the unwanted cross-talk relative to a signal and the flow velocity which fluctuates with the flow profile. In the worst case the acoustic signal is lost. Usually the closer the receiver of one pair is positioned to the transmitter of another pair the stronger the cross-talk between the channels. It is therefore often desirable to position the receiver of one pair and the transmitter of another pair as far apart as possible. An investigation was carried out to define a suitable separation distance between the transmitters and the receivers for this research.

Four different ultrasonic transducers configurations were set up to investigate the cross-talk between a transmitter and a receiver that is not intended to receive the signal from that transmitter. The transducers were placed on a table and held down by re-usable adhesive. The table and transducers were positioned to avoid reflecting objects.

The cross-talk phenomenon can be traced back to the transducer's characteristics. For example, the -3dB angle in the conical beam from the transmitter that was used is 60°. If there is any reflecting object within this angle (but not between the receiver and

transmitter) the receiving transducer will detect a strong signal. By making a simple scale sketch for the 50mm pipe that was used, see Figure 3.9, it can be concluded that to “avoid” cross-talk between the receiving transducers Receiver 2, Rx2 (not intended to receive the signal), has to be located at an axial distance greater than 134mm from Receiver 1, Rx1 (intended to receive the signal). To situate the transducers so that they made the necessary angle to the pipe, the transducers were placed on plastic wedges, see Figure 3.9 and Section 4.3.4. These wedges are shown as blue in Figures 3.9, 3.11, 3.13, 3.15, 3.17, 3.19, 3.20 and 3.22.

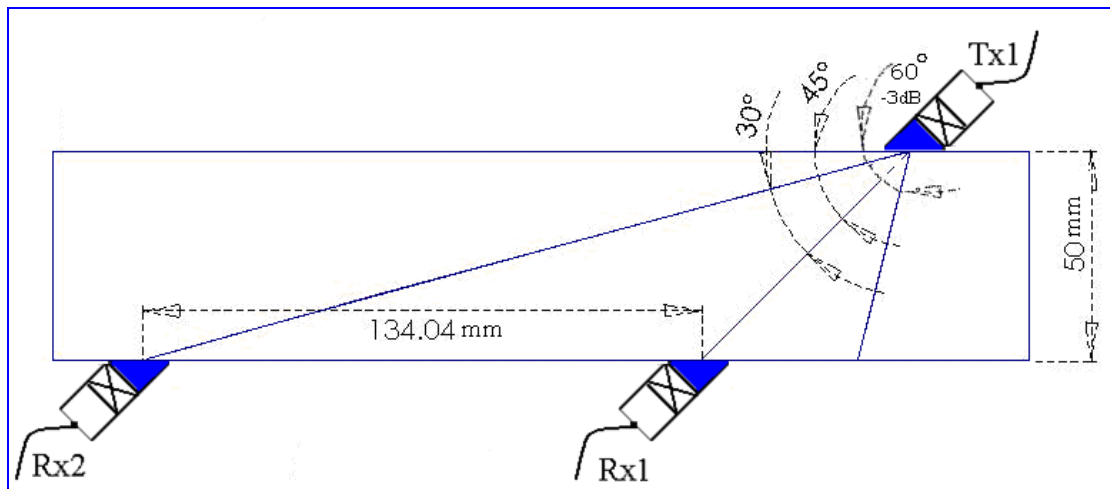


Figure 3.9 Critical separation between receivers (50mm pipe)

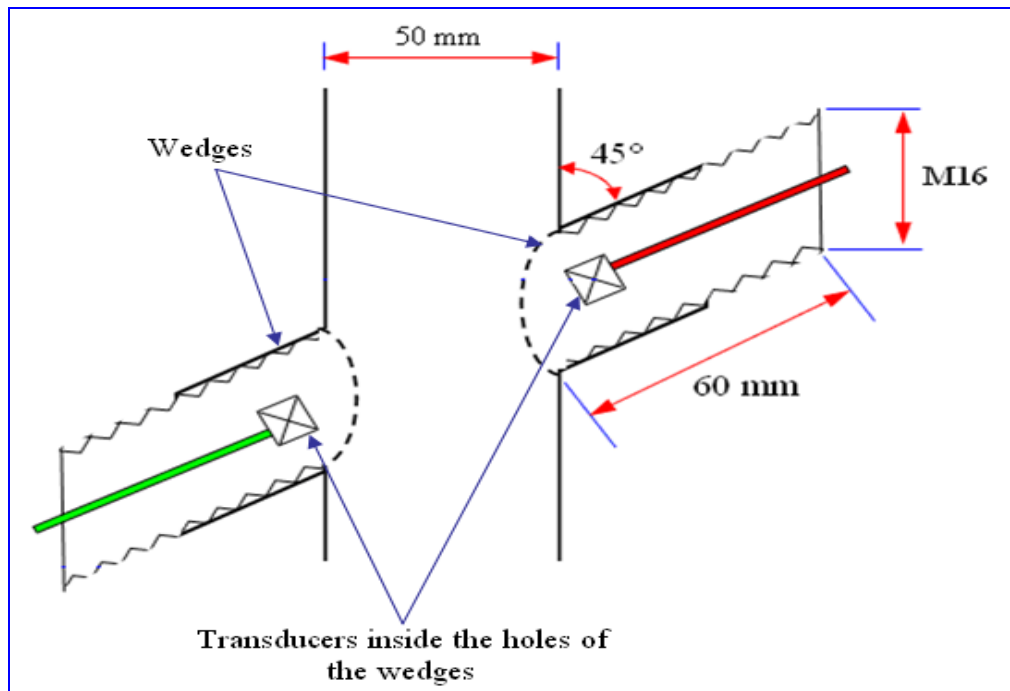


Figure 3.10 Transducers placed in plastic wedges

The following four general statements apply to all of the configurations presented in this section, Figures 3.11, 3.13, 3.15 and 3.17:

- Each configuration has two transmitter-receiver pairs; Transmitter Tx1 and Receiver Rx1, and Transmitter Tx2 and Receiver Rx2.
- Tx1 is on the opposite side of the pipe to Rx1, and Tx2 is on the opposite side of the pipe to Rx2.
- During the bench tests of this particular investigation, a signal was only transmitted from one transmitter, Tx1, and received by its pair receiver Rx1 (Yellow signal in the plotting graphs). The cross-talk signal is the signal picked up by receiver Rx2 from the signal transmitted by transmitter Tx1 (Blue signal in the plotting graphs). Transmitter Tx2 was disconnected to avoid any ambiguity and complexity in the analysis of the received signal by receiver Rx2.
- Ideally, in all of the configurations, the transmitted signal from Tx1 should be received only by receiver Rx1 and not be picked up by receiver Rx2.
- **Configuration A**

In configuration A the transducers have been set up in such a way that the transmitter pairs are parallel to each other and each pair is at an angle of  $45^\circ$  to the pipe axis, see Figure 3.11. Each receiver is positioned upstream of its corresponding transmitter and the pair Tx1 and Rx1 is positioned upstream of Tx2 and Rx2. With the pipe vertical and upward flow, Tx2 is vertically above Tx1 and Rx2 is vertically above Rx1.

It can be seen from Figure 3.11 that the direction of propagation of the acoustic signal is against the flow.

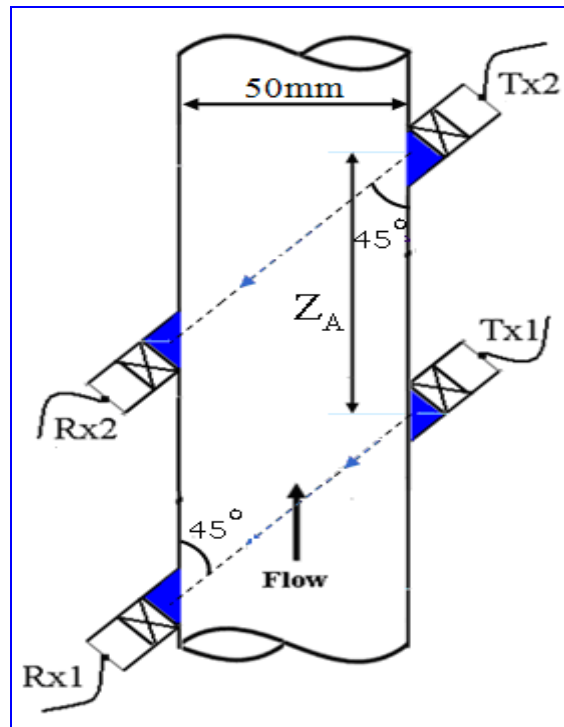


Figure 3.11 Configuration A

While maintaining Tx1-Rx1 parallel to Tx2-Rx2, the separation distance between Tx1 and Tx2,  $Z_A$ , was varied in 50mm steps from 100mm to 200mm. Figure 3.12 shows that as the axial separation of the receiving transducers increases, the cross-talk effect (blue signal picked by Rx2) reduces. In this case at  $Z_A=50\text{mm}$  and  $Z_A=100\text{mm}$ , the cross-talk signal is very noticeable. When  $Z_A$  starts to get bigger than 150mm the cross-talk signal received by Rx2 fades away. A further separation ( $Z_A=200\text{mm}$ ) showed no significant traces of a received signal by Rx2, hence no significant cross-talk.

Obviously, this configuration is not practical since both transmitted waves are against the flow which means a zero phase shift will be always recorded, see Section 3.3.4. However, the purpose of introducing this configuration was to confirm the critical separation distance between the receivers, as previously illustrated in Figure 3.9.

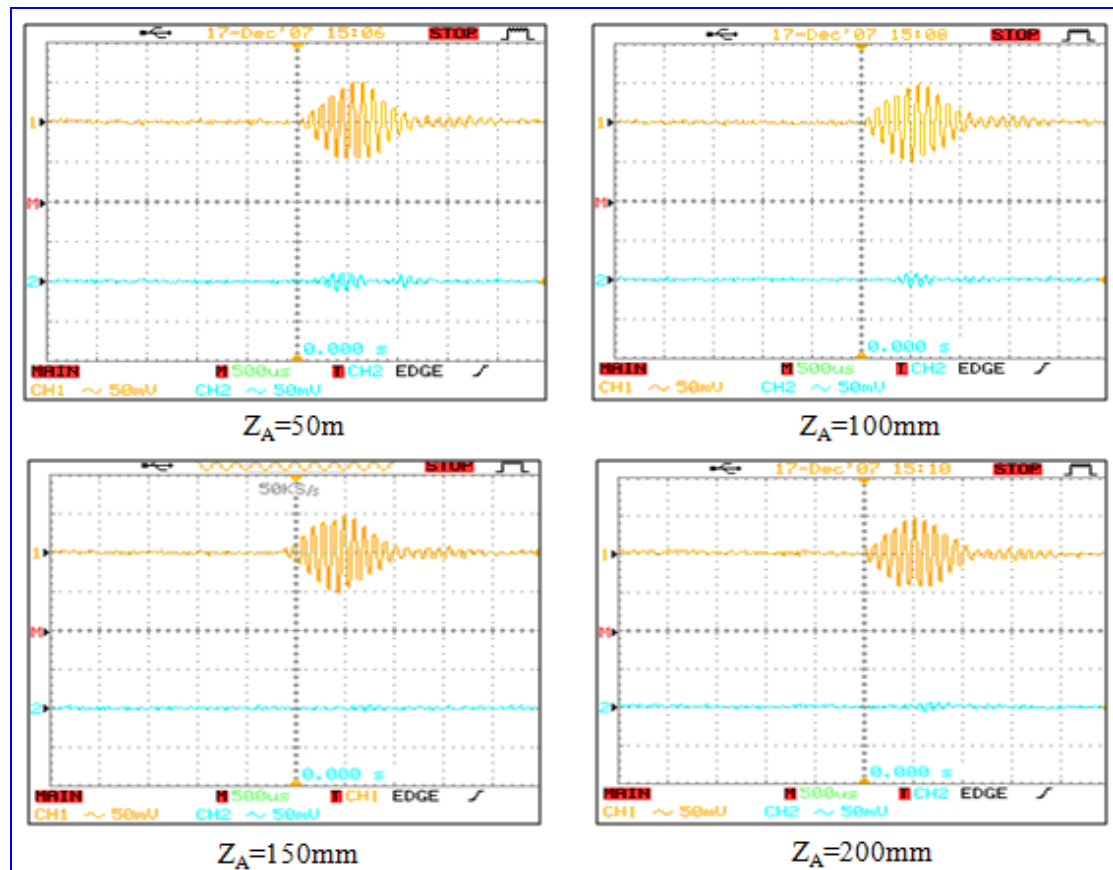


Figure 3.12 Results for configuration A –Yellow signal is received signal at Rx1 and blue signal is cross-talk signal received at Rx2

- **Configuration B**

In configuration B, see Figure 3.13, Tx1, Rx1, Tx2 and Rx2 form the four corners of a rectangle, with the pipe diameter making up two sides of the rectangle. Tx1 and Rx1 are on opposite sides of the pipe at  $45^\circ$  to the pipe axis. Tx1 is downstream of Rx1 so the acoustic signal travels against the flow. Tx2 and Rx2 are on opposite sides of the pipe at  $45^\circ$  to the pipe axis, Tx2 is upstream of Rx2 so that this signal travels with the flow.

In this case the separation distance between Tx1 and Tx2,  $Z_B$ , is fixed because any movement of either pair brings the transmitters or receivers closer. When the angle is set to  $45^\circ$  for a 50mm internal diameter pipe, the separation distance is  $Z_B = 50\text{mm}$ . Cross-talk signal received at Rx2 is present, see Figure 3.14, and this is in agreement with the previous analysis because the axial separation between the receivers was less than 134mm, see Figure 3.9.

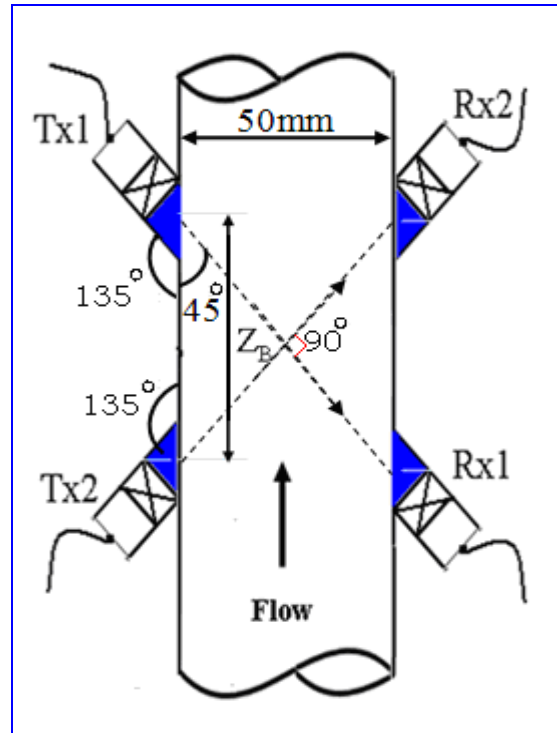


Figure 3.13 Configuration B

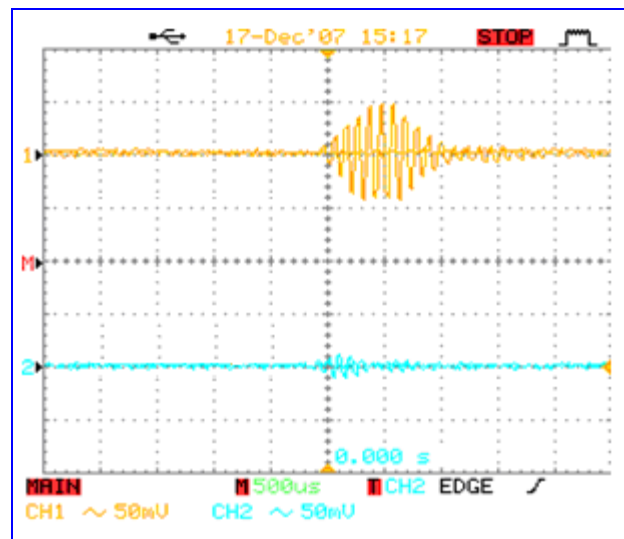


Figure 3.14 Results for configuration B – Yellow signal is received signal at Rx1 and blue signal is cross-talk signal received at Rx2

For a vertical pipe with upflow, Tx1 is vertically above Tx2 and Rx2 is vertically above Rx1. The signal from Tx1 to Rx1 is against the flow while the signal from Tx2 to Rx2 is with the flow.

- **Configuration C:**

This configuration is essentially the same as configuration B but the transducer pair Tx2,Rx2 has been moved parallel to itself, down the pipe to a position below the pair Tx1 and Rx1, see Figure 3.15. The transmitters have the same directionalities as in configuration B. All transducers are in the same axial plane.

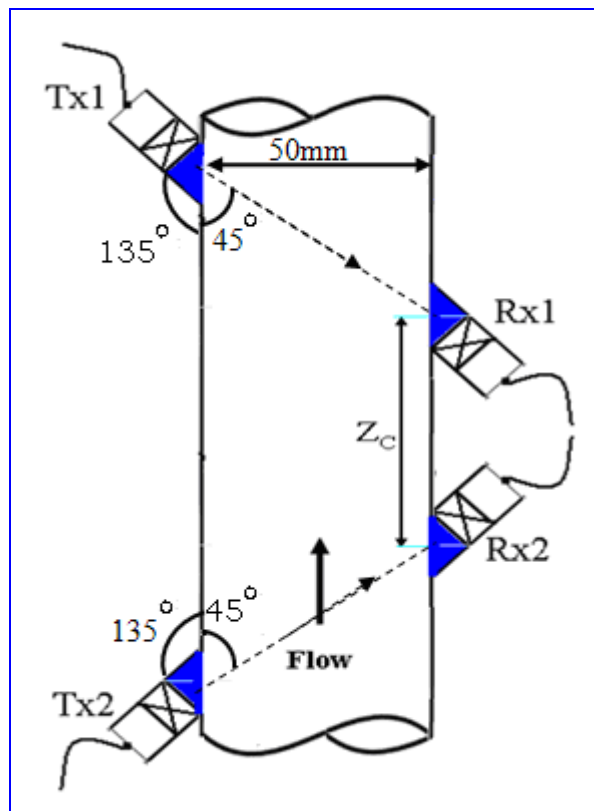


Figure 3.15 Configuration C

$Z_C$  is the separation of the two receivers Rx1 and Rx2. At  $Z_C = 50\text{mm}$ , the cross-talk effect is obvious in Figure 3.16, it has started to fade away at  $Z_C = 100\text{mm}$ , but at  $Z_C = 150\text{mm}$  it has almost disappeared. There was no practical need to proceed to  $Z_C = 200\text{mm}$  since it's obvious the result of  $Z_C = 150\text{mm}$  already gives a sufficiently small level of cross-talk.

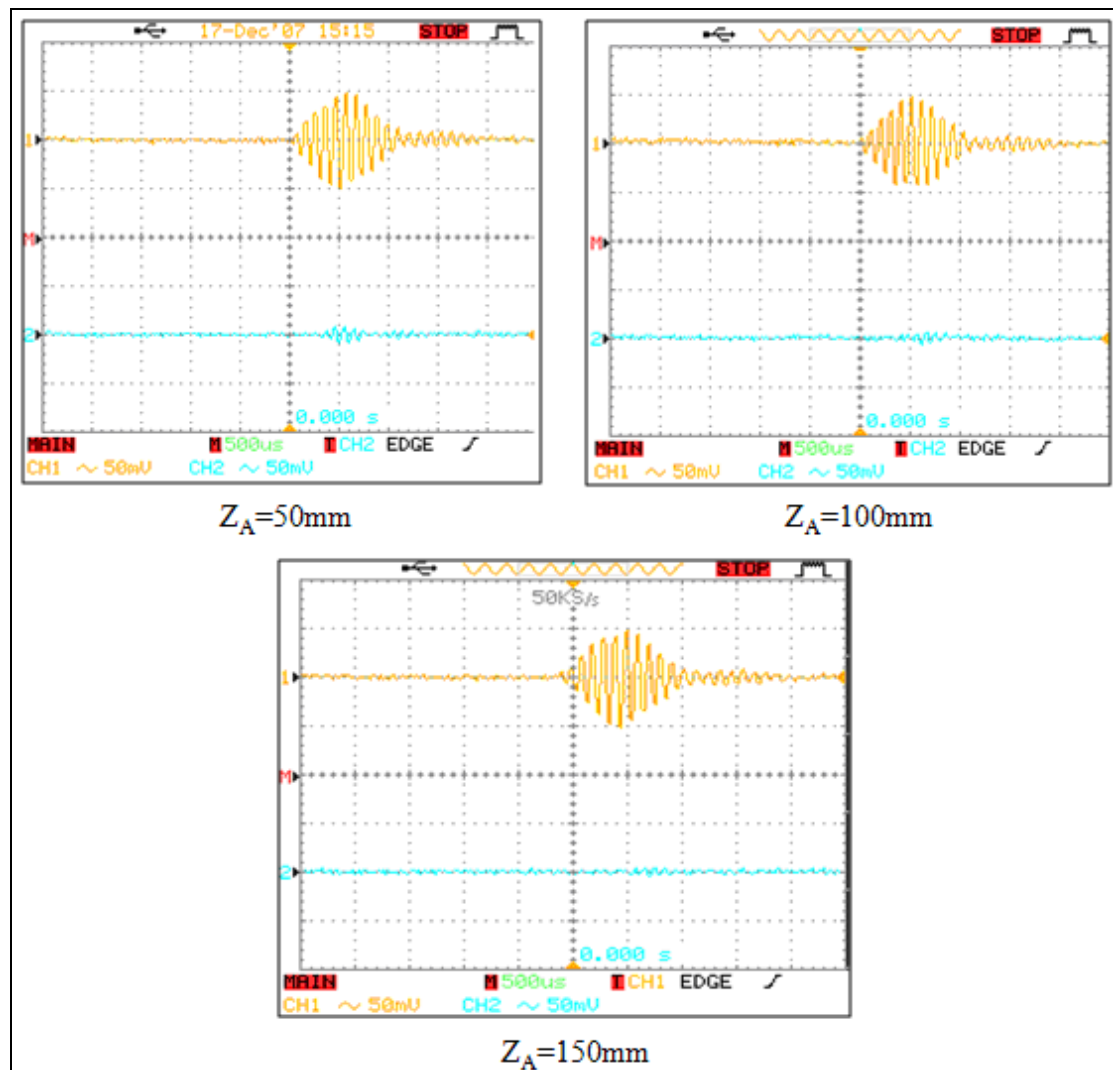


Figure 3.16 Results for configuration C – Yellow signal is received signal at Rx1 and blue signal is cross-talk signal received at Rx2

- **Configuration D:**

This configuration is basically the same as configuration A except that the positions of receiver Rx2 and transmitter Tx2 have been reversed, see Figure 3.17. The fact that the receiver in one pair of transducers is positioned on the same side of the pipe as the transmitter in the other pair of transducers means only a weak possibility of cross-talk in this configuration.

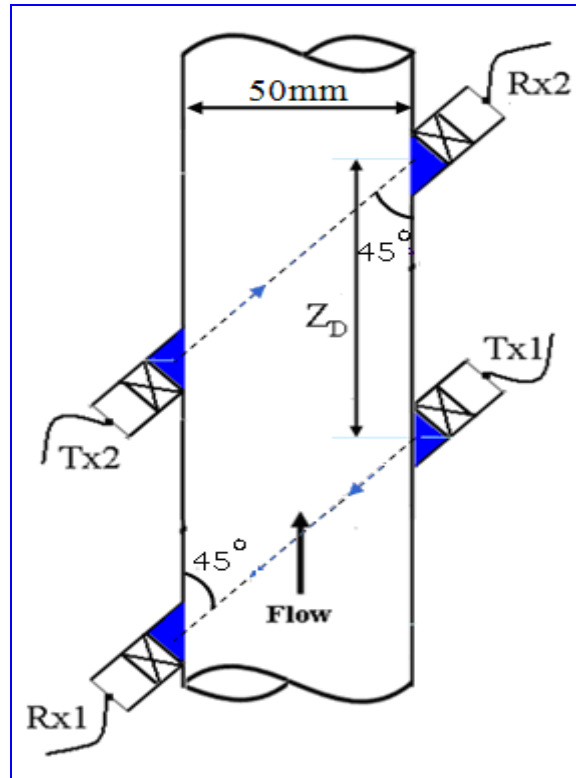


Figure 3.17 Configuration D

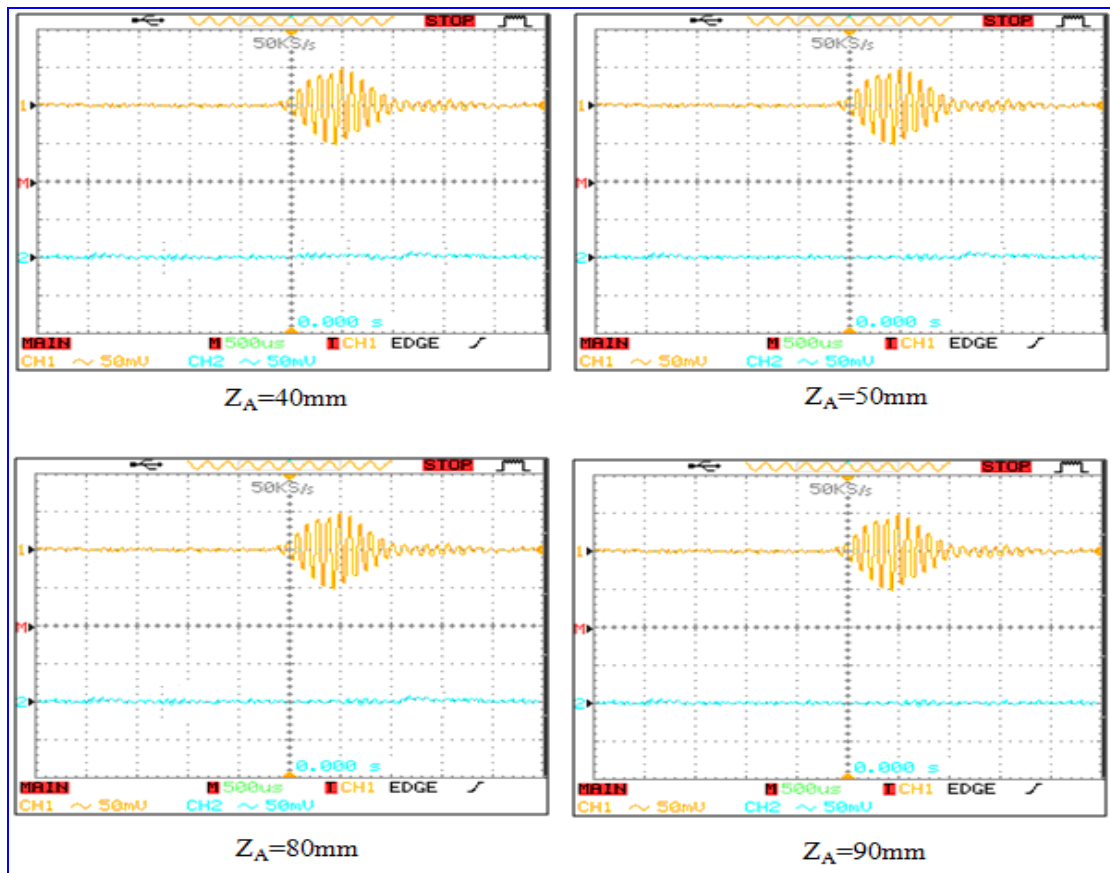


Figure 3.18 Results for configuration D - Yellow signal is received signal at Rx1 and blue signal is cross-talk signal received at Rx2

At axial separations of less than 50mm cross-talk is barely seen, see Figure 3.18. As the separation is increased above 50mm the cross-talk disappears completely. The reason for this is the directionality pattern of the transmitters. With this arrangement virtually no intensity is radiated from the transmitter of one pair in the direction of the receiver of the other pair. Configuration D was chosen to be used in this study. A complete set of details on its design and related electronics control circuit will be presented in Section 4.3.3. The researcher was unable to find a report of this transducer configuration in the literature, and believes this means it's the first time it has been implemented.

As it has been stated earlier, see Section 3.3, that the PW system was only used to investigate the cross-talk phenomenon in term of mechanical design. These results have no effect on the calculation technique associated with CW system which will be discussed in Section 3.3.3. From this stage all the discussion related to the Ultrasonic Flow Meter (USFM) will be about the CW system unless otherwise stated.

### 3.3.2 Recesses or “dead zones” effect

The accuracy with which USFMs measure flow rates in pipes is strongly affected by the profile of the flow velocity, particularly at or near the internal wall of the pipe and sometimes when flow takes place in the recesses of the transducers themselves. Dead zones can occur. The size and geometry of these dead zones are defined by such factors as whether the transducers have been positioned in a recess, size of the gap between the transducer and the housing wall, etc. Recesses are particularly important because of the flow turbulence that can be generated in the region of the recess, and which can disturb the measurements. Kažys (2002) has given the following expressing for the recess depth:

$$l_n = \frac{D_p + 2w}{2 \tan \theta} \quad 3.26$$

where:  $l_n$  is the recess depth,  $D_p$  is the transducer diameter (m),  $w$  is the distance between the edge of the transducer and the nearest point on its holder (m) and  $\theta$  is the

angle (degrees) between the acoustic path and a vector representing the direction in which the medium moves.

Kažys stated that the depth of recesses strongly depends on angle in the range  $\theta=20^\circ$ - $40^\circ$  and is less dependent on the diameter of the transducer. In our design, the angle  $\theta=45^\circ$ ,  $w=0$  and  $D_p = 11.1\text{mm}$ , so the recess depth  $l_n$  was 5.55mm. However, if the “dead zones”, see Figure 3.19, are geometrically the same for (Tx1, Rx1) and (Tx2, Rx2) then this will make no contribution to  $(\Delta t)$ , see Equation 3.32. So, providing the “dead zones” are very similar for both pairs of transducers we can make them whatever shape we want. This means that we can actually put transducers as we want in the transducer holder – with no effect on  $(\Delta t)$ .

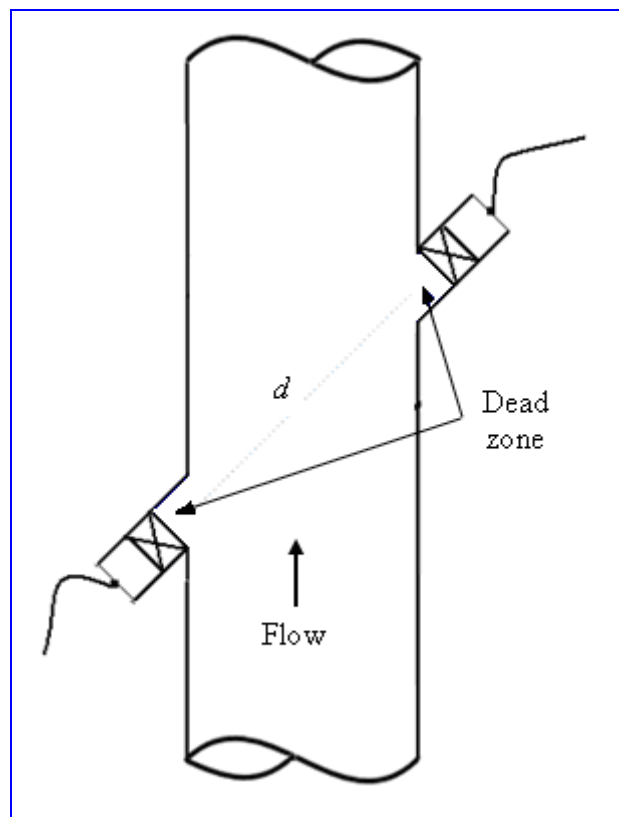


Figure 3.19 Dead zones or recesses

### 3.3.3 Beam reflection

When designing the USFM it was observed that for ideal reflections the ultrasound beam will reflect from the pipe wall at axial distances of  $(n \times 50 \times \tan 45^\circ)\text{mm}$  away

from its initial transmission point. When  $n$  is odd, the reflection point (shown as red circles in Figure 3.20) is on the same side of the pipe as the receiver, when  $n$  is even the reflection point (shown as green circles in Figure 3.20) will be on the opposite side of the pipe to the receiver. Again, Rx1 is the receiver that we wish to receive the signal from Tx1. We do not wish to receive signal from Tx1 at Rx2 i.e. avoid cross-talk.

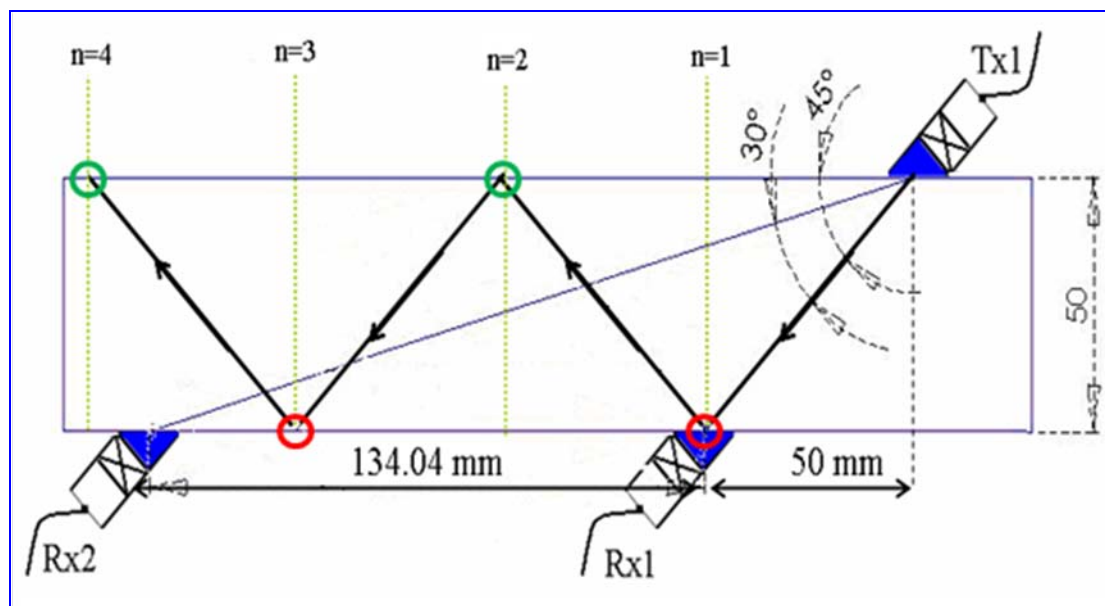


Figure 3.20 Beam reflection analysis (50mm pipe)

According to this, the receiver Rx2 of the other pair of transducers should not be positioned in a reflection zone, i.e. avoid 150mm, 250mm, etc on the same side of the pipe as the receiver Rx1. Rather the second receiver Rx2 should be positioned at 200mm, 300mm, etc on the same side of the receiver Rx1.

The investigations reported in Sections 3.3.1, 3.3.2 and 3.3.3 lead to the following conclusions on the final geometry of the designed USFM in the current study:

- Configuration D, see Figure 3.17, was chosen since it showed no cross-talk effect provided geometrical dimensions are kept at minimum.
- The receivers should be located/positioned in such a way that reflection zone is avoided, see Figure 3.20.

- The Pulse Wave (PW) system was used in this preliminary work only to determine the geometry of the USFM design. The PW will not be used in the final design.

### 3.3.4 Calculation methods

There are three basic modes of operation used for the measurement of the difference in transit time between the upstream and downstream signals ( $\Delta t$ ) and numerous variations of each mode. The modes of operation are:

- the leading edge mode,
- the frequency (sing-around) mode, and
- the phase comparison mode

All of the above modes are essentially time interval ( $\Delta t$ ) measuring systems and can work for either pulse or continuous waves. There would appear to be no significant advantage in choosing one system over the other particularly when one considers that turbulence spreads the time delay, and averaging is required to reduce this effect. The overall accuracy is therefore a function of statistical methods and must be traded off against the response time required (Blackstock, 2000). A number of researchers (Lynnworth and Liu, 2006; Eckert and Gerbeth, 2002; Blackstock, 2000; Papadakis, 1999) have discussed these methods in some detail and concluded that there is no significant advantage in choosing one mode over the other. However, with the availability of the electronic multipliers, e.g. the MC1496 Analogue Multiplier, there was an obvious opportunity for the author to implement the *Phase Comparison System*, see Chapter 4.

- The leading edge mode

In this mode, the transducers are used as both transmitters/receivers. One transducer is used as the transmitter and another as the receiver, and the time taken for the wave to travel from the one to the other is measured. Then the roles are reversed, another wave transmitted and received and a second time measured. The transit time  $\Delta t$  between the two measured times is found by a simple averaging process. Because there is always a

defined leading phase which is the transmitted signal, hence the name leading edge mode. This system has the advantage that only one electronic path is used to measure  $\Delta t$  and so differential delay can be eliminated. This method is not good for measuring relatively long times accurately.

In this mode, the equation governing the velocity is obtained through this equation:

$$\Delta t = \frac{2v(D-2z)\cot\theta}{c^2} \quad 3.27$$

where:  $D$  is pipe diameter (m),  $z$  is the pipe wall thickness (m),  $c$  is sound velocity (m/s),  $\theta$  is the orientation angle (degrees) of the transducer and  $v$  is the flow velocity (m/s).

- The frequency system

Here one transducer acts transmitter and the other as receiver. A wave is transmitted and the moment it is received a second is triggered from the transmitter, and a frequency train is set up. Then the transmitter and receiver are reversed and the procedure is carried out in the opposite direction. The difference in frequency  $\Delta f$  of the frequency trains is a measure of the velocity.

This method, which includes all the measuring electronics in one feedback loop has the problem that  $\Delta f$  is of the order of 1000 times smaller than the transmitted frequency and hence a long response time is required (Murakawa et al., 2005).

$$\Delta f = \frac{2d v \cos\theta + ((c^2 - v^2 \cos^2\theta))}{[d + (c - v \cos\theta)][d + (v \cos\theta)]} \quad 3.28$$

where:  $d$  is the length of the acoustic path (m),  $c$  is sound velocity (m/s),  $\theta$  is the angle (degrees) between the acoustic path and a vector representing the direction in which the medium moves and  $v$  is the velocity of the moving medium (m/s).

- The phase comparison system

If the transducers are used in a continuous or quasi-continuous system then the phase difference between upstream and downstream signals is given by:

$$\phi = \frac{\Delta t}{T} 2 \pi \quad 3.29$$

where:  $\phi$  is the phase difference (degrees),  $T$  is the time period of the signal and  $\Delta t$  is the difference in transit time between the upstream and downstream signals (s).

The advantage of this system is that increasing  $f$  increases the phase difference to be measured and this eases the electronic measurement. Various techniques have been used to improve this method, the chief one being heterodyning (mixing) of the received signals with a local oscillator. Because mixing of signals maintains phase relationships the problem of timing is eased by mixing at a frequency very near to that of the signal itself.

As mentioned at the beginning of this section, with the availability the electronic multipliers, e.g. the MC1496 Analogue Multiplier, there was an obvious opportunity for the author to implement the *Phase Comparison System* using continuous wave (CW). To understand the concept of this technique, assume we have a sine wave transmitted from two identical transducers and received by two receivers. Each point on the transmitted ultrasound wave from Tx1 received at Rx1 takes longer to arrive than the equivalent point on sine wave from Tx2 takes to arrive at Rx2. Since Tx1 and Tx2 are excited by the same source, the measured sine wave at Rx1 lags that at Rx2 by phase difference  $\phi$ , see Equation 3.29.

With reference to Figure 3.21 (the novel configuration D which was presented earlier in Section 3.3.1), the time for an ultrasonic wave to travel in the downstream direction ( $t_d$ ) is given by:

$$t_d = d \frac{1}{(c + v \cos \theta)} = \frac{d}{c} \left(1 - \frac{v}{c} \cos \theta\right) \quad \left[\text{as } \frac{v}{c} \cos \theta \ll 1\right] \quad 3.30$$

The time for an ultrasonic wave to travel in the upstream direction ( $t_u$ ) is given by:

$$t_u = d \frac{1}{(c - v \cos \theta)} = \frac{d}{c} \left(1 + \frac{v}{c} \cos \theta\right) \quad 3.31$$

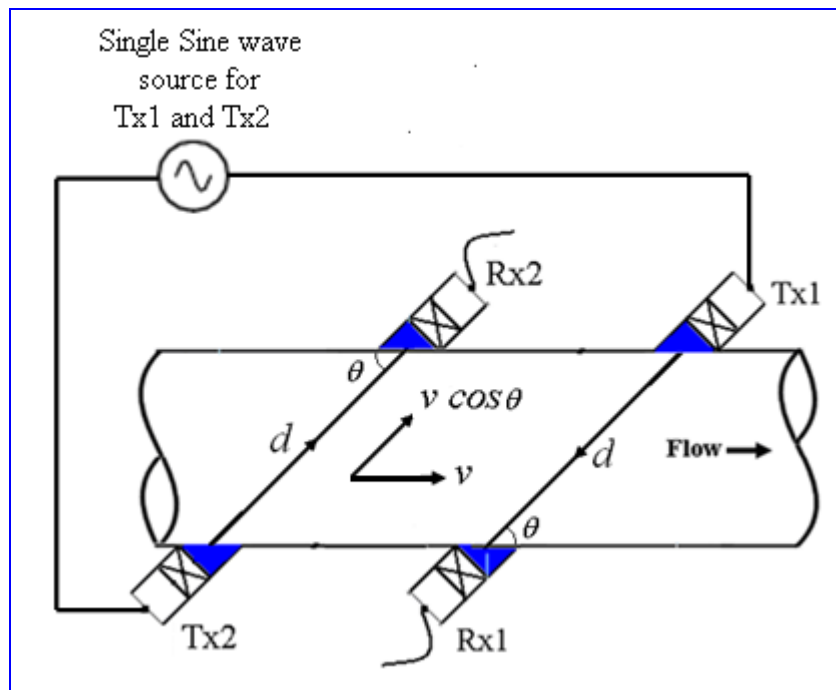


Figure 3.21 Ultrasonic wave directions

The time difference  $\Delta t$  between the durations of travel can be shown to be:

$$\Delta t = \tau_u - \tau_d = \frac{d}{c} \left(1 + \frac{v}{c} \cos \theta - 1 + \frac{v}{c} \cos \theta\right) \quad 3.32$$

$$\Delta t = \frac{2vd}{c^2} \cos \theta \quad 3.33$$

The phase relationship as a function of time delay is given by:

$$\phi = \frac{\Delta t}{T} 2\pi \quad 3.34$$

$$\phi = \left( \frac{4 \pi f d}{c^2} \cos \theta \right) v \quad 3.34a$$

or

$$\phi = \hat{c} U_g \quad 3.35$$

where:  $U_g$  is the gas velocity (m/s) and  $\hat{c}$  is a constant.

Equation 3.35 implies a linear relationship between the phase and the gas velocity, see Figure 3.22, since the value of the terms in brackets in Equation 3.34a can be assumed constant ( $\hat{c}$ ) if  $c$  in Equation 3.34a is assumed constant. Taking the following values:  $c = 329.43 \text{ m/s}$ ,  $d = 0.07 \text{ m}$ ,  $\theta = 45^\circ$ ,  $f = 40 \text{ kHz}$  then  $\hat{c} = 13.26$ . Table 3.2, shows the corresponding calculated phase shifts  $\phi$  for different gas velocities, and Figure 3.22 shows the same information in a graphical form.

<b>Velocity</b> $v \text{ m/s}$	<b>Phase shift</b> $\phi$
1	13.26
5	66.33
10	132.71
15	199.18
20	265.78
25	332.58

*Table 3.1 Phase shift calculation*

The mean volumetric gas flow rate is usually the quantity required:

$$Q_g = A U_g \quad 3.36$$

where:  $Q_g$  is the gas volumetric flow rate ( $\text{m}^3/\text{s}$ ),  $U_g$  is the gas velocity (m/s) and  $A$  is the pipe cross-sectional area of the pipe ( $\text{m}^2$ ).

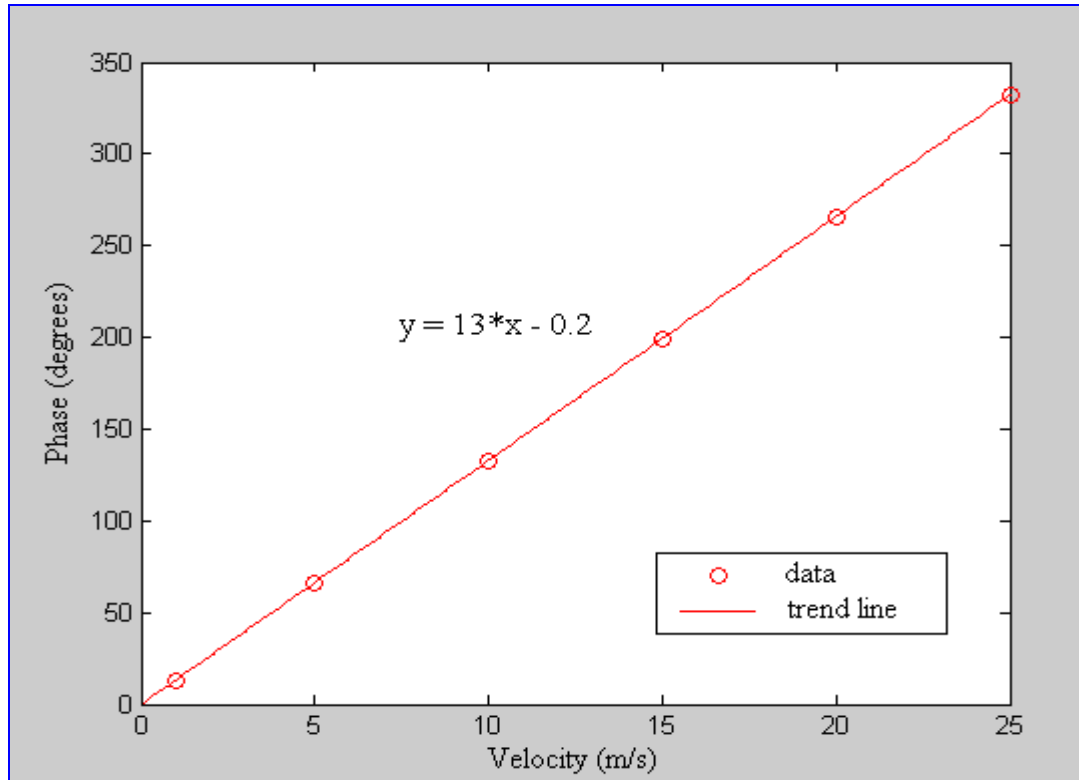


Figure 3.22 Relation between change in phase and the velocity

A similar technique has been used by Pavlović, et al., (1997) but with only one acoustic path with transducers that can both receive and transmit a signal. Also, the application was measurement of liquid flow rate. The design included a complicated electronic circuit whereas a simplified electronics technique is being used in this study.

The idea is for an electronic system to multiply the signals from the two receivers Rx1 and Rx2 (see Figure 3.22) with a suitable, locally generated reference:

$$\sin(\omega_1 t + \theta_1) \sin(\omega_2 t + \theta_2) = \frac{1}{2} \{ \cos[(\omega_1 - \omega_2)t + \theta_1 - \theta_2] - \cos[(\omega_1 + \omega_2)t + \theta_1 + \theta_2] \} \quad 3.37$$

If the two frequencies are the same ( $\omega_1 = \omega_2 = \omega$ ) the result is a DC component and an AC component of frequency  $2\omega$ . A low pass filter allows the DC component through, while the AC “ripple” ( $2\omega$ ) is reduced.

However, without taking any calibration constant into account, Figure 3.22 shows the theoretically calculated output of the circuit at different phase angles.

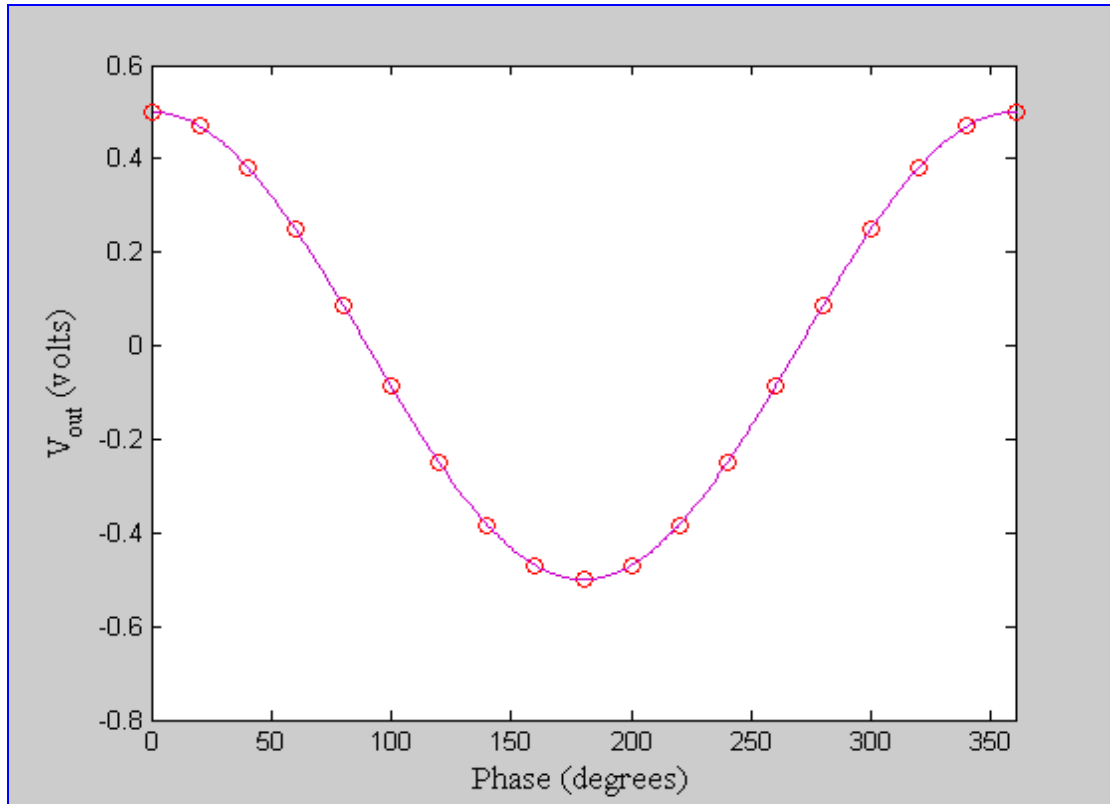


Figure 3.23 Theoretical output of the USFM electronic circuit

Figure 3.23 shows that  $V_{out}$  against  $\phi$  is symmetrical about  $\phi=180^\circ$ . This will introduce a possible ambiguity into the system when taking a reading of different phase angles which give a similar  $V_{out}$ . For example:

$$V_{out} \text{ (at } \phi = 200^\circ \text{ and correspond to } U_{g,s} = 15.12 \text{ m/s)} = -0.47 \text{ volts}$$

$$V_{out} \text{ (at } \phi = 160^\circ \text{ and correspond to } U_{g,s} = 12.12 \text{ m/s)} = -0.47 \text{ volts}$$

So, realistically, we use the designed USFM for changes in phase in the range  $180^\circ < \phi < 360^\circ$  which corresponds to a range gas velocity of  $13.6\text{m/s} < U_{g,s} < 27.23\text{m/s}$ . This range is practical since high gas flow rates are required in this study.

The electronic circuit output when calibrated is given by:

$$V_{out} = \hat{a} \cos(\phi) + \hat{b} \tag{3.38}$$

where:  $\hat{a}$  and  $\hat{b}$  are to be found from the calibration curve and  $\phi$  is the phase-shift angle.

Substituting Equation 3.35 into Equation 3.38 gives:

$$V_{out} = \hat{a} \cos(\hat{c} U_g) + \hat{b} \tag{3.39}$$

This idea can be used to improve the calibration curve of the USFM and that will be discussed later in the next chapter, see Section 4.3.4.

## CHAPTER 4 DESIGN AND CALIBRATION OF SENSOR TUBE, CFM AND USFM

Parallel with the challenge of developing a measurement technique, there was the challenge of designing the measurement devices. A system containing three major devices (Sensor tube, Conductance Flow Meter (CFM) and Ultrasonic Flow Meter (USFM)) to take the required measurements, was successfully designed and implemented.

### 4.1 Film extraction by sensor tube

This section describes the film extraction method with which the volume fractions of oil and water in the liquid film could be determined if required. It comprised, see Figures 4.1 and 4.2, a 15mm inner diameter Perspex tube, 1.2m long, four Burkert solenoid valves, and two pressure taps connected to a Honeywell ST-3000 differential pressure transducer (DP cell). Despite the fact that the sensor tube was not used extensively in the present study, the set up was used to demonstrate the feasibility of extracting the liquid film into the sensor tube that could be used to determine the oil volume fraction  $\alpha_o$  and water volume fraction  $\alpha_w$  in the liquid film.

#### 4.1.1 Principle of operation of sensor tube

Part of the liquid film was periodically extracted into the sensor tube, its density measured off-line and then the liquid was released back into the system. With an oil-water mixture, the oil and water volume fractions could be calculated from this density measurement. From the  $\Delta P$  measured by the DP cell and assuming that the lines between the pressure tappings and the DP cell are water filled, see Figure 4.2, the density  $\rho_m$  of the oil-water mixture can be calculated from:

$$\Delta P = \rho_w g h_{ST} - \rho_m g h_{ST} \tag{4.1}$$

$$\therefore \rho_m = \rho_w - \left[ \frac{\Delta P}{g h_{ST}} \right] \quad 4.2$$

where:  $\Delta P$  is the measured differential pressure,  $\rho_w$  is water density,  $\rho_m$  is mixture density,  $g$  is  $9.81\text{m/s}^2$  and  $h_{ST}$  is the separation of the pressure tapping in the sensor tube (1m). Pressure sensor lines are filled with water during the oil-water mixture density measurement to avoid having air in the pressure lines.



Figure 4.1 Sensor tube, to the left and outside the red line



It is known that:

$$\rho_m = \alpha_{o,l} \rho_o + \alpha_{w,l} \rho_w \quad 4.3$$

where:  $\alpha_{o,l}$  is the oil volume fraction in the liquid film,  $\rho_o$  is the oil density,  $\alpha_{w,l}$  is the water volume fraction in the liquid film and  $\rho_w$  is the density of the water.

Also, we have:

$$\alpha_{o,l} + \alpha_{w,l} = 1 \quad 4.4$$

So, from Equations 4.2, 4.3 and 4.4, knowing  $\rho_m$ ,  $\rho_o$  and  $\rho_w$ , the oil and water volume fractions in the liquid film can be found. These values for oil and water volume fractions are likely to also be the correct values for the oil and water volume fractions for the liquid droplets in the core. However, for the annular flow, the oil volume fraction  $\alpha_{o,l}$  and the water volume fraction  $\alpha_{w,l}$  in the liquid film do not represent the overall oil and water volume fractions of the flow. The overall oil and water volume fractions  $\alpha_o$  and  $\alpha_w$  respectively, are given by Equation 4.5:

$$\alpha_o + \alpha_w + \alpha_g = 1 \quad 4.5$$

Where the overall oil volume fraction is  $\alpha_{o,l} \alpha_l = \alpha_o$  and the overall water volume fraction is  $\alpha_{o,w} \alpha_l = \alpha_w$ , and  $\alpha_g$  is the gas volume fraction.

#### 4.1.2 Liquid film extraction procedure

The sensor tube system is shown in Figure 4.1. To the left of the test section is a 15mm internal diameter Perspex tube (sensor tube), where  $h_{ST}$  (1m) represents the distance between the taps situated at the top and bottom of the sensor tube. Nylon tubes of 6mm internal diameter were used to connect the solenoid valves to the sensor tube. The sensor tube was operated in the following manner: to fill both sensor and nylon tubes, solenoids A and C were both opened while B and D were closed. In this case, solenoid A allowed liquid to fill the tube and solenoid C allowed the air in the tube to escape. Once the liquid reached the downstream pressure point (a tap at the

top of the nylon tube) both solenoids were closed. At this moment the  $\Delta P$  measurement was taken.

To release the liquid back into the test section, solenoids B and D were opened and A and C closed. Now, solenoid B allowed the liquid to return back to the test section. However, the pressure in both the sensor tube and the test section was equal at some point and that prevented a full discharge of the liquid into the test section. In this case, solenoid D allowed air from the air line to flow into the sensor tube and push the liquid out. This process was undertaken automatically using a simple m-file in MATLAB via LABJACK.

## 4.2 Conductance flow meter

From the literature survey, see Section 2.3.2, and the preliminary work, see Section 3.2; the conductance technique was chosen to measure the liquid film thickness. This technique is considered a method that will give a measurement of the local thickness of the film. The designed CFM has two conductance probes and each probe has two electrodes.

### 4.2.1 Principle of operation of CFM

Liquid film thickness can be determined from these conductance measurements by a calibrated linear relationship for the range of measurements, see Section 3.2. In this study, the electrodes are two parallel thin stainless steel needles (the probes). These protrude from the pipe wall supported only at the end outside the pipe. As the film thickness increases, the measured resistance between the electrodes decreases. The voltage output  $V_a$ , see Figure 4.3, depends on the geometry of the probes, their dimensions and on the conductivity of the liquid. The film thickness/voltage output  $V_{out}$  relationship was obtained by prior calibration.

### 4.2.2 Electronic circuitry

The electronic circuitry involved the application of a high frequency, constant amplitude AC signal. The designed circuit consisted of, see Figure. 4.4: **(A)** an inverting amplifier, **(B)** a non-inverting amplifier, **(C)** a half wave rectifier, **(D)** a low-pass filter, **(E)** a non-inverting amplifier, **(F)** a zero offset adjust and **(G)** a low-pass filter as RC ripple filter.

The first stage of the circuit was the inverting amplifier whose output  $V_a$  was proportional to the conductance,  $S_m = \frac{1}{R_m}$ , between the electrodes of the CFM, see Figure 4.4.

The output of this stage is given by:

$$V_a = -\left(\frac{R_{fb}}{R_m}\right)V_i \quad 4.6$$

where:  $R_{fb}$  is the reference feedback resistance,  $V_a$  is the output voltage, and  $V_i$  is the AC input voltage.

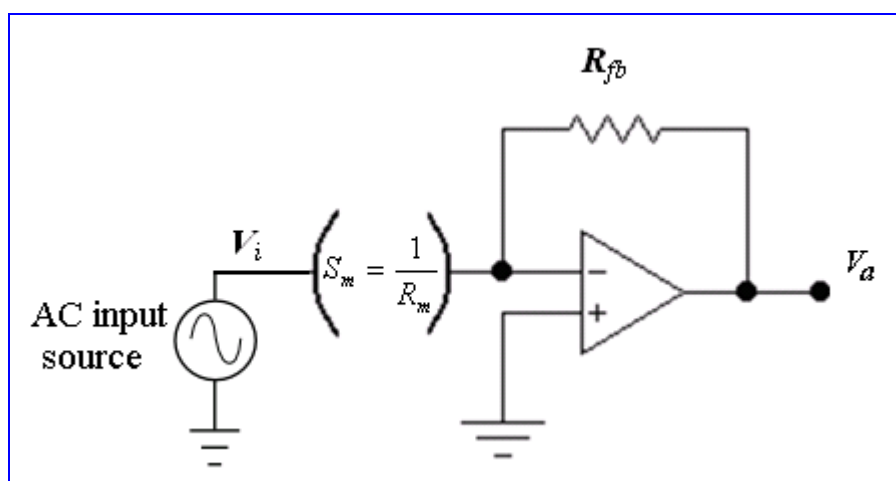


Figure 4.3 First stage of the electronic circuit showing the principle of the initial conductivity measurement

Because the reciprocal of electrical resistance is conductance  $S_m$  the above equation can be rewritten as:

$$V_a = -R_{fb} S_m V_i \quad 4.7$$

$$V_a = K S_m \quad 4.8$$

where:  $K$  is a constant  $= -R_{fb} V_i$ .

Thus any change in the water level between the electrodes which changes the conductance  $S_m$  will (as shown previously by Equations 3.15-3.24) result in a change in the circuit output voltage  $V_a$ .

The choice of excitation frequency was critical to the successful operation of the probe. At low frequencies, the conductance between the electrodes was affected by a number of capacitive and resistive elements that arose at the electrode-electrolyte interface commonly referred to as ‘double layer’ effects (Conte, 2003). Therefore, an excitation frequency high enough to negate the double layer effect was chosen. Kvurt, et al., (1981) extensively studied the influence of frequency of the signal on the measured results and concluded that frequencies of at least 50kHz should be used. In the present study, the designed circuit used a 50kHz sine wave signal and AC voltage amplitude of 2.2 volts peak-to-peak.

Part (B) of the circuit is a non-inverting voltage amplifier. The op-amp gain can be controlled by the variable resistor VR1. The input signal can be amplified theoretically from 1.6 to infinity. So the variable resistor VR1 is used as system gain control.

Part (C) of the circuit is an inverting full-wave voltage rectifier. For the positive half cycle input, the op-amp output goes negative and current flows through the output resistor (100k $\Omega$ ). It acts like an inverting amplifier except for a diode in a series with the op-amp output. For the negative half cycle input, the op-amp output goes positive. Now no current is flowing in the output resistor (100k $\Omega$ ) because the upper diode is

shut. The rectified voltage is DC; however, it is not a steady DC but a fluctuating DC and needs to be smoothed before it is useful.

Part **(D)** of the circuit is a low pass filter. The DC output produced in the previous stage will be smoothed here and the low pass filter output will be a useful DC signal. The gain of the DC output signal will vary between -2 and -2.5 depending on the variable resistance VR2. In this circuit design the variable resistance VR2 is used as a span adjuster.

Part **(E)** of the circuit is a differential amplifier that amplifies the difference between two inputs. One input (the output of part D) has a positive effect on the output signal; the other input (the output of part F) has a negative effect on the output.

Part **(F)** of the circuit is a non-inverting op-amp with a unity gain. The non-inverting side of the op-amp connected to a  $\pm 15\text{V}$  power supply via variable resistor VR3 and two  $2.5\text{k}\Omega$  buffer resistors. This part of the design works as a zero adjustment with a buffer. So the variable resistor RV3 is used as a zero adjuster.

Part **(G)** is the final DC output voltage  $V_{out}$ .

Two electronic circuits were designed and built to serve the two conductance probes of the CFM. One of the conductance probes was used to measure liquid film thickness. However, the two probes together were used to measure the liquid film velocity as described earlier in Section 2.3.3.

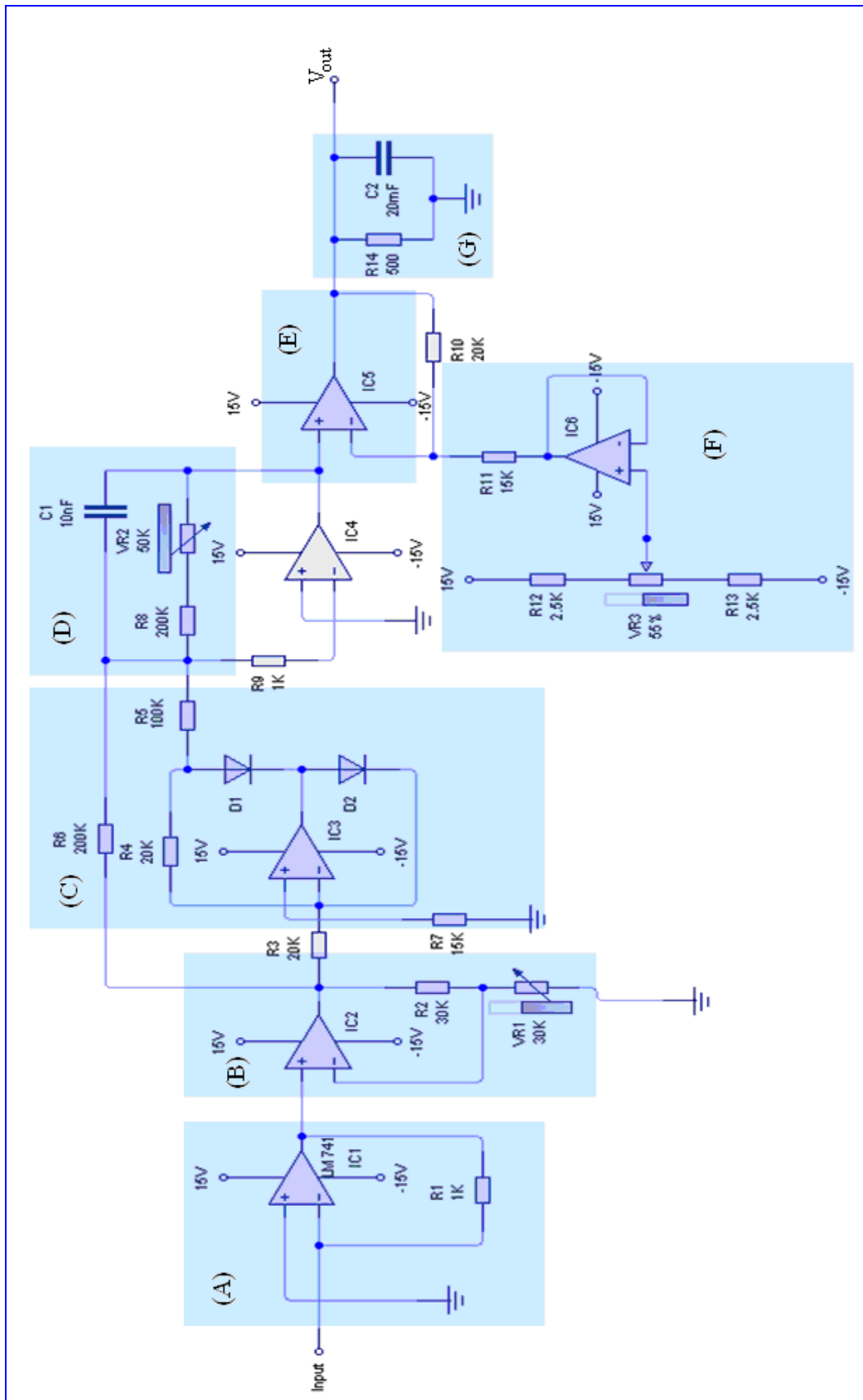


Figure 4.4 Conductance monitoring circuit

### 4.2.3 Design and calibration of CFM

The CFM flow meter consisted of Perspex pipe of 50mm internal diameter to match the test section. Two conductance probes separated by an axial distance of 70mm were mounted in the Perspex pipe. The electrode diameter was 1.3mm. The choice of electrode diameter was critical to the successful operation of the CFM, it had to be small enough to have negligible effect on the flow and yet be large enough to be sensitive to changes in the electrical resistance over the entire range of liquid film height (Koskie et al., 1989). Figure 4.5 shows the final design of the CFM being installed in the flow loop.

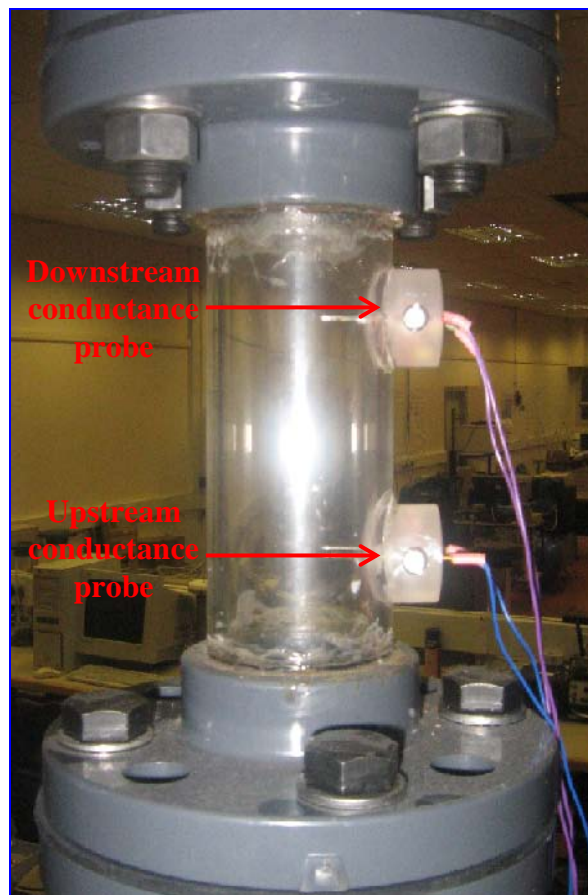


Figure 4.5 Conductance flow meter installed in the flow loop

Two boss connections were fitted in a symmetrical position and separated by an axial distance of 70mm in the direction of the flow. The bosses were machined to match the shape of the inner surface of the main tube, see Figure 4.6. In each boss, a pair of holes was drilled to fit the needle electrodes, with the needle electrodes 20mm apart, centre to centre, so that the plane containing the electrodes was perpendicular to the flow direction. The electrodes protruded 20mm into the 50mm inner diameter pipe. In the middle of each electrode path, a threaded M3 hole was drilled to take a grub screw to hold the electrode tight, see Figure. 4.7.

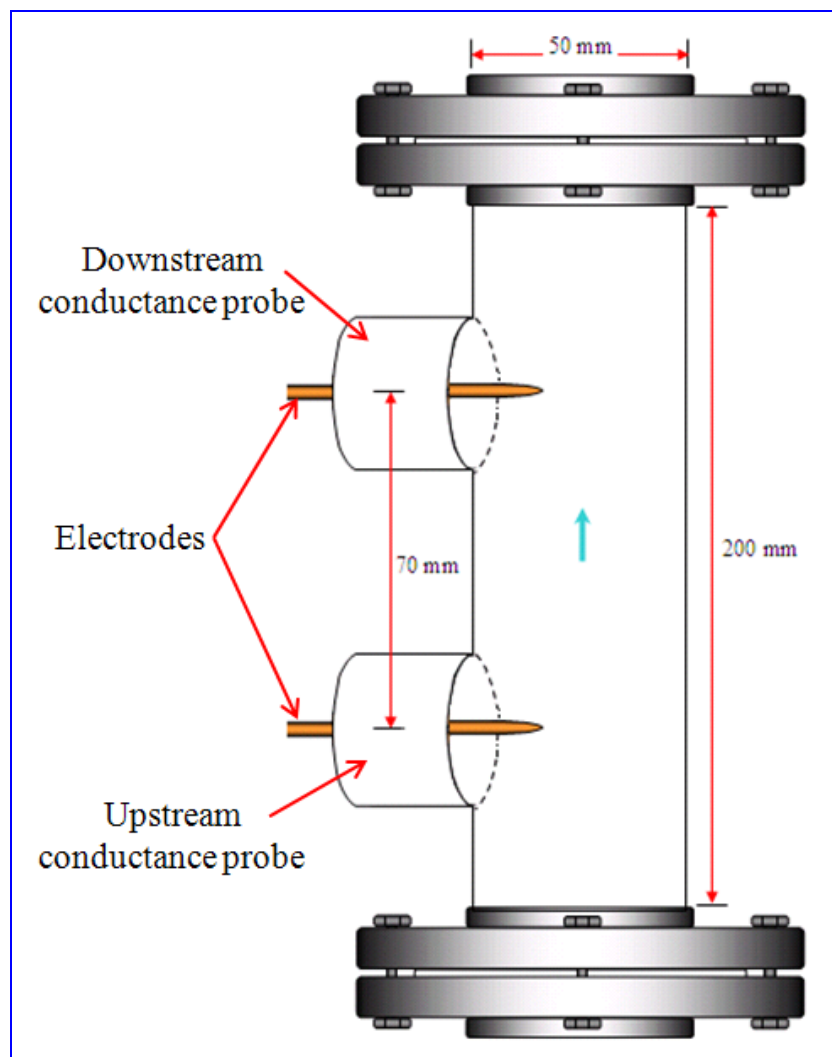


Figure 4.6 Sketch of a side view of the CFM (not to scale)

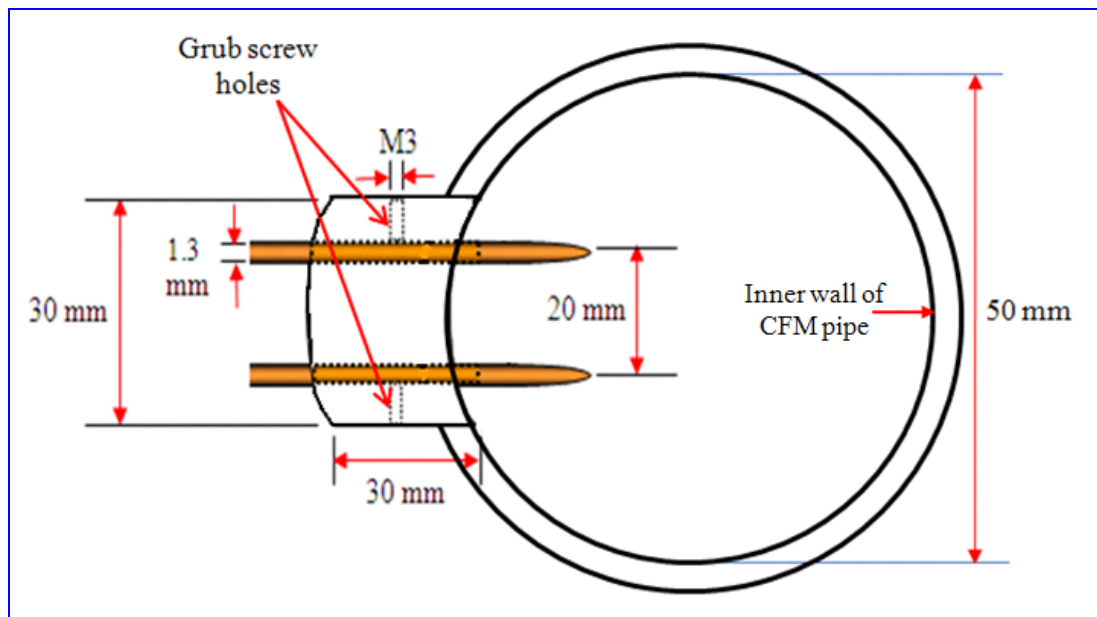


Figure 4.7 Top view showing the boss connection (not to scale)

The aim of having two sets of measurement points (one upstream and one downstream) was:

- To determine the local mean film thickness at two points, one upstream of the other.
- To allow cross-correlation of the two film thickness signals to determine the liquid film velocity.

This technique was less reliable for thin films because of its intrusive nature, and the formation of a meniscus due to surface tension effects. A bench test, see Section 3.2.1, showed that the best separation of the two electrodes to minimise the effect of the meniscus, was 20mm.

Calibration of the probes was performed on a laboratory bench. It was done by placing different sizes of solid cylindrical non-conducting plugs concentrically in the main body of the flow meter, see Figure 4.8. The gap between the pipe inner diameter and the outer diameter of a particular solid core represents an annular film when the gap is filled with water. The cores were made of dry foam material and could be

machined with a sufficient precision to give film thicknesses of 1mm, to 20mm in steps of 1mm. Conte, (2003) reported a similar calibration method.

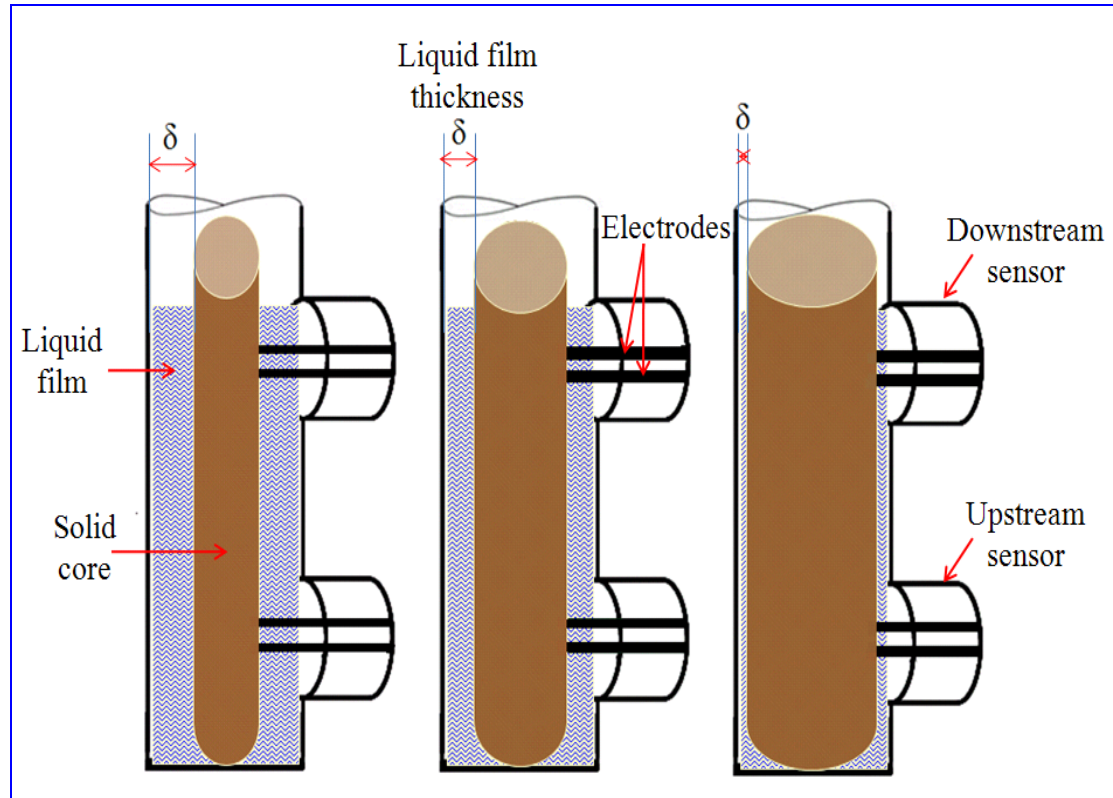


Figure 4.8 CFM calibration process using non-conducting plugs

During the calibration process, voltage readings were acquired from both probes at two stages ( $V_{out,us}$ : upstream probe output voltage and  $V_{out,ds}$ : downstream probe output voltage). In the first stage, voltage readings were taken from each probe separately and compared. In the second stage, readings were taken from both sensors simultaneously and compared to the first stage readings. This was done to investigate if there was any presence of signal cross-talk (defined in Section 3.3.1) between the two probes. Big variations between the readings from both sensors would indicate that sensors are influencing the operation of each other. This investigation also ensured that the electronic circuits for both probes were operating simultaneously and matched output responses were produced.

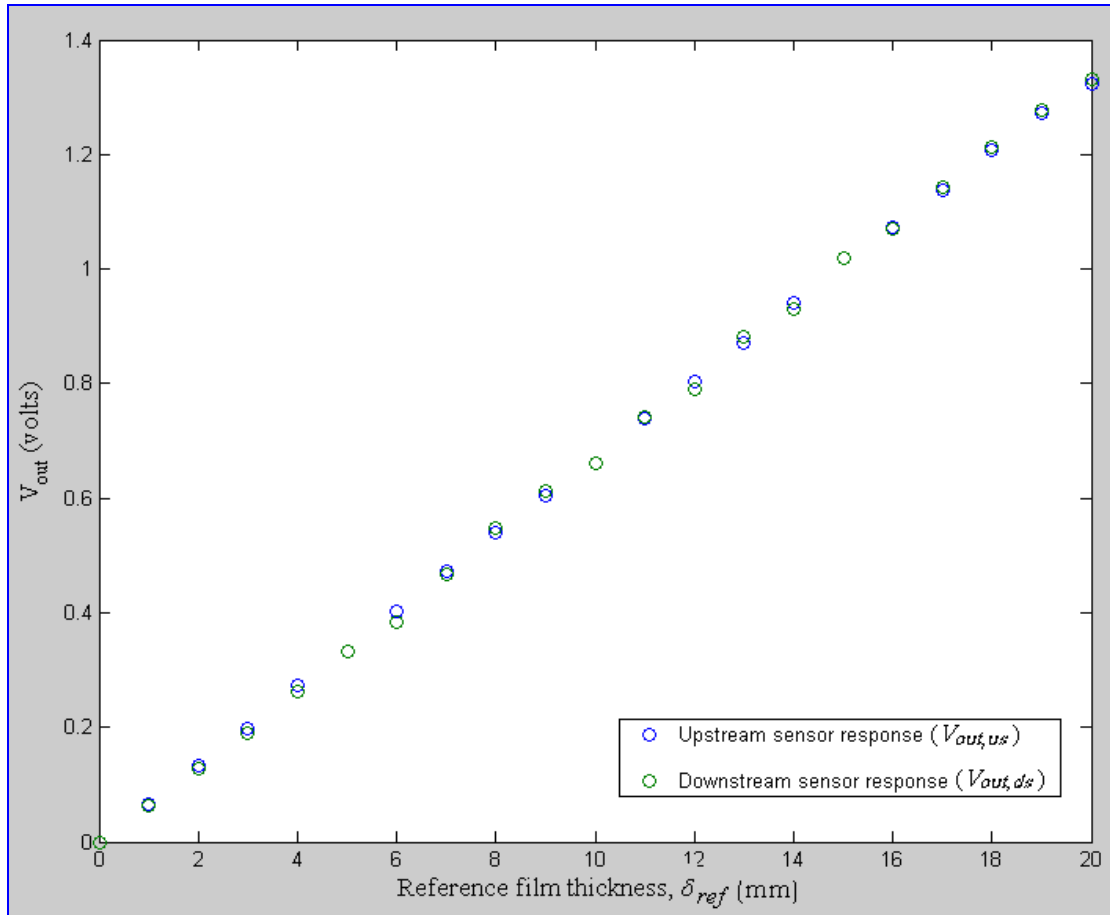


Figure 4.9 Output responses of both sensors; simultaneously

Figure 4.9 shows that both sensors operated similarly in a defined characteristic correspondence to film thickness variations. This gives the option of using either probe to measure the film thickness. However, in this current investigation the downstream probe was used to measure the film thickness. There are some negligible variations which can be attributed to the tolerance of the electronic components. A least squares fit showed that the trend lines for both data sets were the same to within experimental error:

$$V_{out,us} = 0.067 \delta - 0.0017 \quad (\text{Upstream probe}) \quad 4.9$$

$$V_{out,ds} = 0.067 \delta - 0.0053 \quad (\text{Downstream probe}) \quad 4.10$$

This allowed the production of an average trend line by combining both sets of data, see Figure 4.10:

$$V_{out} = 0.067 \delta - 0.0074$$

4.11

where:  $\delta$  is the film thickness in mm.

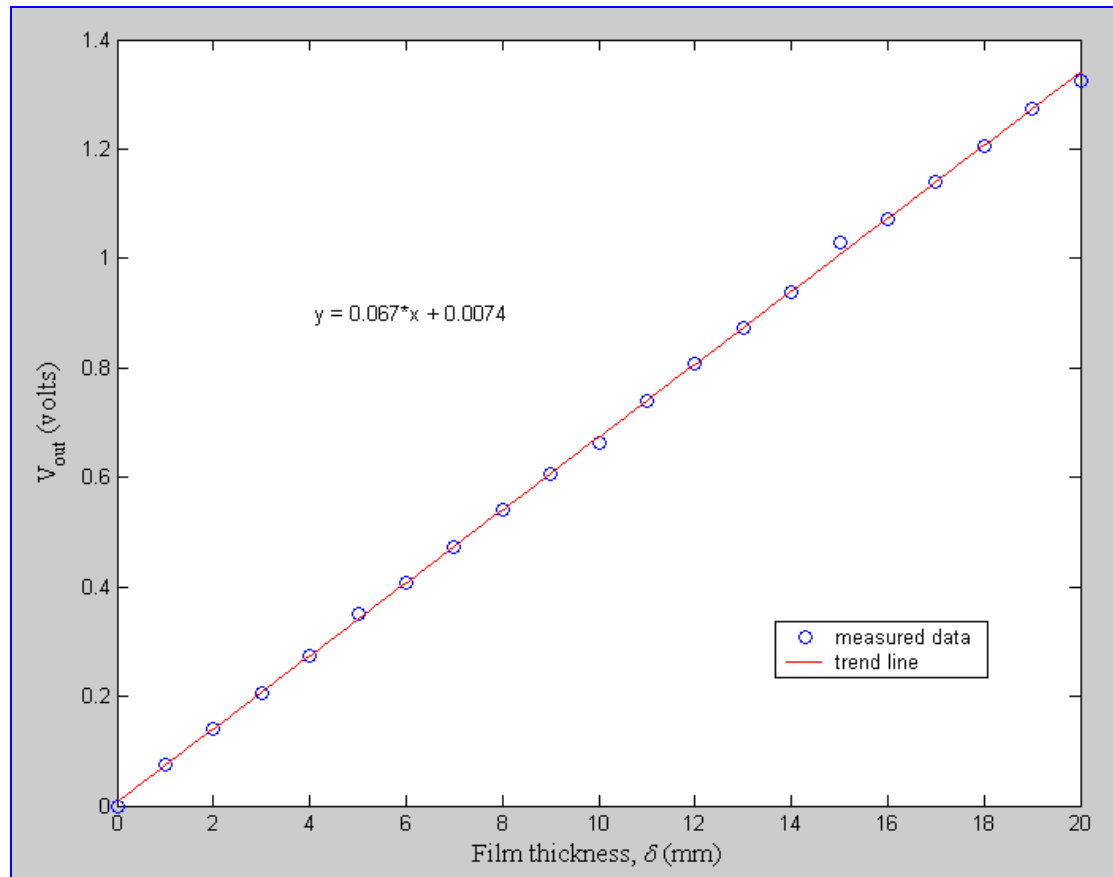


Figure 4.10 Calibration curve for probe separation 20mm

The response of this system was linear and could be used for both thin and thick films. Once again the result in Figure 4.10 confirms the analysis of Section 3.2 which suggested a linear relationship between the voltage output of the CFM and the measured liquid film thickness, see Equations 3.15-3.24.

The output voltages from both probes were found to drift very slightly so they were calibrated once a week. Full tube and empty tube voltages were taken before and after every flow loop run to ensure that there had been no calibration drift during that particular experimental run.

Using a similar argument to Section 3.2.1, estimated values for film thickness could be obtained using the probes and a percentage error in this measured liquid film

thickness could be calculated  $\xi_{f,thickness}$ , see Figure 4.11. The error calculation showed a mean error of 1.52% in the measured value of the film thickness  $\delta$ , though larger errors appeared at smaller film thicknesses.

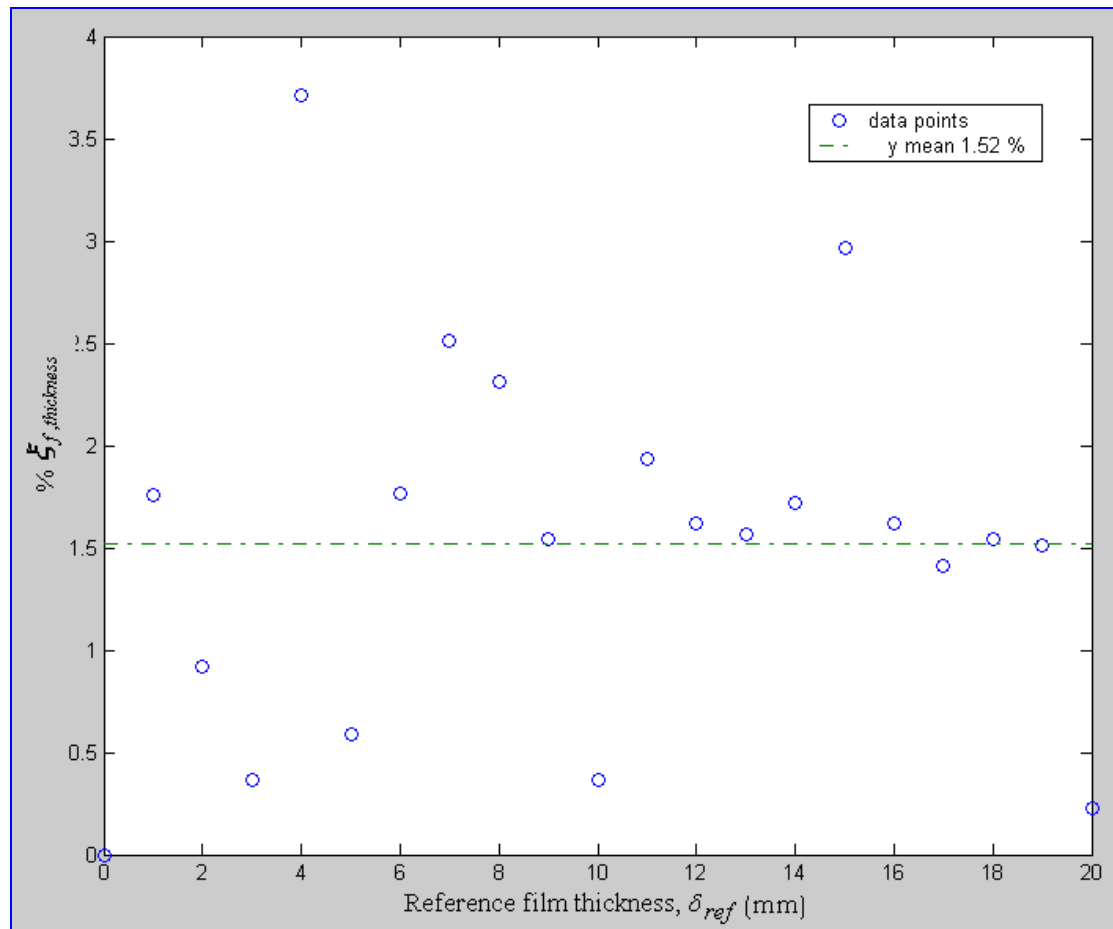
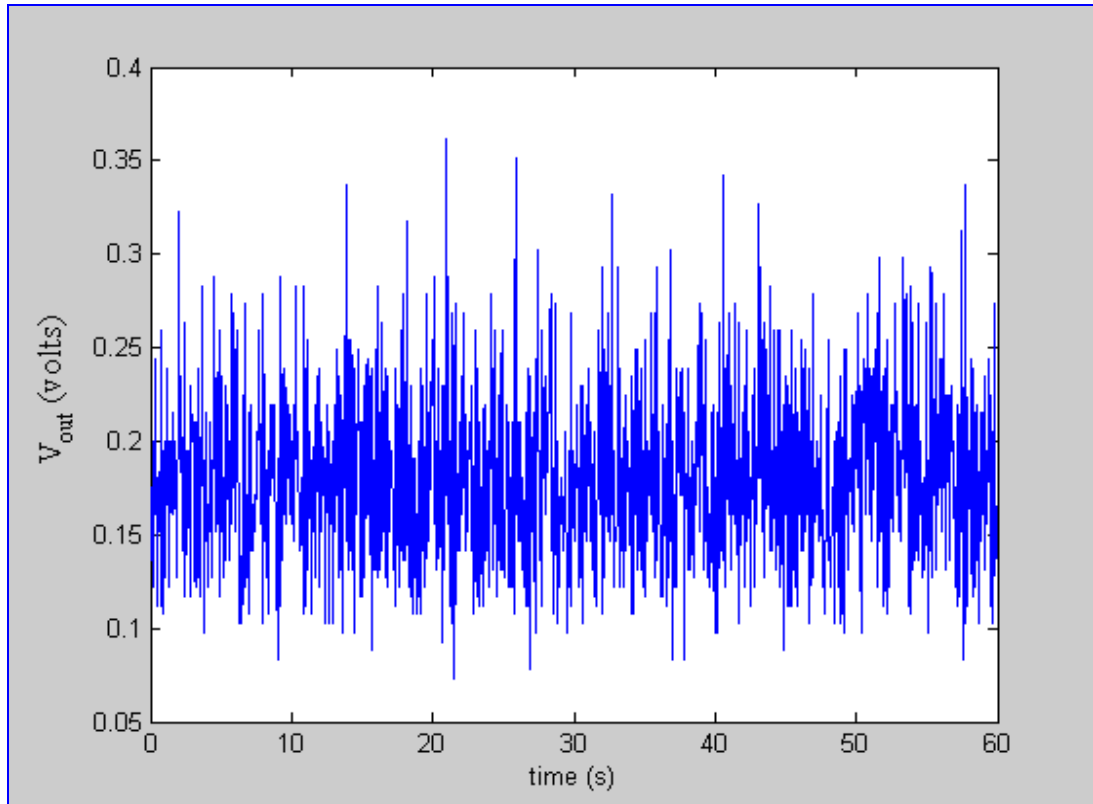


Figure 4.11 Percentage error in liquid film thickness measurement

#### 4.2.4 Signal optimization of the CFM device

With a water flow rate of  $4.17 \times 10^{-4} \text{ m}^3/\text{s}$  and gas flow rate of  $140 \text{ m}^3/\text{hr}$  the output voltages from the CFM probes were monitored and investigated. Figure 4.12 shows the response of the CFM to the liquid film thickness from one of the probes for 60 seconds at the normal sampling frequency, 50Hz, of the LABJACK U12. This response is very noisy and it was difficult to achieve cross-correlation results from both probes with such signals. In this case the sampling frequency was suspected of being too low and, as will be explained in Section 5.3.3, the sampling frequency was increased to 1kHz. This action improved the signal enormously, see Figure 4.13.



*Figure 4.12 CFM output voltage at 50Hz sampling frequency*

However, because of the limited memory with the LABJACK U12 there was a major disadvantage with the faster sampling rate, data for only for about 4.5 seconds could be stored, whereas for the 50Hz sampling rate over 1 minute of data could be stored. To reduce random errors data for each flow condition was collected 10 times and then averaged. Figure 4.13 shows that outputs from the two probes, upstream (blue) and downstream (green), of the CFM device correspond very well to each other and thus, to the liquid film thickness. The downstream signal is delayed with respect the upstream signal.

The signal obtained using the faster sampling frequency (1kHz) was processed using a digital filter to eliminate the very high frequencies which gave rise to the spikes on the signal and which may have been introduced by the pulsating movement of the liquid film. A 3rd order digital filter was tuned by trial and error to obtain the right order of the filter to produce a signal without the unwanted spikes. The mean values of the filtered and non-filtered data were taken separately in order to examine the effect of using the filter. For, both probes, the non-filtered data the mean value was 1.141volts and for the filtered data was 1.136 volts. This indicates that the filter did impose a

small effect on the data when compared to the sensitivity of the device voltage output, about 0.067volts/mm, see Equation 4.11, which was considered acceptable.

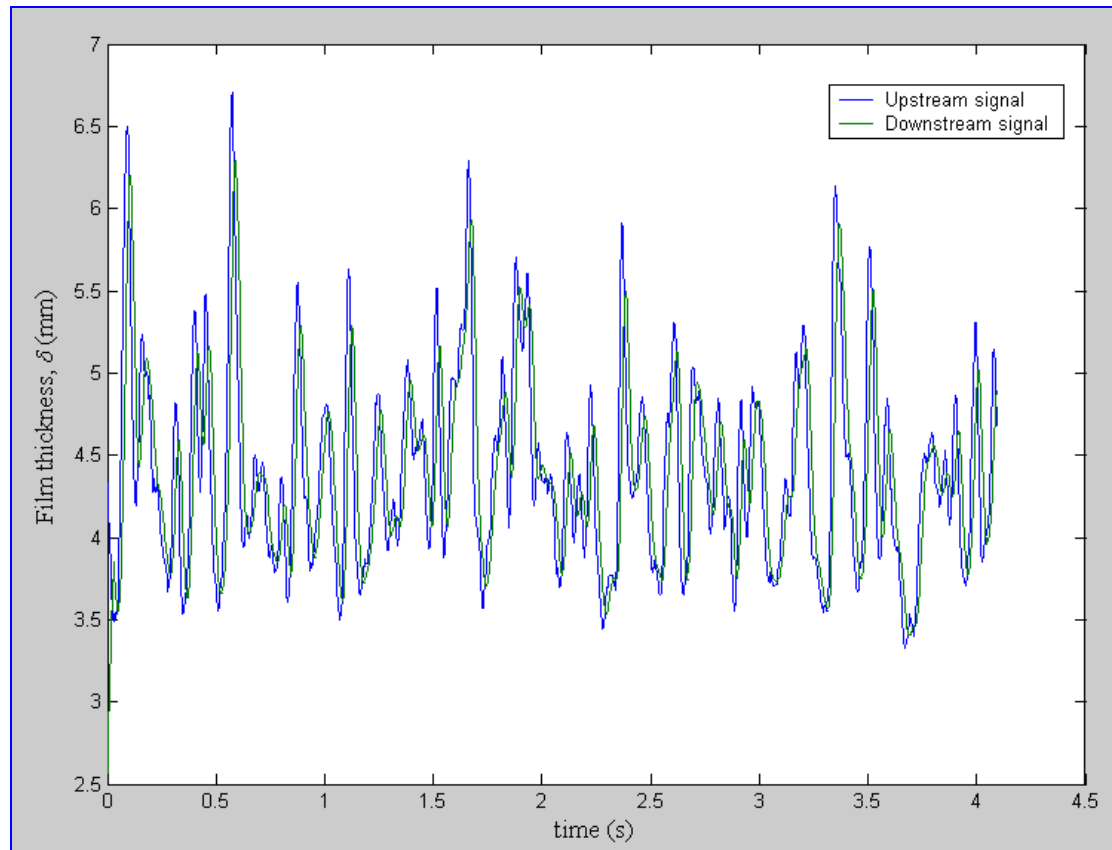


Figure 4.13 CFM film thickness reading at 1 kHz sampling frequency (Upstream sensor blue, downstream sensor green)

#### 4.2.5 Cross-correlating the CFM probe signals

The reason for acquiring signals from the two axially separated probes is to cross-correlate them in order to obtain the liquid film velocity. By cross-correlating upstream and downstream signals, a function  $R_{xy}(\tau)$  with a well defined peak is obtained. However, as was explained at the start of this section it was not possible to achieve a well defined peak using probe signals sampled at 50Hz, see Figure 4.14. The 1kHz sampling frequency improved the cross-correlation result and a further improvement was achieved when 10 sets of cross-correlograms obtained from 10 sets of data (4.5 seconds long) at a given flow condition were ensemble averaged, see Figure 4.15 which shows a well defined peak occurring at the mean time delay between the upstream and downstream signals. The obtained result agrees well with

the cross-correlation theory introduced earlier in Section 2.3.3 and its graphical representation in Figure 2.17.

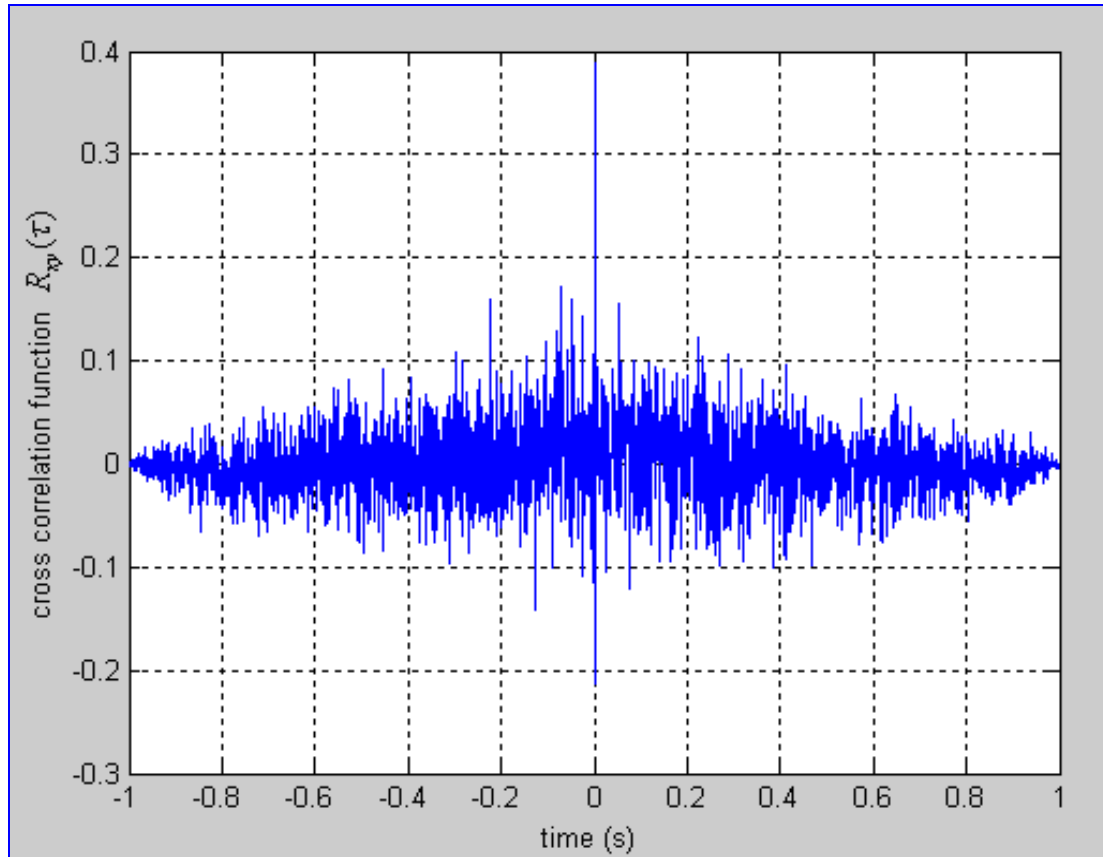


Figure 4.14 Correlogram of the two signals, 50Hz sampling rate

The separation of the probes was 0.07m, for the flow condition shown in Figure 4.13 for which  $U_{g,s}=19.8\text{m/s}$  and  $U_{w,s}=0.212\text{m/s}$  the time taken for the liquid film to travel this distance is 0.108s (see Figure 4.15), so  $U_f = 0.07/0.108= 0.648\text{m/s}$ . the reference volume flow rate of the water was measured, see Section 5.1.2, as  $Q_{w,ref} = 4.17 \times 10^{-4} \text{m}^3/\text{s}$ . Using the relationship:

$$Q_{w,ref} = U_f A_f \quad 4.12$$

It follows that a prediction for the cross-sectional area of the film from Equation 4.12  $A_f = 6.43 \times 10^{-4} \text{m}^2$ .

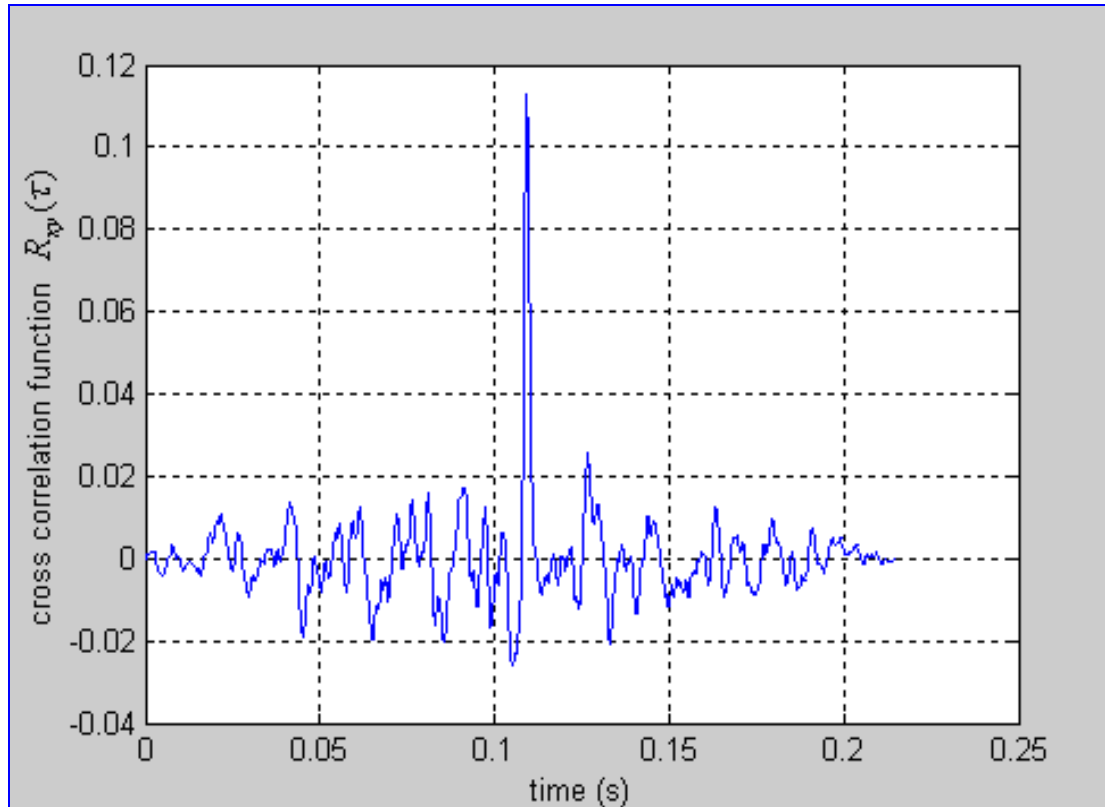


Figure 4.15 Correlogram of the two signals after ensemble averaging, 1kHz sampling rate

The mean liquid film thickness  $\delta$  measured by the CFM for this flow condition was 0.0044m (from downstream probe). So, the value of  $A_f$  can be found directly from simple geometric considerations:

$$A_f = \pi[R^2 - (R - \delta)^2] = 6.30 \times 10^{-4} \text{m}^2 \quad 4.13$$

The two values of  $A_f$  are very close, and confirms that the CFM (downstream) gives reasonable results for the film thickness  $\delta$  because the film cross-sectional area calculated from 4.11 was of similar size to the film area calculated from the measured film thickness  $\delta$ . A difference between the two results would be expected because not all the water is flowing in the film; some is being entrained into the gas core. This is why a lower film area would be expected using Equation 4.13, which uses the film thickness measured by the CFM (downstream probe), than from Equation 4.12 which uses the reference water flow rate and the measured film velocity. This is further discussed in Chapter 6.

#### 4.2.6 CFM operation with both gas and liquid variations

Once the signals from the CFM had been made fit for purpose, the CFM was used with varying gas and water flow rates, see Section 6.1. Figures 4.16 and 4.17, show that the mean film thickness obtained using the CFM measurements (using the level calibrations in Figures 4.8-4.10 explained in Section 4.2.3) conforms with the trends reported in the literature, see Section 2.3.1. The mean film thickness increases with increasing water flow rate, at constant gas flow rate and it decreases with increasing gas flow rate, at a constant water flow rate, once a certain volume flow rate had been reached. Further analysis is presented in Chapter 6.

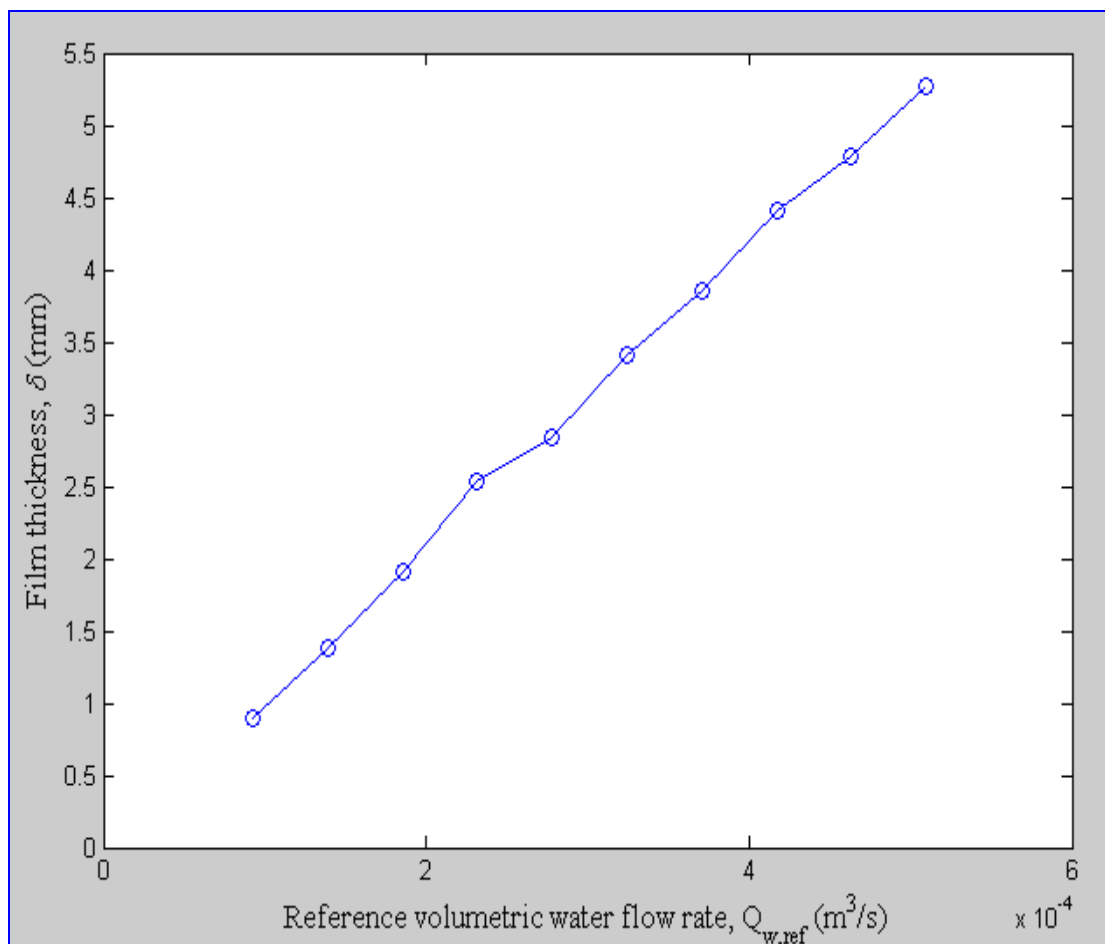


Figure 4.16 Mean water film thickness as a function of increasing water flow rate measured using the CFM

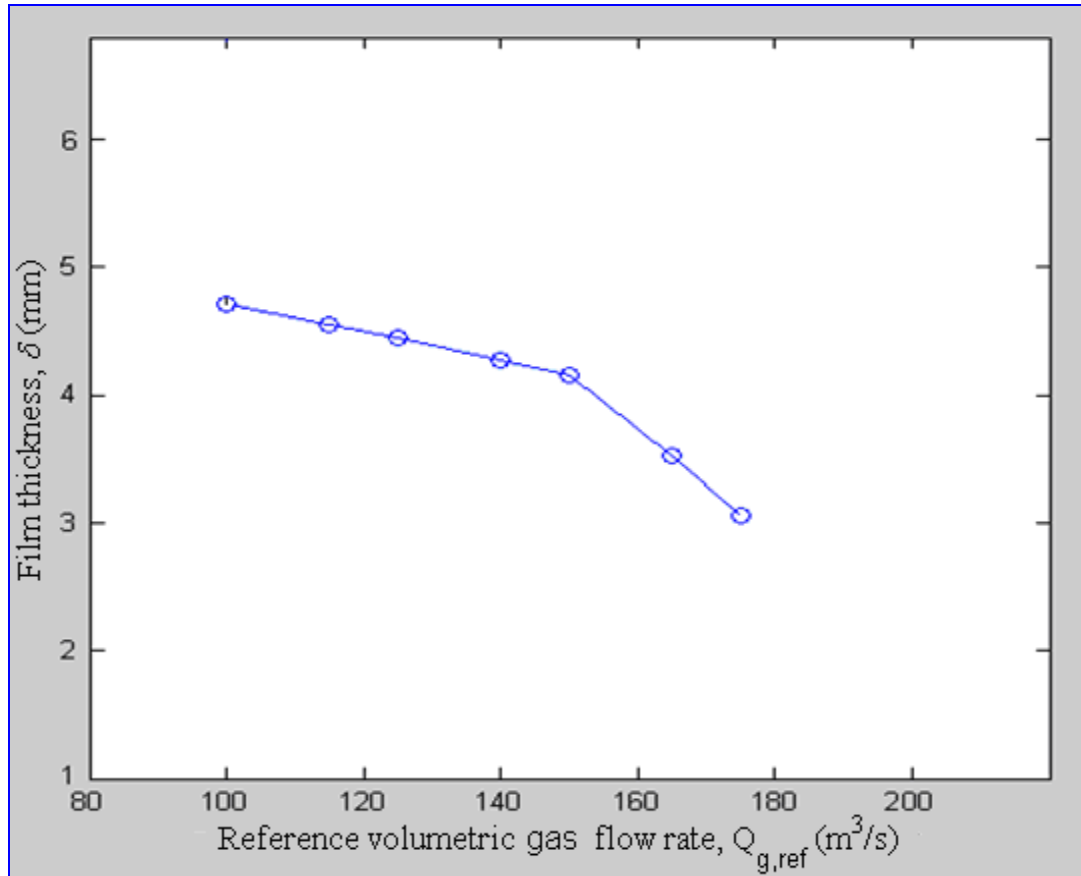


Figure 4.17 Mean water film thickness as a function of increasing gas flow rate measured using the CFM.

### 4.3 Ultrasonic Flow Meter

Based on the results of the preliminary work presented in Chapter 3, the design/manufacture and calibration of the Configuration D shown in Figure 3.17 and described in Section 3.3.1 will now be discussed.

#### 4.3.1 Principle of operation

The USFM measures the time taken for sound to travel between two transducers (Section 2.4.2 and Section 3.3 introduced the ultrasonic technique). One transducer is placed upstream and another downstream. The effect of the fluid velocity makes the upstream time of flight longer than the downstream. The transit times calculations were presented in Section 3.3.4.

USFMs are characterized by: (a) an electronic control unit; and (b) a primary element, composed of a metering pipe on which one or more pairs of piezoelectric transducers have been mounted.

### 4.3.2 Electronic control unit

The electronic control unit varies significantly with the type of flow meter. Signal excitation can be continuous or pulsed, adaptation to attenuation can be automatic or manual, the electronic metering unit can be analogue or digital and different noise filtering strategies can be used. Here, a brief of the designed electronic circuit used in the present investigation is given, see Figure 4.18.

The sine wave oscillator consisted of a non-inverting amplifier, with a variable gain, and a band pass RC filter. The resistors, VR1 and VR2, were varied depending on the frequency adjustment required. The band pass network provided positive feedback with a maximum gain of one-third at a centre frequency given by:

$$f = \frac{1}{2\pi RC} \quad 4.14$$

Variable gain was used so that the adjustable negative feedback would allow the overall loop gain to be set to just greater than 1 at which level it was just enough to sustain oscillation.

The amplitude was regulated by means of the back to back Zener diodes which began to conduct when the voltage across the upper part of the 10k $\Omega$  potentiometer was equal to the Zener voltage plus a diode drop. The consequent drop in loop gain controlled the amplitude.

The op-amp used was a low cost LF356. The 40kHz used was a high frequency, a high speed device, with a good slew rate to avoid non-linear effects.

The MC1496 Analogue Multiplier was a key component of the circuit and contains a cross-coupled differential arrangement of matched transistors. The carrier input voltage causes the current to vary differentially. The MC1496 was used to multiply the two received signals from Rx1 and Rx2, see Section 3.3.4 and Equation 3.37.

The base-emitter voltage of the upper quad arrangement was proportional to the logarithm of the emitter current, and was, therefore, the sum of the logarithms of the carrier and signal input voltages. The current flowing through the cross-connected collector resistors was, therefore, proportional to the anti-logarithm of the sum, hence proportional to the product of signal and carrier inputs.

The Zener diode was used to set up a sufficient base-collector voltage for the correct operation of the lower differential stage. Double-balanced operation ensures maximum dynamic range, greatest linearity and lowest DC errors. The three main advantages of using transformers compared to resistors, capacitors and active circuitry are:

- Ground isolation – avoids ground loops and circulating currents.
- Accurate balance matching (compared with an inverter circuit).
- No DC errors due to input bias currents.

The final output of this circuit is a DC voltage proportional to  $0.5 \cos(\phi)$ , where  $\phi$  is the phase-shift angle. It was shown previously how the cosine function limits the usage of the USFM to a defined range, see Section 3.3.4.

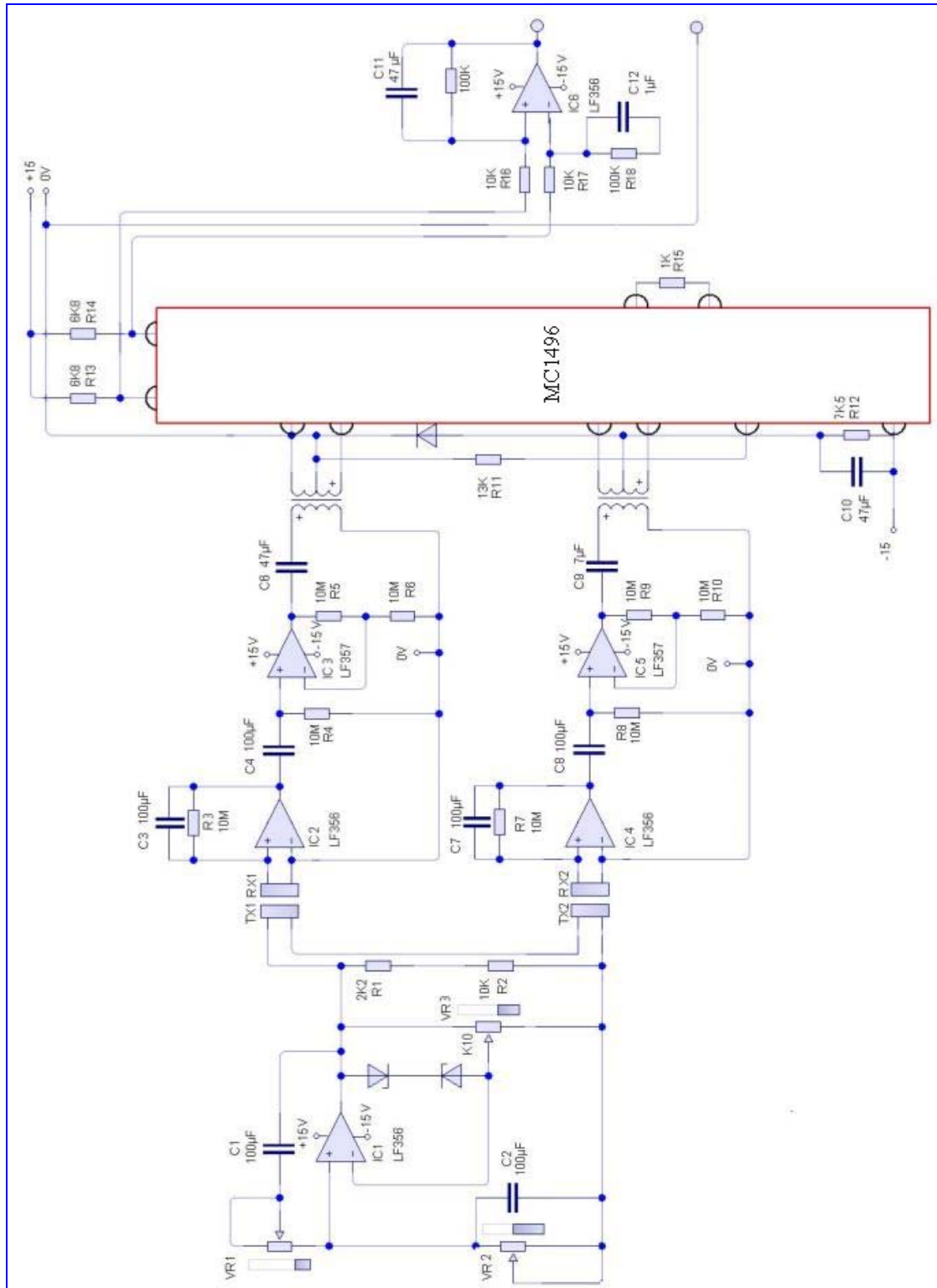
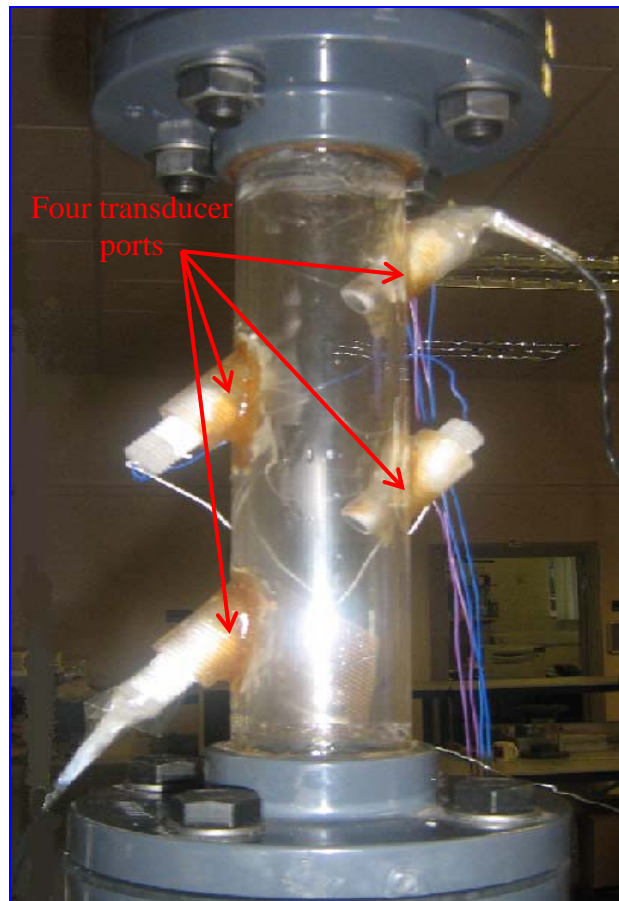


Figure 4.18 Ultrasonic electronic circuit

### 4.3.3 Design and testing of USFM with air only

Figure 4.19 shows the USFM being installed in the test section of the flow loop.



*Figure 4.19 Ultrasonic flow meter installed in the flow loop*

The flow meter was made of Perspex. The total length of the body was 270mm and the internal diameter matched the test section i.e. 50mm. The four transducer ports, see Figure 4.20, had matching dimensions and each pair had a symmetric and parallel finish. The transducer holders were designed to be threaded rod so a fine adjustment of the final transducer position could be achieved. The transducers were fixed into the holders with removable silicon glue.

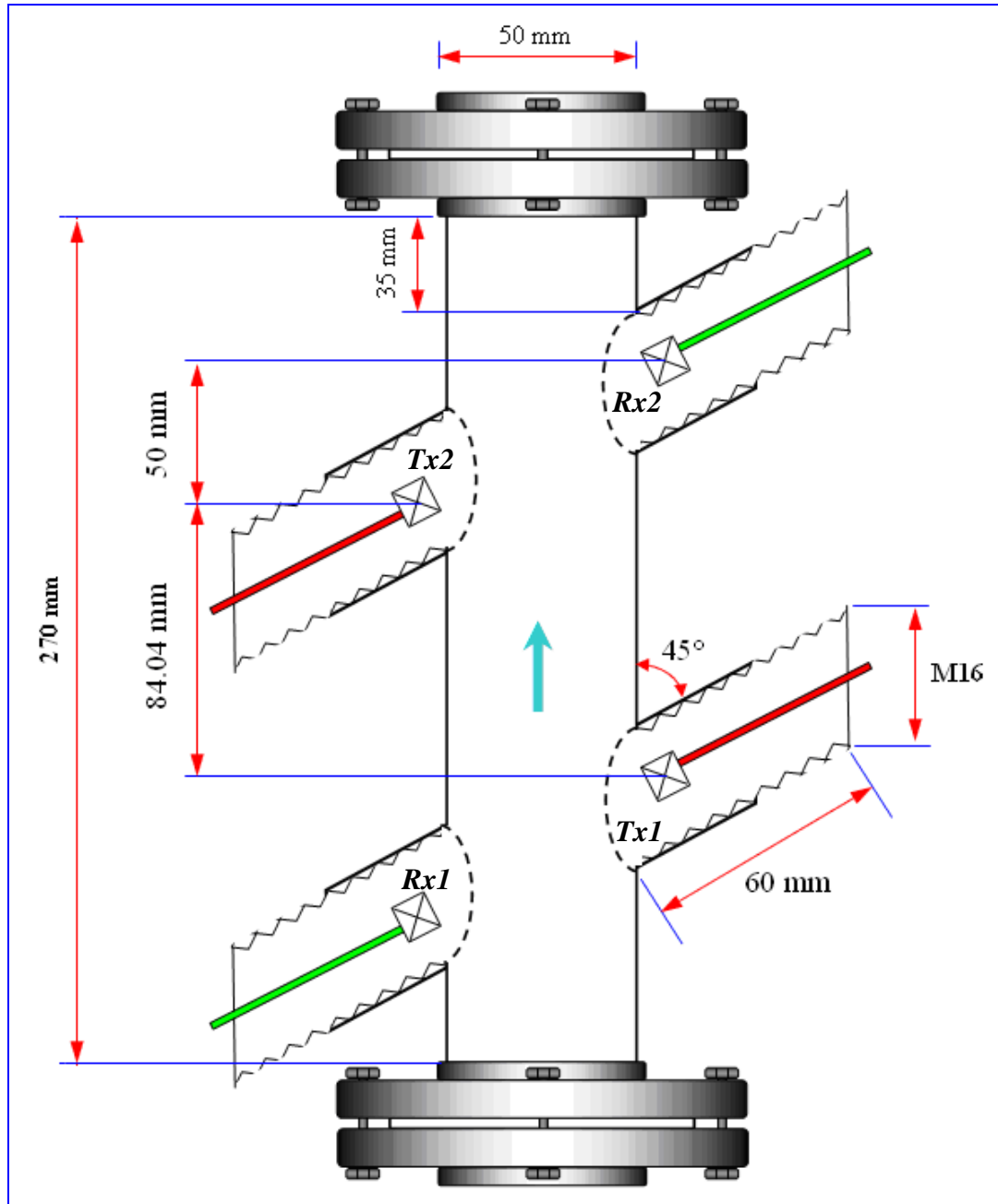
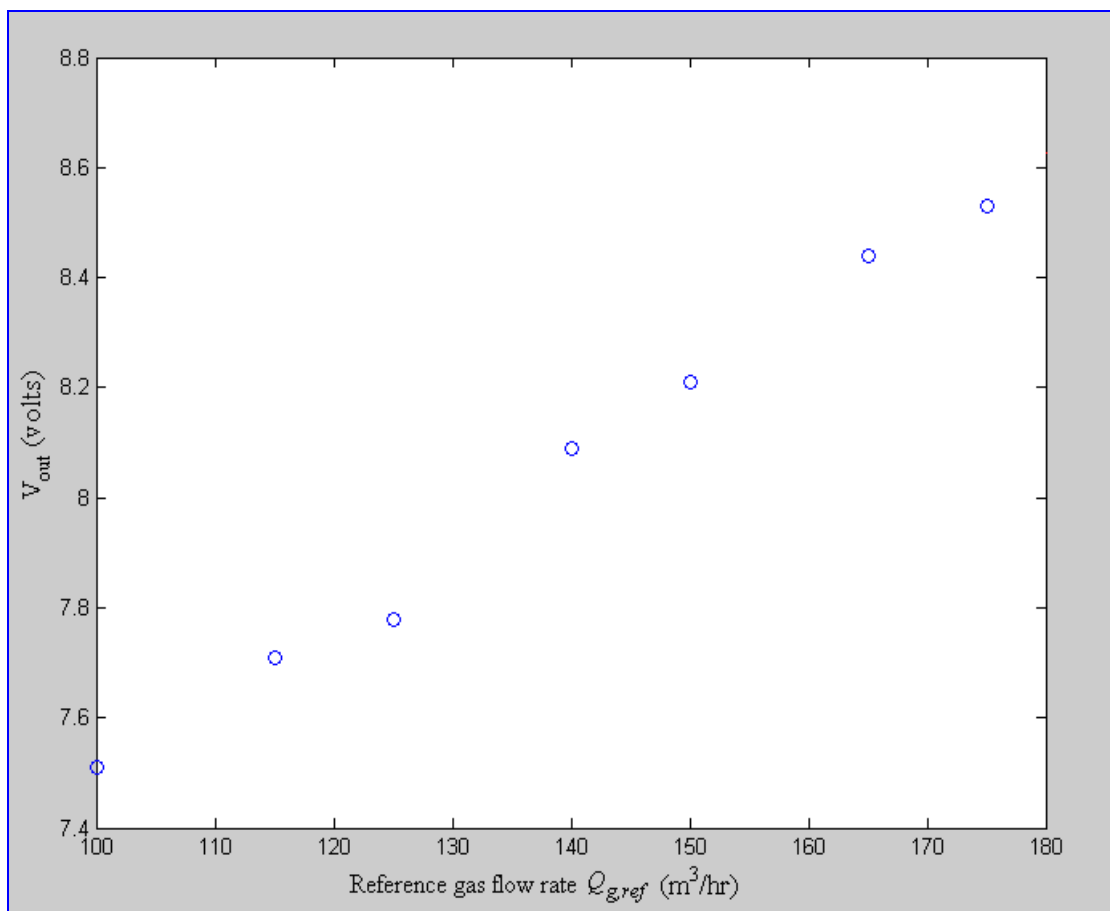


Figure 4.20 Sketch of a side view of the USFM (not to scale)

Operating at 40kHz made the positioning of the transducers in the housing port critical. A slight difference between the two transmission paths could have introduced a large extra phase shift into the measurement, causing inaccuracy in the system. To avoid this problem the transmitters (Tx1 and Tx2) were first fixed, then the receivers (Rx1 and Rx2) were adjusted to give a matched received signal at both receivers. Because this was a critical point, it was vital to repeat this check in each experimental run in case of the position of any of the transducers became distorted.

The flow meter was tested in the test section, see Section 5.1, with only gas phase flow. This test was to gain an understanding of the characteristics of the flow meter. Figure 4.21 shows the characteristic curve obtained for the USFM. The curve shows the relationship between the DC output voltage, measured from the analogue multiplier MC1496 for different gas flow rates, of the USFM and the volumetric flow rate read from the Variable Area Flow Meter (VAFM), see Section 5.1.1, in the operating range. Since this test is gas flow only,  $V_{out}$  was plotted against reference gas velocity, see Figure 4.22.



*Figure 4.21 Characteristic curve for the designed USFM (air only)*

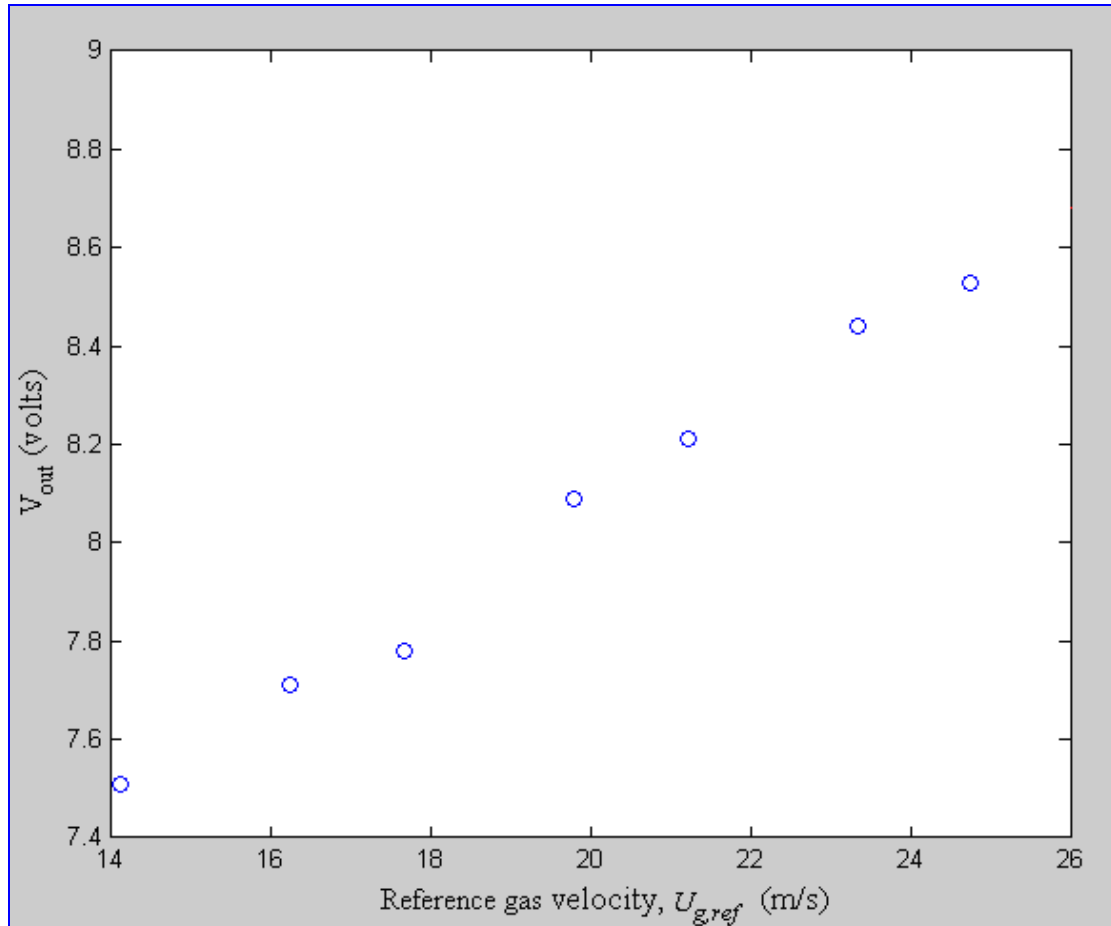


Figure 4.22  $V_{out}$  expressed in term of the gas superficial velocity (air only)

Earlier in Section 3.3.4, a calibration equation, Equation 3.39, was introduced to enable a convenient yet accurate best fit curve to be achieved in the form of:

$$V_{out} = \hat{a} \cos(\hat{c}U_g) + \hat{b} \quad 4.15$$

For zero flow and since it's only air for this test,  $U_g = U_{g,ref} = 0$ , the output  $V_{out}$  obtained from the electronic circuit was 8.67 volts, so the above equation reduces to:

$$V_{out} = \hat{a} + \hat{b} \approx 8.67 \quad 4.16$$

$$\text{When } \hat{c}U_g = \frac{3\pi}{2}$$

$$V_{out} = \hat{b} \quad 4.17$$

The velocity at  $\phi = \frac{3\pi}{2}$  can be obtained as follows,  $\hat{c} = 13.26$  (see Section 3.3.4):

$$\hat{c} = \frac{4\pi fd}{c^2} \cos \theta \quad 4.18$$

$$\text{So, } U_g * \frac{4\pi fd}{c^2} \cos \theta = \frac{3\pi}{2}$$

$$\text{Thus, } U_g = \frac{3c^2}{8fd * \cos \theta} = 20.35 \text{ m/s} \quad 4.19$$

where:  $\theta$  the angle the transducer makes with the pipe =  $45^\circ$ ,  $c$  is the speed of sound in the fluid = 329.4m/s in air,  $d$  is the ultrasound path = 0.07m and  $f$  is the frequency of the ultrasound = 40kHz.

Looking at Figure 4.22, to a best estimate, this velocity obtained from Equation 4.19 corresponds to  $V_{out} = 8.13$  volts. i.e.  $\hat{b} = 8.13$  and hence  $\hat{a} = 0.54$ . This suggests that Equation 4.15 can be stated as:

$$V_{out} = 0.54 \cos(13.26 U_g) + 8.13 \quad 4.20$$

Figure 4.23 shows the new and more accurate characteristic curve for the designed USFM. Hence,  $U_g$  can be obtained from  $V_{out}$ :

$$U_g = \frac{\cos^{-1} \left[ \frac{V_{out} - 8.13}{0.54} \right]}{13.26} \quad 4.21$$

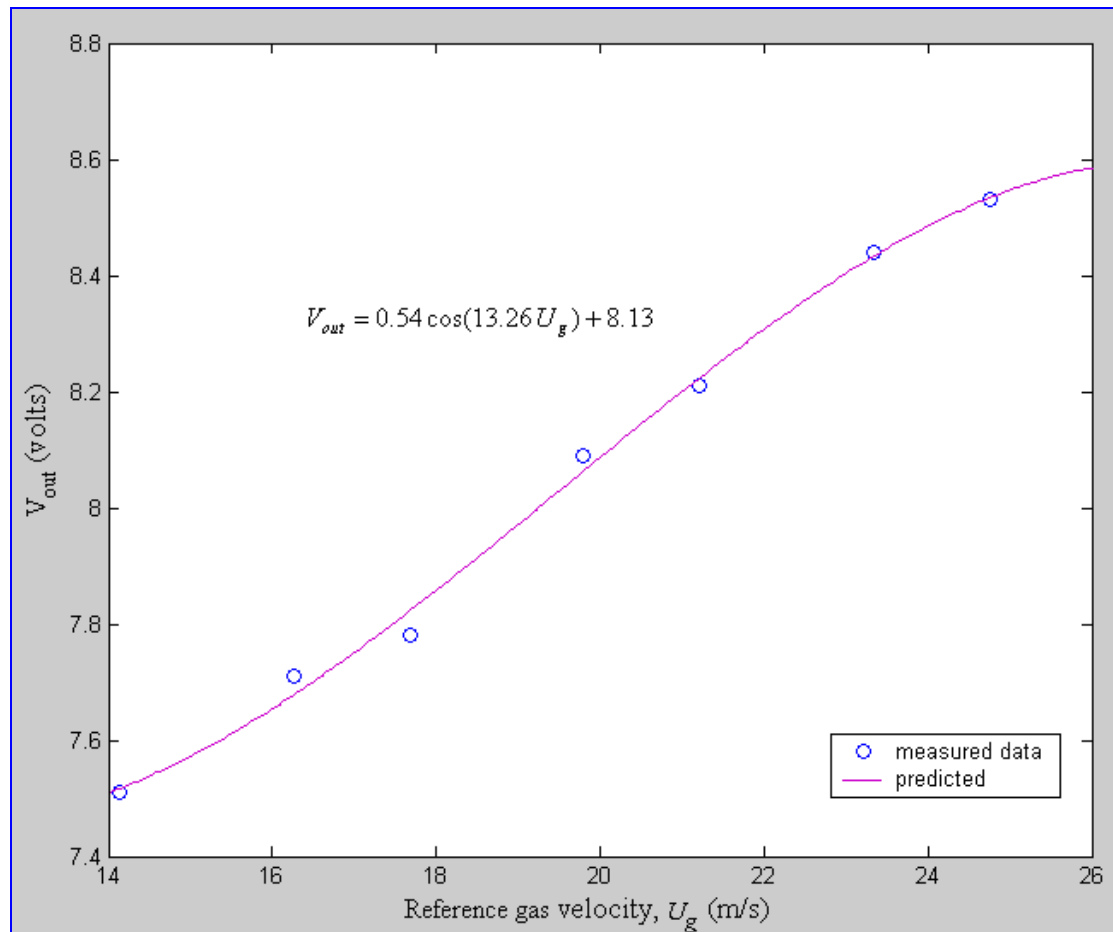


Figure 4.23 Calibration equation (4.20) against measured data (air only)

#### 4.3.4 Liquid film effect on the performance of the USFM

The first calibration tests of the USFM with only gas flow seemed to be very promising, Section 4.3.4. However, when the transducers were covered with liquid film of up to about 0.5mm thickness the device responded, but well away from the calibration settings. If the film thickness was increased to more than 0.5mm, the device stopped responding to changes in gas velocity. This can be put down to the characteristic of the transducers when covered with water.

To overcome this problem, the transducers were moved so that they intruded into the pipe i.e. passing through liquid film as shown in Config.2, see Figure 4.24. This action introduced a slight disturbance to the film but it solved the problem of measuring the gas flow.

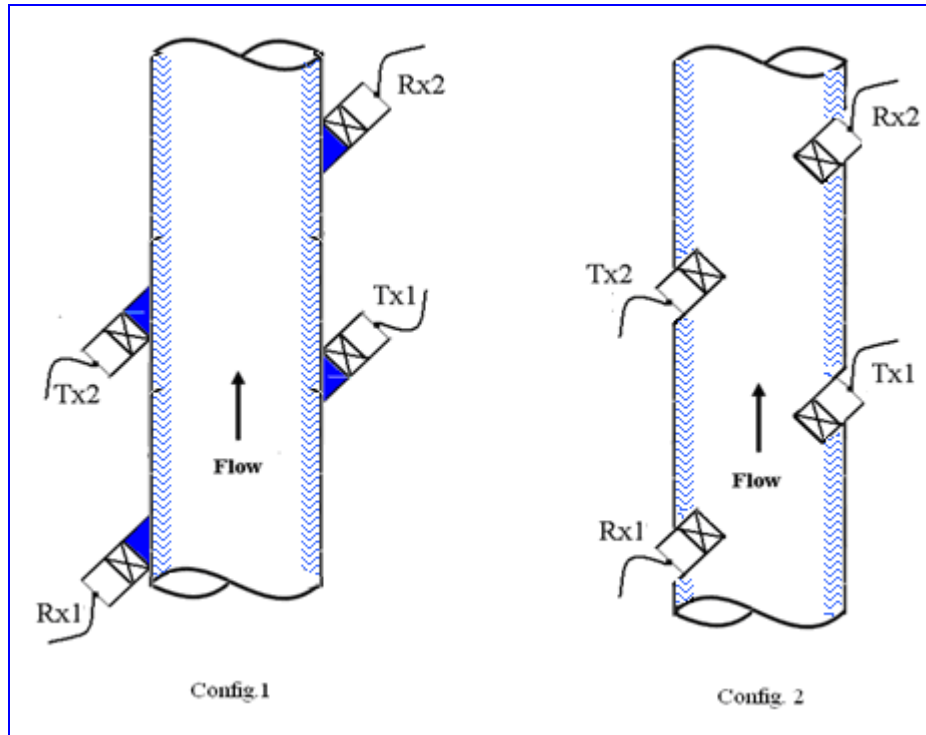


Figure 4.24 Transducers configurations.

The USFM device was calibrated once again, see Figure 4.25, since the length of the acoustic path is different in the new configuration; now  $d = 0.059\text{m}$ , hence  $\hat{c} = 11.07$ . Since we are using water and air, the gas velocity notation is  $U_{g,c}$  to indicate the gas core velocity of the annular flow.

However, since this test was carried with both water and air, a reference gas core velocity was calculated from:

$$U_{g,c,ref} = \frac{Q_{g,ref}}{A_\delta} = \frac{Q_{g,ref}}{\frac{\pi}{4}(D - \delta)^2} \quad 4.22$$

where:  $Q_{g,ref}$  is the gas flow rate read from the Variable Area Flow Meter (VAFM, see Section 5.1.1),  $A_\delta$  is the cross-sectional area of the gas core taking into account the film thickness  $\delta$  and  $D$  is the pipe diameter. Later in Section 6.4.1, it is shown that the entrained droplets are not causing the USFM to overestimate the measurement of the gas core velocity, so the effect of water droplets in the gas core can be neglected.

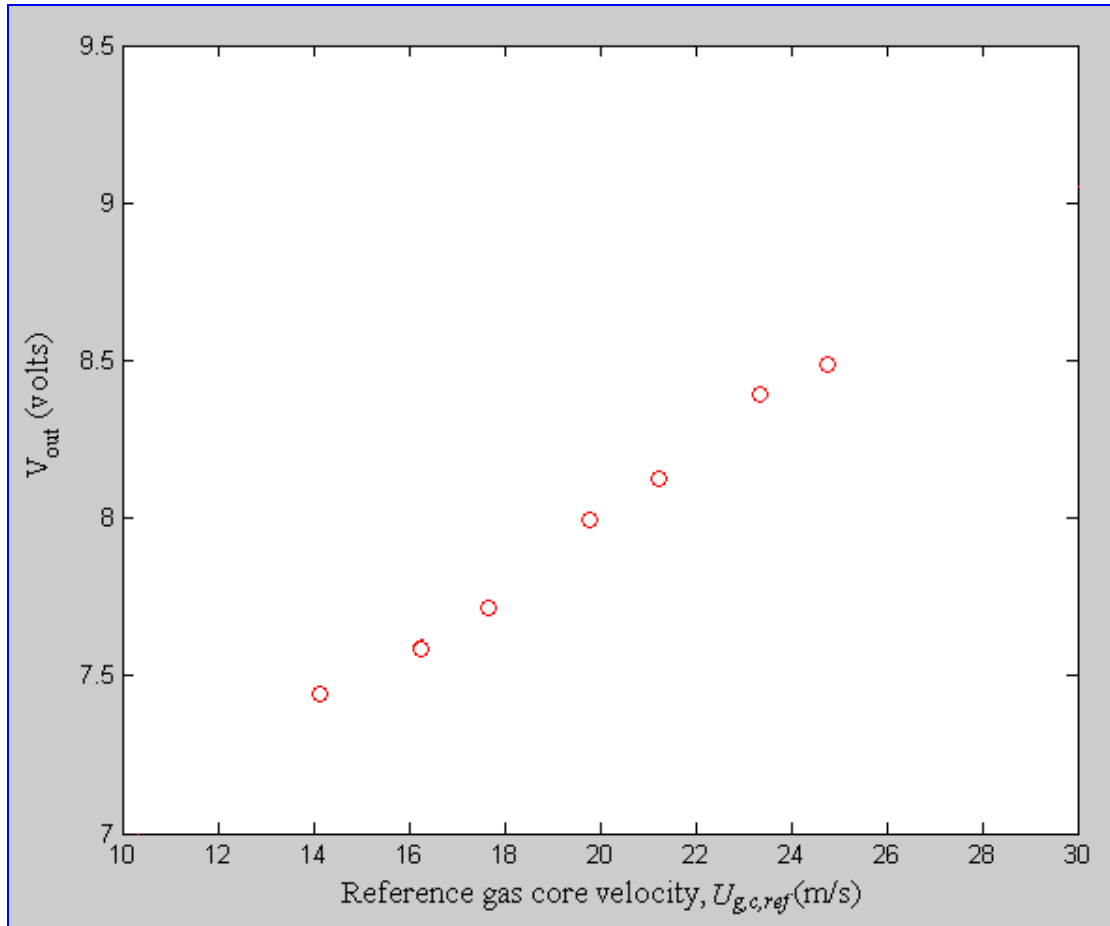


Figure 4.25  $V_{out}$  expressed in term of the reference core gas velocity (air and water)

The same argument that was used to find the constants values of  $\hat{b}$  and  $\hat{a}$  in Section 4.3.4 is repeated here, where  $\hat{c} = 11.07$ .

For zero flow,  $U_{g,c} = U_{g,c,ref} = 0$  the above equation reduces to:

$$V_{out} = \hat{a} + \hat{b} \approx 8.67 \quad 4.23$$

$$\text{When } \hat{c}U_{g,c} = \frac{3\pi}{2}$$

$$V_{out} = \hat{b} \quad 4.24$$

$$\therefore U_{g,c} = \frac{3c^2}{8fd * \cos \theta} = 19.98m/s \quad \text{at } V_{out} = \hat{b} \quad 4.25$$

From Figure 4.25, to a best estimate, this velocity value corresponds to a voltage output of 7.96 volts i.e.  $\hat{b} = 7.96$  and hence  $\hat{a} = 0.644$ . This suggests that Equation 4.20 can be re-stated as:

$$V_{out} = 0.644 \cos(11.07 U_{g,c}) + 7.96 \quad 4.26$$

Figure 4.26 shows how the calibration curve Equation 4.26 fits the measured data. The curve shows some deviation from the measured data, especially at low velocities.

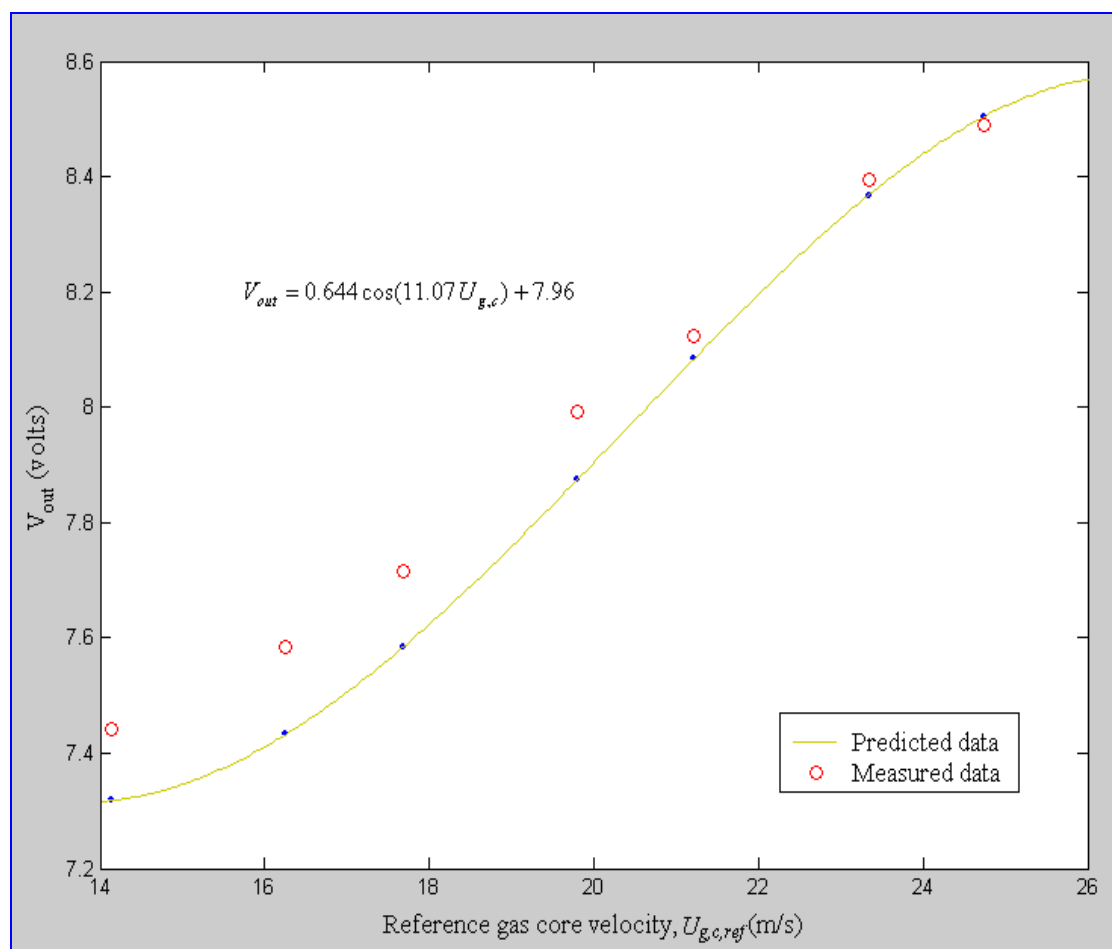


Figure 4.26 The calibration curve fitting with the measured data (air and water)

Most likely this is because the cosine wave used for the calibration curve is derived from a somewhat idealised representation of the output of the USFM electronic circuit. Tuning the values of  $\hat{b}$  and  $\hat{a}$ , by trial and error, can improve the calibration curve to give a better estimate of the measured data for both air and water flow and also for air only flow, see Figure 4.27. Equation 4.26 was modified to:

$$V_{out} = 0.56 \cos(11.07 U_{g,c}) + 8.03 \quad 4.27$$

$$U_{g,c} = \frac{\cos^{-1} \left[ \frac{V_{out} - 8.03}{0.56} \right]}{11.07} \quad 4.28$$

Equations 4.27 and 4.28 will be used in the future experiments and investigations in this study.

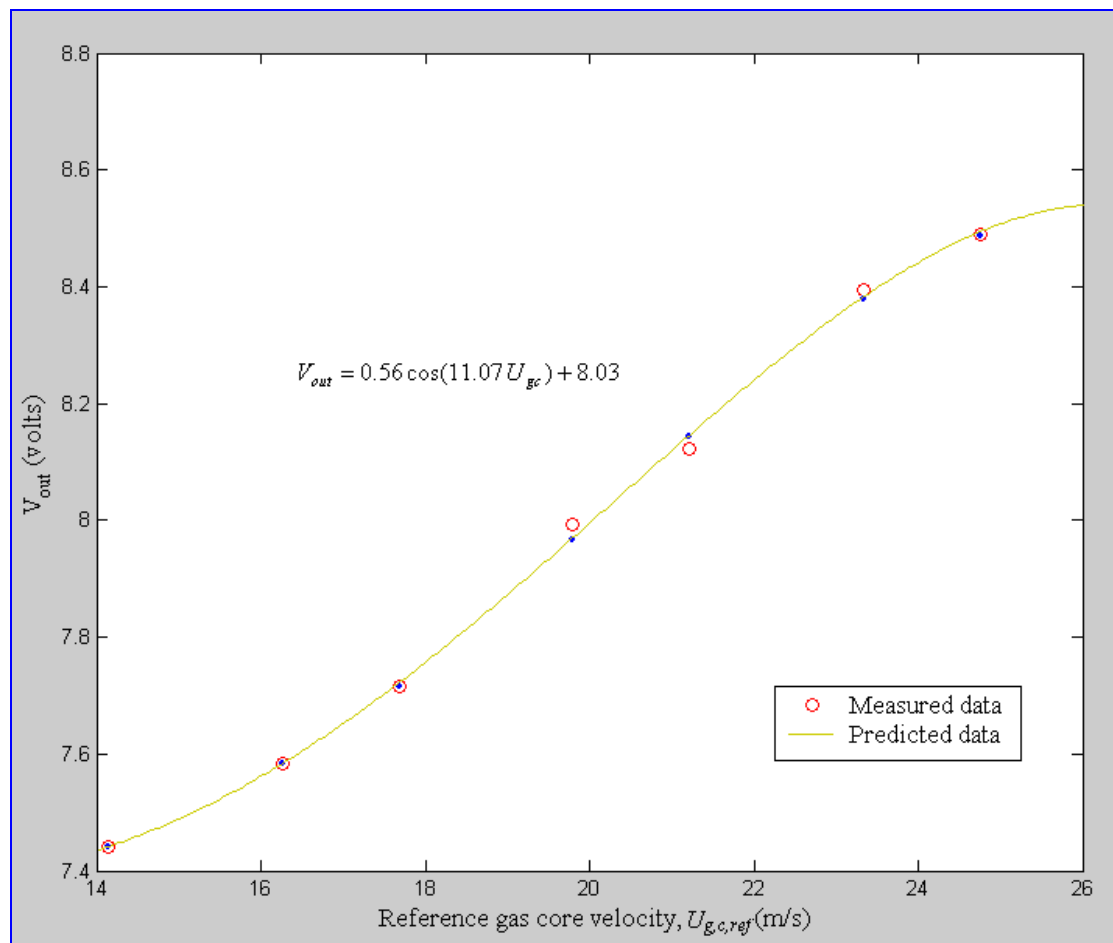


Figure 4.27 Modified version of Equation 4.27 against the measured data (air and water)

### 4.3.5 Temperature effect on USFM readings

In the design process of the USFM device, it was assumed that the temperature of the fluids is constant in the test section and so has a negligible effect on the USFM readings. This assumption was made because each experiment at a given set of flow conditions takes less than 60 seconds to complete and during this short time the

temperature would be constant. Figure 4.28 shows that the output voltages of the USFM for each flow rate are effectively constant with time. This validates if there is any change in the temperature during the run time of the experiment, the USFM output voltage will change accordingly.

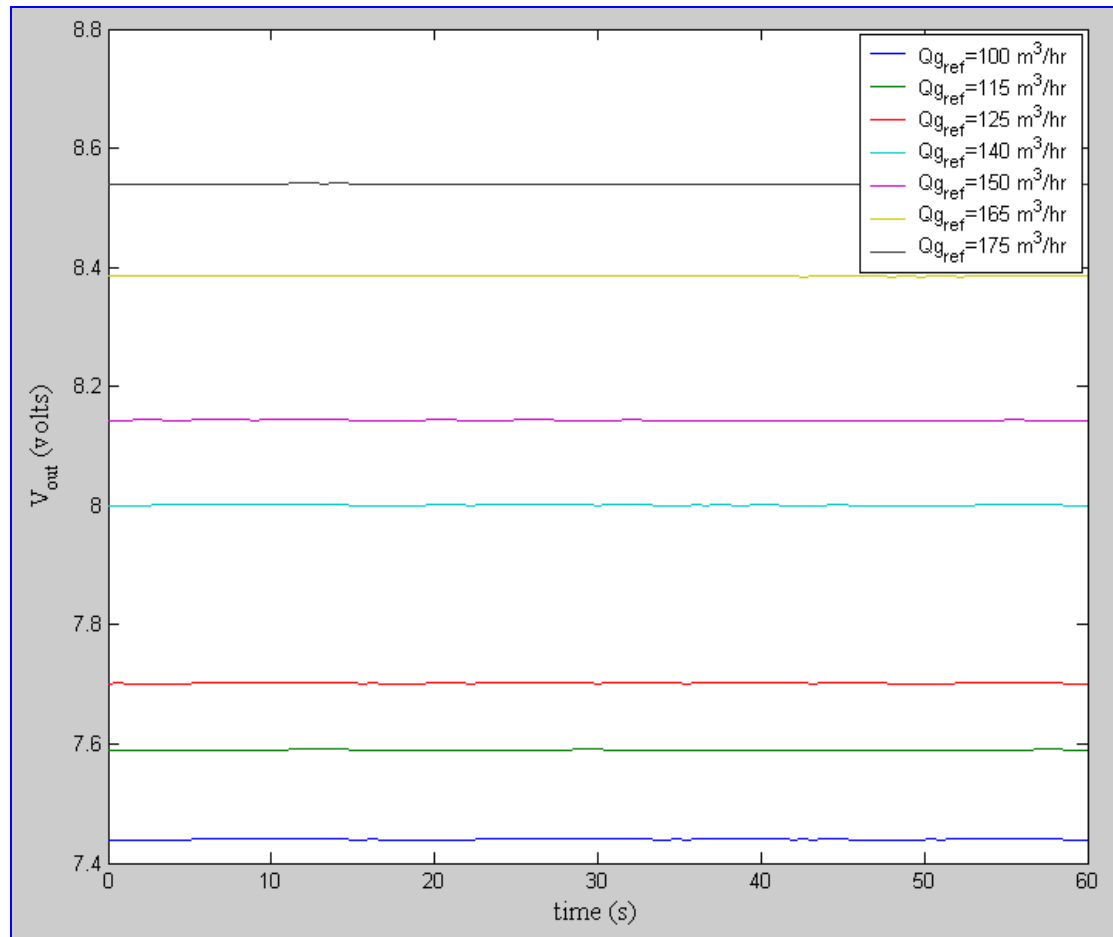
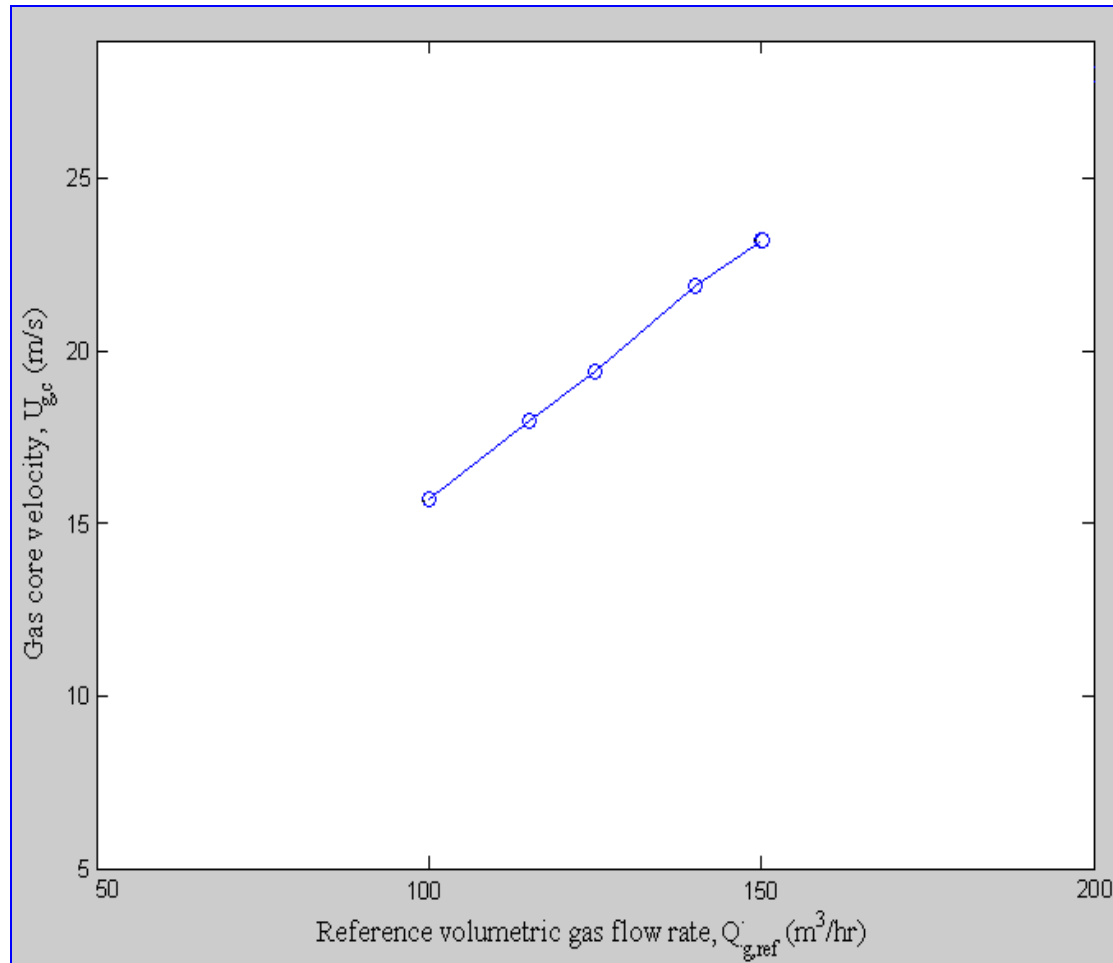


Figure 4.28 Temperature effect on the USFM at different gas flow rates (air and water)

#### 4.3.6 USFM operation with both gas and liquid flows

The transducers protruding into the test section effectively solved the problem caused by the liquid film without introducing any further complication to the measurement technique. This was examined at two flow conditions; first, constant water flow rate of  $9.27 \times 10^{-5} m^3/s$  while increasing the gas flow rate from  $100 m^3/hr$  to  $150 m^3/hr$ , see Figure 4.29. The second flow condition was a constant gas flow rate of  $140 m^3/hr$  with a water flow rate varying between  $9.27 \times 10^{-5} m^3/s$  and  $2.78 \times 10^{-4} m^3/s$ , see Figure 4.30.

Figure 4.29 validates the proportional relationship between the gas flow rate and its velocity ( $Q_g = U_g A_g$ ). Figure 4.30 indicates that the core gas velocity increases as the water flow rate increases because the film thickness increases, reducing the area of the core, resulting in an increase in the gas velocity. More detailed results will be given in Chapter 6.



*Figure 4.29 Response of the USFM to the increase in the gas volume flow rate*

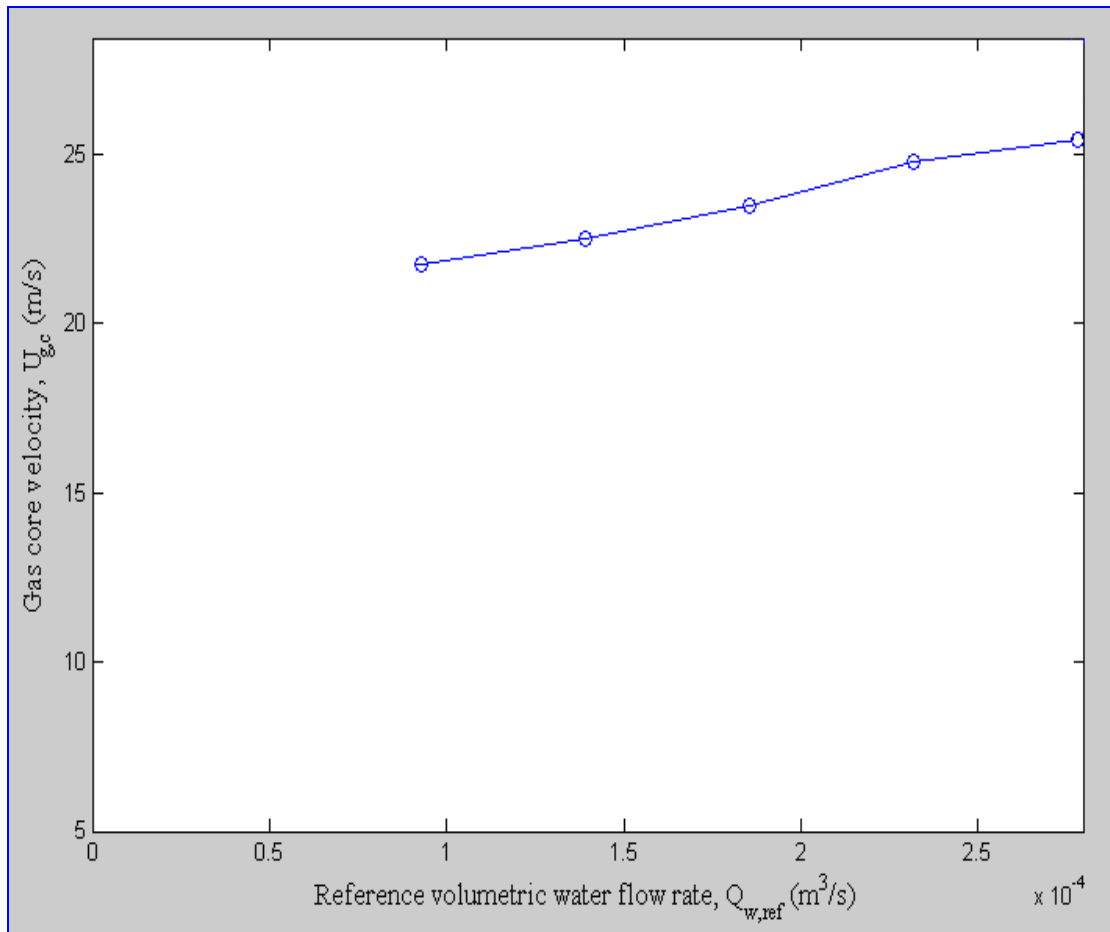


Figure 4.30 Response of USFM to the increase in the water volume flow rate

## CHAPTER 5 FLOW LOOP AND EXPERIMENTAL PROCEDURES

### 5.1 Flow loop Facility

In order to carry out dynamic testing of the measurement probes a flow loop in which annular flow can be established was required. This facility had to be capable of producing the necessary liquid-gas flows for the present investigation, including a range of different gas and water flow rates.

The available literature contains several descriptions of established flow rigs for vertical annular flow (e.g. Lopez de Bertodano, 1997; Whalley, 1987; Keeys et al., 1970; Quandt, 1965). The annular flow is invariably established in an acrylic pipe, called the test section, for ease of visualisation. The outlet from the test section is either passed to a separator or storage tank, and all the above named researchers seem to have had the same idea, given below, for establishing annular flow i.e. the same method of fluid injection system into the test section.

The loop consisted of four sections, **1)** air supply, **2)** water supply, **3)** test section, and **4)** outlet section. The flow loop is capable of producing flows with gas as the continuous phase. This was an open to air system, the water in the system and in the holding tank was replaced every few days to avoid algae growth in the tank.

The annular flow rig was needed in the present study to allow:

- Investigation of the film by the film removal method.
- Determination of the entrainment fraction  $E$  for a variety of gas and liquid flow conditions.
- Investigation of techniques for measuring the film velocity and the film thickness.

An available flow loop at the University of Huddersfield was capable of producing liquid, gas-liquid and solid-liquid vertical and inclined flows, but it did not have the capacity to produce annular flows since all the previous research work carried in this flow loop was at low gas flow rates. The existing flow loop includes a circulating liquid loop, an open gas loop (air outlet is to atmosphere), and a computer based data acquisition and control system.

The loop modifications designed in the present study was based on the preliminary work explained in Section 3.1. The idea for the development of the annular flow rig for the purposes of this study originated with the concept of combining the water with the air supply. Some of the plant necessary to extend the existing capability to include annular flow was available, and were some of the reference measurement devices.

Initially the air supply was taken from the compressed air supply from the university main compressor, supplied by a compressor (COMPAIR Rotary Screw CYCLONE 215). The rate of supply is controlled/set by a hi-flow pressure regulator (FAIRCHILD 100) and measured by a rotameter (ABLE VA METER 50PTnAAI75) with an accuracy of 2%. The university main compressor was used in the early stages of establishing annular flow and investigating the maximum and minimum flow rates of both the air and water. Later, a side channel blower (RT 1900) was installed as an alternative air supply. The side channel blower was used to achieve high air flow rates, giving a maximum flow rate of  $216\text{m}^3/\text{hr}$  (gas superficial velocity in the test section of  $U_{g,s} = 32.2\text{m/s}$ ) at a maximum pressure of 250mbar. Ball valve A, see Figure 5.1, was installed after the RT 1900 to allow the air flow rate from the RT 1900 to be varied.

Water could be pumped through the test section using a vertical multistage in-line centrifugal pump from a reservoir containing water only. The water pump delivered up to  $22\text{m}^3/\text{hr}$  (water superficial velocity in the test section of  $U_{w,s} = 62.3\text{m/s}$ ). Both the air suppliers and the water supply were capable of providing the required water superficial velocity ( $U_{w,s} = 5\text{m/s}$ ) and minimum gas superficial velocity ( $U_{g,s} = 27.2\text{m/s}$ ) found necessary in Section 3.1.1 for annular flow. Both blower and pump

could be independently set, allowing water volumetric flow rate  $Q_w$  and gas volumetric flow rate  $Q_g$  in the test section to be varied separately.

Commercially, it would appear that the pipe sizes of most interest, in industrial situations, (process industries etc,) are in the range 50mm to 150mm diameter with maximum demand for 75-100mm diameter sections (Cosham et al., 2007). However, because we are concerned with the design of an experimental laboratory instrument a choice of section of 50mm diameter test section seemed sensible. This gave the opportunity of upgrading the existing flow loop design using commercial instrumentation. Also, for a given flow rate it's easier to achieve annular flow the smaller the pipe diameter. Using design software *SolidWorks*, a diagram of the design loop was produced, see Figure 5.1.

One of the major challenges in designing the flow loop was the selection of the flow meters, where each flow meter was required to provide a certain flow which resulted in different outlet and inlet conditions for each device. This raised the challenge of accommodating devices with different pipe diameters in a limited space, which made building the loop to the required design all the more challenging, particularly as there was already an existing flow loop for other experimental projects.

Ambient atmospheric pressure (and temperature) conditions were assumed constant across the test section and at the Rotameter (variable area flow meter (VAFM)). This is not unreasonable because there is a low pressure drop across the test section (and VAFM).

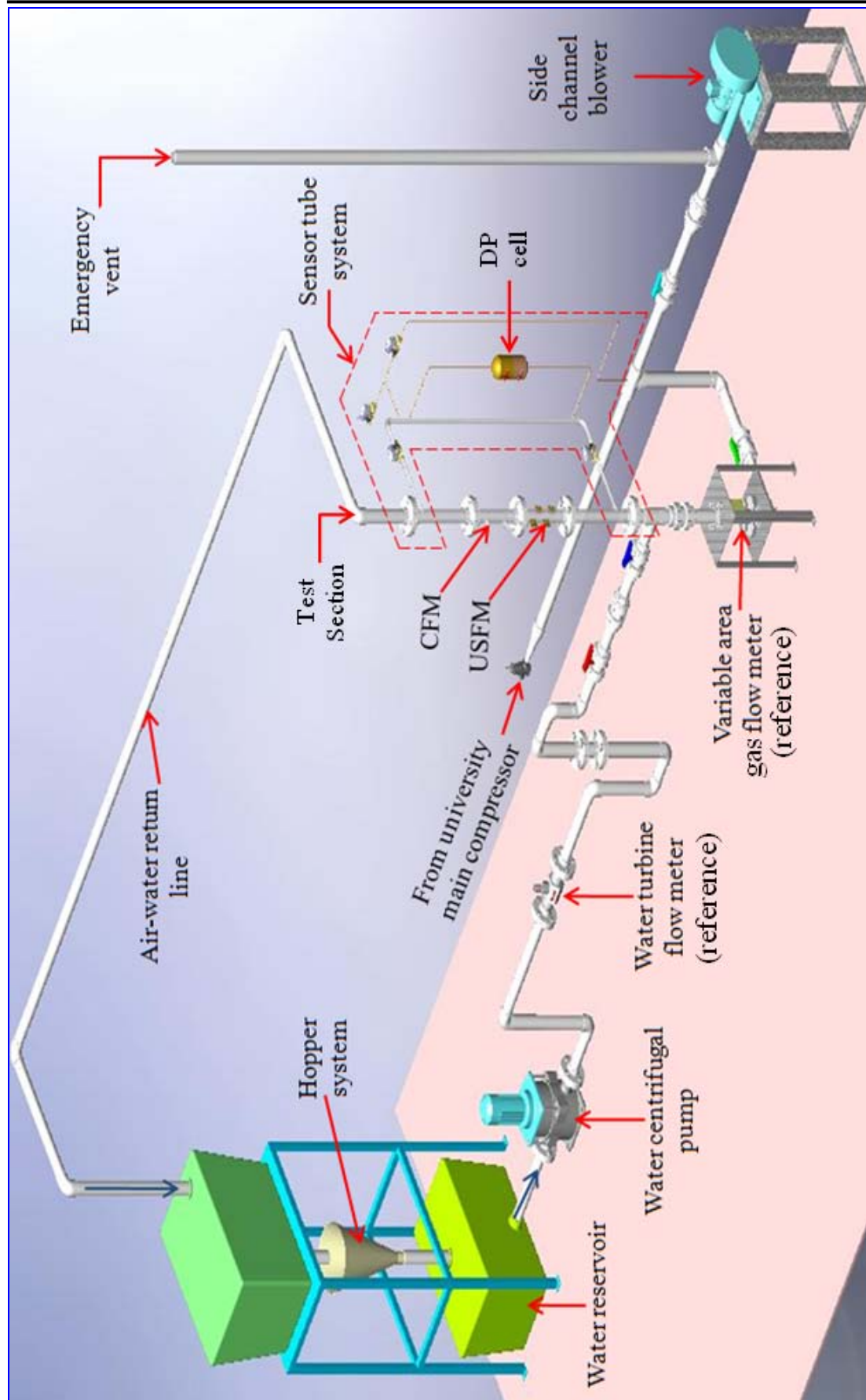


Figure 5.1 Diagram of designed flow loop

### 5.1.1 Air supply and monitoring

In the air supply section, the air flow is supplied by either the University high-pressure air system or the alternative air supply RT 1900. After passing through the test section the air was vented to atmosphere.

➤ Variable Area flow meter (Rotameter)

Rotameters are the most commonly used type of variable area flow meters. The working principle is that the differential pressure remains constant and the flow is measured by the position of a freely moving float in a tube of varying cross-sectional area. A variable area flow meter (50PTnAAI75) type was installed in the gas line, see Figure 5.2. In this flow meter, air passing into the meter moves the profiled float to a position where the forces created by the flow are balanced by the weight of the float.

This device provides a measurement of the reference volumetric gas flow rate  $Q_{g,ref}$  delivered by the air compressor or RT 1900. Hence, the gas superficial velocity  $U_{g,s}$  can be obtained:

$$U_{g,s} = \frac{Q_{g,ref}}{A} \quad 5.1$$

where:  $Q_{g,ref}$  is the reference volumetric gas flow rate and  $A$  is the pipe cross-sectional area.

The 50PTnAAI75 model flow meter has a 2" (50mm) stainless steel flanged body with a flow range of 30-300m<sup>3</sup>/hr. The flow rate can be read directly from the front display, but a magnet in the float sensed by the FloTrak system gives an output from an independent 4 to 20mA transmitter. This required the author to build a current/voltage (I/V) converter to provide a voltage for the LABJACK data acquisition unit, see Section 5.3.1, to read the voltage signals. This circuit is a simple voltage follower with a precision resistor of 250Ω and an AD620 amplifier, see Figure 5.3.



Figure 5.2 ABL E (50PTnAAI75) VAFM

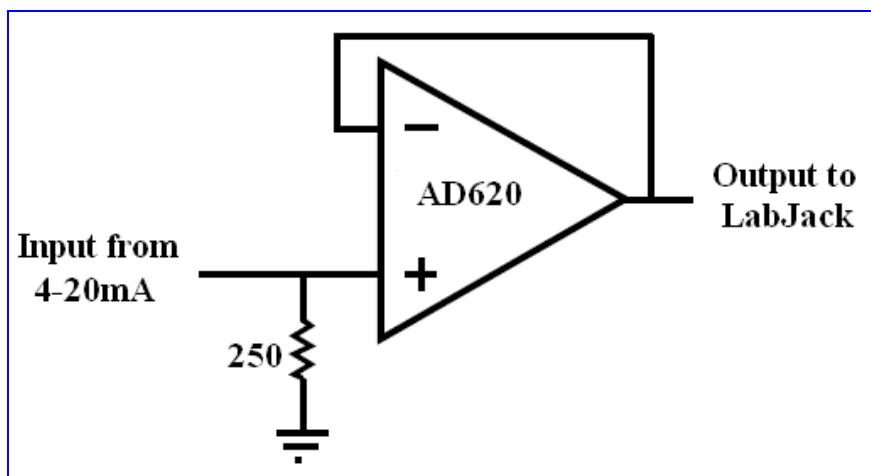
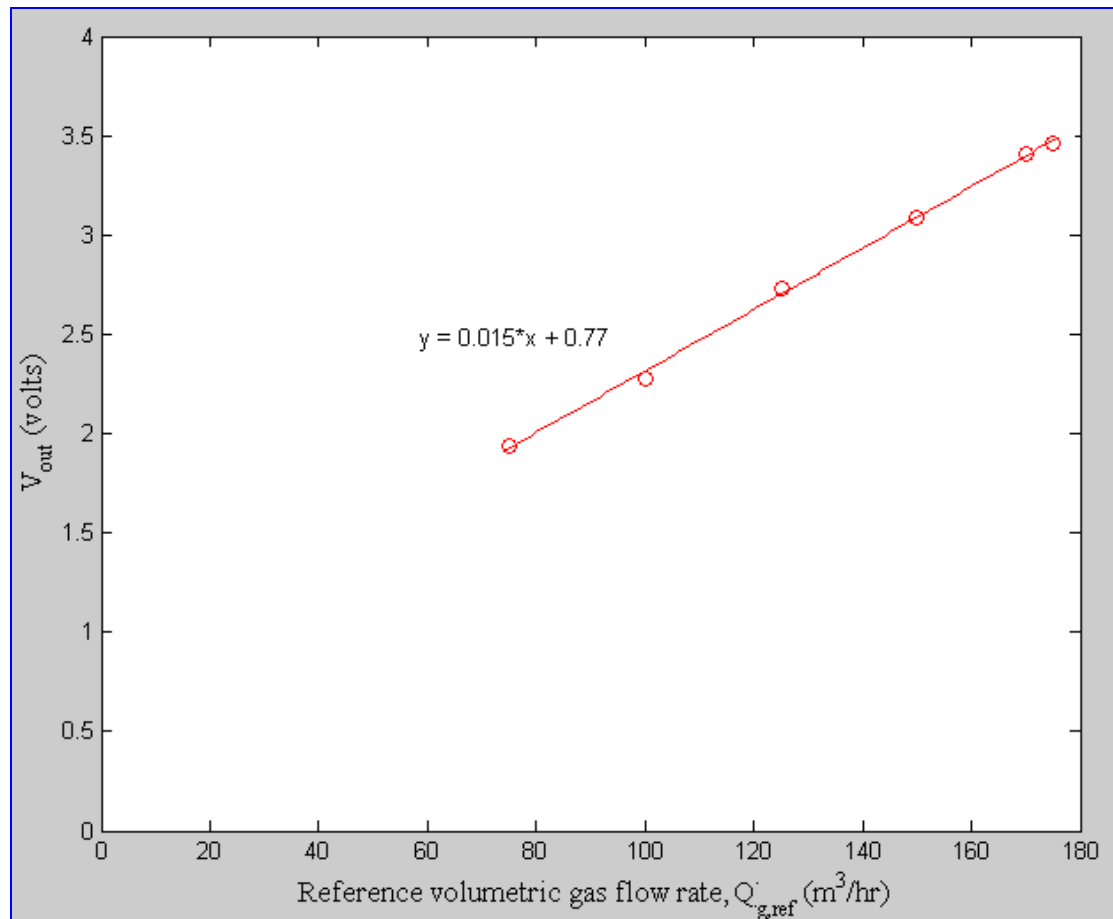


Figure 5.3 I/V converter circuit

Figure 5.4 shows the voltage output of the VAFM plotted against the direct reading from the front display. Due to background noise and vibration of the VAFM, it was only possible used it for flows between  $75\text{m}^3/\text{hr}$  to  $175\text{m}^3/\text{hr}$  which were the minimum and maximum gas flow rates respectively, that would be used in the present study.



*Figure 5.4 Output voltage  $V_{out}$  from the ABLE VAFM flow meter against gas volume flow rate*

A stainless steel frame was constructed to house and support the VAFM, see Figure 5.5. It consisted of two separate platforms that can be attached vertically, side-by-side, to ease the installation and removal of the VAFM. Also, this frame formed a rigid base for the test section of the flow loop, see Figure 5.1.

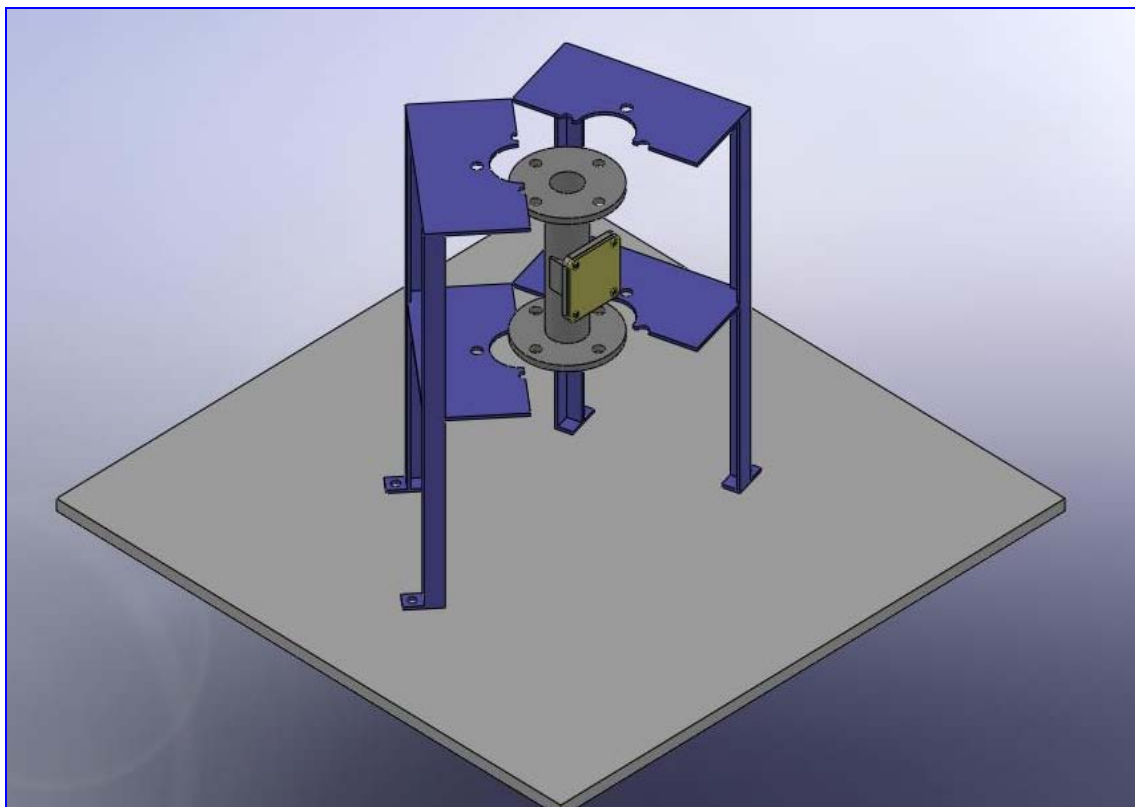


Figure 5.5 VAFM flow meter and support frame.

➤ High flow pressure regulator with filter

The FAIRCHILD Model 100 High Flow Pressure Regulator, see Figure 5.6, has a flow capacity of up to  $2550\text{m}^3/\text{hr}$  with a 7 bar of supply and a 2.8 bar set point. The screw handle of the device allows a fine adjustment for the air flow rate. It was used to regulate the air flow from the main university compressor only, i.e. not used with the RT 1900. The compensating action of the inner valve assembly of the Model 100 allowed complete stabilization of downstream pressure. The choice of this instrument was based on the pressure drops calculated in Section 3.1.2.

The purpose of the compressed air filter installed prior to the regulator was to take out any oil droplets that might originate from the compressor and be carried into the compressed air and which could affect the measurement of liquid related parameters.



Figure 5.6 FAIRCHILD Flow Pressure Regulator

### 5.1.2 Water supply and monitoring

Air was supplied axially to the test section, while water was injected normal to the axis of the test section, see Figure 5.1. Water was drawn from a storage tank using a vertical multistage in-line centrifugal pump and the flow rate was measured by a turbine flow meter (ABLE AT13T).

#### ➤ Turbine flow meter

The turbine meter (ABLE AT13T) was installed in the liquid line of the flow loop, see Figure 5.7, to measure the reference water volumetric flow rate  $Q_{w,ref}$  delivered by the

centrifugal pump. Because the annular flow regime requires only a small amount of water, a low range flow meter was used.



*Figure 5.7 ABL (AT13T) turbine flow meter*

Turbine meters provide measurements of the water volumetric flow rates by counting the rotation frequency of the turbine rotor. Turbine meters are designed so that the rotation frequency  $f$  of the turbine is directly proportional to water flow rate over the specified operational range of the meter.

Calibration of the turbine meter was carried out by comparing the turbine meter output frequency  $f$  with the water volumetric flow rate read from a reference gravimetric flow measurement system. In this gravimetric system, the water flows into a conical stainless steel hopper suspended from a load cell. The hopper has a pneumatic valve at its base which can be closed when required. The mass of water collected in the hopper in a known time is measured so the water mass flow rate  $W_w$  can be determined. Knowing the density of the water  $\rho_w$  the volumetric flow rate  $Q_w$  measured by the gravimetric system can be calculated:

$$Q_w = \frac{W_w}{\rho_w} \quad 5.2$$

Cory (1999) has explained the operation of this system in detail.

The results for the calibration of the turbine meter are shown in Figure 5.8. The calibration was also checked by comparing the calibration factor given by the manufacturer with the factor obtained from the calibration curve in Figure 5.8.

Figure 5.8 shows that there is a linear variation of frequency  $f$  with volume flow rate  $Q_w$  measured from the gravimetric system. The factory calibration for this meter is  $0.0033\text{m}^3/\text{hrHz}$  over a design range of  $0.48\text{m}^3/\text{hr}$  to  $4.8\text{m}^3/\text{hr}$ . The meter factor calculated from the calibration experiments is  $0.0034\text{m}^3/\text{hrHz}$ . This is valid over a range of  $0.33\text{m}^3/\text{hr}$  to  $3.3\text{m}^3/\text{hr}$ . This shows that the meter has experienced little wear and that it is usable at lower flow rates than the manufacturer's specifications suggest.

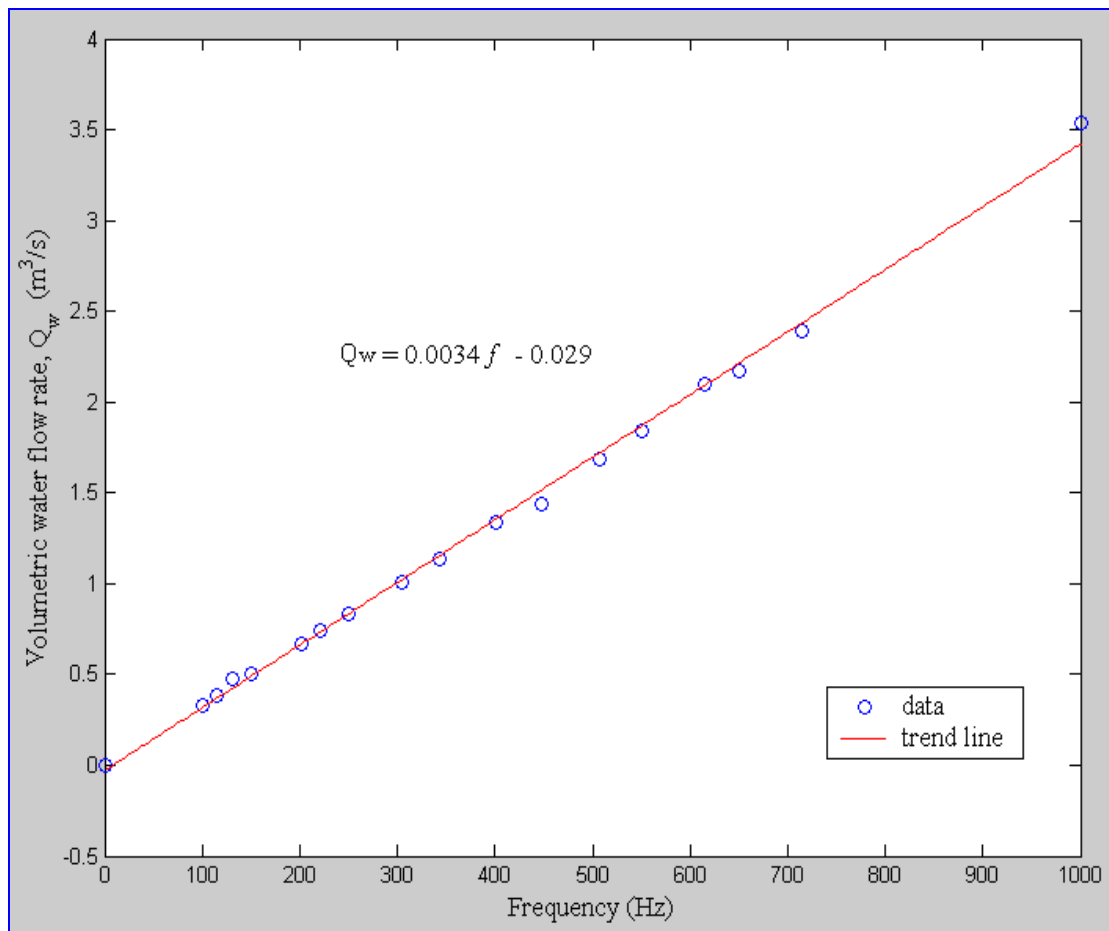


Figure 5.8 Calibration of ABL (AT13T) turbine flow meter using the gravimetric system

### 5.1.3 The test section

Prior to performing experiments, a visual inspection was performed to check for any fluid leakage. So, each time the experiment was setup to run, the pumps were turned on to circulate a small amount of water through the entire system. The mixture of air and water concurrently flows upwards into the test section, which is an acrylic tube of 50mm inner diameter. The tube length is 2000mm ( $L/D = 40$ ), which is long enough to guarantee an annular flow in the test section for the specified flows. The critical ratio of length to diameter for fully developed annular flow is about 72 (Lopez de Bertodano, 2001). The laboratory ceiling was not high enough to allow  $L/D = 72$ , but we were not concerned with obtaining a fully developed flow, our concern was measuring the flows established in the test section.

#### ➤ Differential pressure sensor

A Honeywell ST-3000 differential pressure (DP) sensor was installed on the flow loop, Figure 5.9. This device was used to measure the DP across a one metre vertical length of the sensor tube section, see Figure 5.1. A flushing system was installed in order to ensure that no air could become trapped in either the transducer or the measurement lines. The DP cell could be used to estimate the liquid volume fractions of different liquids flowing in the liquid phase of the annular flow. The method to do this is explained in Section 4.1.1.

In the present study, water only was used as the liquid phase, and so the principle of operation of the sensor tube was tested by measuring the air and water volume fractions when the tube was filled with an air-water mixture. For this purpose the sensor tube, DP cell and associated solenoid valves, see Figure 4.2 in Section 4.1.2, were found to measure the volume fraction accurate to about 1% of reading. Since the sensor tube system could not be fully evaluated due to the fact that oil-water mixtures could not be used as the liquid phase in the present study, further results from the sensor tube will not be presented in Chapter 6.



Figure 5.9 Honeywell ST-3000 DP sensor

➤ Solenoid valves

Two 2-way BURKERT 6013, see Figure 5.10, solenoid valves were used for the sensor tube operation. The 6013 is a direct acting solenoid valve used to close a pipe, and for venting purposes.



Figure 5.10 Burkert 6013 solenoid valve

These Solenoid valves operate on 230volts/50Hz and to accommodate this with the LABJACK, see Section 5.3.1, a switching circuit was built, see Figure 5.11. This circuit is controlled via the LABJACK which sends a digital output of 0 volts (low)

and 5 volts (high) enabling the solenoid valves in the sensor tube to be opened and closed as required.

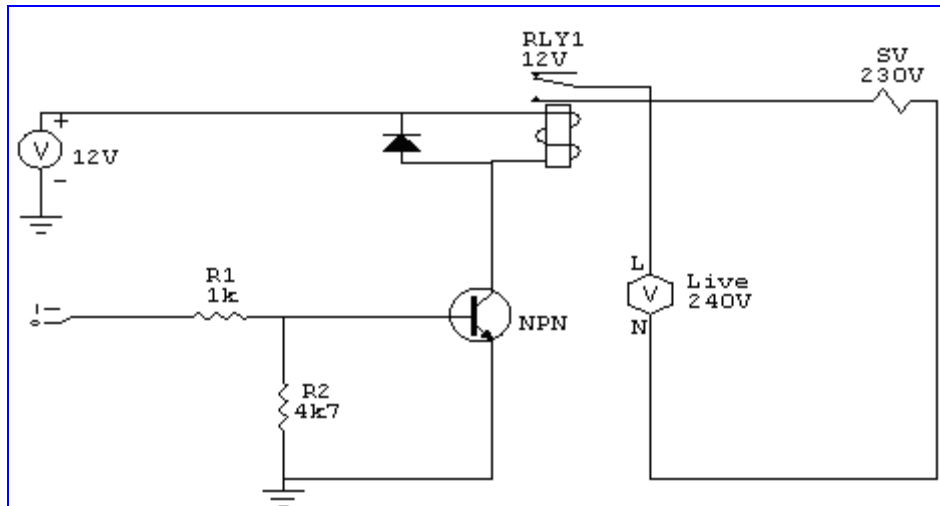


Figure 5.11 Relay on/off switching circuit

### ➤ Temperature sensor

PT100 Chromel/Alumel thermocouple sensor was placed into the base of the test section to monitor the temperature of the flowing mixture (air-water). The probe body is made of stainless steel and the mounting is 1/4" NPT thread. Since the room, in which the flow loop is housed, was kept at a fairly constant temperature, the main source of the heat is the centrifugal pump. Temperature was recorded manually in each experimental run. Thermocouples have a relatively rapid response time and given the practicalities of the situation the response time of this device was quite rapid enough to accurately follow any changes in water temperature.

## 5.2 Integrating the test section components

Vertical annular flow was studied in 50mm internal diameter Perspex pipe called the test section, see Figure 5.1. It consisted of four flanged sections connected with bolts and sealed with EPDM flat gaskets. With the different joints in the test section, it was very important to ensure the section remained vertically aligned, and a double axis spirit level was used to help do this. Pipe supports were used to ensure that this alignment remained in place throughout the experimental runs. To ensure proper

mating of the pipe sections, the PVC flanges were manually reamed with a tapered reamer. The test section accommodated the USFM, CFM, gauge pressure sensor (used to compensate for temperature and pressure effects on gas flow rate  $Q_g$  if required) and temperature sensor. The height of the vertical test section was limited to 2m, due to the height of the laboratory ceiling.

### 5.3 Data acquisition & Control system

#### 5.3.1 LABJACK U12

It was necessary to collect the data rapidly and to be able to store it for further analysis. This was achieved by using a USB based data acquisition card called a LABJACK U12, see Figure 5.12, which acquired the data and controlled the solenoid valves of the sensor tube system.



Figure 5.12 LABJACK U12

There are several functions and terminals provided by the LABJACK U12. For this project the U12 has eight terminals for analogue input signals (AI0-AI7) which can be controlled by using the *EAnalogIn* function for returning a single value or *AIBurst* for acquiring multiple samples of 1-4 channels at a sample rate of 400-8192 Hz. Also, it has two terminals for analogue output voltages (AO0 and AO1). Each analogue output can be set to a voltage between 0 and 5 using the *EAnalogOut* function. The U12 also

provides four digital I/O terminals (IO0-IO3). These can be controlled by either the *EDigitalIn* or *EDigitalOut* functions. DIO lines were used to control the solenoid valves.

### 5.3.2 System interface

Data acquisition and control system was performed via the LABJACK U12 using a computer running MATLAB software, see Figure 5.13. All data acquisition and control was automated through MATLAB based codes developed by the author, except the air and water valves which were controlled manually. Data was collected simultaneously from the test section (USFM and CFM), from the gas line (VAFM), from the water line (turbine flow meter), and the sensor tube section involved controlling the solenoid valves and recording the DP output. The VAFM and turbine flow meter both had 4-20mA outputs and so were connected to the LABJACK via I/V converters. Data were collected at a sampling rate of 1kHz.

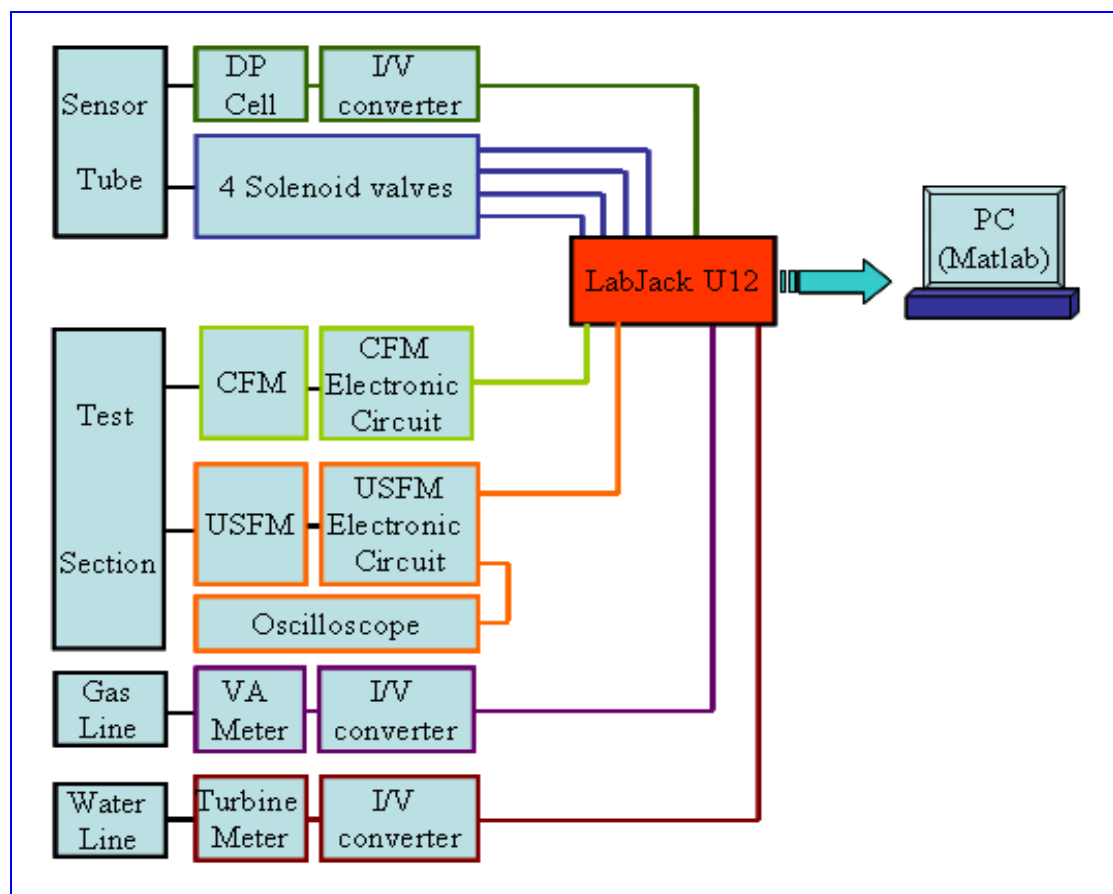


Figure 5.13 System interface and wiring diagram

### 5.3.3 Sampling frequency:

A sampling frequency problem occurred in the first attempts to optimize the operation of the CFM, see Sections 4.2.4 and 4.2.5. This was because the sampling rate was too low, 50Hz, and aliasing occurred. Initially the Nyquist criterion was not met: that the sampling frequency should be at least twice the highest frequency of interest in the signal being sampled. The sampling frequency was increased to 1kHz using the AIBurst function. This function reads from 1, 2, or 4 analogue inputs at a specified scan rate of up to 8192Hz. First, data was acquired and stored in the LABJACK's 4096 sample RAM buffer, then the data was transferred to a PC. The AIBurst function has a limitation on its run time, it can acquire data for only 4.5 seconds. To compensate for this limitation, each data collection was made ten times then averaged using the *Ensemble Averaging* technique to reduce random errors, see Section 4.2.5.

### 5.3.4 .m files (MATLAB programming codes)

The purpose of these programming codes (or .m files) was to call, sample, average and filter the data. The sampling and filtering .m files were created especially by the author to deal with the data collected from the CFM device. This was due to the noticeable noise on the output signal. The main program was written to acquire the raw data and then process it into sampling, averaging and filtering codes. The final data was to be presented in graphical plots to be analysed later. All the calculations and graphical plots were performed using commercially available software, MATLAB.

## 5.4 Experimental runs

### 5.4.1 Parameters and flow conditions

All of the experimental runs were performed in a vertical Perspex pipe of 50mm internal diameter using upward air and water flow in the annular flow regime. In the experiments, air and water were supplied at room temperature. Tables 5.1 and 5.2 list

the range of air and water volumetric flow rates used for the experimental work and their corresponding superficial velocities:

<b>Water volumetric flow rate (m<sup>3</sup>/hr)</b>	<b>Water superficial velocity (m/s)</b>
0.334	0.0473
0.501	0.0708
0.667	0.0944
0.834	0.1180
1.001	0.1416
1.168	0.1652
1.335	0.1888
1.502	0.2124
1.669	0.2360
1.836	0.2597

*Table 5.1 Water volumetric flow rates and superficial velocities*

<b>Air volumetric flow rate (m<sup>3</sup>/hr)</b>	<b>Air superficial velocity (m/s)</b>
100	14.15
115	16.27
125	17.68
140	19.81
150	21.22
165	23.34
175	24.76

*Table 5.2 Air volumetric flow rates and superficial velocities*

The lowest liquid volumetric flow rate chosen (0.334m<sup>3</sup>/h) provided an unbroken liquid film on the tube wall at all gas flow rates used. If the liquid flow rate fell too low the liquid film broke into rivulets which was easy to see.

The maximum air flow in the test section was 175m<sup>3</sup>/hr. In addition to using only air and water, several other experimental parameters were maintained at constant or approximately constant values for all runs, these were:

Water temperature	20-22°C
Air temperature	17-22°C
Water conductivity	143 $\mu\text{S}/\text{cm}$

*Table 5.3 Constant operating conditions*

For each experiment, the run parameters measured were: the liquid film thickness (using CFM, see Section 4.2), the liquid film velocity (using cross-correlation technique, see Section 4.2.5), the gas velocity in the core (using USFM, see Section 4.3), the reference gas and water volume flow rates (using VAFM and Able turbine flow meter, see Sections 5.1.1 and 5.1.2). The liquid volume fraction was measured on only a few of the runs, just to check the validity of the sensor tube measurement at minimum and maximum gas and liquid flow rates.

#### 5.4.2 Data collection process

The common procedure used for each experimental run is described later in the form of a flow diagram, see Figure 6.14. As explained earlier in Chapter 4, the designed devices i.e. CFM and USFM, were calibrated prior to making the experimental measurements. At the “Prompt MATLAB to collect data from measurement devices” stage, voltage measurements are made. These measurements come from VAFM, Turbine flow meter, CFM and USFM.

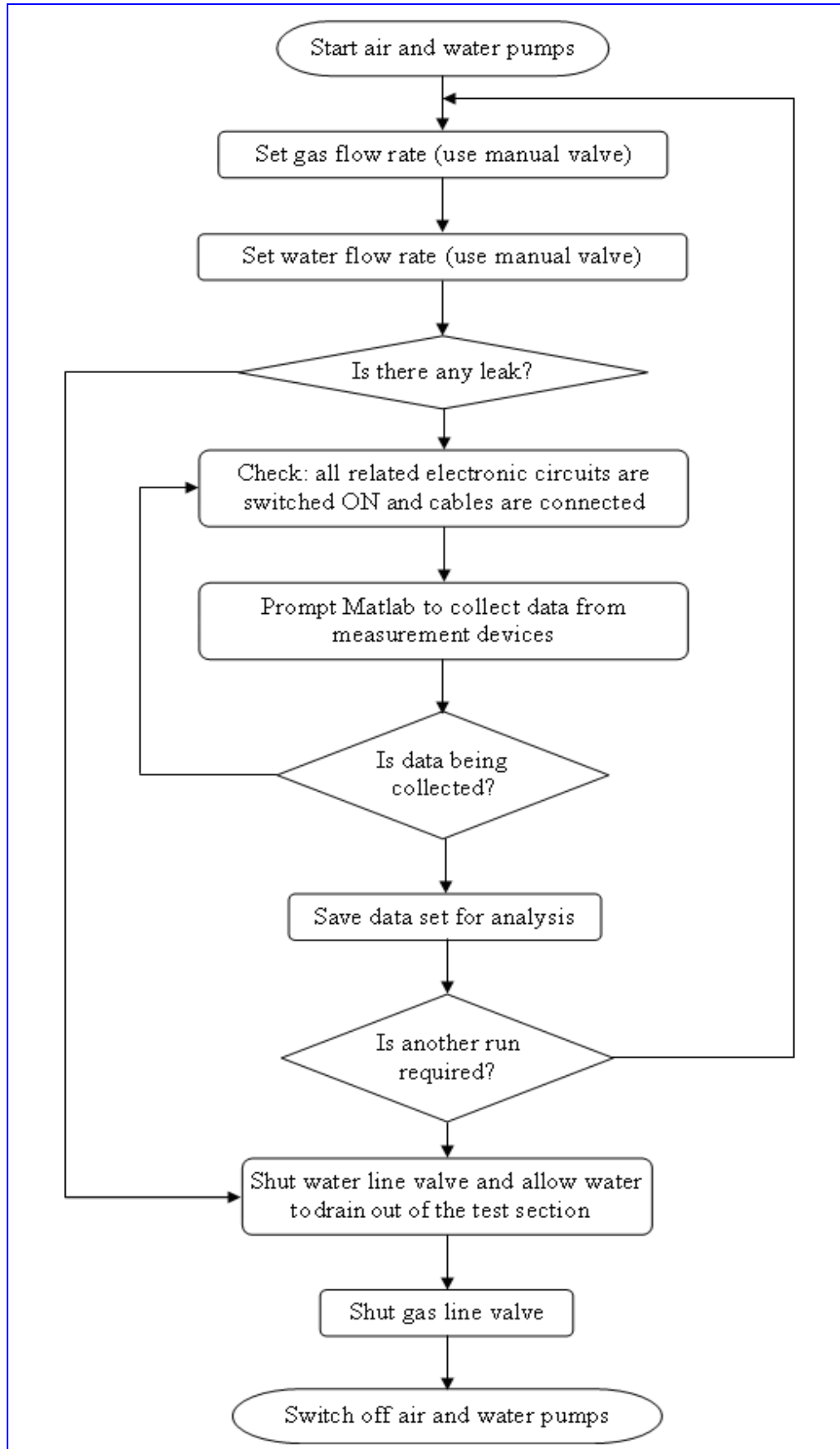


Figure 5.14 Flow chart of data collection process

## CHAPTER 6 RESULTS AND DISCUSSION

The presented results in this chapter will show how accurately the designed devices (CFM and USFM) will measure the individual properties of air-water annular flow i.e. liquid film thickness, liquid film velocity, entrainment fraction and gas velocity. At the end of this chapter it will be shown how these results enable the calculation of volumetric water and air flow rates.

### 6.1 Liquid film

#### 6.1.1 Film thickness

##### *6.1.1.1 CFM measurement of liquid film thickness*

Using the CFM, the film thickness was measured at different gas and water flow rates, see Tables 6.2 and 6.3. Referring back to Figure 4.13 (*CFM film thickness reading at 1kHz sampling frequency*), it can be seen that the CFM showed good measurement signals for the film thickness at both upstream and downstream sensors.

Four different flow conditions were used to investigate the film thickness (presented in this section) and film velocity distribution (presented in Section 6.1.3). These flow conditions were selected in such a way to create four extreme combinations of low and high water and gas flow rates as shown in Table 6.1. The film thickness and film velocity were experimentally measured for the given flow rates. The reason for presenting the film velocities of these four extreme flow conditions beside the film thickness results is to evaluate the relationship between the film thickness and film velocities. However, the results of the film velocity will be presented and discussed more fully later in Section 6.1.2.

Water flow rate $Q_{w,ref}$ (m <sup>3</sup> /hr)		Gas flow rate $Q_{g,ref}$ (m <sup>3</sup> /hr)		Film thickness $\delta$ (mm)	Film velocity $U_f$ (m/s)
1.84 (High)	0.334 (Low)	175 (High)	100 (Low)		
✓		✓		4.1	0.71
	✓		✓	1.0	0.56
✓			✓	5.7	0.63
	✓	✓		0.8	0.65

Table 6.1 Film thickness and film velocity for four different combinations of flow conditions

The output signals of the liquid film thickness from the CFM against time, corresponding to the conditions in Table 6.1, are shown in Figures 6.1-6.4. In each case the blue trace is the signal from the upstream sensor and the green trace is the signal from the downstream sensor. In three of the four conditions, Figures 6.1, 6.3 and 6.4, the CFM shows a clear and well-defined signal for the film thickness. However, at the lowest water flow rate and highest gas flow rate the signal suffers from sudden disturbances due to breaks in the liquid film, discontinuities in the flow (at the downstream sensor only), see Figure 6.2.

Starting from minimum gas and water flow rates, as the gas flow rate was increased in six steps, see Table 6.2. It was noticed that eventually gaps in the film occurred due to shear forces, see Figure 6.2. Reducing the gas flow rate and/or increasing the water flow rate returned stability to the film thickness. Nevertheless, the CFM showed itself capable of responding to the changes in liquid film thickness. Zabarás and Dukler (1986) presented similar variations in their liquid film thickness signals using a parallel wire probe.

Reference gas flow rates and the corresponding gas superficial velocities							
$Q_{g,ref}$ m <sup>3</sup> /hr	175	165	150	140	125	115	100
$U_{g,s}$ m/s	24.8	23.3	21.2	19.8	17.7	16.3	14.2

Table 6.2 Gas flow rates used throughout the investigation

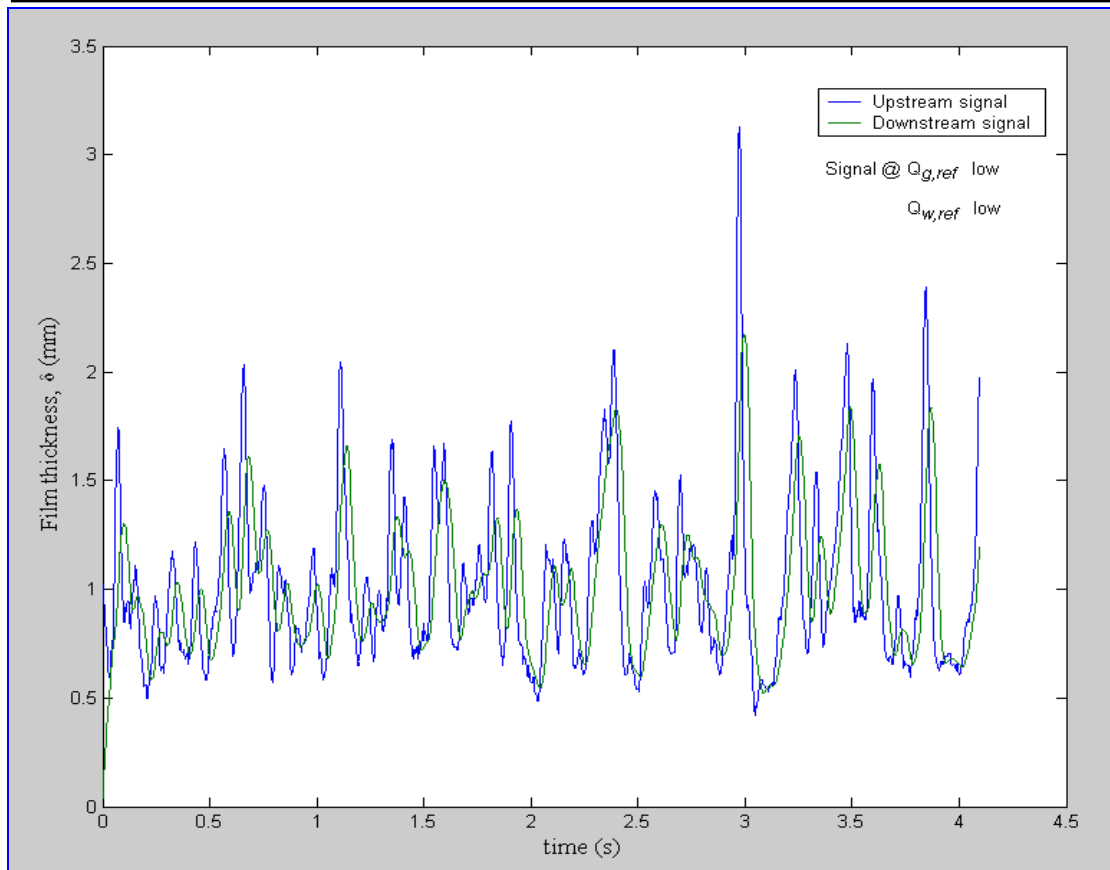


Figure 6.1 Film thickness signal for  $Q_{g,ref} = 100\text{m}^3/\text{hr}$ ,  $Q_{w,ref} = 0.333\text{m}^3/\text{hr}$

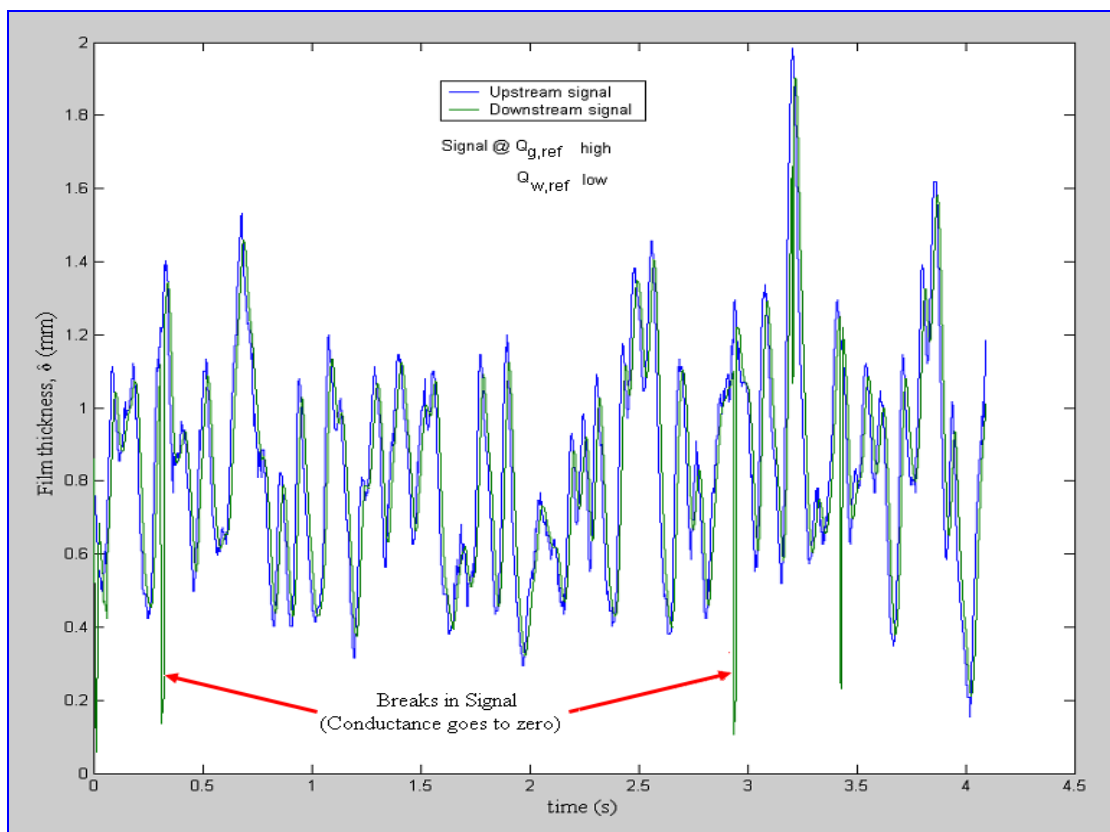


Figure 6.2 Film thickness signal for  $Q_{g,ref} = 175\text{m}^3/\text{hr}$ ,  $Q_{w,ref} = 0.333\text{m}^3/\text{hr}$

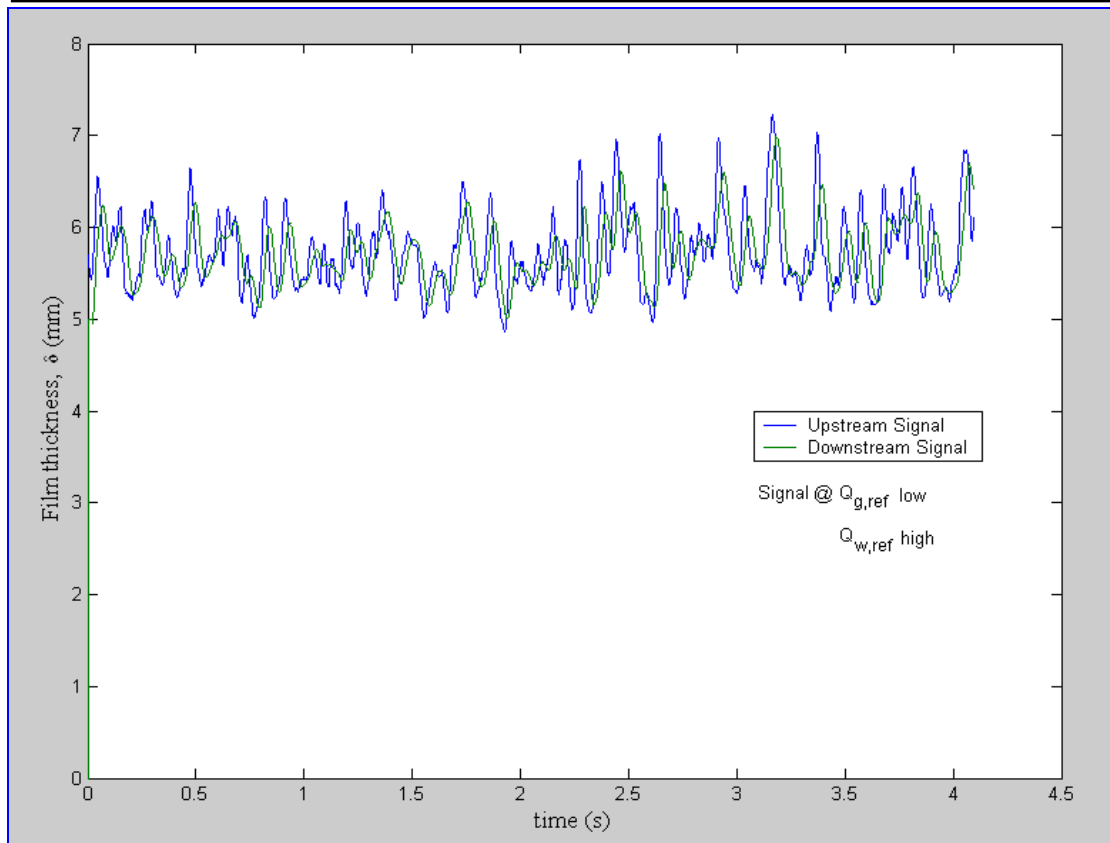


Figure 6.3 Film thickness signal for  $Q_{g,ref} = 100\text{m}^3/\text{hr}$ ,  $Q_{w,ref} = 1.84\text{m}^3/\text{hr}$

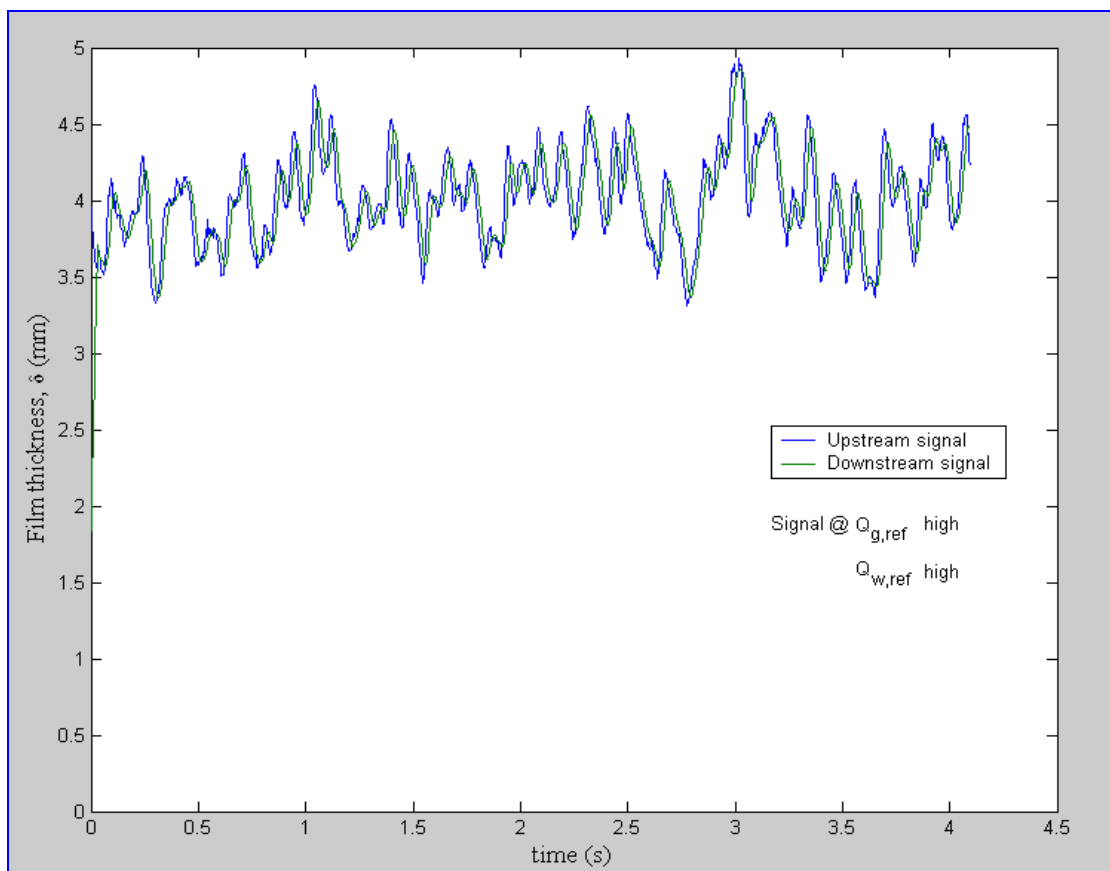


Figure 6.4 Film thickness signal for  $Q_{g,ref} = 175\text{m}^3/\text{hr}$ ,  $Q_{w,ref} = 1.84\text{m}^3/\text{hr}$

### 6.1.1.2 *Effect of gas and liquid superficial velocities on liquid film*

To present as full an analysis as possible of the effect of the gas and liquid superficial velocities on the liquid film, a total of seventy separate flow conditions were used (ten water flow rates between  $0.333\text{m}^3/\text{hr}$  and  $1.84\text{m}^3/\text{hr}$ , for each of seven gas flow rates between  $100\text{m}^3/\text{hr}$  and  $175\text{m}^3/\text{hr}$ ). The mode of application was to maintain either the water or gas flow rate constant and vary the other.

<b>Reference water flow rates and the corresponding water superficial velocities</b>										
$Q_{w,ref}$ $\text{m}^3/\text{hr}$	1.84	1.67	1.50	1.34	1.17	1.00	0.834	0.667	0.501	0.333
$U_{w,s}$ $\text{m/s}$	0.26	0.24	0.21	0.19	0.17	0.14	0.12	0.094	0.071	0.047

*Table 6.3 Gas and water flow rates used throughout the investigation*

Figure 6.5 shows the variations of the liquid film thickness with increasing water superficial velocity at different gas superficial velocities. In Section 4.2.6 it was stated that at a constant gas flow rate the liquid film thickness is expected to increase with increasing water flow rate. The results of measurements, see Figure 6.5, confirm this. At the minimum water superficial velocity the film thickness is much the same for all the gas superficial velocities used although, as mentioned above, at the highest gas superficial velocities the film thickness could become unstable. However, as the water superficial velocity increased the film thickness increased at a faster rate for the lower gas superficial velocities, see Figure 6.5. This phenomenon is attributed to the ability of the gas flow to limit the liquid film growth. Further increase in water superficial velocity above  $1.33\text{m/s}$  resulted in over flooding of the system i.e. liquid film collapses into the gas core of the annular flow.

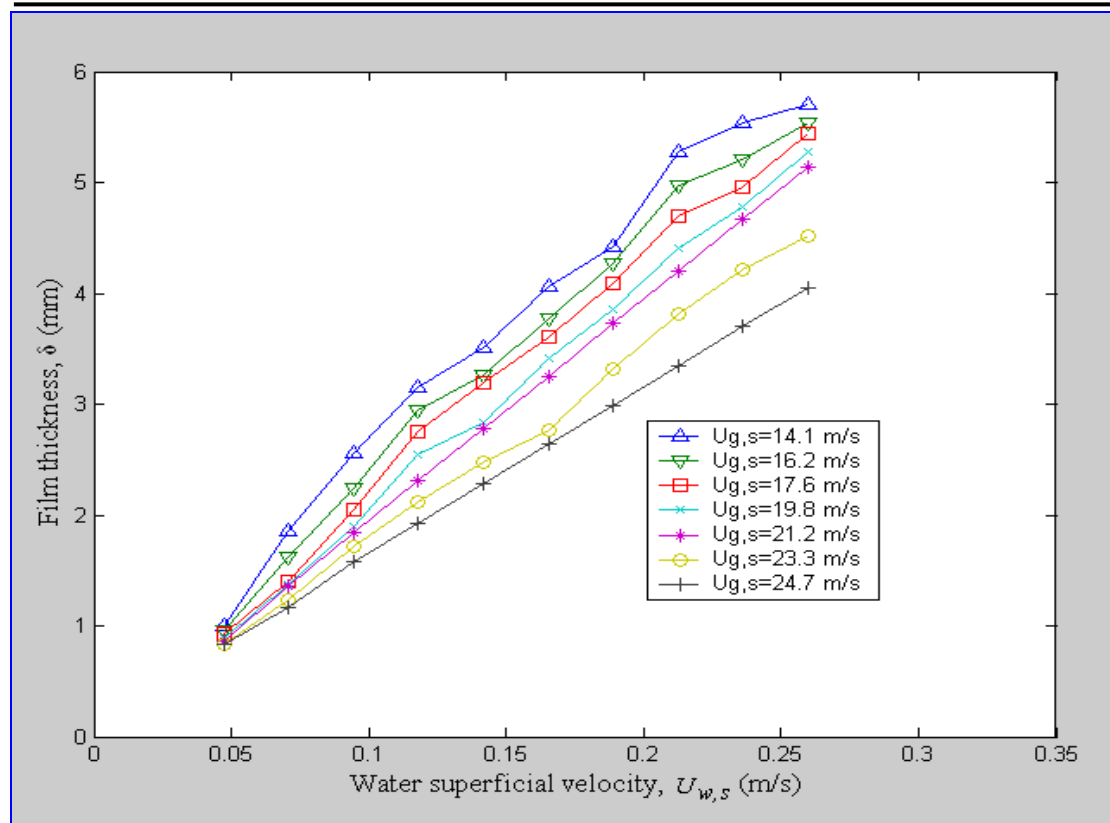


Figure 6.5 Effect of water superficial velocity on liquid film thickness at different constant gas superficial velocities

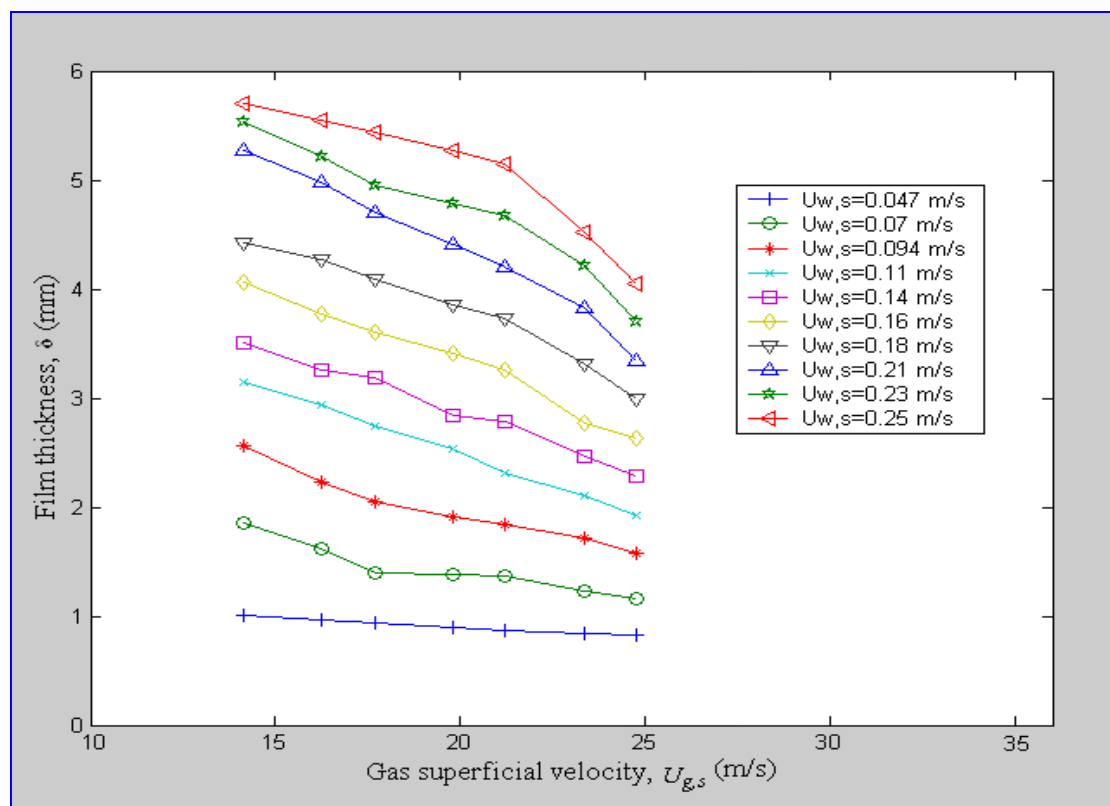


Figure 6.6 Effect of gas superficial velocity on liquid film thickness at constant water superficial velocity

Figure 6.6 shows the variations of the liquid film thickness with increasing gas superficial velocity at different water superficial velocities. Figure 6.6 shows that at a constant water superficial velocity the liquid film thickness decreases as the gas superficial velocity increases. This behaviour is attributed to increased film velocity and increased entrainment. This observation is more obvious at higher water flow rates than the lower water flow rates. Figure 6.6 also suggests that further increase in the gas superficial velocity could cause a dangerous dry-out for the system. Quandt (1965) reported similar decreasing trends in the film thickness using a computational model.

This observation, also mentioned during the liquid film velocity discussion in Section 6.1.2.2, is likely due to the higher gas superficial velocity increasing the liquid film velocity, which would give rise to a reduced film thickness:

$$Q_f = (2\pi R\delta)U_f \quad 6.1$$

where:  $Q_f$  is the volumetric flow rate of the liquid in film,  $U_f$  is the liquid film velocity measured by the CFM,  $R$  is the pipe radius and  $\delta$  is the film thickness.

Equation 6.1, suggests that if the liquid film flow rate is approximately constant; increasing the liquid film velocity results in a decrease in the liquid film thickness.

These trends are very similar to the observations of Drosos et al. (2006). This was taken as a first sign of the success of the CFM device in measuring the liquid film thickness. It also shows that the CFM device can be used to measure the liquid film thickness and hence to predict either over-flooding or drying-out from the measured value of the liquid film thickness for a known pipe diameter. Results, in this study, showed that the CFM was able to read maximum and minimum film thicknesses of 5.7mm and 0.8mm respectively.

## 6.1.2 Film velocity

### 6.1.2.1 CFM accuracy in measuring film velocity

The cross-correlation technique was used in this study to measure film velocity, see Sections 2.3.3 and 4.2.5. The liquid film velocity data and its analysis are given in Sections 6.1.2.2 and 6.1.2.3. However, prior to analysing the effect of the gas and water superficial velocities on the liquid film velocity, it was important to perform an initial check on the accuracy of the CFM readings. A “reference” liquid film velocity can be obtained from the reference water volumetric flow rate obtained from the turbine flow meter, which had been carefully calibrated, see Section 5.1.2, on the assumption that no water flows in the core:

$$U_{f,ref} = \frac{Q_{w,ref}}{A} \quad 6.2$$

It is shown that  $U_{f,ref}$  given by Equation 6.2 is likely to over-estimate the actual liquid film velocity since, obviously, water droplets do flow in the core. Nevertheless, it enables a useful comparison to be made with the film velocity measured by the CFM using cross-correlation.

A percentage error in the liquid film velocity,  $\xi_{f,velocity}$ , could be calculated for each of the seventy flow conditions, and was defined as:

$$\xi_{f,velocity} = \frac{U_f - U_{f,ref}}{U_{f,ref}} \times 100 \% \quad 6.3$$

where:  $\xi_{f,velocity}$  is the percentage error in the measured liquid film velocity,  $U_f$  is the film velocity determined from the cross-correlation technique and  $U_{f,ref}$  is the reference liquid film velocity given by Equation 6.2 and based on water flow rate obtained from the turbine meter.

For the seventy flow conditions mentioned earlier in Section 6.1.1.2, the results of the error calculation of the measured liquid film velocity are shown in Figure 6.7.

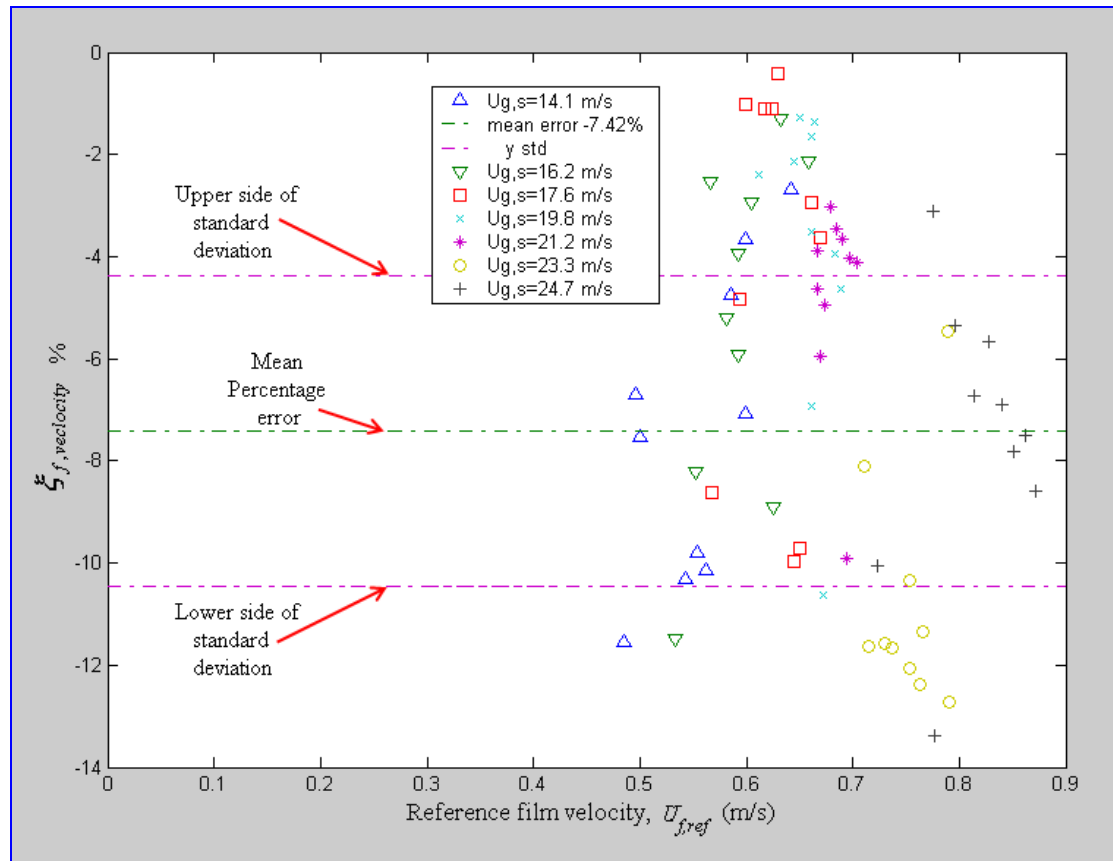


Figure 6.7 Percentage error in measured liquid film velocity at different constant gas superficial velocities

All the calculations gave a negative error as expected because of the assumption that all the water was in the liquid film, but actually some water was entrained as drops in the core, see Figure 6.7. The calculations indicated a mean percentage error of  $-7.4\%$ . In addition the slight vibration of the test section caused by random pressure fluctuations in the air line may have contributed some inaccuracy to the measurement. The measured values by the CFM indicated maximum and minimum liquid film velocities of  $0.71\text{m/s}$  and  $0.56\text{m/s}$  respectively, see Figures 6.8 and 6.9.

Because the “reference” film velocity was known to be too high, the results shown in Figure 6.7 gave good initial confidence that the CFM was indeed measuring the film velocity and not for example, the speed of surface wave on the liquid film.

The need to assume that all the water was in the liquid film was overcome by using a correlation for the entrainment fraction, see Section 6.2.2. The correlation, Equation 6.24, can provide an estimate of the volumetric flow rate of the entrained water in the core and an estimate for the total volumetric flow rate of the water in the pipe can be calculated from:

$$Q_{w,est} = Q_{w,c,est} + Q_f \quad 6.4$$

where:  $Q_{w,est}$  is the estimated water flow rate in the test section,  $Q_{w,c,est}$  is the estimated volumetric flow rate of the entrained water in the core and  $Q_f$  is the volumetric film flow rate calculated from Equation 6.1.

So, a better estimate for a reference value for the liquid film velocity can be given by:

$$U_{f,ref} = \frac{Q_{w,est}}{A} \quad 6.5$$

Referring ahead to the error calculation in the water flow rate in Section 6.6.1, Figure 6.39 indicates that taking into account the entrained water flow rate reduces the mean percentage error to -1.11%.

However, the development of the entrainment method relies on knowing liquid film volumetric flow rate  $Q_f$  which requires liquid film velocity  $U_f$  measured by the CFM. The only relevance of Section 6.1.2.1 to this argument is that the liquid film velocity obtained using the CFM is close to (and always less than) reference liquid film velocity  $U_{f,ref}$  from Equation 6.5. We know from the literature that the entrainment flow represents a small proportion, see Table 6.5, of the total liquid flow rate. Hence, the fact that the measured liquid film velocity was close to the reference liquid film velocity was taken as an indication that we were measuring the correct film velocity.

### *6.1.2.2 Effect of gas and liquid superficial velocities on liquid film velocity*

Figures 6.8 and 6.9 show the variations in the measured liquid film velocity with water and gas superficial velocity respectively. By inspection, both figures show that the liquid film velocity increases with increasing gas and liquid superficial velocity. It is interesting that a fivefold increase in water superficial velocity increased the film velocity by a mere 20 to 30%, because the film thickness also increased. However, for the ranges of values chosen, the gas superficial velocity has a greater influence on the liquid film velocity than the water superficial velocity. The reason behind these variations is the interfacial shear stress. The gas seems to exert a large interfacial shear stress which causes the liquid film to speed up. In the case of the increasing water flow rate, the wall shear stress has a tendency to slow the liquid film.

However, the theory presented earlier in Section 6.1.1.2 concerning the effect of both gas and water superficial velocities on the liquid film thickness is able to explain the obtained results in Figures 6.8 and 6.9. Figure 6.8 indicates that the liquid film velocity increases with increasing the water superficial velocity (i.e. increasing the water film flow rate) at a constant gas superficial velocity. This agrees with Equation 6.1. However, it was also found in Section 6.1.1.2, see for example Figure 6.5, that increasing water superficial velocity and thereby increasing the water film flow rate, results in the liquid film thickness being increased (i.e. increasing the liquid film cross-sectional area). It is this thickening of the liquid film which results in the relatively slow increase in the liquid film velocity with increasing water flow rate.

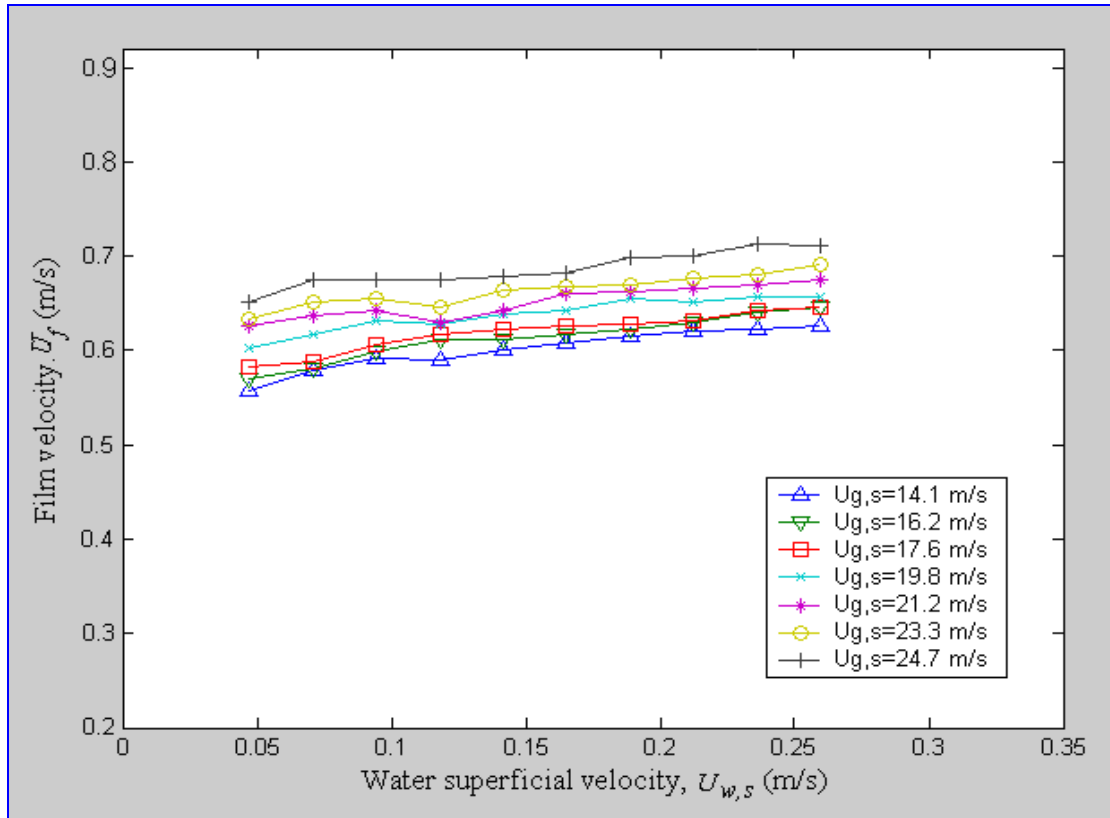


Figure 6.8 Effect of water superficial velocity on liquid film velocity at constant gas superficial velocity

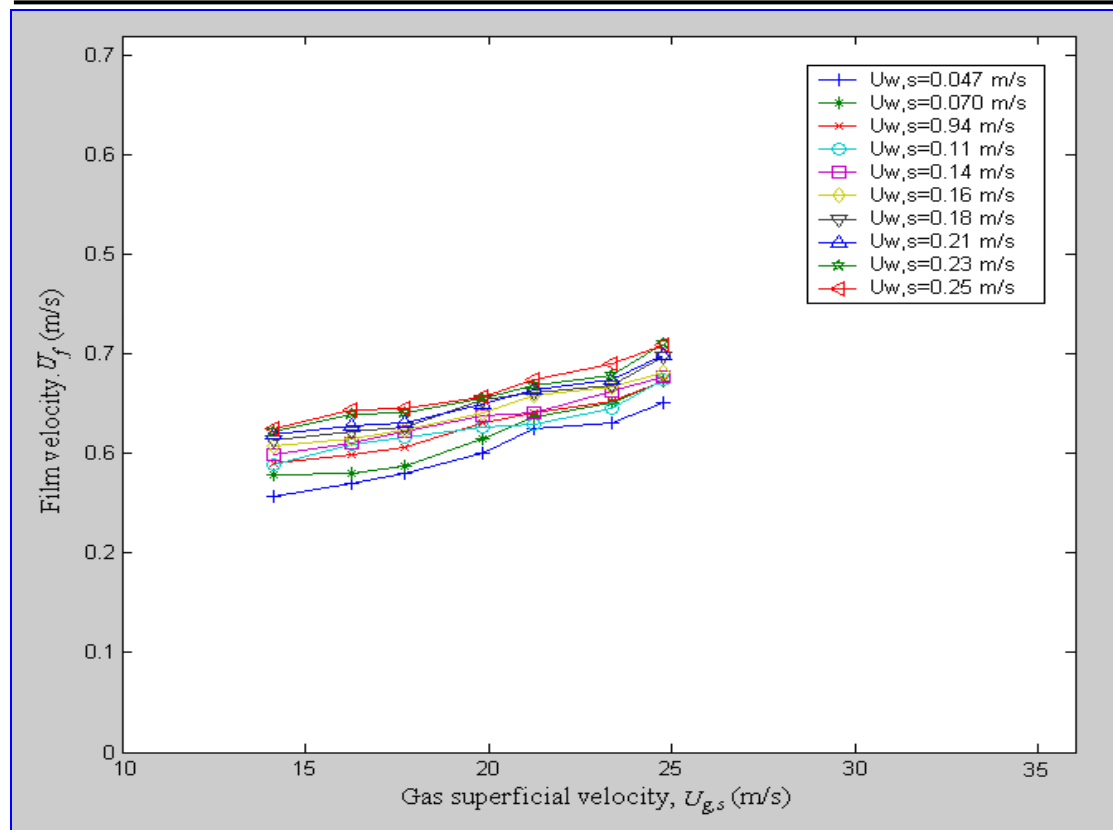


Figure 6.9 Effect of gas superficial velocity on liquid film velocity at constant water superficial velocity

### 6.1.2.3 Comparison of liquid film velocity results with Zabarás and Dukler (1986)

The results obtained in this investigation for the velocity of the liquid film were compared to those of previous workers. A detailed comparison is made with the results of Zabarás and Dukler (1986). The reason these authors have been chosen for this comparison is because they presented a comprehensive set of data gained from a very similar test rig to that used in the present study with a pipe of diameter 50.8mm carrying a vertically upward co-current of air/water mixture.

To make the comparison easier, flow rates were converted to mass flow rates since Zabarás and Dukler (1986) presented their results in these units. Also, they represented their results as a function of the liquid feed Reynolds number  $Re_w$ .

$$Re_w = \frac{4Q_{w,feed}}{\nu} \quad 6.6$$

where:  $\nu$  is the kinematic viscosity ( $1 \times 10^{-6} \text{ m}^2/\text{s}$  for water) and  $Q_{w,feed}$  is the water feed flow rate per unit perimeter.

That is:

$$Q_{w,feed} = \frac{Q_{w,ref}}{\pi D} = \frac{U_{w,s} (\pi D^2)}{4} \frac{1}{\pi D} \quad 6.7$$

$$Q_{w,feed} = \frac{U_{w,s} D}{4} \quad 6.8$$

where:  $U_{w,s}$  is the water superficial velocity and  $D$  is the pipe diameter.

By substituting Equation 6.8 into Equation 6.6 we obtain:

$$Re_w = \frac{U_{w,s} D}{\nu} \quad 6.9$$

$Re_w$	2360	3100	3561	5902	3100 (Z and D)
$U_{w,s}$ m/s	0.047	0.061	0.071	0.118	0.06

*Table 6.4 Corresponding liquid film Reynolds numbers and water superficial velocities*

Zabaras and Dukler (1986) were able to vary the gas mass flow rate  $W_g$  from 0.01kg/s to 0.09 kg/s but chose only to vary it in the range 0.03kg/s to 0.07kg/s. Similarly for the liquid feed Reynolds number, they used only four flows with  $Re_w = 310, 768, 1550$  and 3100. The author of the present study believes that last Reynolds number of 3100, corresponding to a flow velocity of 0.06m/s, is the best for comparison because this was the region where the annular flow was visually observed to be fully developed in the current study.

The values of  $Re_w$  in the present study that are suitable for comparison with the results of Zabaras and Dukler were 2360, 3541 and 5902. Figure 6.10 shows how the film mass flow rate shows a similar trend to the data curve for Zabaras and Dukler between gas mass flow rates of 0.033kg/s and 0.068kg/s.

Zabaras and Dukler used a separation method to obtain the film mass flow rate. In the current study the film volumetric flow rate was obtained from measured parameters of the liquid film, i.e. the film thickness  $\delta$  and film velocity  $U_f$ . Then Equation 6.10 was used to obtain the film mass flow rate:

$$W_f = Q_f \rho \quad 6.10$$

where:  $W_f$  is the film mass flow rate,  $Q_f$  is the film volumetric flow rate given by Equation 6.11 and  $\rho$  is the water density taken  $1000\text{kg/m}^3$ .

$$Q_f = U_f \pi [R^2 - (R - \delta)^2] \quad 6.11$$

where:  $R$  is the pipe internal radius,  $\delta$  is the measured film thickness using the CFM.

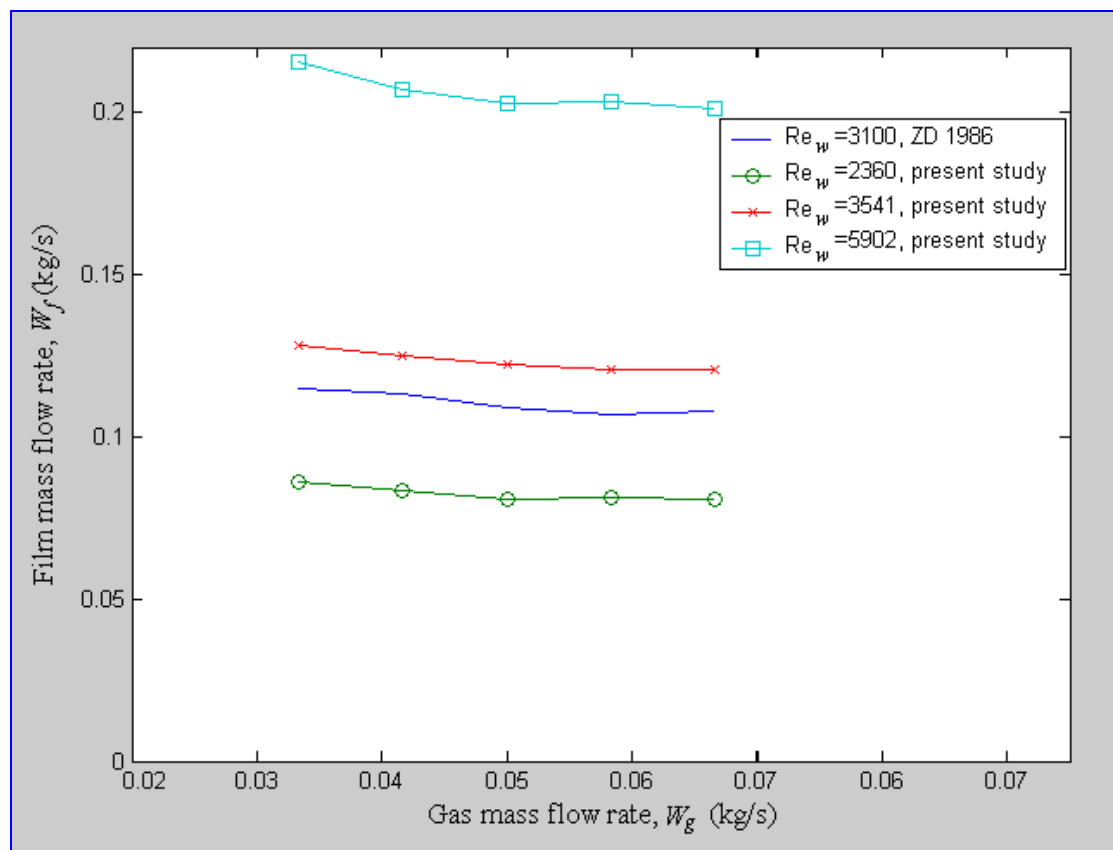


Figure 6.10 Comparison of film mass flow rate when varying the gas mass flow rate with results of Zabaras and Dukler (1986)

Figure 6.10, indicates that the measured liquid film flow rates using the CFM agree with the results obtained by Zabaras and Dukler. This suggests that the measured values of liquid film flow rate  $Q_f$  and hence the measured values of film thickness  $\delta$  and liquid film velocity  $U_f$  are likely to be reasonably accurate. This can be understood from inspecting Equation 6.1. Calculating the film flow rate  $Q_f$  in this equation is totally dependent on the measured values of the film thickness  $\delta$  and the film velocity  $U_f$ . The film thickness is used to obtain the cross-section area of the film, see Equation 6.12, and hence an inaccurate film area measurement would result in an inaccurate film flow rate.

$$\pi[R^2 - (R - \delta)^2] = A_f \quad 6.12$$

A similar argument applies to the film velocity  $U_f$  which was measured using the cross-correlation technique, see Sections 2.3.3 and 4.2.5. Once, again the comparison suggests that the technique used has accurately measured the film velocity by giving

an film flow rate measurement which compares well with the previous study of Zabaras and Dukler.

The film velocity at the gas-water interface is higher than the mean film velocity (Sugawara, 1990). Thus if the CFM has been measuring the surface wave velocity it would be expected that the percentage error shown in Figure 6.7 would be positive not negative, indicating that the CFM device is measuring the actual liquid film velocity.

### 6.1.3 Film velocity profile

For annular flow the velocity profile of the liquid film is important because a better knowledge of the film velocity profile will give a better understanding of the relationship between the film and the gaseous core. In the current study simple liquid film modelling work has been undertaken in order to characterize the liquid film velocity profile. The back-flow or flooding phenomenon, which usually occurs when the gas flow lacks the ability to lift up the entire segment of the liquid film in the annular flow so the liquid at the internal pipe wall will start to flow downwards, was

then investigated. In co-current gas-liquid flow, the onset of flooding is identified by the critical gas flow rate at which partial liquid flow reversal is observed (Wadekar, 2002).

In this section, an attempt at characterizing the liquid film velocity was carried out in order to provide evidence that the measurement of the liquid film velocity is true. The effect of the gas and water flow rates on the thinning of the liquid film can be observed from the velocity distribution curves as it will be shown later, see Figure 6.17.

The simplest approach to modelling annular film flow is to develop a force balance equation for an element of the film. This method assumes mean values of the film properties. Additional assumptions are:

- The surface of the liquid is smooth; there are no surface waves or ripples which imply that the flow rates are restricted.
- The velocity profile of the film is known and it is identical to profiles found in single phase flow, e.g. the universal velocity profile for turbulent flow or the parabolic profile for laminar flow.

With reference to Figure 6.11, a force balance on a cylindrical element of the film under steady state conditions yields:

$$2\pi r_i \hat{\tau}_i \delta Z + P \pi (r^2 - r_i^2) = 2\pi r \hat{\tau} \delta Z + \pi \left( P + \frac{dP}{dZ} \delta Z \right) (r^2 - r_i^2) + \rho_l g \pi \delta Z (r^2 - r_i^2) \quad 6.13$$

where:  $r_i$  is the distance from the centre-line of the pipe to the film surface,  $r$  is the distance from pipe centre-line to the middle of the film ( $r = (r_i + r_0)/2$ ),  $Z$  is the axial coordinate,  $\rho_l$  is the density of the liquid forming the fluid film (it is assumed that the liquid density within the liquid film is constant),  $dP/dZ$  is the pressure gradient,  $\hat{\tau}$  and  $\hat{\tau}_i$  are the shear stress and interfacial shear stress respectively,  $g$  is  $9.81\text{m/s}^2$  and  $P$  is the pressure.

Equation 6.13 can be simplified and rearranged to form Equation 6.14:

$$2\pi r_i \hat{\tau}_i \delta Z = 2\pi r \hat{\tau} \delta Z + \pi \frac{dP}{dZ} \delta Z (r^2 - r_i^2) + \rho_l g \pi \delta Z (r^2 - r_i^2)$$

$$\therefore 2r \hat{\tau} = 2r_i \hat{\tau}_i + \frac{dP}{dZ} (r_i^2 - r^2) + \rho_l g \pi \delta Z (r_i^2 - r^2)$$

$$\therefore \hat{\tau} = \hat{\tau}_i \left( \frac{r_i}{r} \right) + \frac{(r_i^2 - r^2)}{2r} \left( \rho_l g + \frac{dP}{dZ} \right) \quad 6.14$$

The local velocity can be calculated from:

$$\hat{u}_f(r) = \int \frac{\hat{\tau}}{\mu} dr \quad 6.15$$

where:  $\mu$  is viscosity of water,  $1 \cdot 10^{-3}$  kg/ms, and  $\hat{\tau}$  is the shear stress.

The boundary conditions for Equation 6.15 are:

$$\begin{cases} r = 0, & \hat{u}_f = 0 \\ r = \delta, & \frac{d\hat{u}_f}{dy} = \frac{\hat{\tau}}{\mu} \end{cases}$$

$$\hat{u}_f(r) = \frac{1}{\mu} \left\{ \ln \left( \frac{r_0}{r} \right) \left[ r_i \hat{\tau}_i + \frac{r_i^2}{2} \left( \rho_l g + \frac{dP}{dZ} \right) \right] - \frac{1}{4} \left( \rho_l g + \frac{dP}{dZ} \right) (r_0^2 - r^2) \right\} \quad 6.16$$

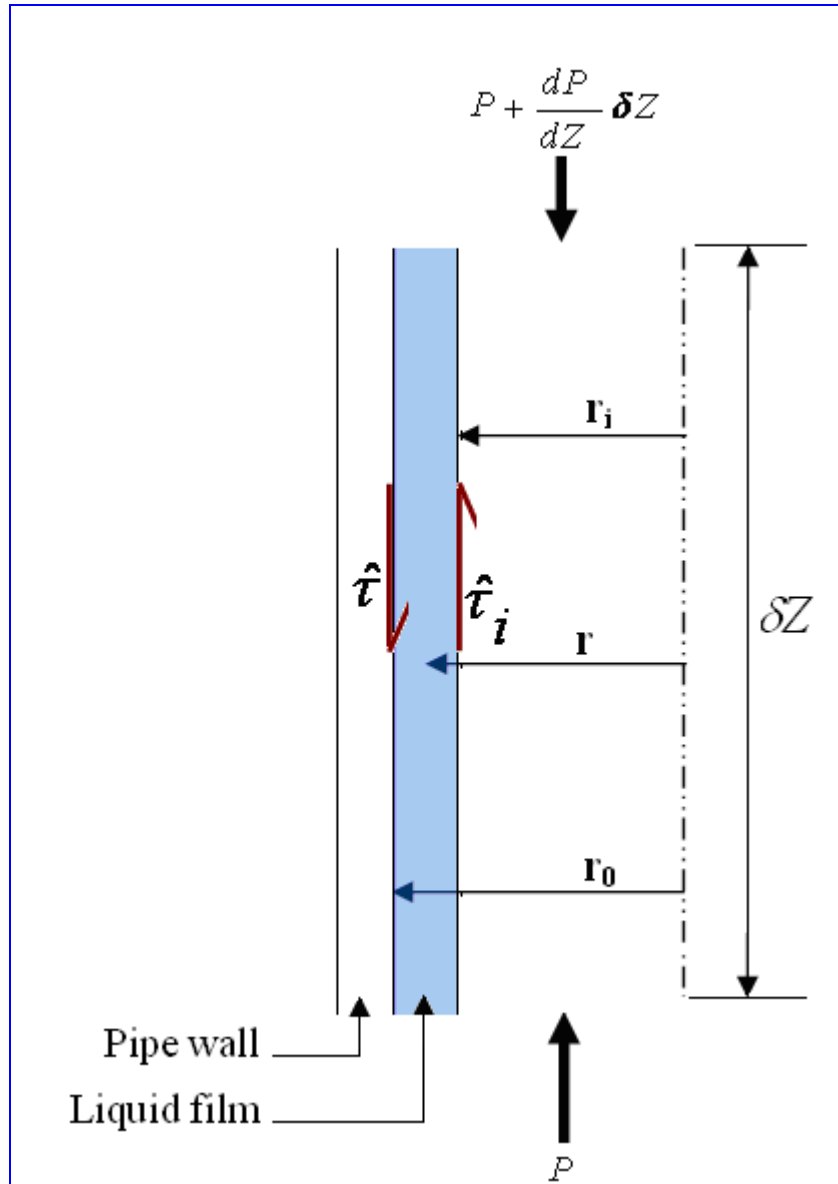


Figure 6.11 Illustration of force balance on the control volume of liquid film for upward annular flow

In the annular flow with which this project is concerned, the gas volume fraction is close to unity and gas density is small compared to that of the fluid, and so gravitational force is negligible compared to the pressure term. Accordingly and with reference to Figure 6.12, the upwards forces sum to zero and the following result is obtained:

$$\pi r_i^2 \left[ P - \left( P + \frac{dP}{dZ} \delta Z \right) \right] = 2\pi r_i \hat{\tau}_i \delta Z$$

$$\pi r_i^2 \left[ -\frac{dP}{dZ} \delta Z \right] = 2\pi r_i \hat{\tau}_i \delta Z \quad 6.17$$

$$-r_i \frac{dP}{dZ} = 2\hat{\tau}_i$$

$$\therefore \hat{\tau}_i = -\frac{r_i}{2} \frac{dP}{dZ} \quad 6.18$$

where:  $dP/dZ$  is negative in the direction of increasing  $Z$ .

The total film volume flow rate from the above equations is given by:

$$Q_w = \int_{r_i}^{r_0} \hat{u}_f(r) * 2\pi r dr \quad 6.19$$

$$\therefore Q_f = \frac{2\pi}{\mu} \left\{ \left[ \hat{\tau}_i r_i + \frac{r_i^2}{2} \left( \rho_l g + \frac{dP}{dZ} \right) \right] \left[ \frac{1}{4} (r_0^2 - r_i^2) - \frac{1}{2} r_i^2 \ln \left( \frac{r_0}{r_i} \right) \right] \right. \\ \left. - \frac{1}{16} \left( \rho_l g + \frac{dP}{dZ} \right) (r_0^2 - r_i^2)^2 \right\} \quad 6.20$$

This expression is known as the “Triangular Relationship” as it relates the three variables: mean film thickness, film flow rate and wall shear stress.

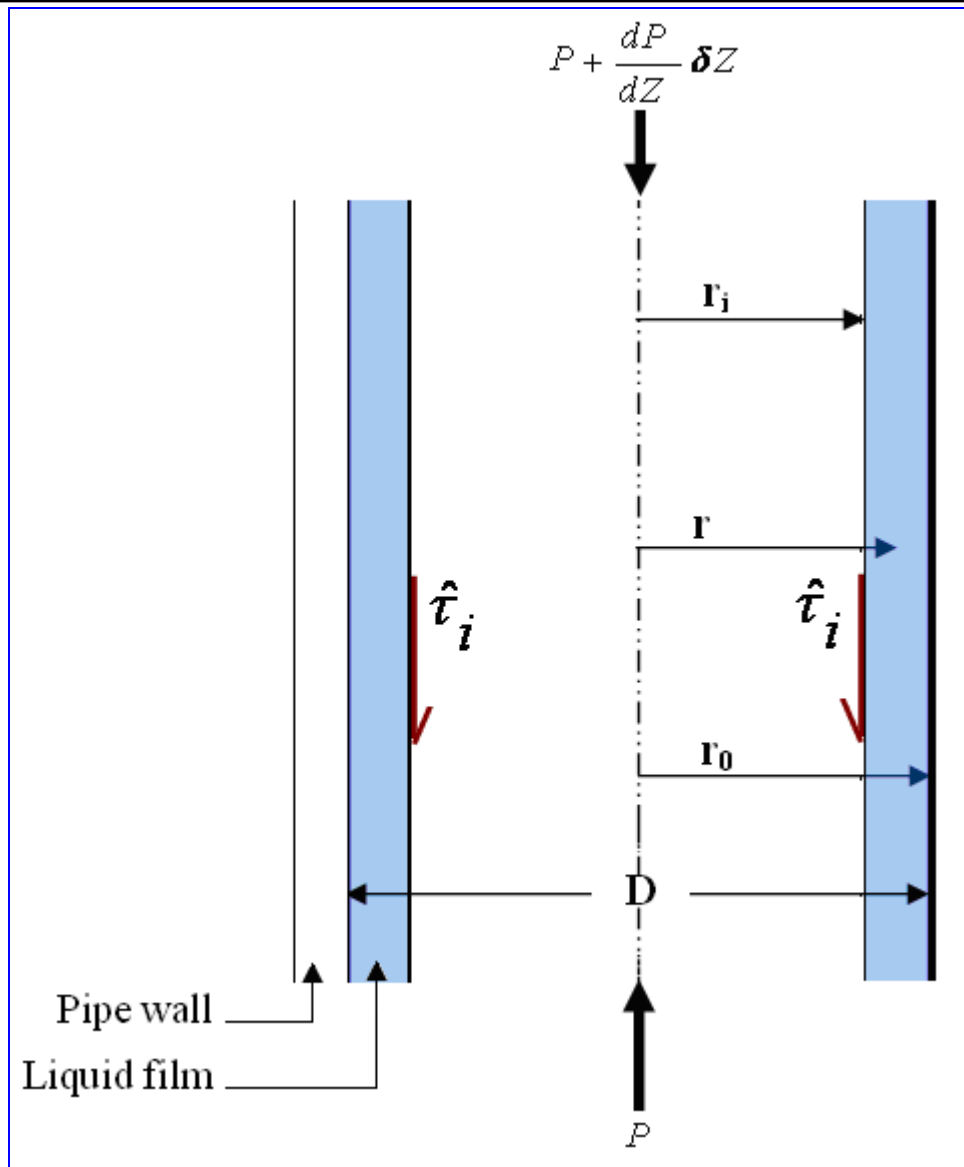


Figure 6.12 Illustration of force balance on the control volume of gas core of upward annular flow

Since the film thickness and velocity can be measured at different flow conditions, using Equations 6.11, 6.18 and 6.20 it enables us to predict the pressure gradient, which can then be used in Equation 6.16 to find the corresponding velocity distribution  $\hat{u}_f(r)$ .

The same extreme flow conditions presented in Section 6.1.1.1 and tabulated in Table 6.1 were used in this modelling investigation. Figures 6.13-6.16 show predicted liquid film velocity distributions  $\hat{u}_f(r)$  versus radial position  $r$  for the given different flow conditions using Equation 6.16. The velocity distribution shows no back flow i.e. no

negative velocity distribution. It's very clear from all figures that the velocity of the film increases from a zero velocity at the pipe wall to a maximum value where the film meets the gas core. This result agrees with visual observation made by the author while carrying out the experiments. This finding emphasises the confidence in using the CFM as a liquid film velocity measurement device.

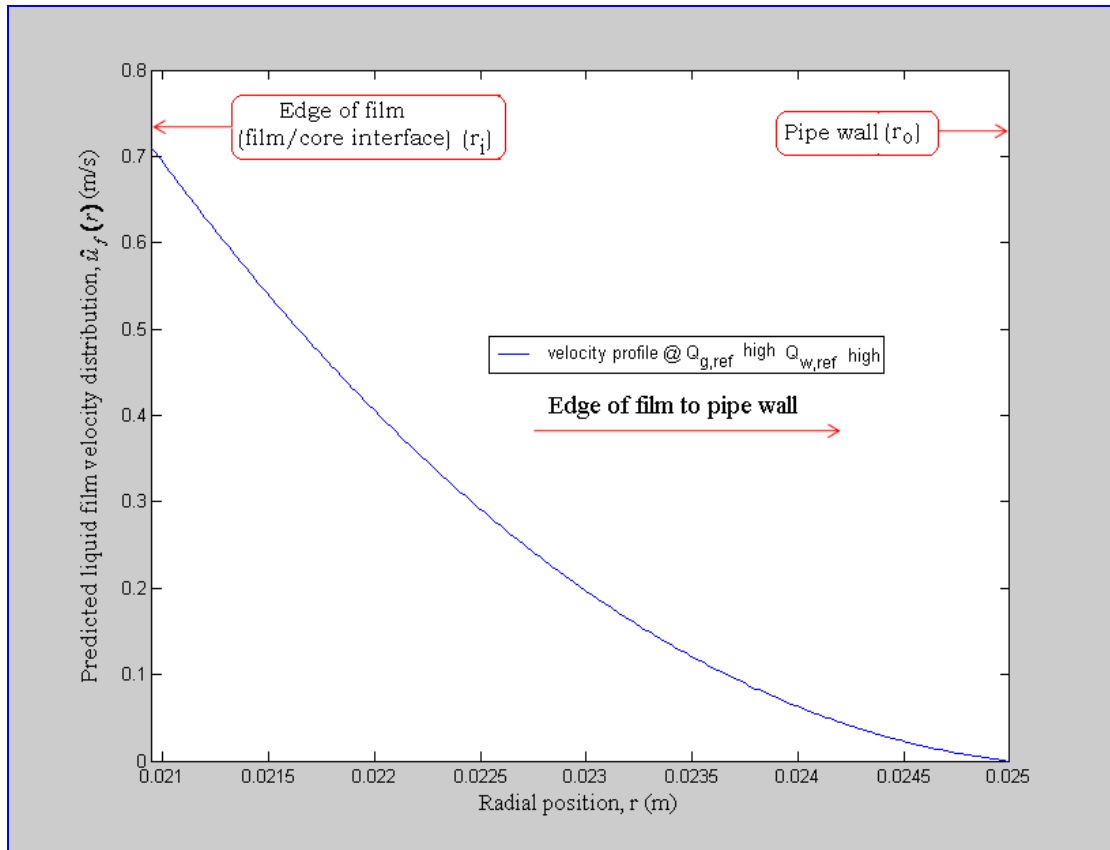


Figure 6.13 Film velocity profile for  $Q_{g,ref}$  high,  $Q_{w,ref}$  high

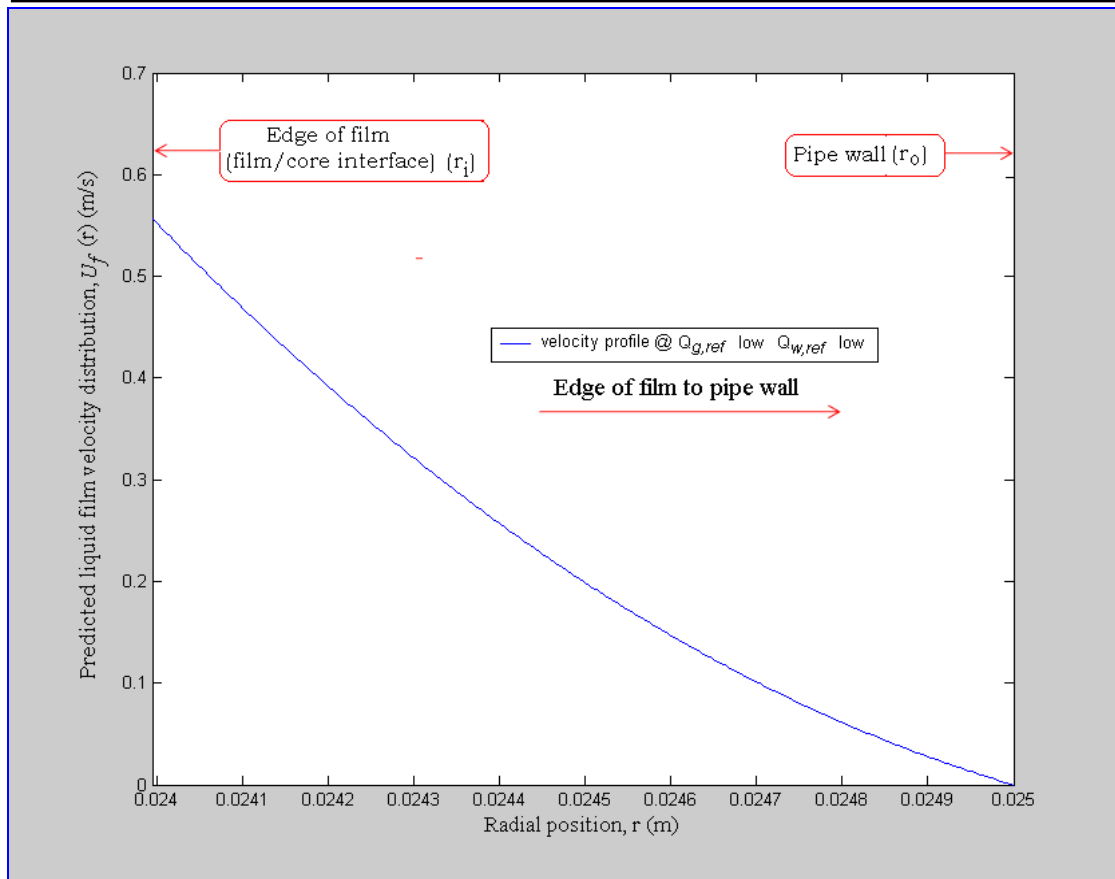


Figure 6.14 Film velocity profile for  $Q_{g,ref}$  low,  $Q_{w,ref}$  low

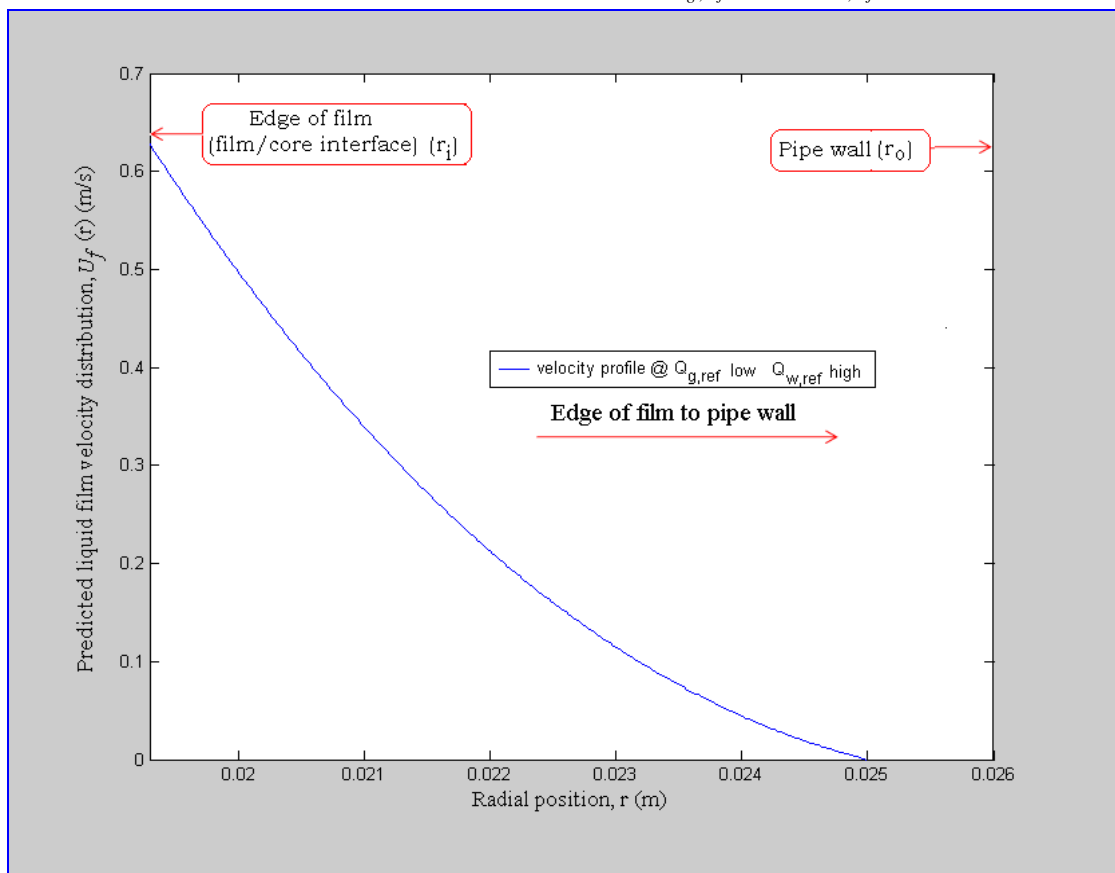


Figure 6.15 Film velocity profile for  $Q_{g,ref}$  low,  $Q_{w,ref}$  high

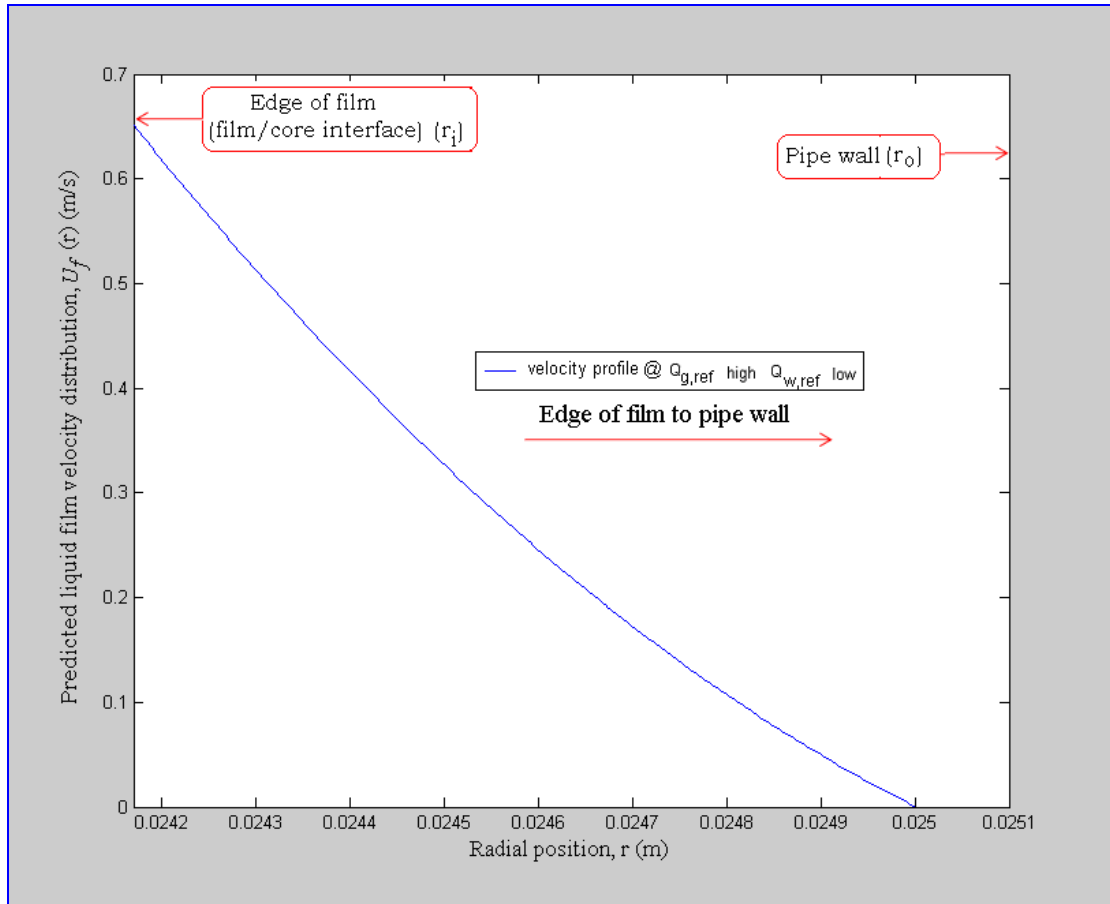


Figure 6.16 Film velocity profile for  $Q_{g,ref}$  high,  $Q_{w,ref}$  low

At this stage it is worth explaining the behaviour of each velocity distribution curve to understand the effect of the gas and liquid flow rates on the liquid film. To start it was useful to plot the distribution curves shown in Figures 6.13-6.16, together in Figure 6.17. Figure 6.17 shows the predicted velocity distribution plotted against non-dimensional distance  $r_{ND}$  from the edge of the liquid film ( $r_{ND} = 0$ ) to the pipe wall ( $r_{ND} = 1$ ).

At high water flow rates (green and turquoise curves in Figure 6.17) the liquid film struggles to build up its velocity i.e. film velocity is slower at small distances from the pipe wall. Close to the pipe wall the liquid film velocity distribution curve for the high water flow rates falls below that for the low water flow rates. This phenomenon helps explain the slower liquid film velocities with higher water flow rates visually observed at the wall.

At low water flow rates and with high gas flow rate, the liquid film velocity at the wall is higher (blue and red lines curves in Figure 6.17). Again this explains the visual observation of high liquid film velocities at the wall with high gas flow rate. It can be seen that with lower water flow rate and higher gas flow rate (red curve in Figure 6.17), the liquid film has higher velocities than the high gas and water flow rates (turquoise line).

These results agree with results and theoretical evaluations obtained by Moalem and Dukler (1984) and Karimi and Kawaji (2000).

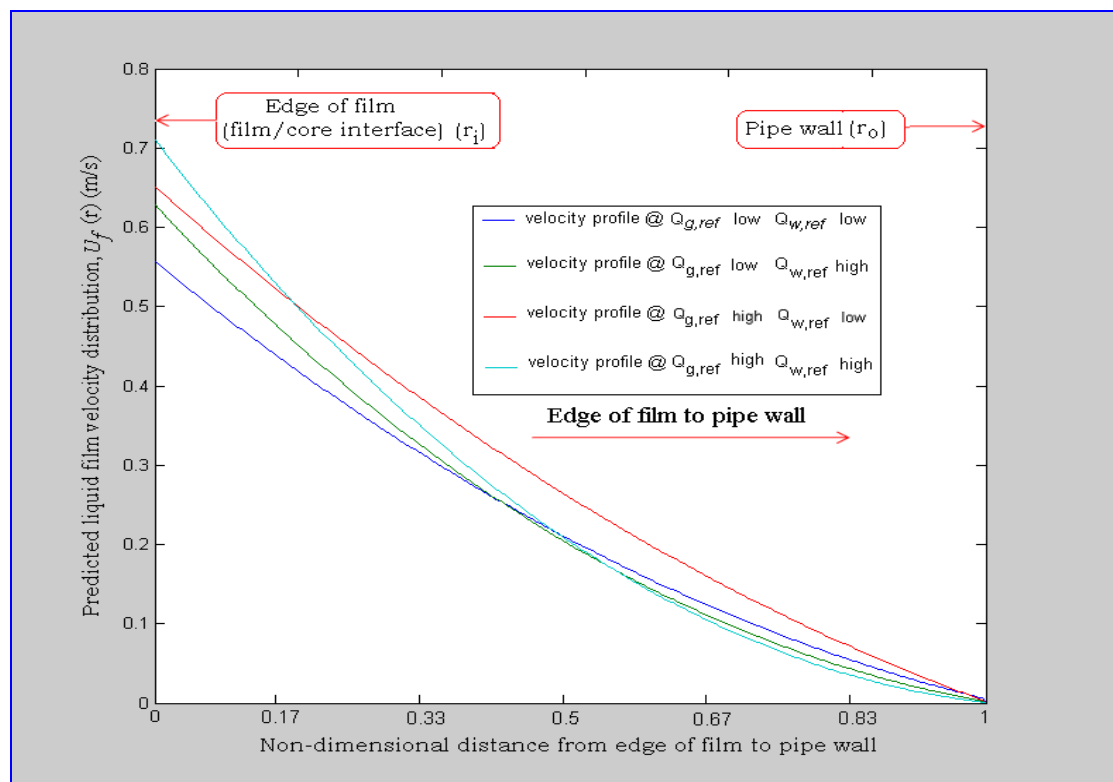


Figure 6.17 A comparison of liquid film radial velocity distribution profiles at different flow conditions

## 6.2 Entrainment

In annular flow the liquid in the film continuously enters the gas core in the form of droplets in a process called liquid entrainment, and the droplets in the gas core continuously deposit on the film in a process called droplet deposition. Knowledge of the entrainment fraction (defined as the water flow rate in the core as a proportion of

the total water flow rate, William et al., 2007) is essential for the development of a relation between entrainment and deposition rate.

Furthermore, the usefulness of the prediction of entrainment fraction is not limited only to the estimation of flow rate measurements but also for many general thermal hydraulic predictions such as how the pressure drop in annular flow can be significantly reduced (Wongwises and Pipathattakul, 2006).

In this study, being able to measure the liquid film thickness and the liquid film velocity meant that the entrainment fraction could be calculated as follows. If  $Q_f$  is the measured water flow rate in the film, then:

$$Q_f = U_f A_f \quad 6.21$$

where:  $U_f$  is the velocity of the fluid film obtained by cross-correlation and  $A_f$  is the cross-sectional area of the film  $= 2\pi R\delta$ ,

If  $Q_{w,c}$  is the water flow rate in the core, then:

$$Q_{w,c} = Q_{w,ref} - Q_f \quad 6.22$$

where:  $Q_f$  is the measured water flow rate in the film and  $Q_{w,ref}$  is the total reference water flow rate through the test section measured on the turbine meter, see Section 5.1.2.

So, the entrainment fraction  $E$  is given by:

$$E = \frac{Q_{w,c}}{Q_{w,c} + Q_f} = \frac{Q_{w,ref} - Q_f}{Q_{w,ref}} \quad 6.23$$

Equation 6.23 can be used with the obtained data to determine the entrainment fraction for the seventy flow conditions tested. Figure 6.18 shows the entrainment fraction variation with the water superficial velocity at different constant gas

superficial velocities. The figure shows two clear and obvious trends for the flow rates used.

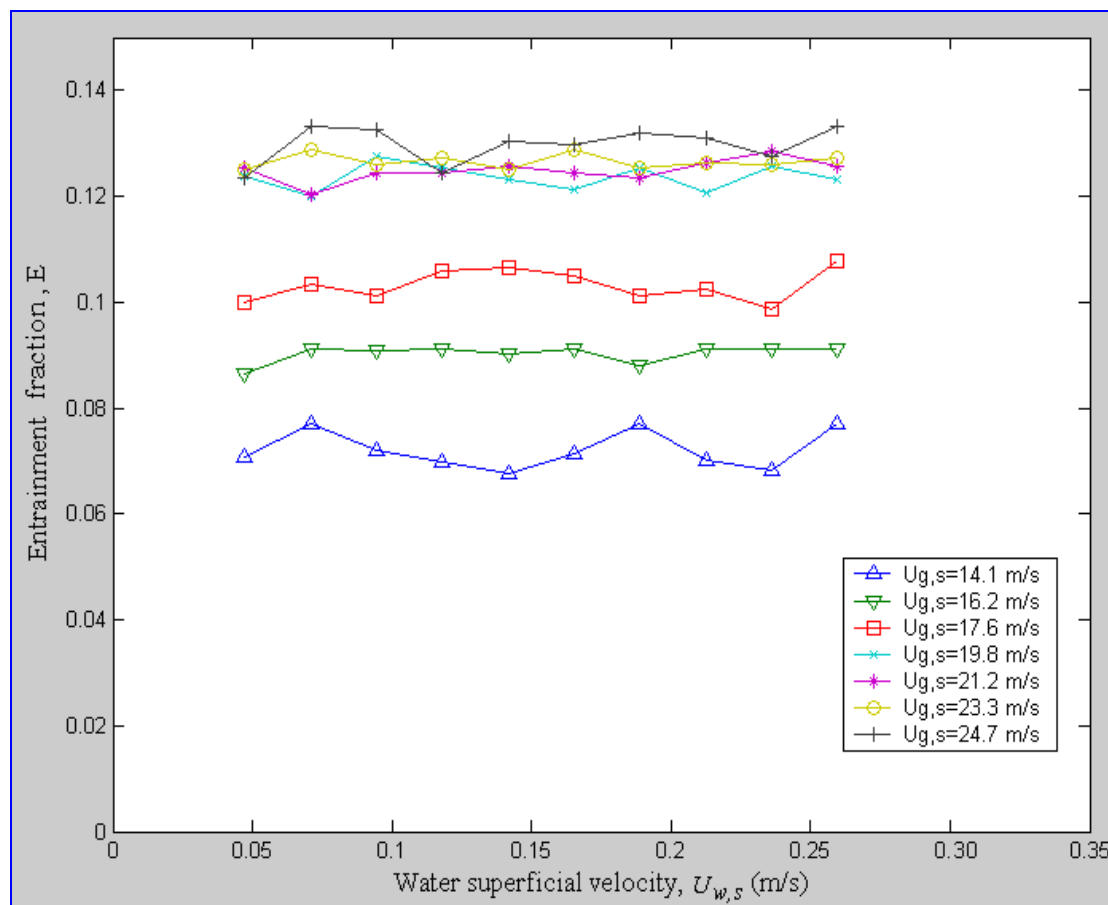


Figure 6.18 Effect of water superficial velocity on entrainment fraction at constant gas superficial velocity

First, the entrainment fraction remained more or less constant across the range of water superficial velocities tested, for constant gas superficial velocity. Second the entrainment fraction appeared to reach a limiting value of about 0.13 when the gas superficial velocity reached about 20m/s. At the lowest gas superficial velocity the average value of the entrainment fraction was 0.075 over the range of water flows used, see Figure 6.18.

Figure 6.19 shows the entrainment fraction plotted against the gas superficial velocity for different values of water superficial velocity. For all of the gas superficial velocities used the curves showed the same general shape. For constant water superficial velocity initially there was a more or less linear increase in the entrainment

fraction with increasing gas superficial velocity but when the gas superficial velocity reaches about 20m/s the value of the entrainment fraction levelled off at about 0.13. This was the maximum value for entrainment fraction for the annular flow of air and water obtained in the current investigation.

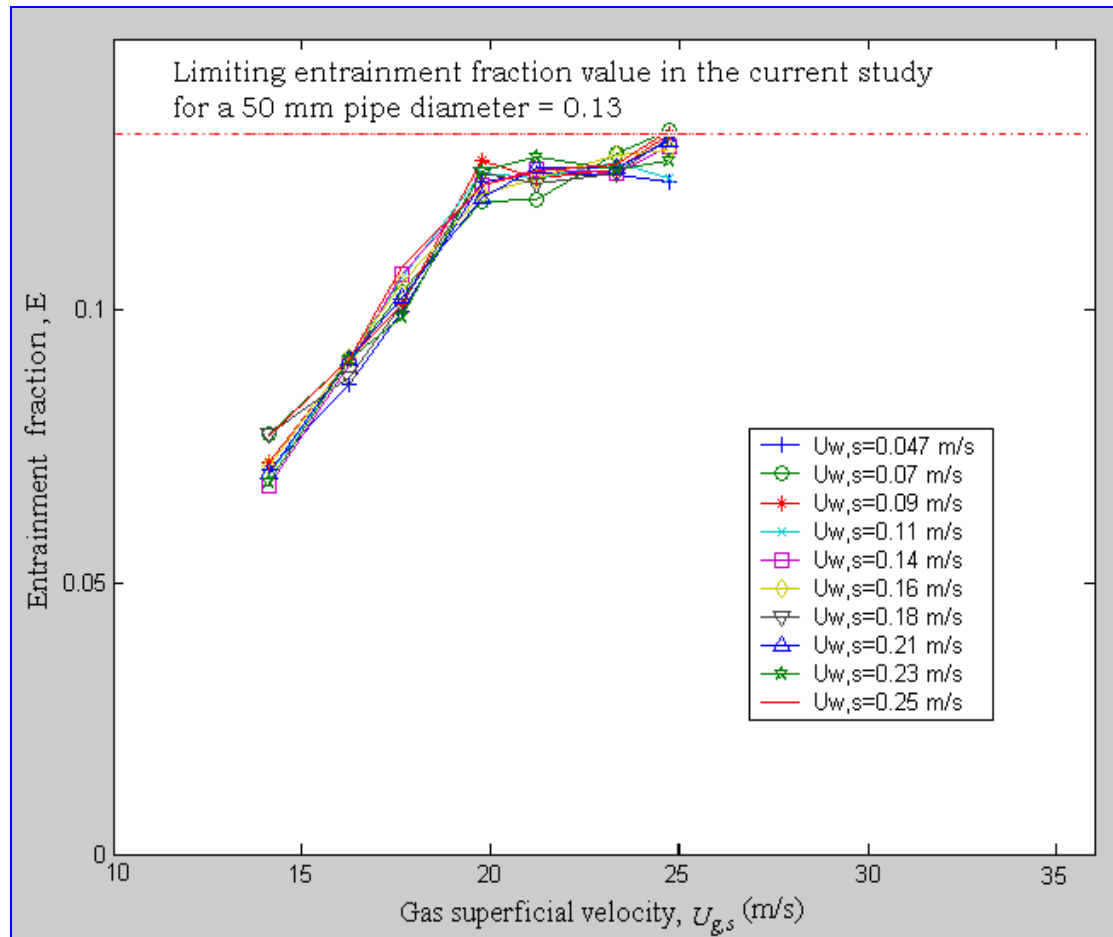


Figure 6.19 Effect of gas superficial velocity on entrainment fraction at constant water superficial velocity

Pan and Hanratty (2002) stated that the occurrence of a limiting value of the entrainment fraction  $E$  is dependent on the pipe diameter. The results shown on Figure 6.19 indicate that a correlation can be formulated for the entrainment fraction as a function of the gas superficial velocity, see Section 6.2.2.

### 6.2.1 Comparison of measured entrainment fraction with recent studies

Han (2005) and Pan and Hanratty (2002) who investigated annular air/water flows, followed a similar way of defining the entrainment fraction to that shown in Equation

6.23, and found a similar variation of entrainment as a function of the gas superficial velocity as that found in the present study. Unfortunately their test rigs had pipes of diameters only 9.5mm and 10mm.

Figure 6.20 (left and right plots) shows the entrainment fraction versus gas superficial velocity at different water Reynolds numbers given by Sawanta et al., (2008) and compared with Assad et al., (1998) (plot on left), and with Pan and Hanratty (2002) (plot on right).

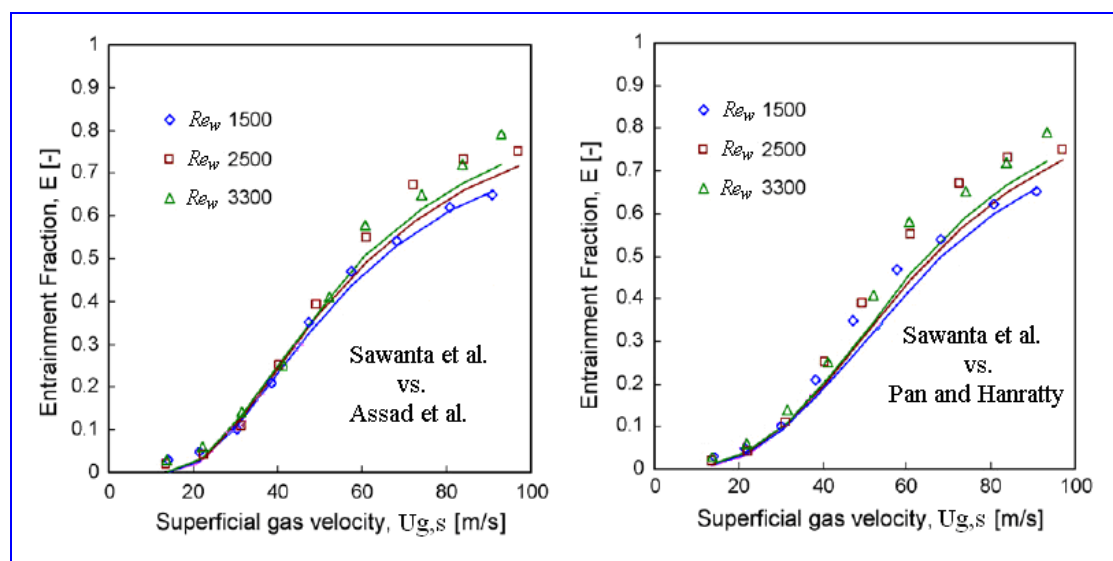


Figure 6.20 Entrainment fraction vs. gas superficial velocity at different water Reynolds numbers from Sawanta et al., (2008).

Regardless of the flow conditions and pipe diameters that had been used by Sawanta et al., the present work shows a similar trend of the entrainment fraction as a function of the gas superficial velocity. However, Sawanta et al. attributed this trend to the gas Froude number  $Fr_g$  which does depend on pipe diameter, but also on the gas superficial velocity, see Section 2.3.1.

Patruno et al., (2009) observed a similar trend in the variation of the entrainment fraction when plotted against the superficial gas velocity when comparing their simulation model with experimental data from Schadel (1990) using a pipe diameter of  $D=40.2$ mm. From all of these previous works by different researchers, it is apparent that the variation of the entrainment fraction with the gas superficial velocity

is similar in all cases. More importantly the CFM shows itself as a technique able to measure other annular flow parameters, namely entrainment fraction.

Zabaras and Dukler (1986) also investigated the entrainment fraction though their graphs plotted entrainment mass flow rate against the gas mass flow rate. For ease of comparison and the lack of information about the density of water being used by Zabararas and Dukler, the author reformulated his results so they could be plotted on the same graph as the findings of Zabaras and Dukler, see Figure 6.21.

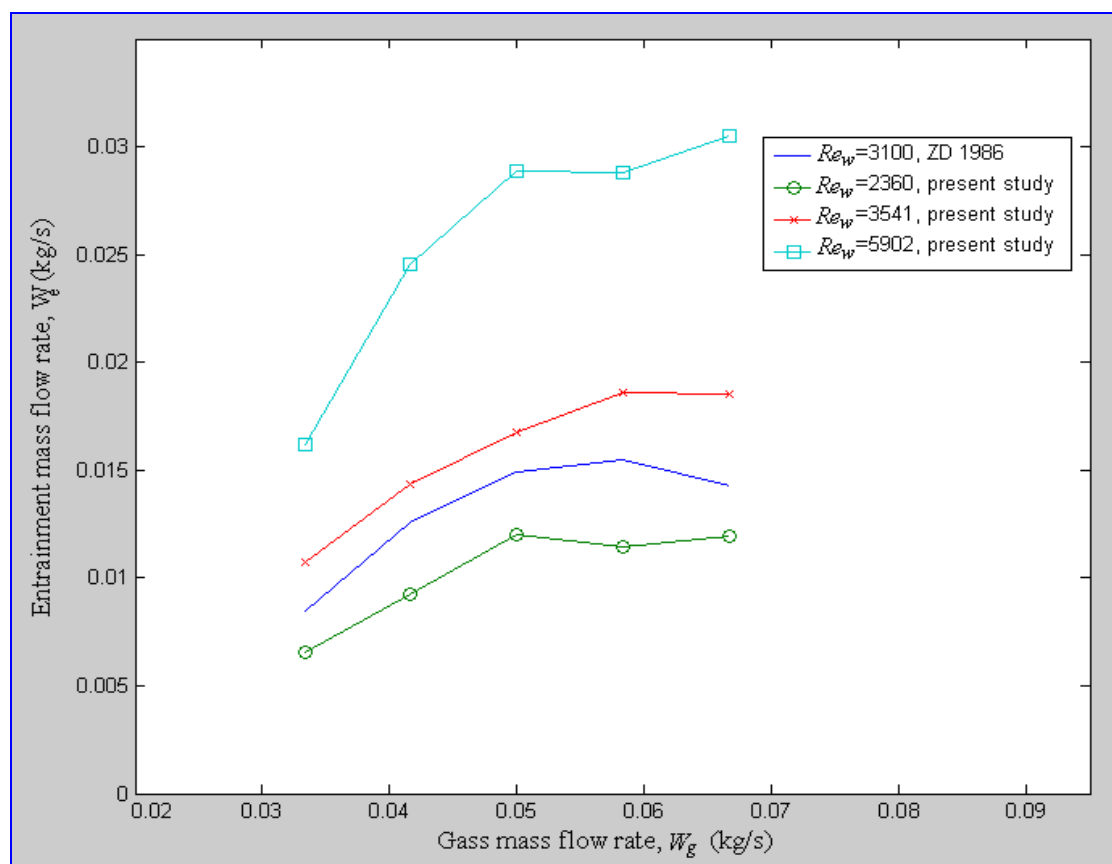


Figure 6.21 Comparison of entrainment rate when varying the gas flow rate with Zabaras and Dukler. (1986)

As the gas mass flow rate  $W_g$  increases, the entrainment mass flow rate  $W_e$  also increases until the dry out point (i.e. liquid film starts to thinning and breaking up) is approached. As discussed above this increase in the entrainment mass flow rate is more dependent on the gas flow rate more than the liquid flow rate. Figure 6.21 shows how the Zabaras and Dukler data fits with the present data. The Zabaras and Dukler data for  $Re_w=3100$  lies between the present data for  $Re_w=2360$  and  $Re_w=3541$ . Also,

Zabaras and Dukler data shows same general increase in the entrainment mass flow rate with the gas mass flow rate as the present data at fixed water Reynolds number.

Table 6.5 summaries available results in the literature for the entrainment fraction  $E$  for annular flow in pipes with reasonably similar diameters to the pipe diameter  $D$  used in the present study i.e. 50mm. The obtained range of entrainment fraction in this study fits nicely between the ranges of the entrainment fraction cited in the literature. However, the tabulated experiments do not show a defined trend in the values of the entrainment fraction in regard to the pipe diameter. This drives the author to conclude that the entrainment fraction is more likely to be affected by the flow properties and conditions.

<b>Author</b>	<b>Fluids</b>	<b>Pipe ID (mm)</b>	<b><math>E</math></b>
<b>Owen et al.</b>	air-water	31.8	0.17-0.38
<b>Asali</b>	air-water	42	0-0.38
<b><i>Present study</i></b>	<i>air-water</i>	<i>50</i>	<i>0.075-0.13</i>
<b>Zabaras and Dukler</b>	air-water	50.8	0.01-0.16
<b>Pan &amp; Hanratty</b>	air-water	57.2	0.3-0.7

*Table 6.5 Summary of some experiments on entrainment fraction*

Once again this comparison suggests that the CFM device was measuring the liquid film velocity because measuring the surface wave velocity on the film would have resulted in values of entrainment fraction  $E$  grossly different from those found in the literature.

### 6.2.2 Development of an entrainment fraction correlation

By referring back to Figure 6.19, it was concluded that the entrainment fraction is dependent on the gas superficial velocity. In Figure 6.22 values for entrainment fraction (which are the average values of the entrainment fraction at each gas superficial velocity in Figure 6.19) are plotted against gas superficial velocity and a least squares fit programme has been used to produce a cubic equation to fit the data,

Equation 6.24. This equation expresses the entrainment fraction as a function of the gas superficial velocity.

$$E_{est} = -2.8e^{-5} U_{g,s}^3 + 0.001 U_{g,s}^2 - 0.002 U_{g,s} - 0.027 \quad 6.24$$

where:  $E_{est}$  is estimated entrainment fraction and  $U_{g,s}$  is the known gas superficial velocity.

Equation 6.24 is considered to be a good correlation of the entrainment fraction as a function of the gas superficial velocity for the experimental conditions in the present study.

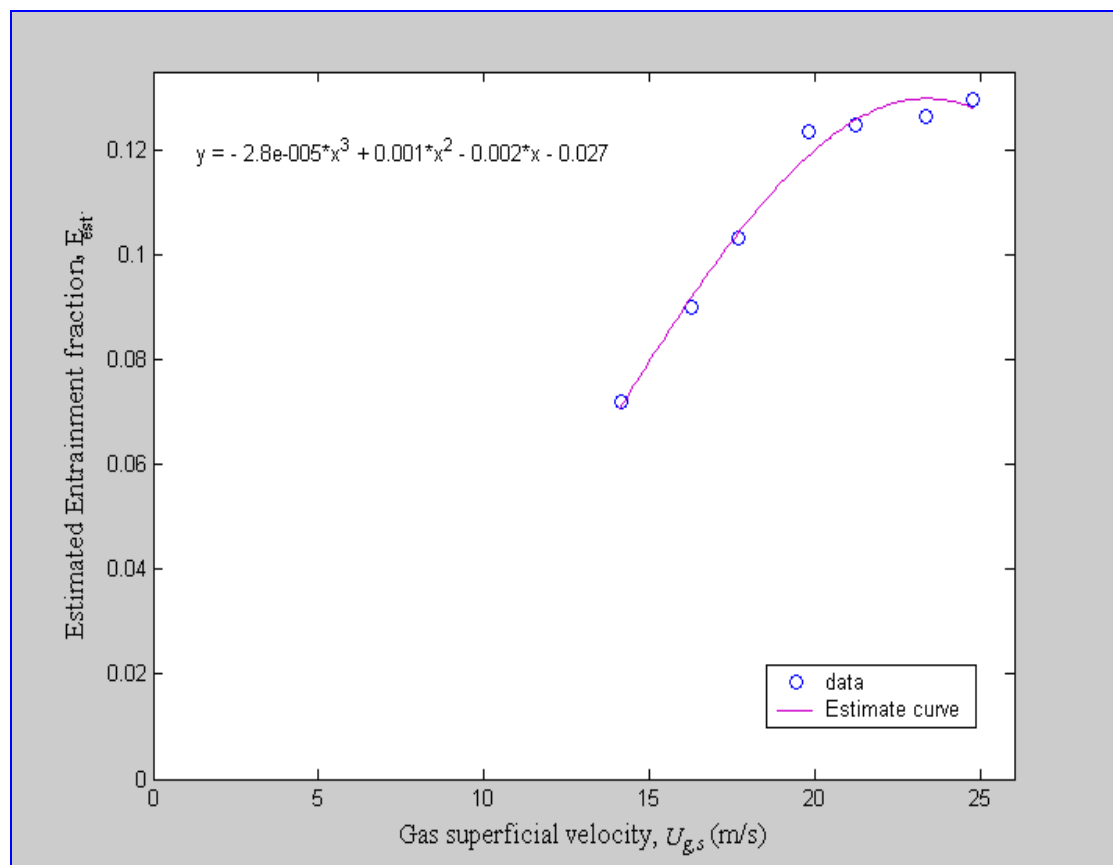


Figure 6.22 Estimated entrainment fraction as a function of the gas superficial velocity (pipe ID = 50mm)

The vital importance of this correlation is presented in Section 6.6.1 where it is used to estimate the water flow rate in the pipe. This estimated value of the water flow rate was then compared to the reference water flow rate to enable calculation of the percentage error in the measured water flow rate which enabled the accuracy of the CFM as a flow measurement technique to be evaluated.

### 6.3 Prediction of the liquid film thickness from film velocity and entrainment data

The author was able to predict the liquid film thickness from the analysis of the liquid film velocity and the entrainment data presented in Sections 6.1.2 and 6.2.2 respectively. The prediction is based on the fact that both the liquid film velocity and the entrainment fraction are functions of the superficial gas velocity. This can be understood from the following set of equations:

$$Q_{w,ref} = Q_f + Q_{w,c} \quad 6.25$$

where:  $Q_{w,ref}$  is the reference water flow rate,  $Q_f$  is the film flow rate and  $Q_{w,c}$  is the entrained water flow rate in the core.

$$Q_{w,ref} = 2\pi R\delta U_f + Q_{w,c} \quad 6.26$$

$$\therefore \delta = \frac{Q_{w,ref} - Q_{w,c}}{2\pi R U_f} \quad 6.27$$

where:  $R$  is the pipe radius,  $U_f$  is the liquid film velocity and  $\delta$  is the liquid film thickness.

In Equation 6.27,  $Q_{w,c}$  is obtained as an estimated value which is defined by Equation 6.24. Where,  $U_f$  is known from Figure 6.9 at any given gas superficial velocity at a constant water superficial velocity. So, for convenient notations Equation 6.27 can be re-written as:

$$\therefore \delta_{est} = \frac{Q_{w,ref} - Q_{w,c,est}}{2\pi R U_{f,est}} \quad 6.28$$

where: the subscript 'est' indicates an estimated value.

The values of liquid film thickness predicted from Equation 6.28 are plotted against the measured liquid film thickness values from the CFM probes in Figure 6.23. The result shows that the prediction method is very good with higher water superficial velocities. However, at lower water superficial velocities the results seem to drift slightly away from the rest of the data. In general, there is a remarkable degree of agreement between the two quantities and the conclusion must be that prediction method presented by the present study can successfully predict the liquid film thickness if both the gas superficial velocity and liquid film velocity are both well known at certain water superficial velocities, at least for the 50mm ID pipe.

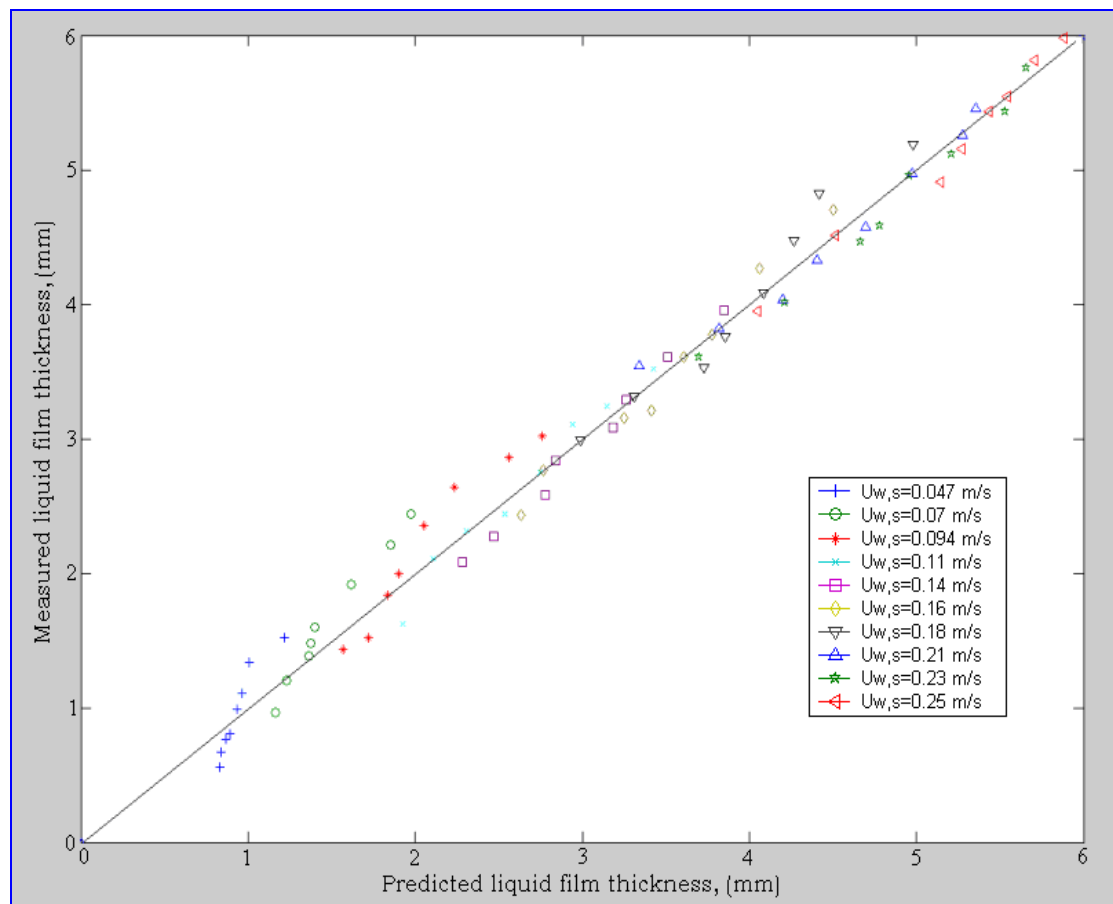


Figure 6.23 Comparison of measured and predicted liquid film thickness

#### 6.4 Volume fraction

To accurately predict the phase velocities and mixture properties requires a good knowledge of the volume fraction, see Figure 6.24. The gas volume fraction of a gas-

liquid flow is defined as the ratio of the volume of gas to the total volume of the gas-liquid mixture in a finite length of the pipeline.

The volume fraction of each phase is an important quantity in measuring and predicting the average density, pressure drop, flow pattern, etc. of a flowing gas-liquid mixture in a pipe. By knowing the volume fraction and the velocity of each flowing phase one can estimate the mass flow rate of each phase.

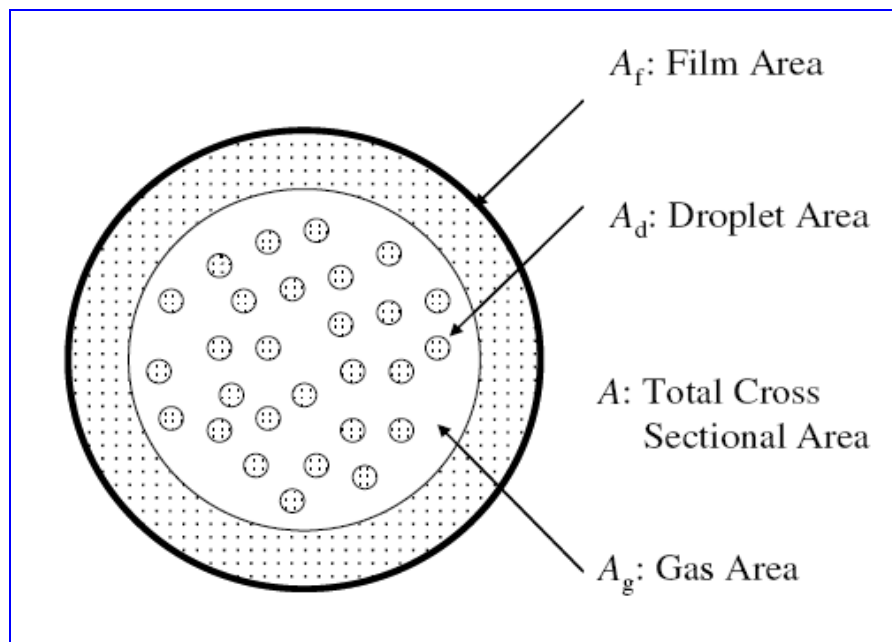


Figure 6.24 Schematic of flow phases distribution in annular flow

#### 6.4.1 Volume fraction of water film ( $\alpha_{w,f}$ )

The volume fraction of the water film  $\alpha_{w,f}$  is given by Equation 6.29, and is defined as the ratio of the cross-sectional area of the film to the total cross-sectional area of the pipe:

$$\alpha_{w,f} = \frac{A_f}{A} \quad 6.29$$

where:  $\alpha_{w,f}$  is the volume fraction of the liquid film,  $A_f$  is the area of the liquid film and  $A$  is the total cross-sectional area of the pipe.

The liquid film thickness was measured by the CFM, so knowing the radius of the pipe (25mm) it is possible to calculate the water film volume fraction:

$$\alpha_{w,f} = \frac{\pi R^2 - \pi(R - \delta)^2}{\pi R^2}$$

$$\alpha_{w,f} = \frac{\pi R^2 - \pi(R^2 - 2R\delta + \delta^2)}{\pi R^2}$$

$$\alpha_{w,f} = \frac{\pi(2R\delta + \delta^2)}{\pi R^2} \tag{6.30}$$

But since  $\delta \ll R$ :

$$\alpha_{w,f} \cong \frac{2\delta}{R} \tag{6.31}$$

$$\delta = \left(\frac{R}{2}\right) \alpha_{w,f} \tag{6.32}$$

where:  $\delta$  is the thickness of the liquid film and  $R$  is the radius of the pipe.

By inspection, Figures 6.25 and 6.26 appear very similar to Figures 6.5 and 6.6 for the film thickness, see Section 6.1.1.2. This is because the liquid film thickness is directly proportional to its volume fraction, the constant of proportionality being  $(R/2)$ , see Equation 3.32. Figure 6.25 emphasises the fact that increasing the gas superficial velocity increases the velocity of the film, see Section 6.1.1.2. This can be concluded from the decreasing volume fraction of the water in the film.

In Figure 6.26, it's clear that the volume fraction of the water film increased with increase of the water superficial velocity.

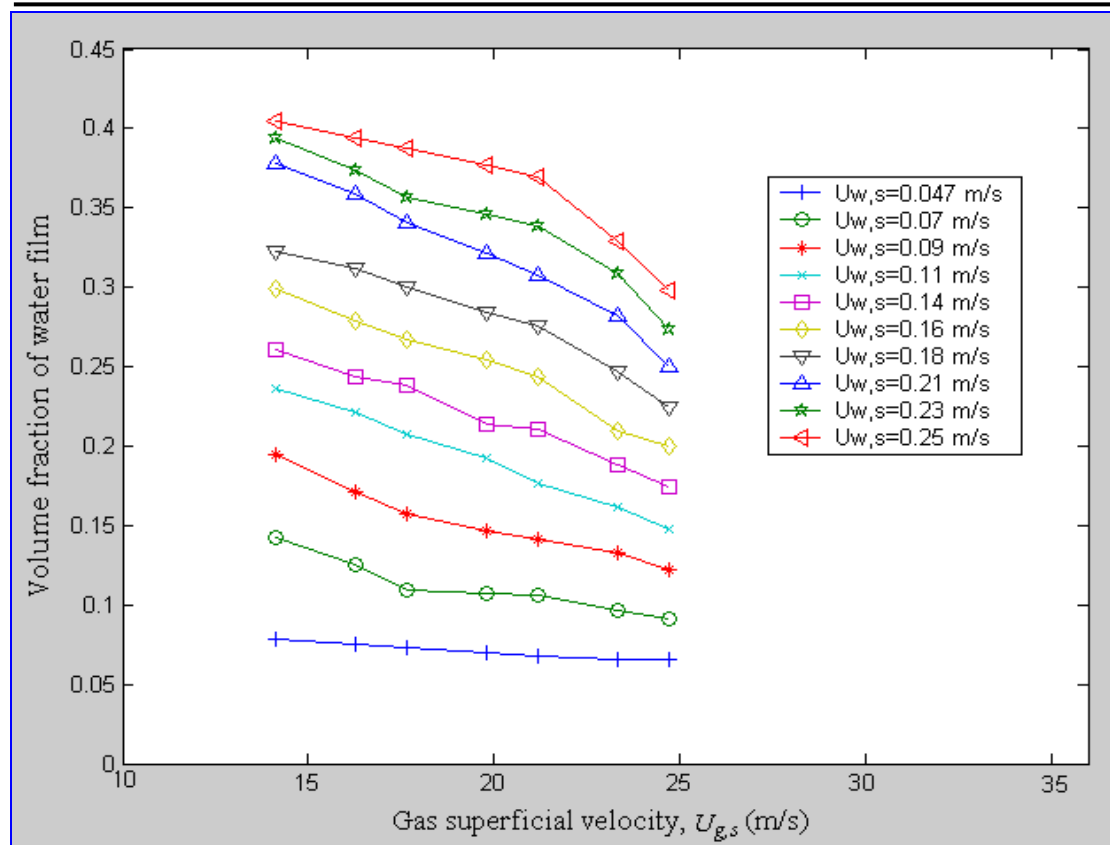


Figure 6.25 Effect of gas superficial velocity on volume fraction of water film at different water superficial velocities

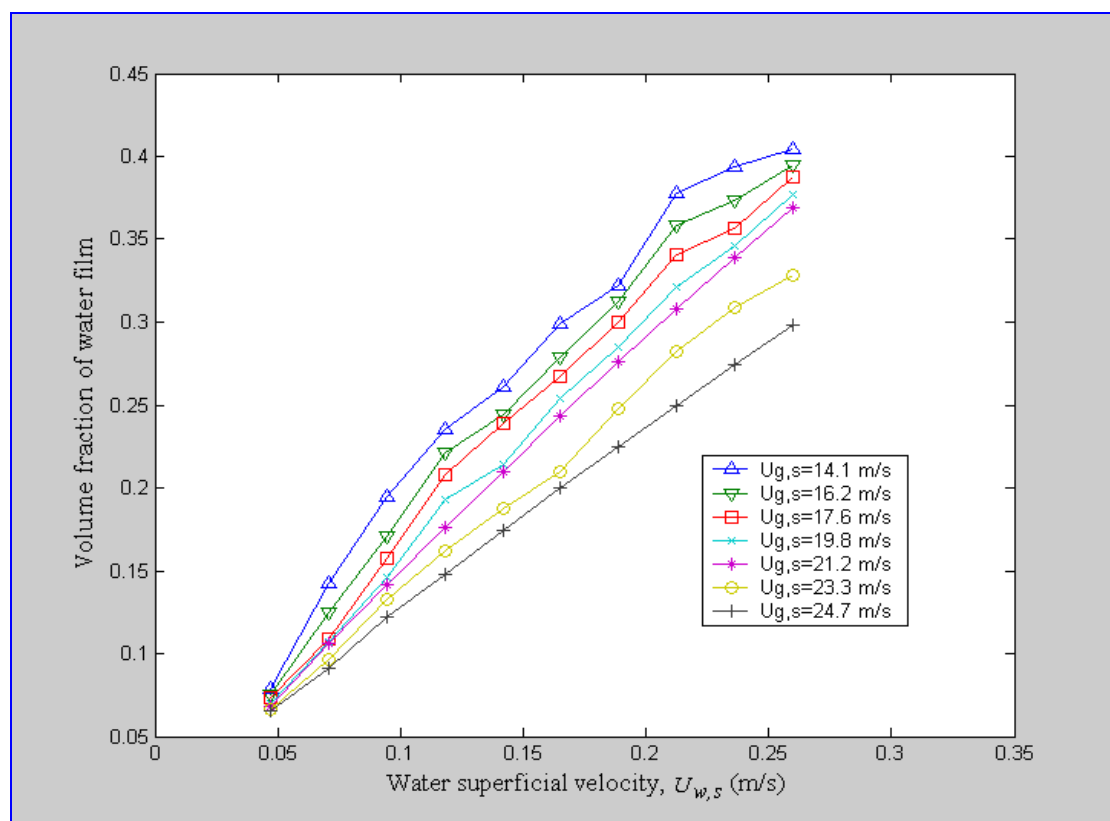


Figure 6.26 Effect of water superficial velocity on volume fraction of water film at different gas superficial velocities

The measurements indicate maximum and minimum water volume fraction values of 0.404 and 0.065 in the present study. The author can conclude, using Equation 6.32, from the previously mentioned work of Zabaras and Dukler that they have achieved volume fraction of water film between a maximum and minimum of 0.11 and 0.015 respectively. However, the larger water film volume fractions found in the present study are due to the high water Reynolds number  $Re_w$  with a minimum value of 2360 and maximum of 13000. Where with Zabaras and Dukler the maximum of  $Re_w$  was set at 3100 and the minimum value of  $Re_w$  was of 300.

#### 6.4.2 Volume fraction of entrained water droplets ( $\alpha_{w,c}$ )

The volume fraction of the entrained water droplets  $\alpha_{w,c}$  is given by Equation 6.33, and is defined as the ratio of the cross-sectional area of the entrained water droplets to the total cross-sectional area of the pipe:

$$\alpha_{w,c} = \frac{A_{w,c}}{A} \quad 6.33$$

From the entrainment fraction equation:

$$Q_{w,c} = \frac{E Q_f}{(1 - E)} \quad 6.34$$

where:  $Q_{w,c}$  is the water flow rate in the core,  $E$  is the entrainment fraction and  $Q_f$  is the water film flow rate.

Because the entrained droplets are very small (Nigmatulin et al., 1996), they are likely to be travelling at close to the gas velocity. The water volume fraction in the core,  $\alpha_{w,c}$ , is given by Equation 6.33, which is based on the assumption that the entrained droplets are moving with the same gas axial velocity as the gas, i.e.  $U_{w,c} = U_{g,c}$ , so we can say:

$$Q_{w,c} = A_{w,c} U_{g,c} \quad 6.35$$

where:  $U_{w,c}$  is the velocity of water in the core and  $A_{w,c}$  is the equivalent cross-sectional area of the water in the core.

From Equations 6.34 and 6.35:

$$A_{w,c} U_{g,c} = \frac{E Q_f}{(1-E)} \quad 6.36$$

$$\alpha_{w,c} = \frac{1}{A} \left( \frac{E}{1-E} \right) \frac{Q_f}{U_{g,c}} \quad 6.37$$

where:  $\alpha_{w,c}$  is the water volume fraction in the core,  $E$  is the entrainment fraction,  $Q_f$  is the liquid film flow rate,  $U_{g,c}$  is the gas core velocity and  $A$  is the pipe cross-sectional area.

Using Equation 6.37 with measured values of the entrainment fraction  $E$  (see Section 6.2), film flow rate  $Q_f$  and gas core velocity  $U_{g,c}$  (see Section 6.5), the water volume fraction in the core  $\alpha_{w,c}$  is shown for the experimental conditions of the present study in Figures 6.27 and 6.28. The results presented in Figures 6.27 and 6.28 show an increase in the water volume fraction in the core with increasing water superficial velocity then a levelling off, similar to Figure 6.19. Some fluctuations are seen after the water volume fraction in the core has levelled off but this is likely to be due to random fluctuations or experimental errors.

Similar behaviour is seen in Figure 6.28 with the water volume fraction in the core  $\alpha_{w,c}$  increasing with superficial water velocity up to a maximum value. The maximum and minimum recorded values for water volume fractions in the core are  $9.2 \times 10^{-4}$  and  $2.1 \times 10^{-4}$  respectively compared with maximum and minimum water volume fraction  $\alpha_{w,f}$  values of 0.404 and 0.065 in the present study. These values seem to be reasonable when they are compared to the entrainment rates of 0.13 and 0.075 obtained in Section 6.2. However, here we observe a new phenomenon. The water volume fraction in the core remains approximately constant as the gas superficial velocity increases but there appears to be a definite maximum in water volume fraction in the core  $\alpha_{w,c}$  at a superficial gas velocity of about 20m/s, see Figure 6.28.

Note also that the water volume fraction in the core, see Figure 6.28, does not vary greatly with gas superficial velocity. It is much more dependent upon the water superficial velocity. This is unlike the entrainment rate  $E$ , which is much more dependent upon the gas superficial velocity. This indicates that the flow rate of liquid droplets in the core is predominantly dependent upon the velocity of the core rather than the liquid volume fraction in the core.

The available data in the Zabaras and Dukler (1986) work indicates that a large amount of the water is being entrained into the gas core. Using their data in Equation 6.37 revealed that the entrained water droplets volume fraction varied between  $9.6 \times 10^{-3}$  and  $7.3 \times 10^{-4}$ . The range of the gas superficial velocities being used by Zabaras and Dukler extended up to 37m/s whereas the current investigation was set at a maximum of 25m/s.

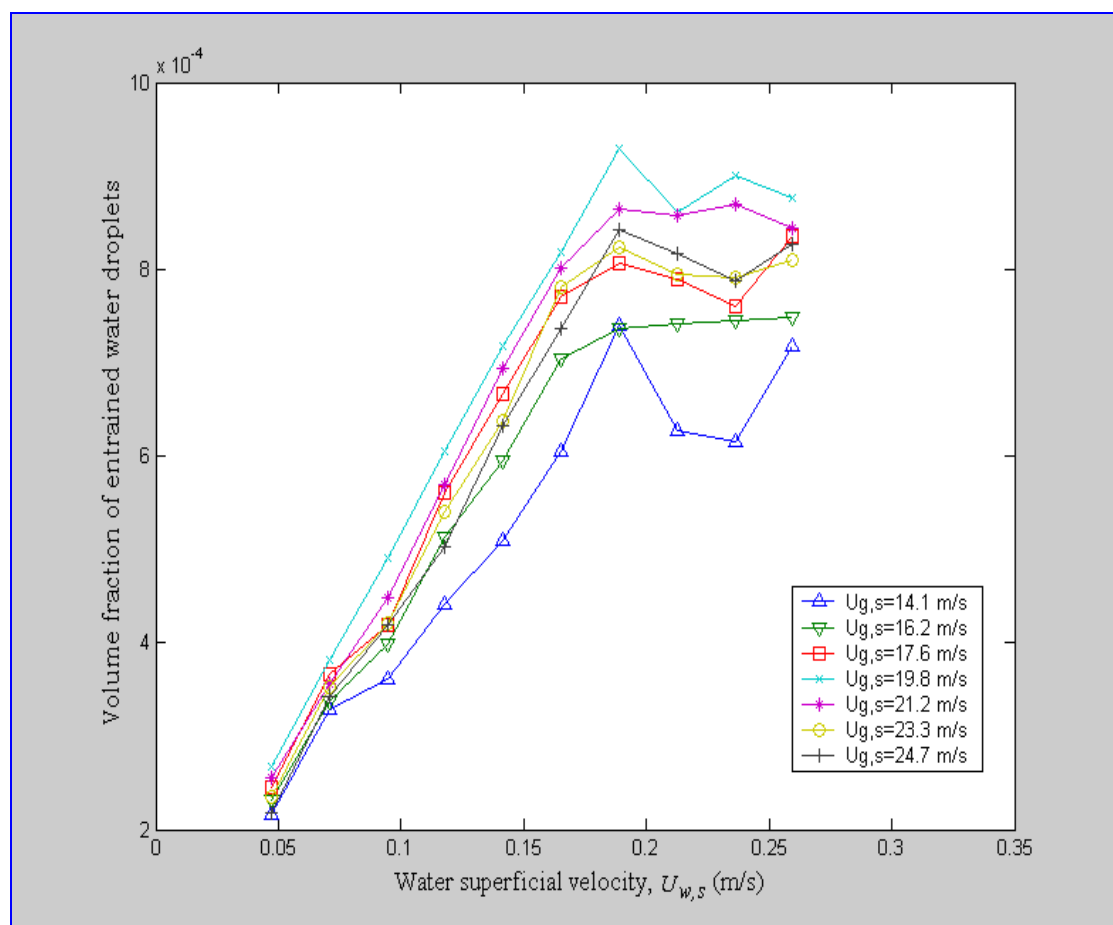


Figure 6.27 Effect of water superficial velocity on volume fraction of entrained water droplets at different gas superficial velocities

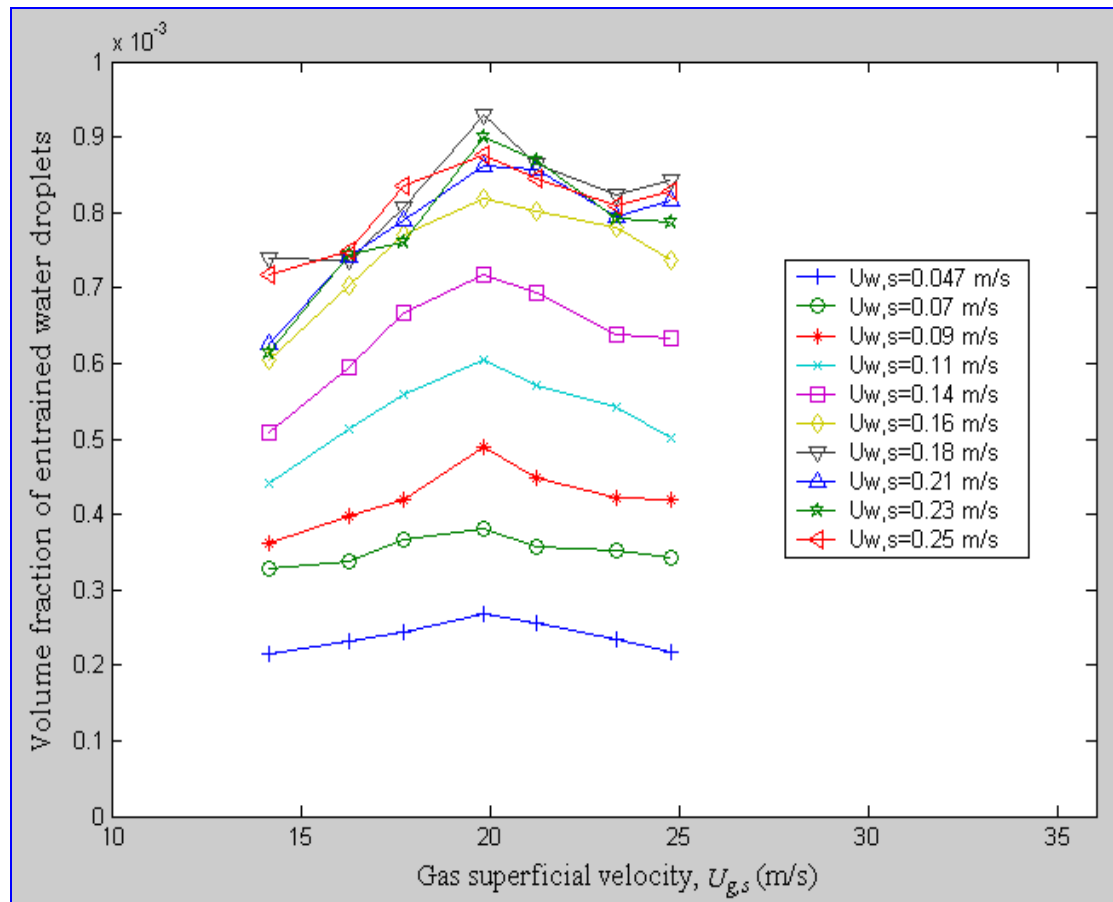


Figure 6.28 Effect of gas superficial velocity on volume fraction of entrained water droplets at different water superficial velocities

### 6.4.3 Total water volume fraction ( $\alpha_{w,tot}$ )

The overall volume fraction of the water in the pipe  $\alpha_{w,tot}$  was obtained by simply summing the volume fraction of entrained water droplets  $\alpha_{w,c}$  and the volume fraction of the water film  $\alpha_{w,f}$ . The results, see Figures 6.29 and 6.30 show the variation of the total volume fraction of water with water and gas superficial velocities respectively. The results indicate that the maximum and minimum total volume fraction values obtained in this study are 0.405 and 0.065 respectively.

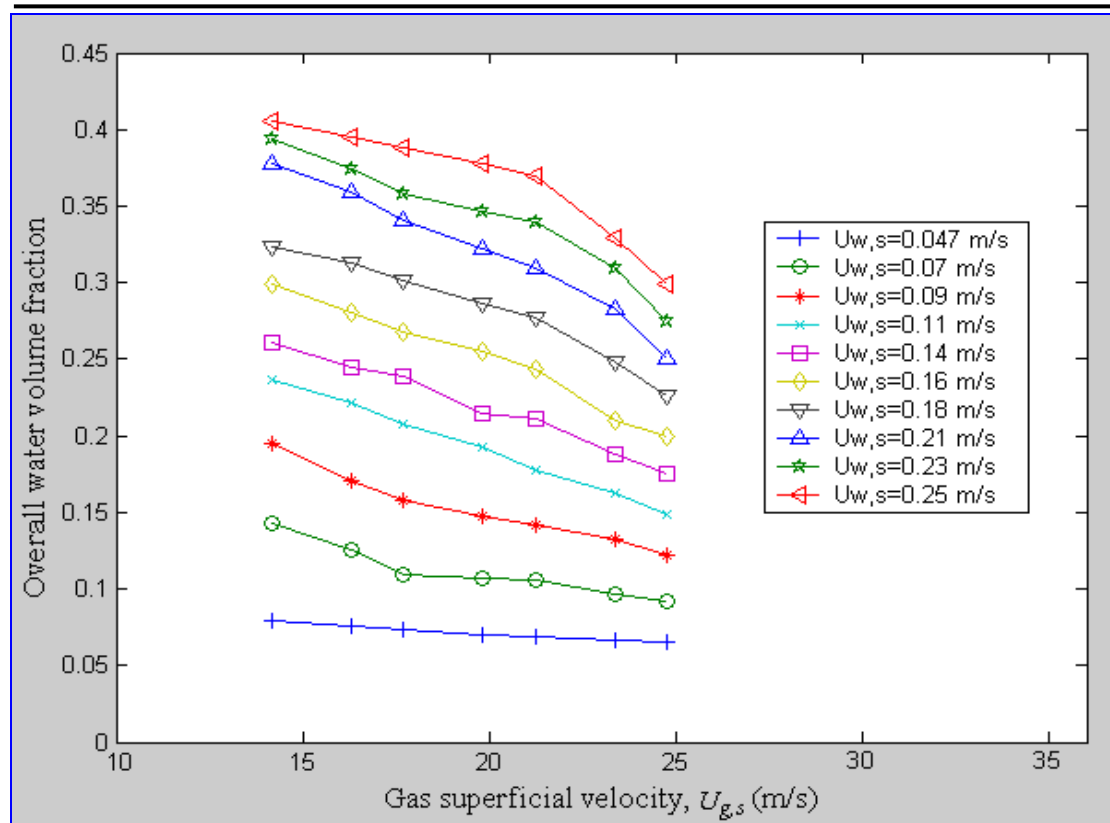


Figure 6.29 Effect of gas superficial velocity on overall water volume fraction at different water superficial velocities

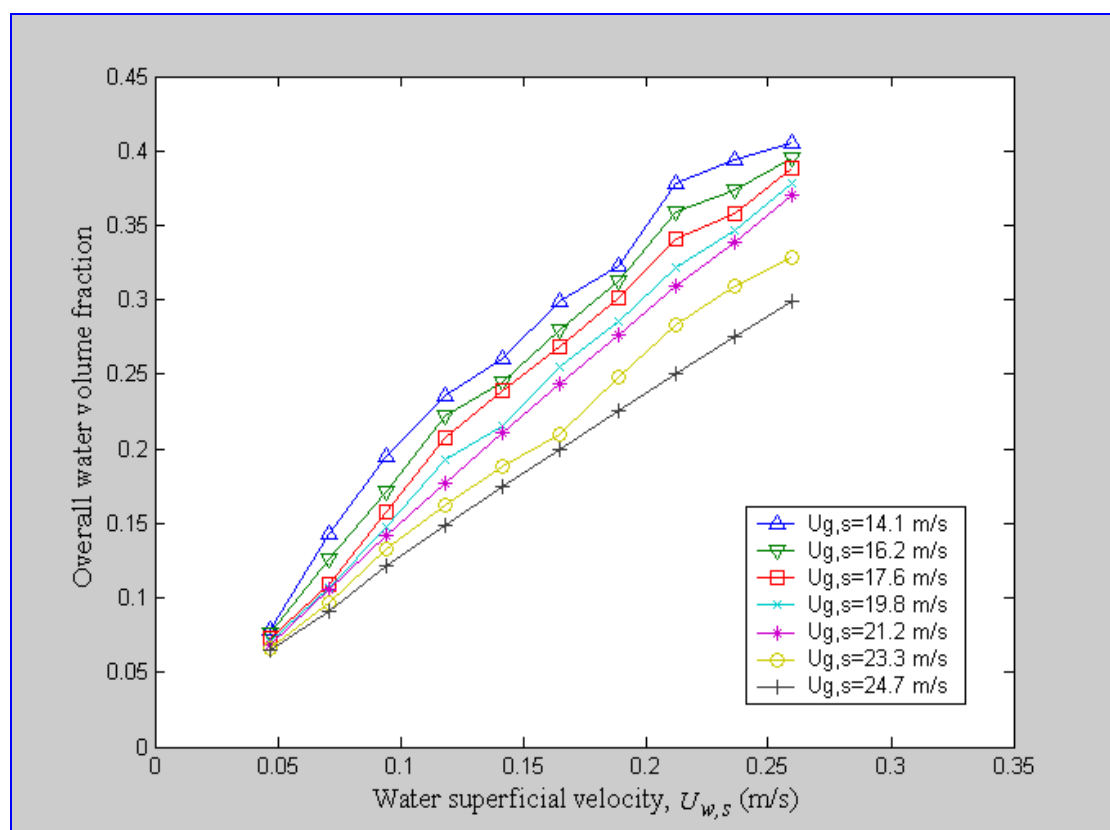


Figure 6.30 Effect of water superficial velocity on overall water volume fraction at different gas superficial velocities

#### 6.4.4 Gas volume fraction ( $\alpha_{g,c}$ )

Since the flow in the test rig comprised only water and gas, the gas volume fraction is simply given by:

$$\alpha_{g,c} = 1 - \alpha_{w,c} - \alpha_{w,f} \quad 6.38$$

where:  $\alpha_{g,c}$  is the gas volume fraction,  $\alpha_{w,f}$  is the volume fraction of the liquid in the film and  $\alpha_{w,c}$  is the volume fraction of entrained water droplets.

Graphs of gas volume fraction versus water and gas superficial velocity are shown in Figures 6.31 and 6.32 respectively. Inspecting the figures, it can be concluded that, as expected, they show the results of the total water volume fraction in the pipe. As the water superficial velocity increases i.e. water volume fraction increases, the gas volume fraction decreases. This observation can be attributed to the increased liquid film thickness.

The film thickness increases with the water flow rate and so water occupies a larger fraction of the cross-sectional area of the pipe, so less area is available to the gas. The reverse effect happens when the gas superficial velocity is increased. The gas shears off parts of the liquid film and also causes liquid film to travel faster, see below, resulting in an increase in the area occupied by the gas.

As mentioned above, the film velocity was also found to increase with the increase in gas superficial velocity, see Section 6.1.2.2. This also caused the liquid film thickness to reduce for a given water flow rate (i.e. not all the film thickness reduction may be due to increased entrainment). The maximum and minimum gas volume fraction values that they have been observed in this study are 0.935 and 0.595 respectively. Calculation show that Zabarás and Dukler (1986) established annular flow with larger gas volume fractions of 0.98 and 0.88, maximum and minimum values respectively.

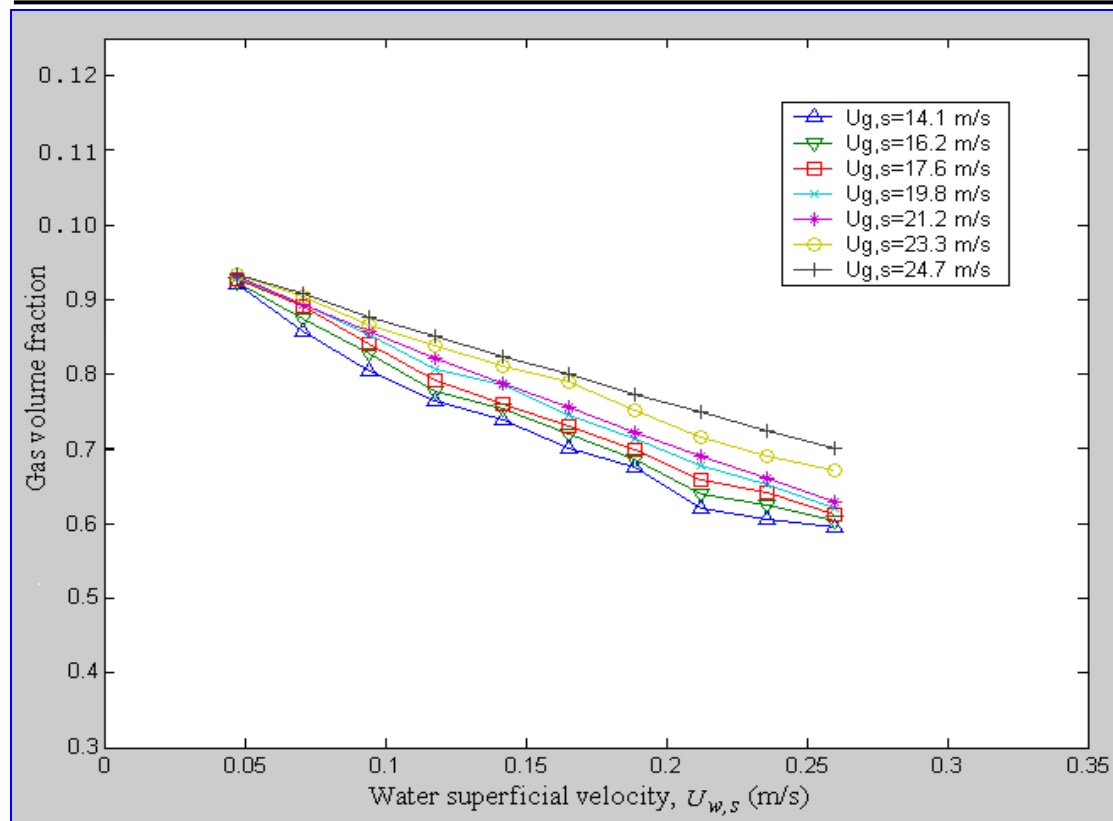


Figure 6.31 Effect of water superficial velocity on gas volume fraction at constant gas superficial velocity

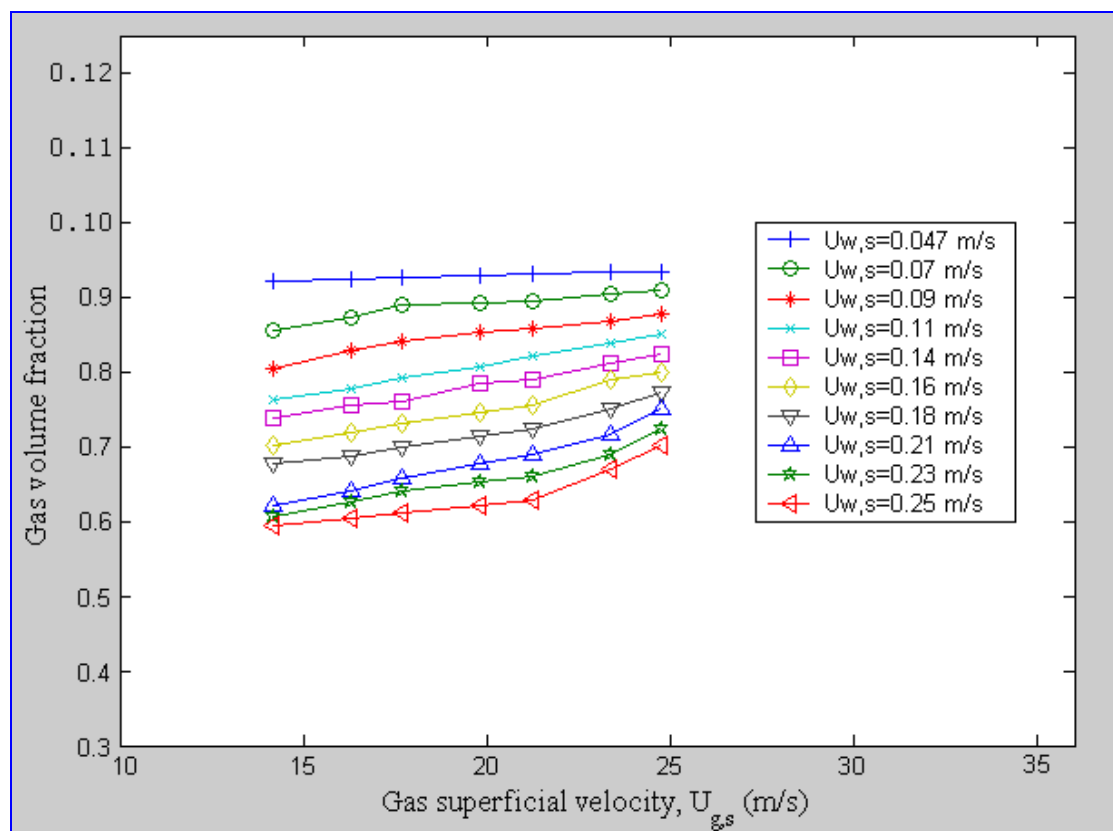


Figure 6.32 Effect of gas superficial velocity on gas volume fraction at constant water superficial velocity

The above gas and water volume fraction measurements in the present study confirm the accuracy of the CFM device since the volume fraction measurements were based on the measurement of the liquid film thickness. The values of water and gas volume fraction obtained in this study are well within the range of the range of values reported in the literature (Wada et al., 2006).

## 6.5 Gas core velocity

### 6.5.1 USFM accuracy in measuring gas core velocity

Prior to carrying out any analysis of the USFM results, it was essential to determine how accurate the USFM device was in measuring the core gas velocity. A reference gas velocity  $U_{g,ref}$  was obtained from:

$$U_{g,c,ref} = \frac{Q_{g,ref}}{A_g} = \frac{Q_{g,ref}}{\frac{\pi}{4}(D - \delta)^2} \quad 6.39$$

where:  $Q_{g,c,ref}$  is the gas flow rate read from the VAFM (see Section 5.1.1),  $A_g$  is the cross-sectional area of the gas core (which does not take into account the cross-sectional area occupied by droplets in the gas core) and  $D$  is the pipe diameter.

The measured value of the core gas velocity  $U_{g,c}$  were obtained from the USFM calibration equation, see Equation 4.27 in Section 4.3.5:

$$U_{g,c} = \frac{1}{\hat{c}} \cos^{-1} \left( \frac{V_{out} - \hat{b}}{\hat{a}} \right) \quad 6.40$$

where:  $\hat{a} = 0.5604$ ,  $\hat{b} = 8.0283$  and  $\hat{c} = 13.26$ .

From  $U_{g,c,ref}$  and  $U_{g,c}$ , a percentage error in the measured gas core velocity  $\xi_{g,c,vel}$  could be calculated:

$$\xi_{g,c,vel} = \frac{U_{g,c} - U_{g,c,ref}}{U_{g,c,ref}} \times 100\% \quad 6.41$$

For annular two phase flow and for a range of values of water superficial velocity  $U_{w,s}$  (between 0.047m/s and 0.141m/s) and range of values of gas superficial velocities  $U_{g,s}$  (between 14.1m/s and 21.2m/s), Figure 6.31 shows the percentage error in the measured gas core velocity  $\xi_{g,c,vel}$  plotted against the reference gas core velocity  $U_{g,c,ref}$ . The calculation indicates a small percentage error of average value of 1.2% with a standard deviation of 0.43. This result encouraged further investigations related to the core gas velocity.

However, it was essential to see the effect of the presence of the water droplets in the gas core on the accuracy of the USFM i.e. causing the core velocity to be overestimated by the USFM. This was done by taking the area of the droplet in the core into the calculation of the reference value of the gas flow rate in the core. Hence, Equation 6.39 can be adjusted to give:

$$U_{g,c,ref,d} = \frac{Q_{g,ref}}{A_{g,d}} \quad 6.42$$

where:  $U_{g,c,ref,d}$  is the new value for the reference gas velocity in the core and  $A_{g,d}$  is the cross-sectional area of the gas core taking the entrained droplet area into account and defined by:

$$A_{g,d} = A(1 - \alpha_{w,c} - \alpha_{w,f}) \quad 6.43$$

where:  $\alpha_{w,c}$  is the volume fraction of entrained water defined by Equation 6.37 and  $\alpha_{w,f}$  is the volume fraction of water film defined by Equation 6.29.

Figure 6.33 shows the new percentage error calculation in the measured gas core velocity. The errors settle to a mean percentage error of 0.85% with a standard deviation of about 0.43. Introducing the area of the entrained droplets has reduced the mean percentage error in the measured gas velocity from 1.2% to 0.85%.

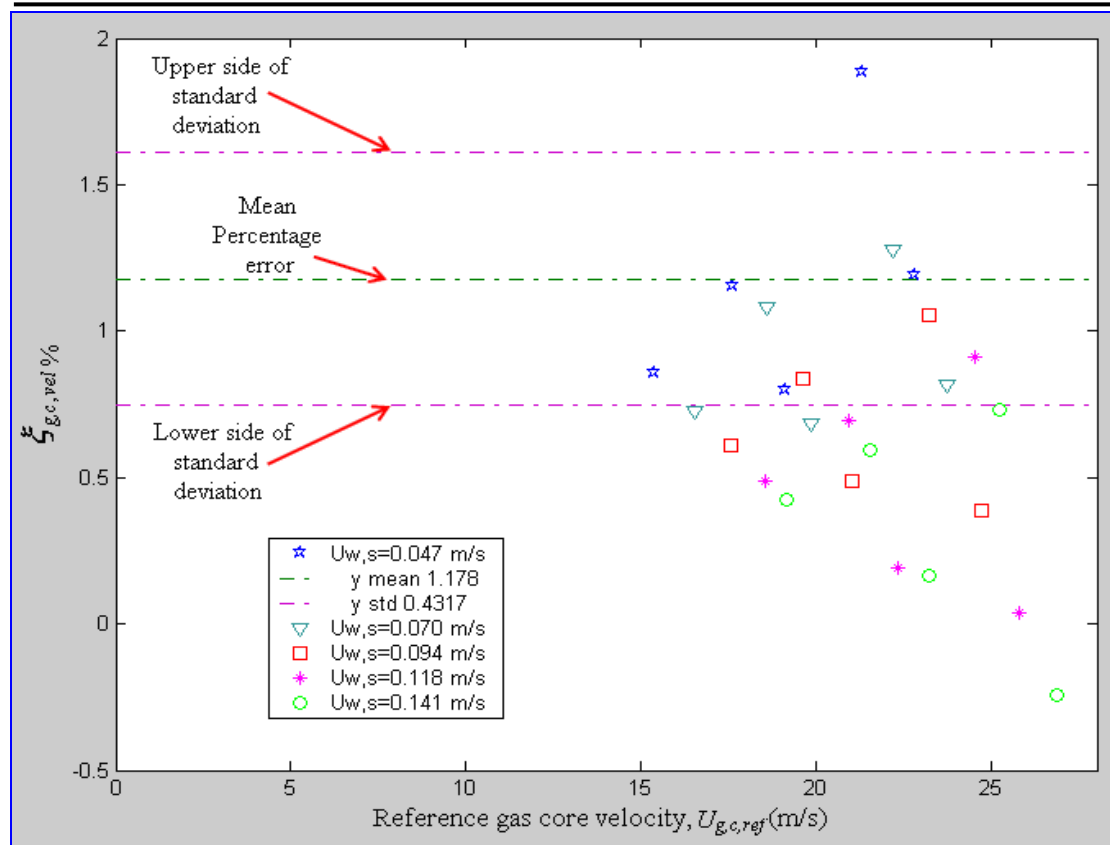


Figure 6.33 Percentage error in measured gas core velocity at different constant water superficial velocities

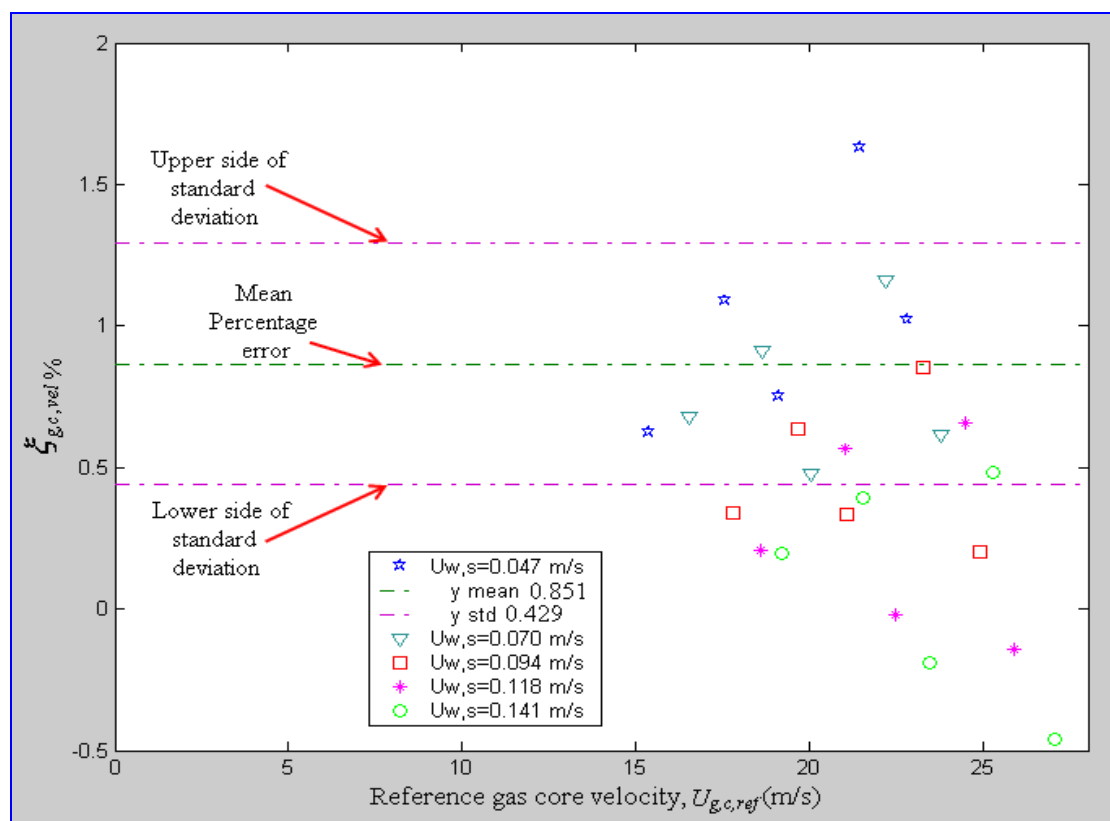


Figure 6.34 Percentage error in measured gas core velocity at different water superficial velocities

The accuracy achieved by the USFM was taken to indicate that the gas velocity measurements were not affected by the disturbance caused by the transducers protruding through the liquid film. In this study the maximum and minimum recorded values of gas core velocities were 26.8m/s and 15.4m/s respectively, see Figures 6.37 and 6.38.

### 6.5.2 Measuring core gas velocity using USFM

From the basic flow rate equation  $Q = U * A$ , the volume flow rate is controlled by the velocity of the flow and the cross-sectional area of the flowing medium. If the volume flow rate is to be kept constant then the cross-sectional area and the flow velocity must change in an inverse proportion. In our case, the cross-sectional area of the gas was affected by the liquid film thickness. Hence, it was of interest to investigate how the film thickness affects the core gas velocity. This will widen our knowledge of how such changes affect flow rate measurement of vertical upward annular flows.

#### 6.5.2.1 Effect of gas and liquid superficial velocities on core gas velocity

Because the variation of the output voltage of the USFM with the velocity of gas has the form of a cosine function, see Section 3.3.4, it is possible to obtain the same output voltage value for different gas velocities. Thus it was necessary to be careful in choosing the range of the gas flow rates for which the USFM could be used, see Section 3.3.4. The number of the flow conditions in the present study for which the USFM could be unambiguously used was twenty five (five water flow rates and five gas flow rates).

The results from the experiments on the effect of the gas superficial velocity on the gas core velocity are shown in Figure 6.35. The gas core velocity increases linearly with increasing gas superficial velocity, at a constant water flow rate. With the gas flow rate kept constant and by increasing the water flow rate, the relationship between the water superficial velocity and the core gas velocity was investigated, see Figure 6.36. The increase in the core gas velocity with increasing water flow rate is predictable. This is due to the increase in the film thickness for a constant gas flow

rate; hence the gas core area is getting smaller forcing the gas flow to travel faster to maintain the same flow rate.

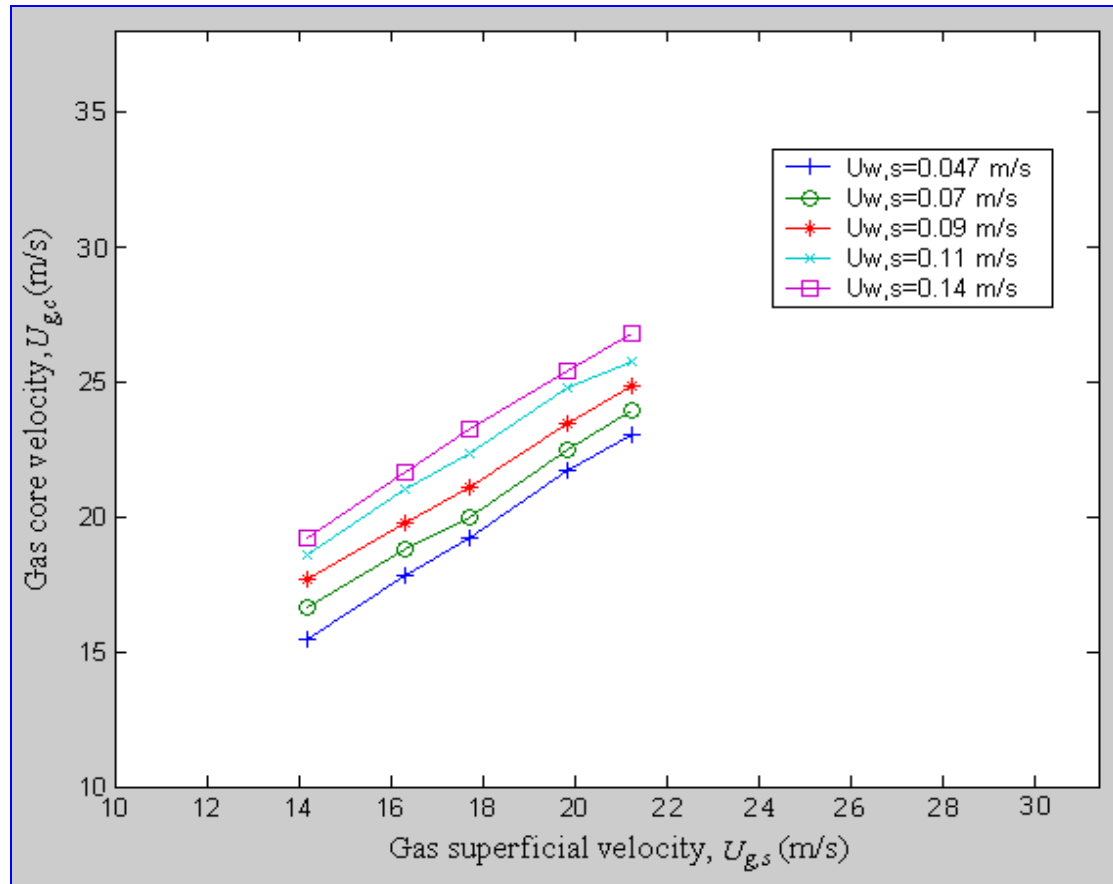


Figure 6.35 Effect of gas superficial velocity on gas core velocity at different water superficial velocities

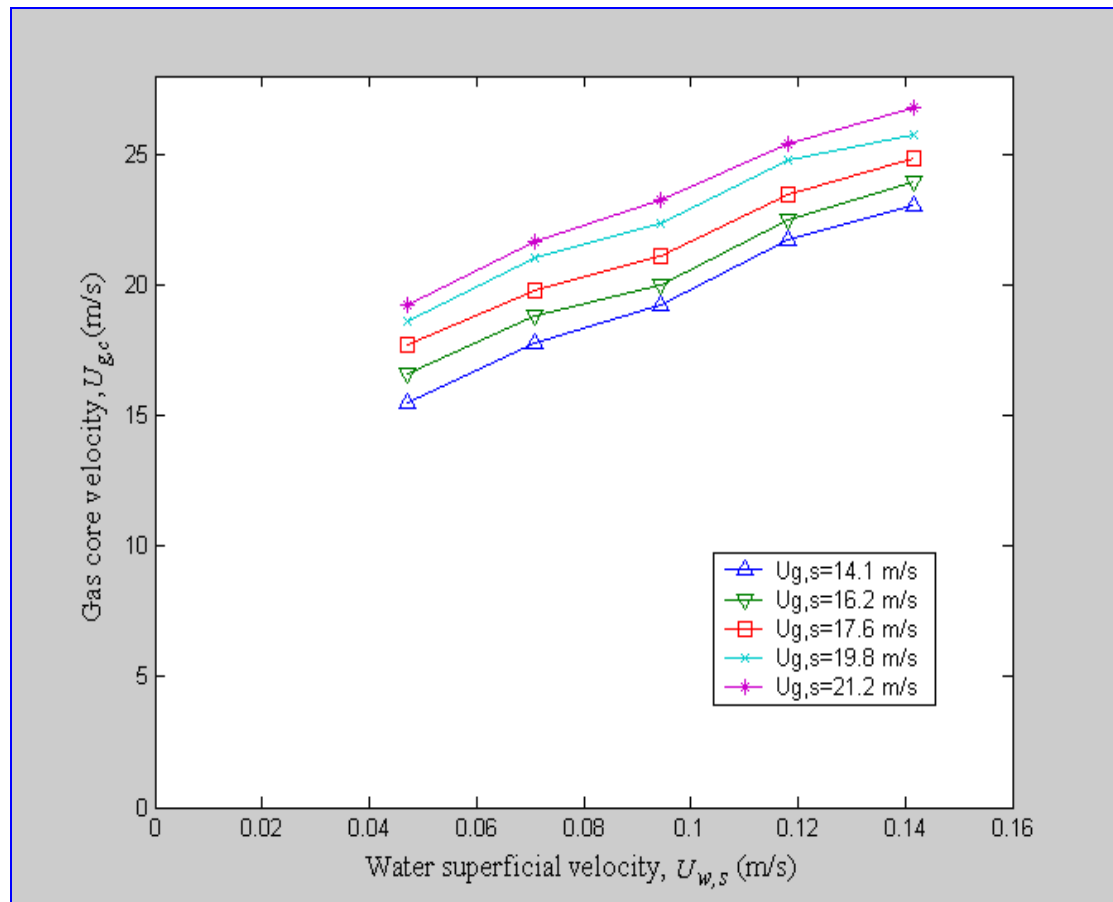


Figure 6.36 Effect of water superficial velocity on gas core velocity at different gas superficial velocities

### 6.5.2.2 Relationship between the gas core velocity and liquid film thickness

The main reason for carrying out this part of the investigation was to validate the performance of the USFM. In this section both the film thickness  $\delta$  and the gas core velocity  $U_{g,c}$  were monitored while the gas and liquid flow rates were varied, see Figures 6.37 and 6.38. Results shown in Figure 6.37 agree with the expectation of an inverse relationship between area of the core and the gas core velocity in the basic flow rate equation. For a constant gas volume flow rate (as indicated by the VAFM), as the water flow rate increased the liquid film thickness increased resulting in a decrease in the gas cross-sectional area and an increase in the core gas velocity (measured by the USFM).

As the gas flow rate increased at constant water flow rate, the liquid film thickness decreased, see Figure 6.38. The larger the water volume flow rate the greater was the decrease in film thickness.

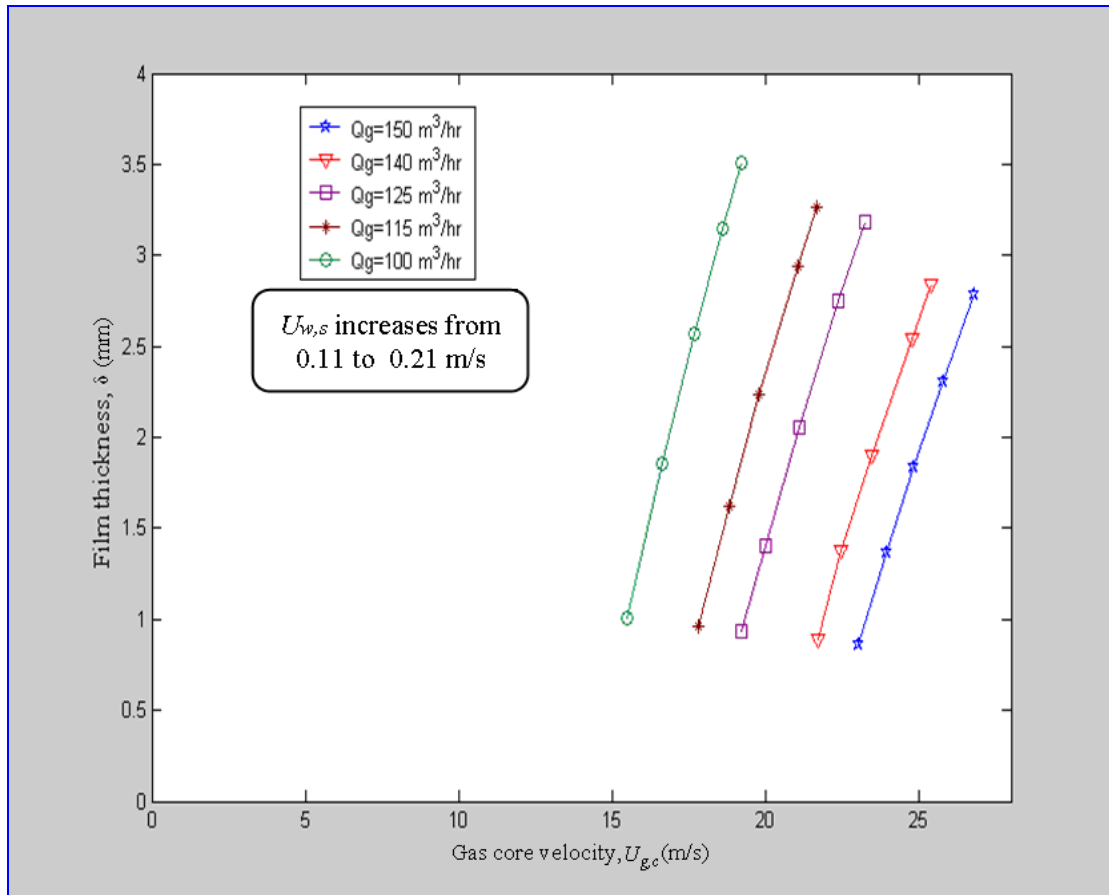


Figure 6.37 of water flow rate on core gas velocity and film thickness at different gas flow rates

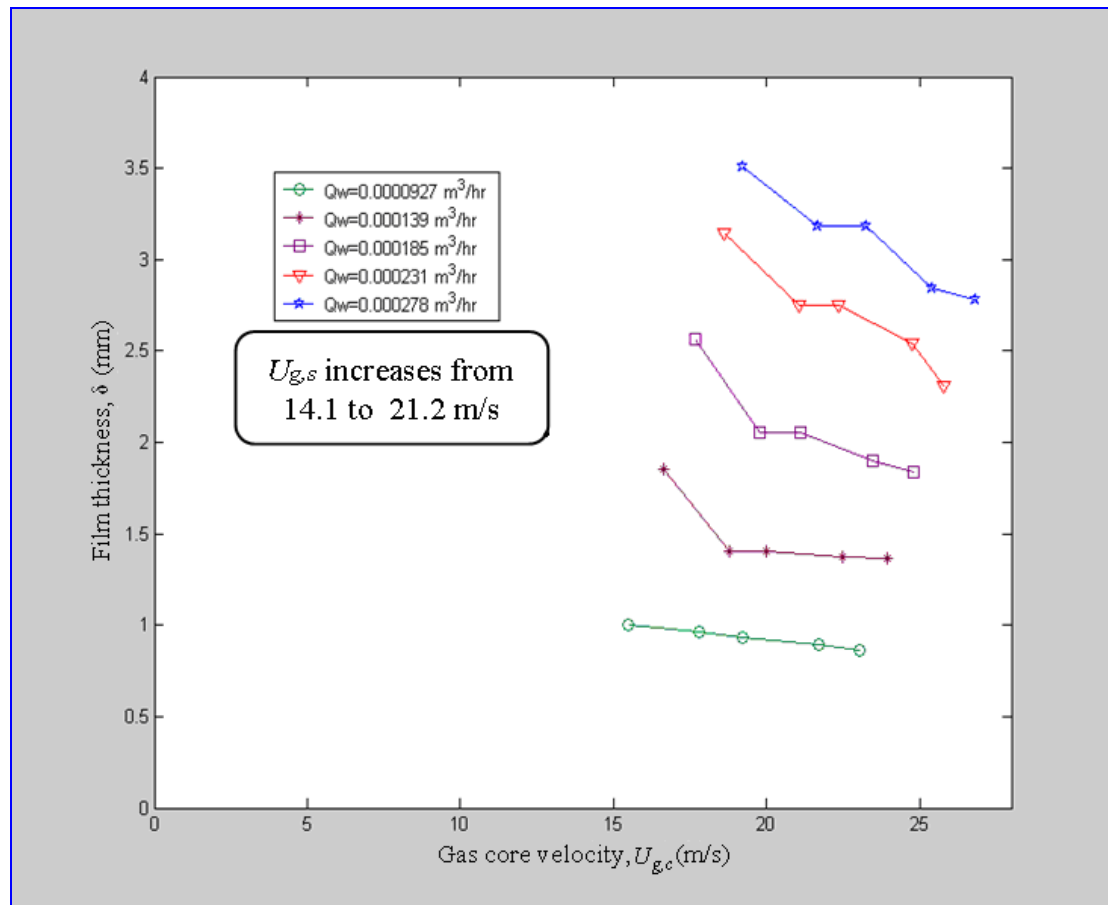


Figure 6.38 Effect of gas flow rate on core gas velocity and film thickness at different water flow rates

## 6.6 Comparison of reference and measured flow rates

The results previously obtained in this chapter are used in this section to examine the accuracy of the combined CFM and USFM system for measuring the water and gas flow rates. Errors are further assessed in the next chapter, see Section 7.4.

### 6.6.1 Water flow rate ( $Q_w$ )

It was shown earlier that Equation 6.24 can be used to estimate the entrainment fraction  $E_{est}$  if the gas superficial velocity is known, see Section 6.2.2. If  $Q_f$  is found using the CFM then  $E_{est}$  can be used to provide an estimate of the liquid volumetric flow rate in the core  $Q_{w,c,est}$ . Provided the gas superficial velocity in the core is known, see Section 6.2.2, this can give an estimated value for the water flow rate  $Q_{w,est}$  in the pipe.

The process for estimating the total water flow rate  $Q_{w,est}$  in the pipe is as follows; knowing  $U_{g,s}$  from the USFM measurement,  $E_{est}$  is estimated from the entrainment fraction correlation:

$$E_{est} = -2.8e^{-5} U_{g,s}^3 + 0.001 U_{g,s}^2 - 0.002 U_{g,s} - 0.027 \quad 6.44$$

Then, having found the water flow rate in the film,  $Q_f$ , by measuring the film thickness and film velocity measurements using the CFM (see Section 6.1),  $E_{est}$  is used to estimate liquid volumetric flow rate  $Q_{w,c,est}$  in the core.

$$Q_{w,c,est} = \left( \frac{E_{est}}{1 - E_{est}} \right) Q_f \quad 6.45$$

The estimated value for the total water flow rate in the pipe  $Q_{w,est}$  is:

$$Q_{w,est} = Q_{w,c,est} + Q_f = \frac{Q_f}{(1 - E_{est})} \quad 6.46$$

where:  $Q_{w,est}$  is the estimated total water flow rate in the pipe,  $Q_{w,c,est}$  is the entrained water flow rate and  $Q_f$  is the liquid film flow rate.

Using the reference water flow rate  $Q_{w,ref}$  obtained from the turbine flow meter, the percentage error in the estimated water flow rate estimated  $\xi_w$  using the method given in Equations 6.44-6.46 above can be calculated as:

$$\xi_w = \frac{Q_{w,est} - Q_{w,ref}}{Q_{w,ref}} \times 100\% \quad 6.47$$

Figure 6.39 shows how the estimated errors in the measured water flow rate vary with reference water flow rate at constant reference gas flow rates. The estimated errors in the water flow rate appear to be scattered randomly between a maximum positive value of +7.4% and a maximum negative value of -7.0%. However, the mean error is -1.1% with a standard deviation of +3.8% from the mean value.

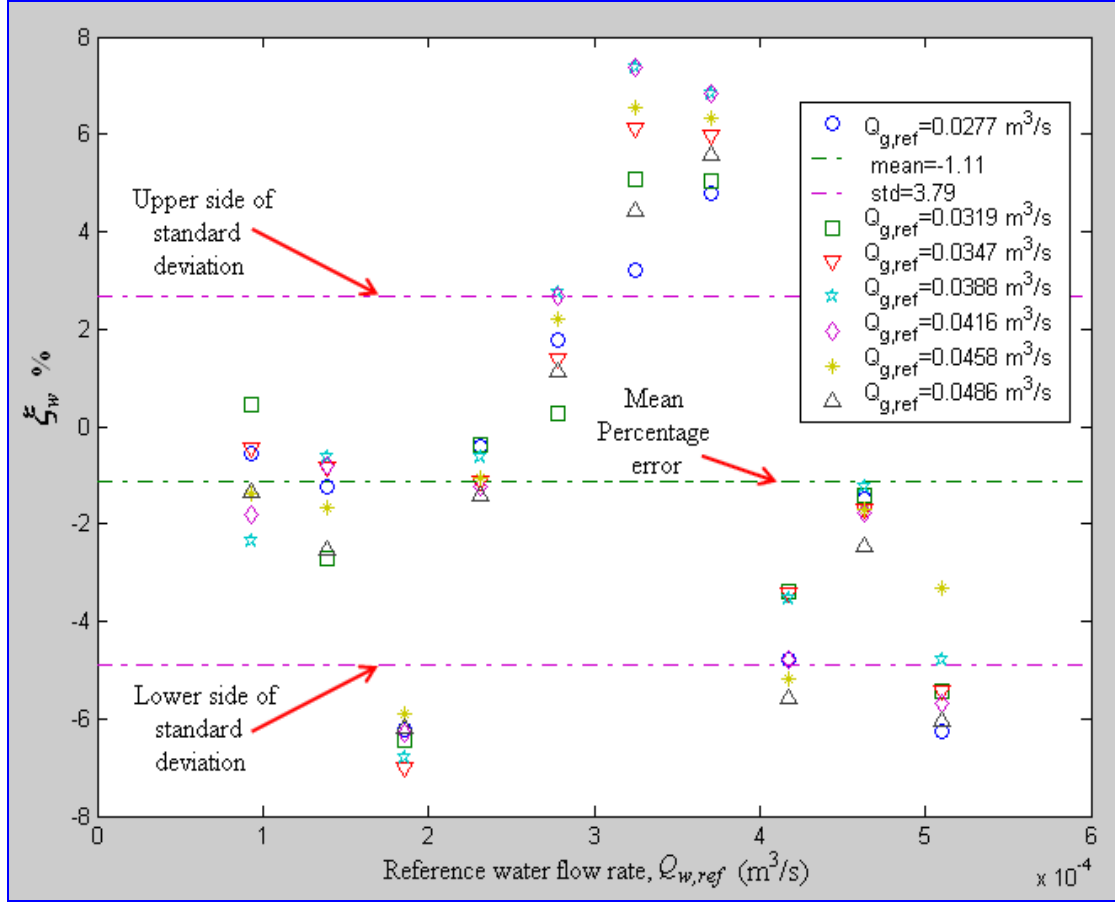


Figure 6.39 Percentage error in the measured water flow rate at different constant gas flow rates.

### 6.6.2 Gas flow rate ( $Q_g$ )

Using the reference gas flow rate  $Q_{g,ref}$  obtained from the VAFM, the estimated percentage error in the estimated gas flow rate  $\xi_g$  can be calculated as follows:

$$\xi_g = \frac{Q_{g,est} - Q_{g,ref}}{Q_{g,ref}} \times 100\% \quad 6.48$$

where:  $Q_{g,est}$ , see Equation 6.49, is obtained from the measured value of the  $U_{g,c}$  defined by Equation 6.40, and  $A_{g,d}$  is the cross-sectional area of the gas core taking the entrained droplet area into account and defined by Equation 6.43:

$$Q_{g,est} = U_{g,c} A_{g,d} \quad 6.49$$

The estimated percentage error in the measured gas flow rate is plotted against the reference gas flow rate at different constant reference water flow rates, see Figure 6.40, which shows that the errors appear scattering randomly with most below 1%. The mean estimated percentage error is 0.8% with a standard deviation of about 0.4%. There is one outlying data point in Figure 6.40 which caused the standard deviation to slightly increase.

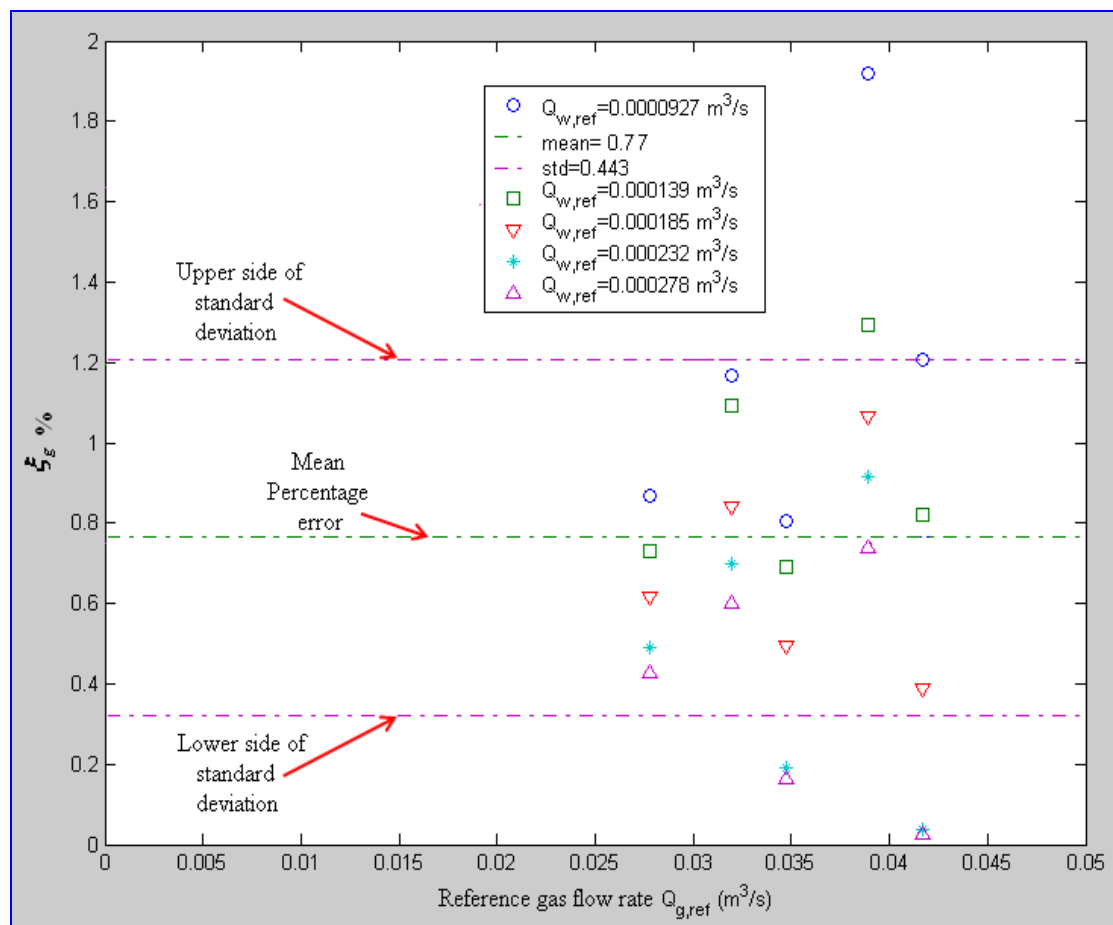


Figure 6.40 Percentage error in the measured gas flow rate at different constant water flow rates

In both error calculations, gas and water flow rates, the total error is an accumulation of different physical error sources that could affect the measurement. These physical errors could include:

- (i) Presence of the meniscus; during calibration it was found that when the thickness of the reference film was less than about 3mm the presence of the meniscus could introduce errors of as much as -0.5% and +3.5% (see Figure 3.5).

- (ii) Conductivity measurement, the presence of electrodes of a definite physical size will disrupt the film flow to an extent. The separation of 20mm was determined for zero flow conditions and under those conditions gave an accurate and reproducible measure of film thickness, but in the presence of flow it is quite possible that some small errors might be introduced.
- (iii) The voltage output  $V_{out}$  measurements are expected to be accurate to a very high degree, it is the constant of proportionality in converting  $V_{out}$  to  $\delta_{ref}$  which introduces the errors in (ii) above.
- (iv) The errors in the USFM measurements are likely to be very small, providing the timing device is correctly set up and calibrated. It is assumed that was the case. However, the measurement of the gas core velocity in the presence of water droplets is more problematic. It was assumed that the droplets were sufficiently small to be carried along at the mean gas flow rate. Obviously, in practice this will not always be the case. With vertical flows the mean droplet velocity will be less than the mean gas flow velocity and, in addition there will be a (small) range of droplet velocities. Obviously this effect will vary with the water volume flow rate. But it is likely that the presence of droplets will affect the USFM measured gas velocity. Indications are that the error introduced is not large (less than one or two %), but it is not possible to be precise at the moment.

## CHAPTER 7 WET GAS FLOW METER PROPOSAL

The importance of wet gas metering was introduced in Section 1.2.3. The Literature Review shows that wet gas metering is becoming increasingly important to the Oil and Gas Industry and different proposals have been made by different researchers, Richard (2001). Each separate proposal was usually made to overcome one or other of the common practical problems of wet gas metering as listed below:

- Practical Problems with Flow Conditioners,
- Practical Problems with Flow Patterns,
- Practical Problems in Determining Fluid Properties,
- Practical Problems in Meter Survivability, and
- Practical Problems in Finding the Liquid Content in the Gas Flow.

The majority of published proposals on Wet Gas Flow Metering are concerned with Orifice Plates. More recently researchers have given greater emphasis to the Venturi Meter although much of this research consisted of taking Venturi Meter readings and then applying them to existing Orifice Plate Meter to check their suitability. The V-Cone, see Section 2.4.1, is not in general use because it is relatively new and largely untested, and so not yet trusted by many industries (Svedeman, 1997).

In this chapter, the author will attempt to summarise the different aspects of a proposed wet gas flow meter based on the results presented in this thesis including, hardware, electronics, analysis and accuracy.

### 7.1 Proposed Flow meter hardware

The aim of any research study in the oil and gas field is invariably directed to produce economic and less bulky measurement systems. The proposed wet gas flow meter in this investigation consists of three major components, see Figure 7.1; Conductance Flow Meter (CFM), Ultrasonic Flow Meter (USFM) and Sensor Tube system.

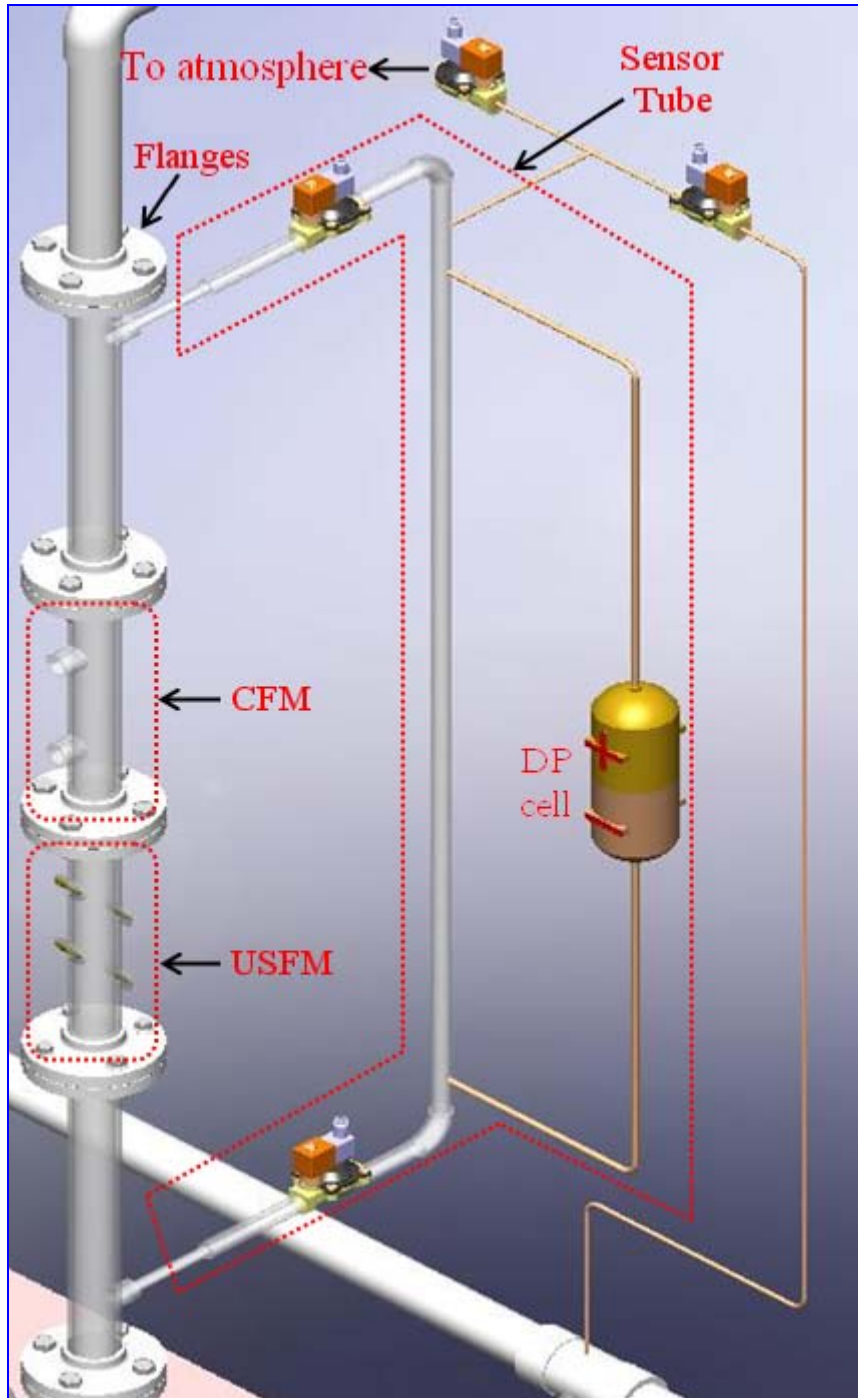


Figure 7.1 Hardware components of the proposed flow meter

It can be seen from Figure 7.1 that the system can be disassembled and reassembled (using the connecting flanges between each component) which enables the orientation of the components to be changed to fit the space intended to accommodate the device. Each component has its own subcomponents i.e. transducers, needle electrodes, solenoid valves, DP cell etc. The position of these components can be changed to suit the available space as long as a certain minimum is available.

The approximate size of CFM, used in the present study, is 0.15x0.15x 0.25m with its flanges. The USFM is 0.15x0.15x0.30m with its flanges. When the sensor tube is attached, the three components together form a system of approximately 0.5x0.15x1m. It was mentioned in Section 1.2.1 that there are a number of constraints on the design of any proposed multiphase flow meter. One of these constraints is that it should not occupy a footprint of more than 0.5m x 1.0m and should be less than 2.0m high. The dimensions provided by the proposed wet gas flow meter in this study, for a 50mm pipe size, meet this requirement.

It was mentioned in Section 5.1 that the pipe sizes of most interest in industrial situations are in the range 50mm to 150mm diameters with maximum demand for 75-100mm diameter sections (Cosham et al., 2007). This places the proposed flow meter in this study in a good position in the scale of the pipe sizes used in actual gas wells. However, the proposed devices can be further developed to better suit the range 50mm to 150mm pipe internal diameters.

## 7.2 Proposed flow meter electronics

The electronic circuit developed for measurement of liquid film thickness was based upon the conductance technique used by the CFM, see Section 4.2.2, and Figures 4.3 and 4.5. By using an inverting amplifier an output was obtained which was proportional to the conductance of the multiphase between the electrodes of the CFM.

The voltage output  $V_a$  is given by Equation 4.7, see Section 4.2.2:

$$V_a = -R_{fb} S_m V_i \quad 7.1$$

where:  $R_{fb}$  is the reference feedback resistance,  $V_i$  is the AC input voltage and  $S_m$  is the conductance of the multiphase.

The complete electronic circuit whose voltage output is a DC signal was fully detailed and presented in Section 4.3.2. The accuracy of the measurement using this circuit was investigated in Section 3.2.1 and discussed in Section 6.6.2.

For the USFM the designed electronic circuit was based upon the trigonometrical relationship between the product of two sine waves and the difference of two cosine terms to obtain the phase difference between the two signals, see Section 3.3.4:

$$\sin(\omega_1 t + \theta_1) \sin(\omega_2 t + \theta_2) = \frac{1}{2} \{ \cos[(\omega_1 - \omega_2)t + \theta_1 - \theta_2] - \cos[(\omega_1 + \omega_2)t + \theta_1 + \theta_2] \} \quad 7.2$$

If the two frequencies are the same ( $\omega_1 = \omega_2 = \omega$ ) the result is a DC component ( $0.5\cos(\theta_1 - \theta_2)$ ) and an AC component ( $-0.5\cos(2\omega t + \theta_1 + \theta_2)$ ) which can be filtered out.

The DC component is proportional to cosine of the two received ultrasound signals – which can be related, see Equations 3.38 and 3.39, to the gas velocity in the core of the wet gas flow. To achieve this multiplication, the MC1496 analogue electronic multiplier was used. The complete design of the USFM electronic circuit was presented in Section 4.3.2. Testing the electronic circuit with the designed USFM hardware showed a mean percentage error in the measured gas core velocity of 1.17% without taking the effect of the presence of the water droplets in the gas core and 0.851% when taking into account the effect of the presence of the water droplets in the gas core, see Section 6.5.1.

### 7.3 Proposed flow meter analysis

This section summarises the analytical arguments used to obtain the different flow parameters from the measurements.

#### 7.3.1 Three phase annular flow [oil, water, gas]

The three phase annular flow considered is when oil, water and gas flow together. This section discusses how we can measure the volumetric flow rates of all three phases using the proposed CFM, USFM and Sensor Tube devices.

To accurately predict the phase velocities and mixture properties requires a good knowledge of the volume fraction. The proposed wet gas flow meter in this study

introduces the Sensor Tube, see Section 4.1, which can be used to measure the volume fractions of a three phase annular flow. Some of the liquid film is extracted into the sensor tube and its density measured off-line, after which the liquid is released back into the system. With an oil-water mixture, the oil and water volume fractions could be calculated from this density measurement.

The differential pressure,  $\Delta P$  in the sensor tube can be measured by the DP cell as:

$$\Delta P = \rho_w g h_{ST} - \rho_m g h_{ST} \quad 7.3$$

From which it follows that:

$$\therefore \rho_m = \rho_w - \left[ \frac{\Delta P}{g h_{ST}} \right] \quad 7.4$$

where:  $\Delta P$  is the measured differential pressure,  $\rho_w$  is water density,  $\rho_m$  is mixture density,  $g$  is  $9.81\text{m/s}^2$  and  $h_{ST}$  is the separation of the pressure tappings in the sensor tube (1m). Pressure sensor lines are filled with water during the oil-water mixture density measurement to avoid having air in the pressure lines.

It is known that:

$$\rho_m = \alpha_{o,l} \rho_o + \alpha_{w,l} \rho_w \quad 7.5$$

where:  $\alpha_{o,l}$  is the oil volume fraction in the liquid film,  $\rho_o$  is the oil density,  $\alpha_{w,l}$  is the water volume fraction in the liquid film and  $\rho_w$  is the density of the water.

Also, we have:

$$\alpha_{o,l} + \alpha_{w,l} = 1 \quad 7.6$$

So, from Equations 7.3-7.6, having measured  $\rho_m$  and knowing  $\rho_o$  and  $\rho_w$ , the oil and water volume fractions in the liquid film can be found.

Hence, by measuring the film velocity  $U_f$  (using cross-correlation, see Section 4.2.5) and the film thickness  $\delta$  (using CFM, see Section 4.2 and 6.1.1), the following equations can be used:

$$(\pi R^2 - \pi(R - \delta)^2)U_f = Q_f \quad 7.7$$

$$\left[ (\pi R^2 - \pi(R - \delta)^2)U_f \right] \alpha_{o,l} = Q_{o,f} \quad 7.7a$$

$$\left[ (\pi R^2 - \pi(R - \delta)^2)U_f \right] \alpha_{w,l} = Q_{w,f} \quad 7.7b$$

where:  $R$  is the pipe radius,  $\delta$  is the film thickness,  $U_f$  is the film velocity,  $Q_{w,f}$  is the water volume flow rate in the liquid film,  $Q_{o,f}$  is the oil volume flow rate in the liquid film and  $Q_f$  is the total film volume flow rate.

The total liquid volume flow rate in the film is given by:

$$Q_f = Q_{o,f} + Q_{w,f} \quad 7.8$$

It is assumed that:

- (i) The ratio of the droplet mass flow rate  $W_d$  to the total liquid mass flow rate ( $W_d + W_f$ ) (where  $W_f$  is the film mass flow rate) is equal to the entrainment fraction  $E$ .

and

- (ii) For the droplets in the core flow,  $\alpha_o$  and  $\alpha_w$  are the same as in the film, then the entrainment fraction  $E$  can be expressed as:

$$E = \frac{\rho_d Q_d}{\rho_d Q_d + \rho_f Q_f} \quad 7.9$$

where:  $\rho_d$  is the average droplet density,  $Q_d$  is the droplet total volume flow rate,  $\rho_f$  is the film density and  $Q_f$  is the film volume flow rate.

Since the average droplet density is equal to the film density,

$$\rho_d = \rho_f = \alpha_o \rho_o + \alpha_w \rho_w \quad 7.10$$

Equation 7.9 can be rearranged in the form:

$$Q_d = \left( \frac{E}{1-E} \right) Q_f \quad 7.11$$

By knowing  $E$  and  $Q_f$  (from Equations 7.8 and 7.9) we can find  $Q_d$ .

Because  $\alpha_{o,l}$  and  $\alpha_{w,l}$  for the droplets are assumed to be the same as for the film, it follows:

$$Q_{o,d} = \alpha_{o,l} Q_d \quad 7.12$$

$$Q_{w,d} = \alpha_{w,l} Q_d \quad 7.13$$

where:  $Q_{o,d}$  is the droplet volume oil flow rate and  $Q_{w,d}$  is the droplet volume water flow rate.

The mean gas core velocity  $U_{g,c}$  can be measured using the USFM, see Sections 4.3 and 6.5, and the mean gas flow rate  $Q_g$  can be obtained from:

$$Q_g = (A - 2\pi R\delta) U_{g,c} \quad 7.14$$

where:  $Q_g$  is the gas volume flow rate,  $U_{g,c}$  is the mean gas velocity averaged over the pipe cross-section measured by the USFM,  $\delta$  is the liquid film thickness measured by the CFM,  $R$  is the pipe cross-sectional area and  $A$  is the cross-sectional area of the pipe.

Hence, we can determine the total volume flow rates for water  $Q_w$  (Equations 7.7b and 7.13), gas  $Q_g$  (Equation 7.14) and oil  $Q_o$  (Equations 7.7a and 7.12).

### 7.3.2 Two-phase annular flow [conducting liquid and gas]

This section deals with two phase annular flow where only two phases are flowing together. The proposed wet gas flow meter deals with conducting liquid phases e.g. water. For two-phase annular flow, the proposed CFM and USFM devices of the proposed flow meter are the only required techniques to perform the measurements of the two-phase annular flow.

From the analysis above it follows at once that the entrainment fraction  $E$  is given by:

$$E = \frac{Q_{w,c}}{Q_{w,c} + Q_f} \quad 7.15$$

and

$$Q_{w,c} = \frac{E Q_f}{(1 - E)} \quad 7.16$$

where:  $Q_{w,c}$  is the water flow rate in the core defined previously by Equation 6.22 and  $Q_f$  is the film flow rate

Because the entrained droplets are very small, they are likely to be travelling at close to the gas velocity. This lead to the assumption  $U_{w,c} = U_{g,c}$ , so we can say:

$$Q_{w,c} = A_{w,c} U_{g,c} \quad 7.17$$

where:  $U_{w,c}$  is the velocity of water in the core and  $A_{w,c}$  is the equivalent cross-sectional area of the water in the core.

From Equations 7.16 and 7.17:

$$A_{w,c} U_{g,c} = \frac{E Q_f}{(1-E)} \quad 7.18$$

$$\alpha_{w,c} = \frac{1}{A} \left( \frac{E}{1-E} \right) \frac{Q_f}{U_{g,c}} \quad 7.19$$

where:  $\alpha_{w,c}$  is the water volume fraction in the core.

From the liquid film thickness measurement, the area of the liquid film  $A_f$  can be calculated and hence:

$$\alpha_{w,f} = \frac{A_f}{A} \quad 7.20$$

where:  $\alpha_{w,f}$  is the volume fraction of the liquid in the film.

The total water volume fraction  $\alpha_{w,tot}$  is given by:

$$\alpha_{w,tot} = \alpha_{w,c} + \alpha_{w,f} \quad 7.21$$

where:  $\alpha_{w,tot}$  is the volume fraction of the total water in the pipe.

The volumetric water flow rate then can be calculated from:

$$Q_w = \alpha_{w,tot} U_f A \quad 7.22$$

where:  $Q_w$  is the total volume water flow rate,  $U_f$  is the film velocity measured using the cross-correlation technique,  $\alpha_{w,tot}$  is the volume fraction of the total water in the pipe and  $A$  is the cross-sectional area of the pipe.

Since the sum of the volume fractions of each component of the phase/flow is 1, it follows that:

$$\alpha_{g,c} = 1 - \alpha_{w,c} - \alpha_{w,f} \quad 7.23$$

where:  $\alpha_{g,c}$  is the volume fraction of the gas core.

Also, the core gas velocity  $U_{g,c}$  can be measured from the USFM device, see Sections 4.3 and 6.5. So, taking into account the liquid film thickness measurement to calculate the cross-sectional area of the gas core  $A_{g,c}$  (defined by Equation 6.43), the gas flow rate  $Q_g$  can be calculated from:

$$Q_g = \alpha_{g,c} U_{g,c} A \quad 7.24$$

#### 7.4 Proposed flow meter discussion and summary

As stated in Section 1.2.3, no technique presently available comes close to the industry's desired standards for the simultaneous metering of the liquid and gas phase flow rates in wet gas flow. This is partly because operators are not willing to allow meter tests on actual production flows due to possible financial penalties that might be incurred with consequent production delays. Meter manufacturers are forced to test their meters on wet gas laboratory test loops which have the major drawback that nowhere does the test equipment available replicate the real flow conditions found in wet natural gas production lines.

In parallel to developments aimed at improving the accuracy of flow metering systems will be negotiations as to what is an acceptable accuracy for partners and governments associated with an oilfield development. These two aspects (technology and accuracy) will probably both have to progress in order for metering of flow to become a reality.

For the proposed wet gas flow meter used in this investigation, the error calculations showed that the flow meter is capable of measuring water and gas volume flow rates with a mean percentage errors of about -1.11% and 0.77% respectively. These values seem promising and suggest promoting this flow meter for commercial development, use since the range of the available accuracy is between +/-5 and 10%.

Figure 7.2 presents a schematic of the procedures for the measurement of the various flow parameters. If the volume fraction is required than DP cell is used – the Pressure Difference Measurement Technique shown on the left of the diagram. If the core gas velocity is required than the diagram shows that the USFM is required. Should it be necessary to measure liquid film thickness then the diagram shows that the CFM will be required.

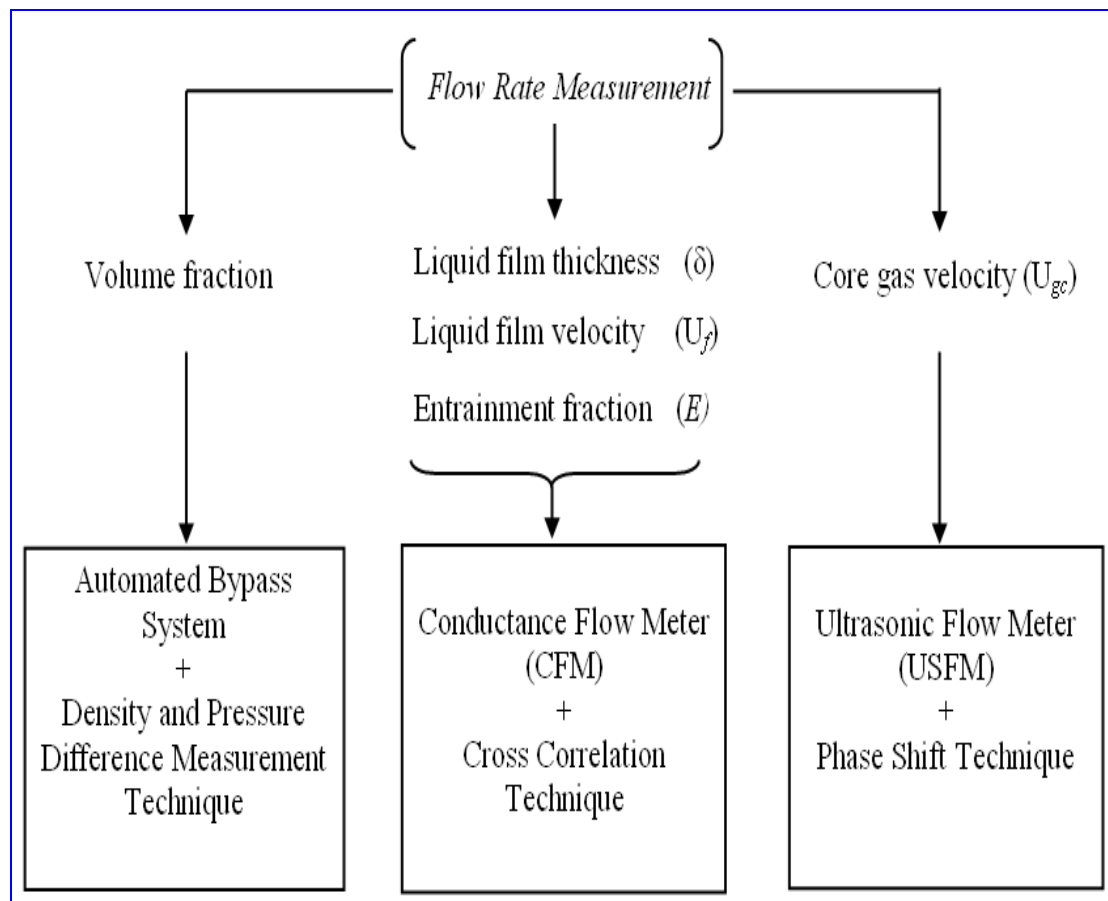


Figure 7.2 Measurement sources for the proposed flow meter

## CHAPTER 8 CONCLUSIONS

The completion of this research study has produced a number of different contributions to knowledge. These contributions are the outcome of the different conclusions drawn from this study.

### 8.1 Conclusions

The primary aims and all objectives listed in Chapter 1 of this thesis were achieved. In addition to achieving the primary objectives a number of specific conclusions have been reached as a result of the measurement techniques and the flow meters that were developed. The results of the experiments have been compared with previous data available for this pipe diameter. However, not a great deal of previous work has been carried out on 50mm diameter pipes and so it was not possible to compare all the results obtained in this thesis with previous work. In general the agreement between the current and data and previous data was good.

The literature review revealed that for annular two-phase flow, where the volumetric flow rate of the liquid phase is much less than the volumetric flow rate of the gas, the annular flow is defined by measuring four properties of the flow in any of the possible combinations given below:

- (I) Film thickness  $\delta$ , film velocity  $U_f$ , gas core velocity  $U_{g,c}$  and the gas volume fraction  $\alpha_{g,c}$ .
- (II) Film volume fraction  $\alpha_{w,f}$ , volume fraction of liquid in the core  $\alpha_{w,c}$ , film velocity  $U_f$  and gas core velocity  $U_{g,c}$ .
- (III) Film volume fraction  $\alpha_{w,f}$ , film velocity  $U_f$ , gas core velocity  $U_{g,c}$  and entrainment fraction  $E$ .

The designed techniques in the current study (CFM and USFM) were integrated into a single, relatively simple measurement system and used with an entrainment model to enable determination of the parameters in (III) above for a two-phase annular flow. For three phase flow a sensor tube system designed in the study can be additionally used for measuring the volume fractions of oil and water in the liquid.

A test flow loop has been designed and built to investigate the two-phase (gas-water) annular flow under different known flow conditions. The loop consisted of four sections, **1)** air supply, **2)** water supply, **3)** test section, and **4)** outlet section. A turbine flow meter for measuring the water volume flow rate was calibrated in the laboratory and this calibration was checked against that of the manufacturer. Good agreement was obtained. A Rotameter (Variable Area Flow Meter) with manufacturer's calibration was used to measure the gas (air) volume flow rate, see Sections 5.1.1 and 5.1.2. The ambient temperature and liquid conductivity was monitored each time the loop was run. However, the author recommends carrying out a calibration at least once every two weeks to maintain accuracy and repeatability patterns.

A new technique, the conductance flow meter (CFM) has been built that is capable of measuring the film thickness when the liquid film is electrically conducting. Measuring the conductance using a conductance probe, containing a pair of steel electrodes protruding into the pipe, it was possible to measure the thickness of the liquid film on the wall of the pipe, see Sections 3.2 and 6.1.1. The CFM device was configured as containing a pair of such conductance probes, set a known longitudinal distance apart, thus enabling the CFM device to also be used to measure the liquid film velocity using cross-correlation, see Sections 3.2 and 4.2.

The CFM designed and built for this project covers a wide range of film thicknesses, see Section 6.1.1.2. It was found that a sampling rate of about 1kHz was required. For the experiments undertaken in the present study the experimental data shows a minimum film thickness of 0.8mm in flows where  $Q_g = 175\text{m}^3/\text{hr}$  and  $Q_w = 0.33\text{m}^3/\text{hr}$ , and a maximum film thickness of 5.7mm in flows where  $Q_g = 100\text{m}^3/\text{hr}$  and  $Q_w = 1.83\text{m}^3/\text{hr}$ . However, the calibration process showed that the flow meter can measure film thicknesses up to 20mm, see Section 4.2.3.

Using the upstream and downstream pairs of probes the CFM was also used as a cross-correlation velocity flow meter to measure the velocity of the liquid film, and showed good repeatability, see Section 6.1.2.1. Under test conditions the mean error in the flow velocity obtained from the CFM, as compared with a reference velocity calculated from the turbine meter reading and the measured film thickness, was about -1.11%, see Section 6.1.2.1. Analyzing the data obtained from the CFM, the film thickness, velocity and entrainment depended virtually exclusively on the gas flow rate and very little on the liquid flow rate. As the gas flow rate increases, there was a simultaneous increase occurs in all of the three parameters, see Sections 6.1.1.2, 6.1.2.2 and 6.2.1.

The core gas velocity of the annular flow was measured using a new design of ultrasonic flow meter (USFM), in which the novel feature was the arrangement of the electrodes, see Section 3.3.4. The phase difference between two received ultrasonic signals was converted to a DC voltage which was a measure of the gas core velocity and hence the core gas flow rate, see Section 4.3. Testing the flow meter under different annular flow conditions showed good repeatability.

The error in the gas velocity measured with the USFM had a mean value of 1.2% (section 6.5.2). Introducing different gas and water flow rates in the test section, the disturbance to the film caused by the presence of the ultrasound transducers did not affect the film thickness measurements. This was concluded from the error calculations carried in Section 6.5.1.

The entrainment fraction is defined as the ratio of the '*total water volumetric flow rate minus the film volumetric flow rate*' to the '*total water volumetric flow rate*' (see Section 6.2). However, the author has developed an expression for the entrainment fraction in terms of the gas superficial velocity, see Section 6.2.2. The relationship was successfully used to estimate the entrained water flow rate in the core thus enabling a better estimate of the total water flow rate in the pipe, see section 6.6.1. Also, with knowing the liquid film velocity at a certain gas superficial velocity, this correlation was able to successfully contribute in the prediction process of the liquid film thickness, see Section 6.3.

A newly designed extraction technique – the sensor tube – was proposed and investigated to measure the liquid volume fractions in flows where the liquid film and the entrained droplets consist of a mixture of two different liquids of different density (e.g. oil and water) see Section 4.1. This is considered a significant outcome of the research project. Its advantages are (i) its ease of use and (ii) its short duration time of less than 2 minutes. Previously sampling techniques have not been used for this purpose and the use of sampling techniques cited in the literature (for example in the measurement of entrainment) has always been associated with tubes of relatively small internal diameters ( $5\text{mm} < \text{ID} < 15\text{mm}$ ). In this project, with the aid of automatic control (solenoid valves), the sampling technique was extended to a larger pipe diameter and different parameters of measurement, namely the liquid volume fractions, see Section 4.1.2. However, the technique was not able to extract liquid films at gas flow rates of less than  $Q_g = 50\text{m}^3/\text{hr}$ . This limitation was due to the lack of pressure inside the test section to force out the liquid film.

On the basis of a number of simplifying assumptions a model has been developed to predict the liquid film thickness (see Section 6.3) and water and gas volume fractions (see Section 6.4). The velocity profile predicted by the model agreed with visual observations and the analysis presented by Maron et al., (1984) (see Section 6.1.3).

By examining the overall system accuracy of the CFM combined with the USFM, see Section 6.6, the error calculation showed a  $-1.11\%$  mean error in the total water flow rate measurement with a standard deviation of  $3.8\%$ . This error is believed to be mainly due to inaccuracies in the entrainment fraction model rather than in the measured water flow rate of the liquid film. This is due to the fact that the entrainment fraction varies slightly with water flow rate (section 6.2) and this is not accounted for in the entrainment fraction model. The mean error in the gas flow rate measurement was  $0.77\%$  with a standard deviation of  $0.4\%$ . These values of mean error represent a significant improvement over existing annular flow measurement techniques (see chapter 2) where typical errors on phase flow rate measurements are of the order of plus or minus  $5\%$  to  $10\%$  for each phase.

The combination of the designed CFM and USFM with the sensor tube offers the opportunity to develop a wet gas flow meter to measure three-phase flow at relatively low cost and enhanced accuracy, see Chapter 7. The combined device would have the advantage that it would be substantially smaller than measurement techniques based on the use of separators (see chapter 2) and could even be retrofitted onto off-shore platforms. A best estimate of overall dimensions that the device would fit into is a cubic space of 1.5m high x 1.5m x 0.5m, see Section 7.1. It is believed that such a device, if successful would be of great interest to oil companies. For the proposed wet gas flow meter, error calculations based on the results of this thesis suggest a mean accuracy in the measured water and gas volume flow rates of less than 1% for both. These values seem promising when compared to the range of currently available accuracies of between 5% and 10%, see Section 7.4.

## 8.2 Present contribution

The contribution made to knowledge by this thesis includes:

- The design of a new experimental loop to establish annular flow and which can be upgraded for use with different diameters and orientations of test sections, if required.
- A novel configuration for a film extraction technique to measure the volume fractions of different liquids in gas-liquid annular flow.
- Designing a novel device to successfully measure the liquid film velocity and thickness.
- Development of an entrainment fraction correlation that can be used to predict the entrained water flow rate from the gas superficial velocity. (Alternatively the entrainment model enables the liquid film thickness to be estimated from the gas superficial velocity if the film velocity is known and the total water flow rate is measured using an auxiliary reference measurement, see section 6.3).

- Designing a successful device with a novel transducer configuration to measure the core gas velocity in annular flow.
- The work has resulted in a novel combination of online measurement techniques to measure the gas and liquid flow rates in annular flow.
- A new technique is also proposed in the next chapter to measure the liquid film conductivity in multiphase annular flows, see Section 9.1.

## CHAPTER 9 FURTHER WORK

This study covered a significant area in term of flow rate measurement, but there remain a large number of possible directions for further work such as:

### 9.1 Alternative method for measuring volume fraction in multiphase annular flows:

Electrical impedance techniques have proven attractive for many applications because of their generally fast response and relative simplicity of operation. Measurements obtained from these devices rely upon the change of permittivity or the conductance of a two-phase mixture with the volume fraction of the disperse phase.

For the film that occurs with annular flows, non-conducting mixtures (such as water-in-oil) use measurement of capacitance, whereas conducting mixtures (such as oil-in-water) require conductance measurements.

The capacitance technique is used in oil continuous multiphase volume fraction measurements. Here, the fluid permittivity decreases with increasing gas volume fraction and increases with increasing water volume fraction.

The conductance technique is used in water continuous multiphase volume fraction measurements. Here, the conductance decreases with increasing gas and oil volume fractions, and increases with increasing water volume fraction.

A conductance probe method, the Flush Mounted Sensor (FMS), is proposed to measure the fluid conductivity using much the same technique as used with the Conductance Flow Meter (CFM). This technique relates the conductance to the impedance between two electrodes which are set flush with the inside wall of the tube, see Figure 9.1. As the impedance between the two flush electrodes changes the conductance changes. The FMS will provide a conductance measurement which can

be used to refine the CFM film thickness measurements. The aim of the FMS device is to respond independently of the film thickness of the annular flow.

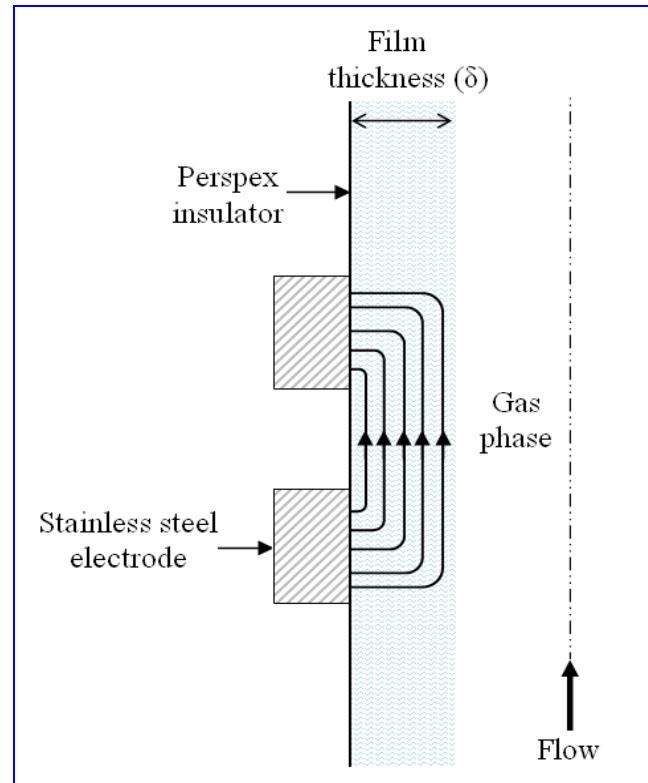


Figure 9.1 Principle of operation of Flush Mounted Sensor

A model sensor, see Figure 9.2, was designed, built and bench tests carried out. The model sensor could be in either of one of two configurations. The first was Config.1, with two 1.3mm diameter probes placed 6.3mm centre to centre. This was calibrated in a similar manner to the CFM, see Section 4.2.3. 20 cylindrical dry foam plugs were placed longitudinally in the centre of the 50mm ID pipe to produce films of different thicknesses in the range 1mm to 20mm (only water film used). For film thicknesses in the range 1mm to 6mm the relationship between voltage drop and film thickness appears linear, see Figure 9.3. However, for films in the range of 6mm to 10mm the curve changes direction and from about 10mm to 20mm resumes a near linear relation but with a different, shallower gradient. The suggestion is that different mechanisms determine the voltage measurement in the two ranges. Figure 9.3 shows the measured voltage drop between the electrodes for each film thickness and should be compared with the calibration curve for the CFM, Figure 4.10.

However, when tested with liquids of different conductivities this probe configuration was deemed not fit for purpose. Figure 9.4 suggests that as the film thickness changes the impedance between the two flush electrodes changes and hence the conductance changes i.e. the voltage output of the FMS is dependent on both the liquid film thickness and the conductivity of the liquid film.

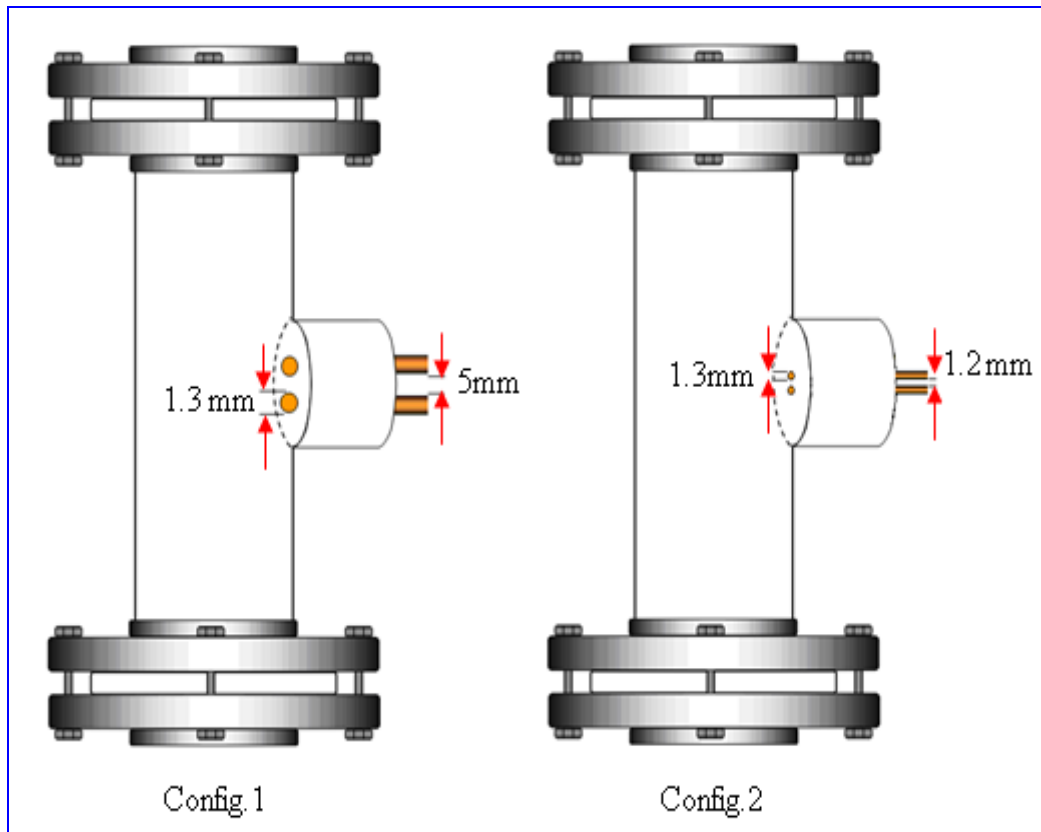


Figure 9.2 Flush Mounted Sensor configurations (not to scale)

To overcome this problem of output voltage dependency on the film thickness, different probe and electrode configurations were investigated using COMSOL software. From the COMSOL investigation it was found that there are five factors to be considered when finding the best sensor configuration for this technique. These elements are: film thickness, excitation frequency  $f$ , liquid film conductivity  $\sigma_f$ , spacing between electrodes  $l_{sp}$  and the electrode dimensions. Figure 9.5 shows the COMSOL predictions and it is clear that to minimize the influence of the film the probe separation should be minimal. The new probe configuration (Config.2) used in this investigation retained the 1.3mm diameter electrodes but separation between the pair of electrodes was reduced to  $l_{sp}=1.2\text{mm}$ .

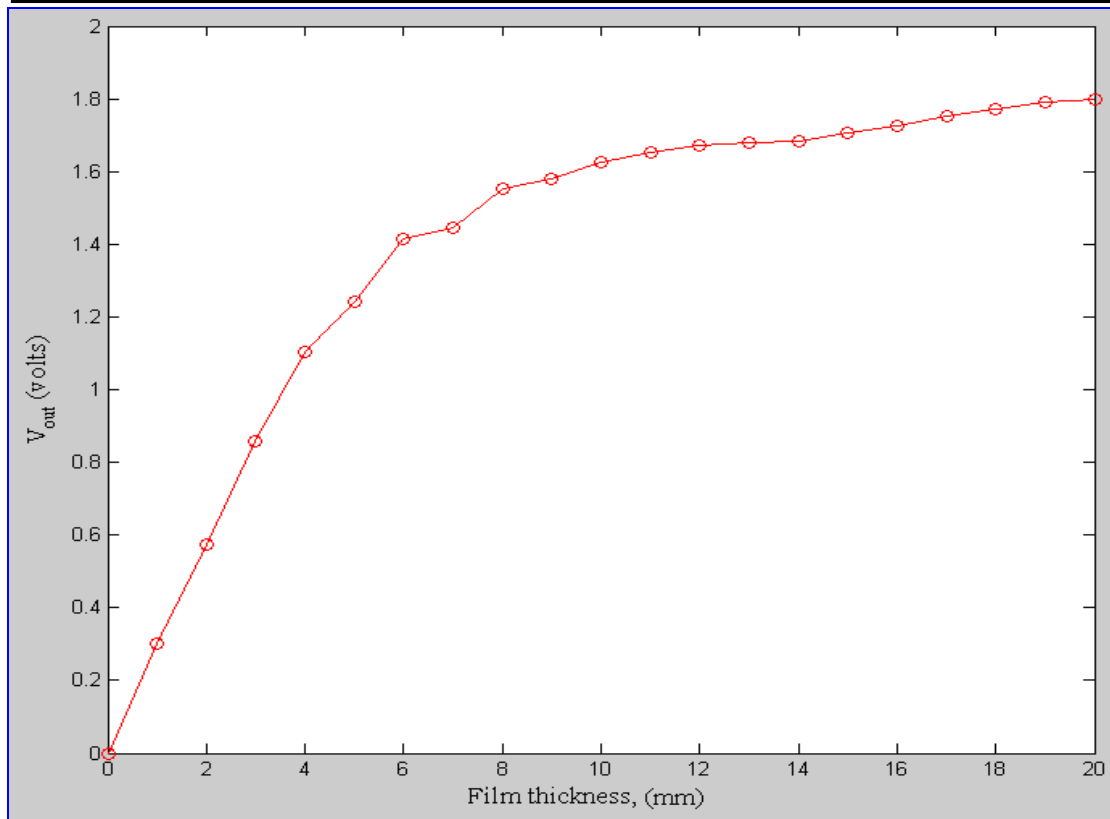


Figure 9.3 Flush Mounted Sensor calibration curve (Config.1)

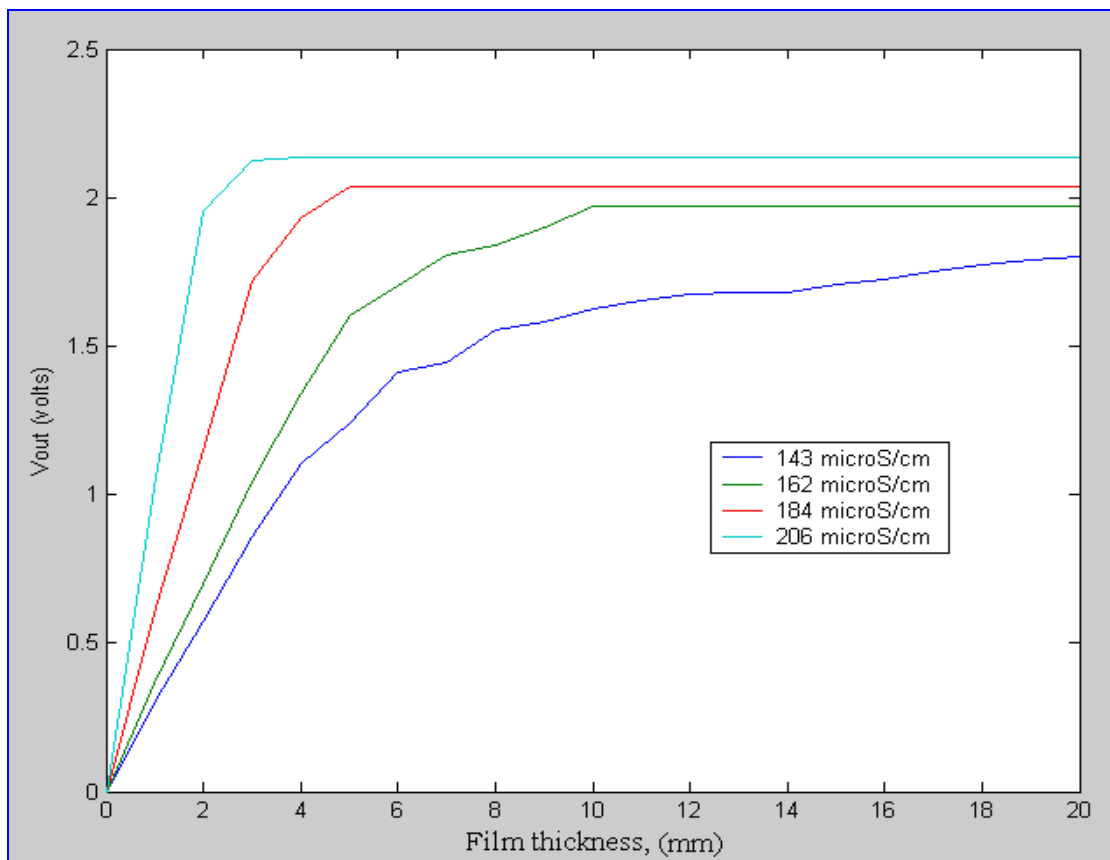
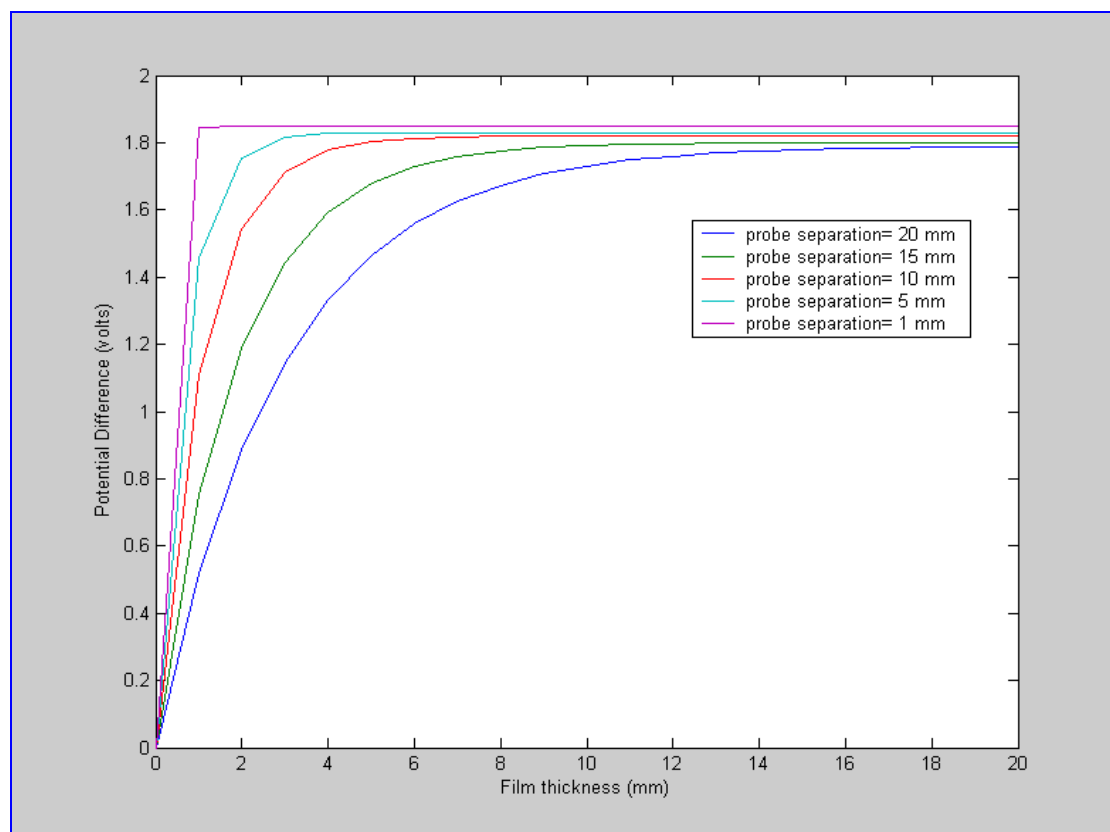


Figure 9.4 Voltage output of Flush Mounted Sensor for different liquid conductivities (Config.1, bench test)



*Figure 9.5 Voltage output of Flush Mounted Sensor for different probe separations (Config.II, COMSOL prediction)*

For the combination of low excitation frequency (50Hz), a short separation distance between the electrodes (1.2mm) and small electrode diameter (1.3mm), The COMSOL results predicted for the new sensor configuration (Config.2) show the voltage output was found to be dependent on the liquid film conductivity and largely independent of the liquid film thickness, see Figure 9.6. The COMSOL results agree with the bench test result carried out for the new sensor configuration, see Figure 9.7.

To vary the conductivity of the water, an electrolyte (sodium chloride) was added to the water. A quantity sufficiently small that it would not affect the other properties of the water (0.3g/l) substantially increases its conductivity (Martin, 1983). To avoid introducing unnecessary variables all the bench tests performed on FMS technique were carried out at in a controlled temperature environment.

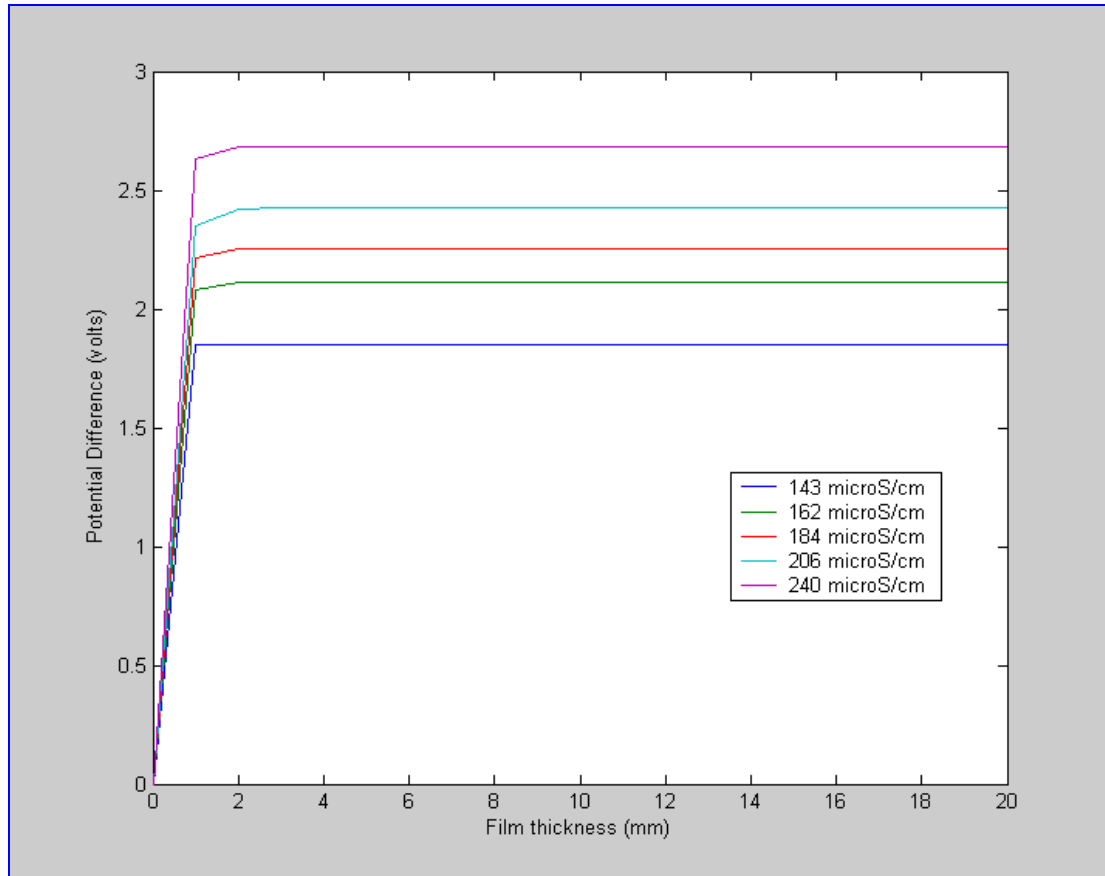


Figure 9.6 Voltage output of Flush Mounted Sensor for different liquid conductivities (Config.2, COMSOL)

The bench test of the FMS shows that, provided film thickness  $\delta > 1\text{mm}$ , the output voltage of the FMS device is directly proportional to the liquid film conductivity  $\sigma_f$ , and independent of film thickness, see Figure 9.7. For  $\delta < 1\text{mm}$ , the voltage output is directly proportional to film thickness for a constant film conductivity.

A parallel investigation of the CFM with different water conductivities shows that for a given conductivity the output voltage is directly proportional to film thickness, see Figure 9.8. For a given film thickness it can be seen that the output voltage increases with conductivity, however below an output of 0.1 volts the curves are so close together that it can be said CFM does not differentiate between conductivities.

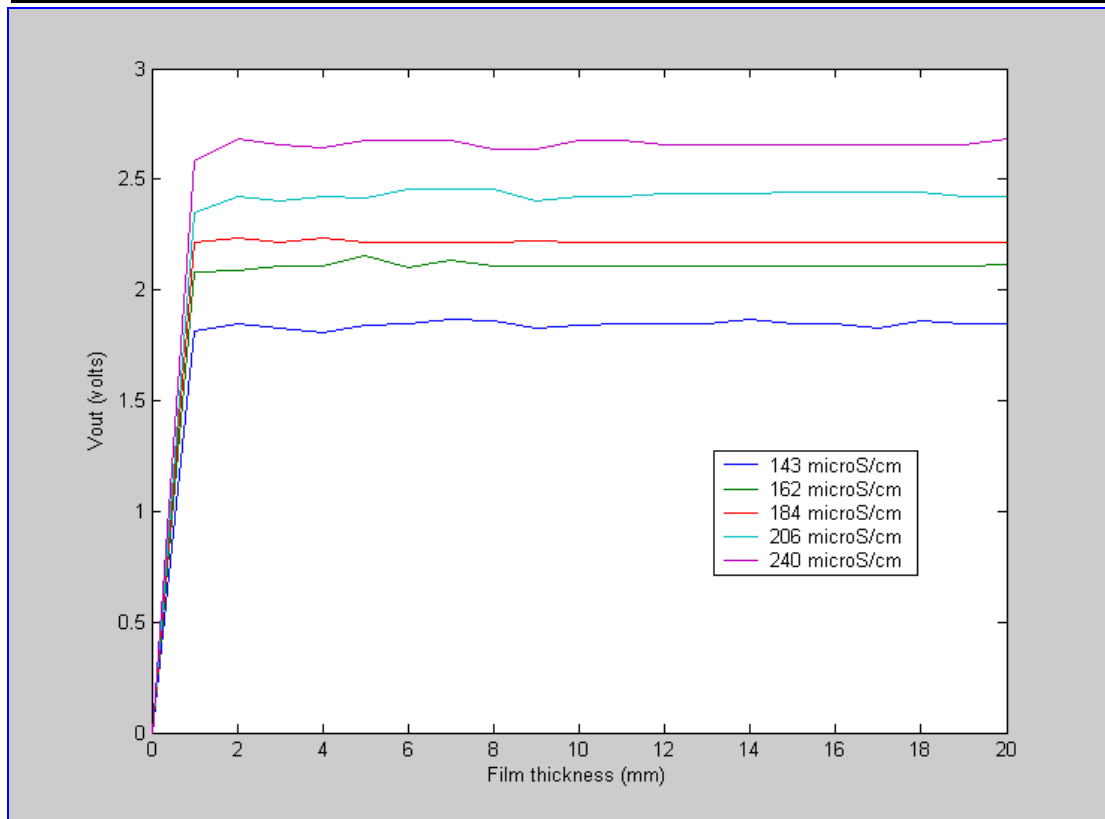


Figure 9.7 Voltage output of Flush Mounted Sensor for different liquid conductivities (Config.2, bench test)

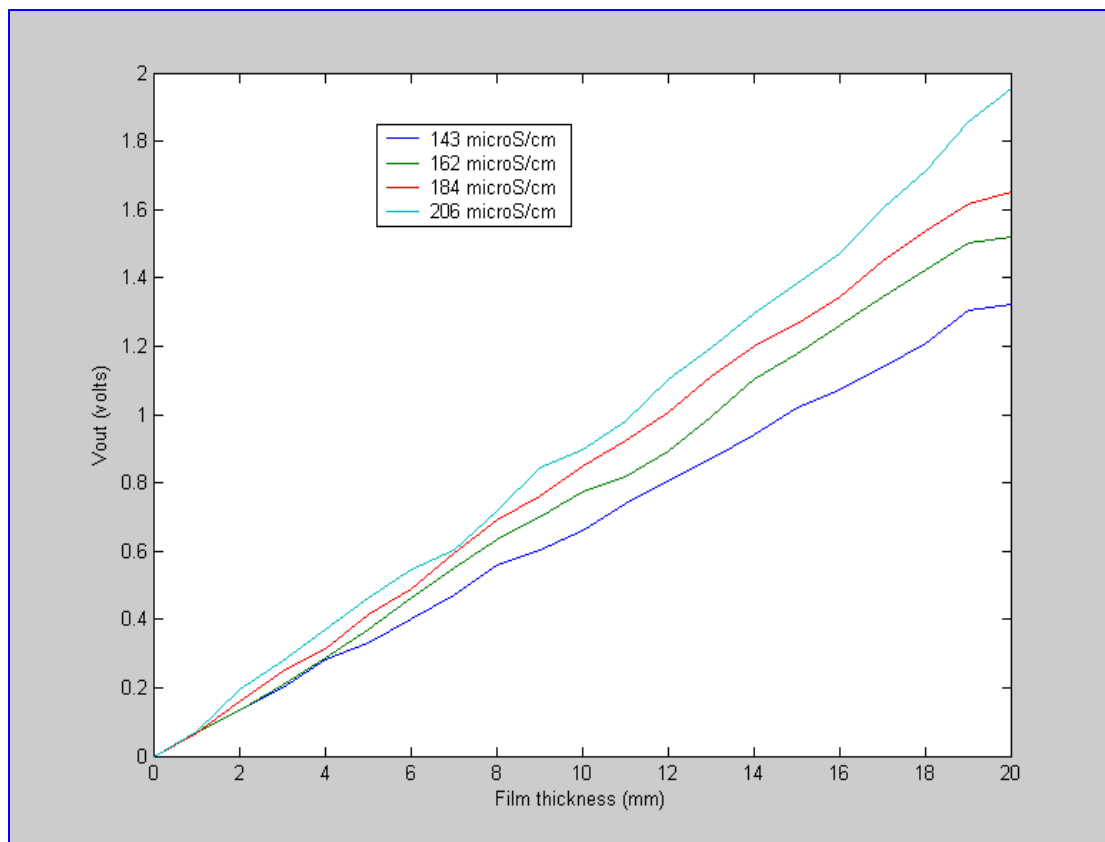


Figure 9.8 Voltage output of CFM device for different liquid conductivities (bench test)

From both systems, CFM and FMS, a working system to cross-check the measurement film thickness would be:

*If* the CFM reads  $\leq 0.1$  volts, *then* the liquid film thickness  $\delta$  would be measured directly and only by the CFM.

*If* the CFM reads  $> 0.1$  volts, *then* the liquid film thickness  $\delta > 1\text{mm}$ . In this case the FMS can be used to measure the liquid film conductivity  $\sigma_f$  and this can be used to check the film thickness measured by the CFM.

## 9.2 Integrate the flow metering devices developed in this thesis into a multiphase flow rig:

The proposed system has proved successful for a two-phase gas-liquid system. However, it is common to have three-phase gas-oil-water flow from production wells as production progresses. Therefore, it is essential to extend the system to multiphase flow. A possible future project could be the integration of the flow meters designed for this project into a three phase (oil-water-air) flow rig. This project will develop better understanding about:

- The range of three-phase flow rates that can be used with the CFM and USFM developed for this project. The range of flow rates could be extended to beyond those used in this project to further analyze the behaviour of the annular flow parameters i.e. liquid film thickness, liquid film velocity, entrainment, gas core velocity and liquid film flow profile. The knowledge gained could be used to improve the performance of the flow meters.
- The behaviour of the test system could be further validated using multiphase flow. In this way the techniques for determining volume fraction could be improved. This may result in a better design configuration than that used in this project.

### 9.3 Investigate the robustness of the system:

The system capability and accuracy should be tested in real life work stations, in particular the robustness of the USFM and the CFM devices, which have been the focal points of the present research. This investigation should include installation effects and consequent errors in the flow measurements. Such effects could be static (effects that do not change with time such as: single or double elbows, diameter reduction, partially open valve and bluff bodies) or dynamic (effects which arise from rapid time dependent changes in the flow field or by pulsations in the flow e.g. from pumps and compressors, control valves and pressure regulators or by flow induced oscillations).

### 9.4 Commercial development of an online flow meter:

The author believes that the USFM and the CFM devices could produce an excellent commercial online flow meter. Such a step would require the reconstruction of the devices so they fit real applications including improved electronic circuits that can cope with field applications and can be integrated into a DSP system.

## **REFERENCES**

Addlesee, A.J. and Cornwell, K. (1997). Liquid film thickness above a bubble rising under an inclined plate. *Chem. Eng. Research and Design*.

Al-Yarubi, Q.S. (2006). The modelling of electromagnetic flow meter to determine phase flow rates in vertical gas-liquid slug flows. *M.Sc. Thesis, University of Huddersfield*.

Alimonti, C., Bilardo, U. (2001): "Measurement of three-phase flow rates using neural network approach", *4th Int. Conf on Multiphase Flow*, New Orleans, Louisiana, USA, May 27- June 1, 2001.

Ambrosini, W., Andreussi, P. and Azzopardi, B.J. (1991). A physically based correlation for drop size in annular flow. *Int. J. Multiphase Flow*.

Aragaki, T., Nakayama, S., Suzuki, M., and Toyama, S. (1987). Characteristics of a falling liquid on a vertical tube. *Int. Chem. Eng.*

Ariyadasa, U. (2002). An Investigation of Film Thickness and Pressure in Upward and Downward Annular Two-Phase Flow. *M.Sc. Thesis, Department of Mechanical Eng., University of Saskatchewan*.

Ariyadasa, U. and Rezkallah, K.S. (2001). An investigation of pressure and film thickness in co-current annular upward and downward two-phase flow. *4th Int. Multiphase Flow Conf.*

Ashkuri, S. and Hill, T.J. (1985). Measurement of Multiphase Flows in Crude Oil Production Systems. *Pet. Rev.*

Atkinson, A., Theuveny, B., Berard, M., Conort, G., Lowe, T., McDiarmid, A., Mehdizadeh, P., Pinguet, B., Smith, G., Williamson, K. J. (2004-2005): "A New Horizon in Multiphase Flow Measurement", *Schlumberger Oilfield Review*.

Azzopardi, B.J. and Wren, E. (2004). What is entrainment in vertical two-phase churn flow? *Int. J. Multiphase Flow*.

Azzopardi, B.J. Sanoullah, K.S. (2002). Re-entrainment in wave-plate mist eliminators. *Chem. Eng. Sci.*

Azzopardi, B.J., Zaidi, S.H. and Jepson, D.M. (1997). Entrained fraction in inclined annular gas/liquid flow. *Gas Liquid Flow in Fluid Mechanics and Heat Transfer, ASME*.

Azzopardi, B.J. (1983). Mechanisms of entrainment in annular two-phase flow. *UKAEA Report AERE-R 11068*.

---

## REFERENCES

---

- Barbosa, J.R., Jr., Hewitt, G.F., Konig, G., and Richardson, S.M. (2002). Liquid entrainment, droplet concentration and pressure gradient at the onset of annular flow in a vertical pipe. *Int. J. Multiphase Flow*.
- Baker, R.C. (2000). *Flow measurement handbook: industrial designs, operating principles, performance, and applications*. Cambridge University press, UK.
- Beck, M.S. and Mazille, J. (2002). A study of a pressure differential flow meter that is insensitive to inlet conditions. *Flow Meas. and Inst.*
- Beck, S. and Plaskowski, A. (1987). *Cross Correlation Flowmeters - Their Design and Application*. Taylor & Francis, Inc.
- Bilgesu, H. (1994). A new multiphase flow model for horizontal, inclined, and vertical pipes. *Society of Pet. Engrs.*
- Blackstock, D.T. (2000). *Fundamentals of Physical Acoustics*. Wiley & Sons.
- Bousman, W.S. (1995). Studies of two-phase gas liquid flow in microgravity. *Ph.D. Thesis, University of Houston*.
- BP Review of World Energy 2005, *downloaded from the bp website*.
- Burns, J.R., Ramshaw, C. and Jachuck, R.J. (2003). Measurement of liquid film thickness and the determination of spin-up radius on a rotating disc using an electrical resistance technique. *Chem. Eng. Sci.*
- Clark, W.W. (2002). Liquid film thickness measurement. *Multiphase Sci. and Tech.*
- Collins, D.B. and Gacesa, M. (1971). Measurement of steam quality in two-phase up flow with venturies and orifice plates. *J. Basic Eng.*
- Conte, G. and Azzopardi, B.J. (2003). Film thickness variation about a T-junction *Int. J. Multiphase Flow*.
- Cory, J. (1999). The measurement of volume fraction and velocity profiles in vertical and inclined multiphase flows. *Ph.D. Thesis, University of Huddersfield*.
- Cosham, A., Hopkins, P. and Macdonald, K.A. (2007). Best practice for the assessment of defects in pipelines. *Corrosion Eng. Failure Analysis*.
- Dell'Isola M., Cannizzo, M. and Diritti, M. (1997). Measurement of high-pressure natural gas flow using ultrasonic flow meters. *Elsevier Sci.*
- Dou, J.W., Xiao, Q.Q. and Chen, J.G. (1996). Development and Trial Application of Haimo Multiphase Flow meter. *The 8th int. conf. on flow meas., Beijing, China*.

---

## REFERENCES

---

- Drosos, E.I., Paras, S.V. and Karabelas, A.J. (2006). Counter-current gas–liquid flow in a vertical narrow channel-Liquid film characteristics and flooding phenomena. *Int. J. Multiphase Flow*.
- Dziubinski, M., Fidos, H. and Sosno, M. (2004). The flow pattern map of a two-phase non-Newtonian liquid–gas flow in the vertical pipe. *Int. J. Multiphase Flow*.
- Eckert, S. and Gerbeth, G. (2002). Velocity Measurements in Liquid Sodium by Means of Ultrasound Doppler Velocimetry. *Experiments in Fluids*.
- Ferrari, V., Ghisla, A., Marioli, D. and Taroni A. (2005). Silicon resonant accelerometer with electronic compensation of input-output cross-talk. *Sensors and Actuators A: Physical*.
- Fossa, M. (1998). Design and performance of a conductance probe for measuring the liquid fraction in two-phase gas-liquid flows. *Flow Meas. and Inst.*
- Franco, A. (2007). An apparatus for the routine measurement of thermal conductivity of materials for building application based on a transient hot-wire method. *Applied Thermal Eng.*
- Fukano, T. and Furukawa, T. (1998). Prediction of the effects of liquid viscosity on interfacial shear stress and frictional pressure drop in vertical upward gas-liquid annular flow. *Int. J. Multiphase Flow*.
- Gamisans, X., Sarrà, M. and Lafuente, F. (2004). The Role of the Liquid Film on the Mass Transfer in Venturi-Based Scrubbers. *Chem. Eng. Research and Design*.
- Geraci, B.J. Azzopardi, van Maanen, H.R.E. (2007). Effect of inclination on circumferential film thickness variation in annular gas/liquid flow. *Chem. Eng. Sci.*
- Govan, A.H. and Hewitt, G.F. (1990). Phenomena and prediction in annular two-phase flow, advances in gas-liquid flows. *Presented at the winter annual meeting, American Society of Mech. Engrs.*
- Govier, G.W. and Aziz, K. (1972). *The flow of complex mixtures in pipes*. Van Nostrand Reinhold, New York.
- Han, H., Zhu, Z. and Gabriel, K. (2006). A study on the effect of gas flow rate on the wave characteristics in two-phase gas–liquid annular flow. *Nuc. Eng. and Design*.
- Han, H. (2005). A study of entrainment in two phase upward cocurrent annular flow in a vertical tube. *Ph.D. Thesis, University of Saskatchewan*.
- Hans, V. and Windorfer, H. (2003). Comparison of pressure and ultrasound measurements in vortex flow meters. *Meas.*
- Hatlo, A. and Sorensen, S. (1999). North Sea field test of a multiphase flow meter. *North Sea flow meas. workshop*.

---

## REFERENCES

---

- Hori, K., M. Nakazatomi, K. Nishikawa, and Sekoguchi, K. (1979). On ripple of annular two-phase flow: effect of liquid viscosity on characteristics of wave and interfacial friction factor. *Bulletin of the JSME*.
- Huang, Z., Xie, D., Zhang, H. and Li, H. (2005). Gas-oil two-phase flow measurement using an electrical capacitance tomography system and a Venturi meter. *Flow Meas. and Inst.*
- Hurlburt, E.T. and Newell, T.A. (1996). Optical measurement of liquid film thickness and wave velocity in liquid film flows. *Experiments in fluids*.
- Jackson, M.L. (1955). Liquid films in viscous flow. *American inst. of Chem. Eng. J.*
- James, F.T. (1965-1966). Metering of steam-water two-phase flow by sharp-edged Orifices. *Process. Inst. Mech. Eng.*
- Jonathan, W. and Mark, S. (2002). Modern developments in shear-stress measurement. *Progress in Aerospace Sci.*
- Kang, H.C. and Kim, M.H. (1992). The development of a flush-wire probe and calibration method for measuring liquid film thickness. *Int. J. Multiphase Flow*.
- Karimi, G. and Kawaji, M. (2000). Flooding in vertical counter-current annular flow. *Nuc. Eng. and Design*
- Kataoka, I., Ishii, M. and Mishima, K. (1983) Generation and size distribution of droplet in annular two-phase flow. *J. Fluids Eng.*
- Kažys, R., Vladišauskas, A. and Raišutis, R. (2002). Experimental investigation of gas flow in pipes with recesses for ultrasonic transducers. *Prof. K.Baršauskas ultrasound institute, Kaunas University of Technology*.
- Keeys, R.K., Ralph, J.C., and Roberts, D.N. (1970). Liquid entrainment in adiabatic stream water flow at 500 and 1000 Psi. *UKAEA*.
- Keshock, E.G. and Lin, C.S. (1996). Two-Phase Annular Flow in Helical Coil Flow Channels in a Reduced Gravity Environment. *Proceedings of the 1996 3<sup>rd</sup> Microgravity Fluid Physics Conf.*
- Koskie, J.E., Mudawar, I., Tiederman, W.G. (1989). Parallel-wire probes for measurement of thick liquid films. *Int. J. Multiphase Flow*.
- Kvurt, P., Kholpanov, L.P., Malyusov, V.A. and Zhavoronkov, N.M. (1981). Influence of the alternating-current on the results of measurement of the thickness of liquid films by the conductivity method. *J. App. Chem. in the USSR*.
- Kwon, J.T., Ahn, Y.C. and Kim, M.H. (2001). A modeling of in-tube condensation heat transfer for a turbulent annular film flow with liquid entrainment. *Int. J. Multiphase Flow*.

---

## REFERENCES

---

- Lin, Z.H. (1982). Two-phase flow measurements with sharp-edged orifices. *Int. J. Multiphase Flow*.
- Lioumbas, J.S., Paras, S.V. and Karabelas, A.J. (2005). Co-current stratified gas-liquid down flow-Influence of the liquid flow field on interfacial structure. *Int. J. Multiphase Flow*.
- Lopez de Bertodano, M.A., Assad, A. and Beus, S.G. (2001). Experiments for entrainment rate of droplets in the annular regime. *Int. J. Multiphase Flow*.
- Lopez de Bertodano, M.A., Jan, C.S., and Beus, S.G. (1997). Annular flow entrainment rate experiment in a small vertical pipe. *Nuc. Eng. and Design*.
- Lowe, D.C. and Rezkallah, K.S. (1999). Flow regime identification in microgravity two-phase flows using void fraction signals. *Int. J. Multiphase Flow*.
- Lucas, G.P. (1987). The measurement of two-phase flow parameters in vertical and deviated flows. *PhD thesis*, UMIST.
- Lynnworth, L.C. and Liu, Y. (2006). Ultrasonic flow meters: Half-century progress report, 1955–2005. *Elsevier, Ultrasonics*.
- Lyons, W.C. and Plisga, G.J. (2004). *Standard Handbook of Petroleum and Natural Gas Engineering*. (Second Edition).
- MacGillivray, R. (2004). Gravity and Gas Density Effects on Annular Flow Average Film Thickness and Frictional Pressure Drop. *Ph.D. Thesis, University of Saskatchewan*.
- Martyn, J. (1999). Tomographic multiphase flow measurement. *Ph.D. Thesis, University of Surrey*.
- Matsuura, K., Kataoka, I. and Serizawa, A. (1995). Prediction of droplet deposition rate based on Lagrangian simulation of droplet behavior, *Proc. Of the 3<sup>rd</sup> JSME/ASME Joint Int. Conf. on Nuc. Eng., Kyoto, Japan*.
- McLeod, W.R., Rhodes, D.F. and Day, J.J. (1971). Radio-traces in gas-liquid transportation problems - a field case. *J. Pet. Tech*.
- Moalem, D. and Dukler, A. (1984). Flooding and upward film flow in vertical tubes: speculations on film flow mechanism. *Int. J. Multiphase Flow*.
- Morud, J. and Skjetne, P. (2005). Simulation of gas-liquid flows with liquid films at walls, *Conf. of CFD*.
- Murakawa, H., Kikura, H. and Aritomi, M. (2005). Application of ultrasonic Doppler method for bubbly flow measurement using two ultrasonic frequencies. *Experimental Thermal and Fluid Sci*.

---

## REFERENCES

---

- Murdock, J. W. (1962). Two-phase flow measurements with orifices. *J. Basic Eng.*
- Mus, E.A., Toskey, E.D., Bascoul, S.F., Norris, R.J.(2001). Added value of a multiphase flow meter in exploration well testing. *Offshore Technology Conference.*
- Nigmatulin, R.I., Nigmatulin, B.I., Khodzhaev, Ya.D. and Kroshilin V.E. (1996). Entrainment and deposition rates in a dispersed-film flow. *Int. J. Multiphase Flow.*
- Oddie, G. and Anthony, J.R. (2004). Flow-rate measurement in two-phase flow. *Schlumberger, Cambridge Research.*
- Ohba, K., Origuchi, T. and Shimanaka, Y. (1984). Multi-fiber optic liquid film sensor. *Proceedings of the 4th Sensor Symposium.*
- Okawa, T., Kitahara, T., Yoshida, K., Matsumoto, T. and Kataoka, I. (2000). Numerical simulation of annular dispersed flows in round tubes and annuli using multi-fluid model. *Proceedings of the 3<sup>rd</sup> UK-Japan Seminar on Multi-phase Flow and Nuc. Safety.*
- Oliemans, R.V., Pots, B.F. and Trompe, N. (1986). Modelling of annular dispersed two-phase flow in vertical pipes. *Int. J. Multiphase Flow.*
- Olsen, AB. and Hanssen B.V. (1994). Framo multiphase flow meter – field testing experience from Statoil Gullfaks A and B platforms and Texaco Humble test facilities. *The North Sea flow meas. workshop, Bergen, Norway.*
- Omebere-Iyari, N.K. and Azzopardi, B.J. (2007). A study of flow patterns for gas/liquid flow in small diameter tubes. *Chem. Eng. Research and Design.*
- Oriol, J., Pierre, J., Jallut, C., Tochon, P. and Clement, P. (2008). Characterization of the two-phase flow regimes and liquid dispersion in horizontal and vertical tubes by using coloured tracer and non-intrusive optical detector. *Chem. Eng. Sci.*
- Owen, D.G. and Hewitt, G.F. (1987). An improved annular two-phase flow model. *3<sup>rd</sup> Int. Conf. on Multi-phase Flow,*
- Pan, L. and Hanratty, T.J. (2002). Correlation of entrainment for annular flow in vertical pipes. *Int. J. Multiphase Flow.*
- Papadakis, E. P. (1999). *"Ultrasonic Instruments and Devices."* Academic Press.
- Pascal, H. (1984). On some new techniques in flow metering of two-phase compressible mixtures. *J. Fluids Eng.*
- Pascal, H. (1983). Compressibility effect in two-phase flow and its application to flow metering with orifice plate and convergent-divergent nozzle. *J. Fluids Eng.*

---

## REFERENCES

---

- Patruno, L., Dorao, C., Svendsen, H. and Jakobsen, H. (2009). On the modelling of droplet–film interaction considering entrainment, deposition and breakage processes. *Chem. Eng. Sci.*
- Pavlović, V., Dimitrijević, B., Stojćev, M., Golubović, Lj., Živković, M. and Stamenković, L. (1997). Realization of the ultrasonic liquid flow meter based on the pulse-phase method. *Elsevier, Ultrasonics*.
- Peng, S.W. (2008). Heat flux effect on the droplet entrainment and deposition in annular flow dry-out. *Com. in Nonlinear Sci. and Numerical Simulation*.
- Pu, F., Sui-Zheng, Q. and Dou-Nan, J. (2006). An investigation of flow characteristics and critical heat flux in vertical upward round tube. *Nuc. Sci. and Tech.*
- Purvey, R. (1998). Water in oil: On-line measurement. The MFI water cut meter in offshore applications. *The North Sea flow meas. workshop, Bergen, Norway*.
- Quandt, E.R. (1965). Measurement of some basic parameters in two-phase annular flow. *American Ins. of Chem. Engrs. J.*
- Richard, S. (2001). Wet Gas Metering. *PhD. Thesis, University of Strathclyde*.
- Richardson, T.J. and Rubin, M. D. (2001). Liquid phase deposition of electrochromic thin films. *Electro-chimica Acta*.
- Rodríguez, D.J. and Shedd, T.A. (2004). Entrainment of gas in the liquid film of horizontal, annular, two-phase flow. *Int. J. Multiphase Flow*.
- Roger C. Baker. (2004). *An Introductory Guide to Flow Measurement*. ASME, Mexico.
- Sawanta, P., Ishii M., Hazukub, T., Takamasab, T. and Moric, T. (2008). Properties of disturbance waves in vertical annular two-phase flow. *Nuc. Eng. and Design J.*
- Schadel, S.A., Lemana, J.L., and Hanratty, T.J. (1990). Rates of atomization and deposition in vertical annular flow. *Int. J. Multiphase Flow*.
- Sekoguchi, K., Fukano, T., Ousaka, A. and Ishida, K. (1978). Two-phase flow measurements with orifice-couple in horizontal pipe line. *Bulletin of JSME*.
- Spendel, K.D. (1985). On non-invasive ultrasonic flow measurement. PhD. Thesis Cranfield Institute of Technology
- Sugawara, S. (1990). Droplet deposition and entrainment modelling based on the three-fluid model. *Nuc. Eng. Design*.
- Svedeman. S. (1997). V-Cone Meter Measurement Accuracy for Wet Gas Flow. *McCrometer Inc.*

---

## REFERENCES

---

- Tayebi, D., Nuland S. and Fuchs P. (2000). Droplet transport in oil/gas and water/gas flow at high gas densities. *Int. J. Multiphase Flow*.
- Taitel, Y., Barnea, D. and Brill, J.P. (1995). Stratified three phase flow in pipes. *Int. J. Multiphase Flow*.
- Taitel, Y., Shoham, O. and Brill, J.P. (1989). Simplified transient solution and simulation of two phase flow in pipelines. *Chem. Eng. Sci.*
- Tibiriçá, C.B., Nascimento, F.J. and Ribatski, G. (2009). Film thickness measurement techniques applied to micro-scale two-phase flow systems. *Experimental Thermal and Fluid Sci.*
- Thomas P. and Paul F., (2008). A novel experimental technique for accurate mass flow rate measurement. *Flow Meas. and Inst.*
- Ting, V.C. and Jones, E.H. (1996). Wet Gas Metering Performance. *Proceedings of the Int. Conf. on Offshore Mech. and Artic Eng., ASME*.
- Upp, E. and LaNasa, J. (2002). Fluid Flow Measurement. *A Practical Guide to Accurate Flow Meas. (2nd Edition), Elsevier*.
- Van't Westende J.M., Kemp, H.K., Belt, R.J., Portela, L.M., Mudde, R.F. and Oliemans, R.V.A. (2007). On the role of droplets in cocurrent annular and churn annular pipe flow. *Int. J. Multiphase Flow*.
- Wada, S., Kikura, H. and Aritomi, M. (2006). Pattern recognition and signal processing of ultrasonic echo signal on two-phase flow. *Flow Meas. and Inst.*
- Wadekar, V.V. (2002). Heat transfer coefficient prediction for falling film evaporation used for solvent removal from highly viscous liquids. *Chem. Eng. Research and Design*.
- Webster, J.G. (2000). *The measurement, instrumentation, and sensors handbook*. CRC Press in cooperation with IEEE press.
- Whalley, P.B. (1987). *Boiling, Condensation, and Gas-Liquid Flow*. Oxford University Press, New York, United States.
- Whitaker, T.S. (1997). Multiphase flow measurement: current and future developments. *Advances in Sensors for Fluid Flow Meas.*
- William, P., Xiqing, L. and Shoeleh, A. (2007). Deposition and re-entrainment dynamics of microbes and non-biological colloids during non-perturbed transport in porous media in the presence of an energy barrier to deposition. *Advances in Water Resources*.
- Williams, L.R., Dykhno, L.A. and Hanratty, T.J. (1996). Droplet flux distributions and entrainment in horizontal gas-liquid flows. *Int. J. Multiphase Flow*.

---

## REFERENCES

---

Wongwises, S. and Pipathattakul, M. (2006). Flow pattern, pressure drop and void fraction of two-phase gas-liquid flow in an inclined narrow annular channel. *Exp. Thermal and Fluid Sci.*

Yeung, H. (2003). Editorial to: Multi-Phase Flow Measurement. *Flow Meas. and Inst.*

Yoshida, K. and Tadayoshi, M. (2005). Turbulence modification in vertical upward annular flow passing through a throat section. *Int. J. Heat and Fluid Flow.*

Yu, S.M. and Tso, C.P. (1995). Simulation of fiber optic sensors in determination of thin liquid film thicknesses. *Advances in Eng. Software.*

Zabaras, Dukler and Moalem-Maron, D. (1986). Vertical upward cocurrent gas-liquid annular flow. *AIChE J.*

Zhao, T.S. and Bi, Q.C. (2001). Co-current air-water two-phase flow patterns in vertical triangular microchannels. *Int. J. Multiphase Flow.*

Zheng, G., Jin, N., Jia, X., Lv, P. and Liu, X. (2008). Gas-liquid two phase flow measurement method based on combination instrument of turbine flow meter and conductance sensor. *Int. J. Multiphase Flow.*

[www.efunda.com/DesignStandards/sensors/flowmeters/flowmeter\\_cor.cfm](http://www.efunda.com/DesignStandards/sensors/flowmeters/flowmeter_cor.cfm) - accessed 05-08-09

[www.AMS-Instrumentation-and-Calibration/Large-line-size-Coriolis-flow-meter - n686517](http://www.AMS-Instrumentation-and-Calibration/Large-line-size-Coriolis-flow-meter-n686517) - accessed 05-08-09